

Assessment and evaluation of visual function measurement in inherited retinal degeneration; focusing on optimisation

A thesis submitted to the Nuffield Department of Clinical Neurosciences for the degree of Doctor of Philosophy Hilary 2020

Jasleen Kaur Jolly

Supervisors: Prof Robert MacLaren

Prof Holly Bridge





FUNDED BY

NIHR | National Institute for Health Research

Merton College

University of Oxford



Acknowledgements

I am deeply grateful to both my supervisors, Holly Bridge and Robert MacLaren for their mentorship and for being such wonderful role models. Robert has shaped the researcher I am today with his training and support for the past 8 years. I feel very fortunate to have the opportunity to work with such an incredible team and wonderful patients. Holly has been incredibly patient and encouraging, showing me how to develop as a scientist. I am thankful that I have had both of you as my supervisors and am looking forward to continuing to work together.

I am also grateful to the NIHR for funding my fellowship and allowing me to complete my DPhil after so many years of working in the field and the RDS for advising on my application. Merton College have been wonderful in providing financial and social support, with special thanks for Simon Jones. I am also grateful to the graduate office at NDCN for their support at several points. I could not have done this work without the support of the Eye Research Group Oxford (ERGO) in Oxford Eye Hospital. ERGO are a great team and a pleasure to work with.

I am grateful to my friends and colleagues who have helped me along and kept my sanity. This includes Iain Wilson, Caroline Peddle, Laura Wood, Laurel Chandler, Aman Josan, Tom Buckley, Lewis Fry, Imran Yusuf, Mital Shah, Matt Gabel, Ivan Alvarez, Aislin Sheldon, Betina Ip, Zeena-Britt Sanders, Hannah Willis, Moreno Menghini, Connie Han, Ben Davis, Shraddha Shah. Plus my friends and neighbours Bruce and Natacha Huggett, who are wonderful people.

I would like to thank my parents and my wonderful sister Kavneet as they have always had confidence in me and pushed me to achieve me dreams. Their belief in me has helped me keep going, especially at the low points.

Finally, I would like to thank all the patients. You are my inspiration and my driving force.

Abstract

Assessment and evaluation of visual function measurement in inherited retinal degeneration; focusing on optimization.

Jasleen K Jolly, Merton College

Thesis submitted for the degree of Doctor of Philosophy, Trinity Term 2020

Photoreceptors at the back of the eye are the first step in producing our sense of vision, able to capture photons of light of differing wavelength. These connect to retinal circuits, which feed into visual pathways and networks in the brain, where the responses from the eye are processed to provide rich visual perception. Loss of these photoreceptors leads to severe visual impairment, as light can no longer be detected. While degeneration has a direct effect on the photoreceptors, there are also secondary effects on retinal circuits, in addition to the pathways processing visual information in the brain.

Recently there has been an increase in the development of novel interventions for the treatment of inherited retinal degenerations, with the first retinal gene therapy approved as an NHS treatment in 2019. Yet little work has been conducted on establishing the most appropriate outcome measures to quantify success. In this thesis I probe the practical impact of visual field loss on the conduct of visual function tests such as visual acuity and colour vision. I discuss factors affecting test reliability and propose solutions to improve measurement. I place emphasis on providing an understanding of the basis of the measurements to allow the appropriate measures to be chosen in trials, including for the first time a comprehensive assessment of local and global scotopic function. Beyond the retina, I show that the secondary changes in the inner retina can be detected with the use of ocular coherence tomography imaging and have an impact on visual function testing with microperimetry. I show changes in the integrity of the white matter in the visual brain pathways as a result of retinal disease. This could potentially pose a limiting factor in reversing visual deficits by treating the retina alone.

Vision is a result of interconnecting circuits between the eye and the brain and therefore, changes from retinal disease must be considered in terms of their wider effects along the visual system.

Table of Contents

Acknowledgements 1
Abstract 2
List of Figures 9
List of Tables 15
List of Abbreviations 16
1. Introduction 19
1.1 Introduction to the visual system 19
1.2 The eye 19
1.2.1 Retina 20
1.2.1.1 Photoreceptors 20
1.2.1.2 Retinal circuits 22
1.2.2 Structural analysis of the retina 23
1.2.2.1 Fundus autofluorescence 23
1.2.2.2 Ocular coherence tomography (OCT) 24
1.2.3 Visual functional measures 25
1.2.3.1 Microperimetry 25
1.2.3.2 Gaps in knowledge 27
1.3 The Visual Brain 28
1.3.1 The visual pathway 28
1.3.2 Preservation of the visual field along the visual pathway 28
1.3.3 Brain adaptability 30
1.3.4 Assessment of the visual brain 33
1.4 Rod-cone dystrophies 34
1.4.1 General introduction 34
1.4.2 Choroideremia 37
1.4.3 RPGR retinitis pigmentosa 38
1.5 Gene therapy outcome measures: Current practice 39
1.5.1 Introduction to gene therapy 39
1.5.2 Scoping review methodology 41
1.5.3 Scoping review results 42
1.5.3.1 Listed outcome measures 42
1.5.3.2 Published trials 48
1.5.4 Justification of thesis 49
1.6 Scope of the thesis 52
1.7 Colour schemes used 52

2. Photopic Function 55
2.1 Optimisation of visual acuity measurement in the presence of visual field loss. 55
2.1.1 Abstract/Summary 55
2.1.2 Importance of visual acuity measurement 55
2.1.3 Methods 58
2.1.4 Results 61
2.1.4.1 Patient demographics 61
2.1.4.2 Visual acuity measurement in healthy volunteers 62
2.1.4.3 Visual acuity measurement in patient group 64
2.1.4.4 Relationship to visual field 65
2.1.4.5 Longitudinal VA measurement 67
2.1.5 Discussion 68
2.1.6 Conclusion 70
2.1.7 Implications for clinical practice 70
2.2 Colour vision in rod-cone dystrophies 70
2.2.1 Abstract/Summary 70
2.2.2 Introduction to colour vision 71
2.2.3 Methods 75
2.2.3.1 Assessments and statistical analyses 75
2.2.3.2 Participants 78
2.2.4 Results 78
2.2.4.1 Comparison between groups shows early tritan loss 78
2.2.4.2 Comparison with 100 Hue reveals the Cambridge Colour Test is more discerning 81
2.2.4.3 Relationship with PERG indicates colour vision is not just related to macular function 81
2.2.5 Discussion 82
2.2.6 Future directions 86
2.2.7 Novel findings 86
2.2.8 Implications for clinical practice 86
3. Scotopic Function 88
3.1 Introduction to scotopic vision 88
3.1.1 Rod photoreceptors 88
3.1.2 Retinal circuits for the rod 90
3.2 Measurement of scotopic vision 91
3.3 Investigation of global scotopic function 92

3.3.1 Abstract/Summary 92
3.3.2 Introduction to FST 92
3.3.3 Methods 93
3.3.3.1 Dark adaptation curves 93
3.3.3.2 Full field stimulus threshold testing 95
3.3.3.3 Statistical analyses 96
3.3.3.4 Participants 97
3.3.4 Results 97
3.3.4.1 Dark adaptation patterns are reflective of disease severity 98
3.3.4.2 FST can provide information about the dark adaptation curve expected 99
3.3.4.3 Retinal AF area influences FST measurement in disease 101
3.3.4.4 Factors affecting FST measurement 102
3.3.5 Discussion 103
3.3.6 Future directions 104
3.3.7 Novel findings 105
3.3.8 Implications for clinical practice 105
3.4 Scotopic visual fields 105
3.4.1 Abstract/summary 105
3.4.2 Introduction to scotopic perimetry 105
3.4.3 Methods 107
3.4.4 Results 108
3.4.4.1 Repeatability 109
3.4.4.2 Group comparisons 109
3.4.4.3 Spatial differences 110
3.4.5 Discussion 115
3.4.6 Future Directions 115
3.4.7 Novel findings 116
3.4.8 Implications for clinical practice 116
4. Retinal remodelling in photoreceptor disease 118
4.1 Summary 118
4.2 Introduction to retinal remodelling 118
4.3 Method 122
4.4 Results 125
4.4.1 Retinal Thickness 125
4.4.2 Relationship with Visual Field 128
4.5 Discussion 129

4.6 Conclusion 132
4.7 Novel findings 132
4.6 Implications for clinical practice 132
5. Impact of visual field loss on the visual pathway investigated with diffusion MRI 134
5.1 Summary 134
5.2 Introduction 135
5.2.1 Visual brain in eye disease 135
5.2.2 White matter tracts 136
5.2.3 Ventral and dorsal visual streams 136
5.2.4 Diffusion-weighted MRI 139
5.3 Methods 141
5.3.1 Structural MRI acquisition 141
5.3.2 Diffusion MRI acquisition 141
5.3.3 Diffusion analysis 142
5.3.3.1 Pre-processing 142
5.3.3.2 Tract based spatial statistics (TBSS) 143
5.3.3.3 Tractography 143
5.3.3.4 Optic radiations tracking 145
5.3.3.5 Statistical analyses 146
5.3.4 Octopus visual fields 147
5.3.5 Microperimetry: central visual field 148
5.3.6 Retinal OCT 148
5.3.7 Participants 149
5.4 Results 149
5.4.1 Whole brain analysis show a correlation between white matter microstructure and visual function 149
5.4.2 Central visual field loss affects both macular and peripheral bundles in the optic radiations 152
5.4.3 Impact of visual field loss on the ventral versus dorsal streams 155
5.5 Discussion 160
5.6 Future Directions 163
5.7 Novel findings 164
5.8 Implications for clinical practice 164
6. General Discussion 166
6.1 Discussion 166
6.2 Conclusion 171

Bibliography 174
Supplementary Data 199
Appendix 1: Standard Operating Procedures 211
A1.1 Measurement of Visual Acuity with ETDRS Charts 211
A1.2 Measurement of Visual Acuity with EVA Using Single Line Presentation 214
A1.3 Measurement of Visual Acuity Using Automated EVA E-ETDRS Protocol 216
A1.4 MAIA Microperimetry 10-2 Standard Grid 218
A1.5 Fundus Autofluorescence 220
A1.6 Farnsworth-Munsell 100 Hue Test 221
A1.7 Cambridge Colour Low Vision Version Trivector Test 223
A1.8 Pattern Electroretinogram 227
A1.9 Measurement of Dark Adaptation Curve 229
A1.10 Full-Field Stimulus Threshold 232
A1.11 Scotopic Microperimetry 235
A1.12 Retinal Imaging With Ocular Coherence Tomography (OCT) 238
A1.13 Octopus Perimetry 240
A2.1 **Jolly JK**, Bridge H, MacLaren RE. Outcome Measures Used in Ocular Gene Therapy Trials: A Scoping Review of Current Practice. *Frontiers in Pharmacology* 2019 doi: 10.3389/fphar.2019.01076 242
A2.2 **Jolly JK**, Juenemann K, Boagey H, Nadsady M, Bridge H, MacLaren RE. Validation of Electronic Visual Acuity (EVA) Measurement Against Standardised ETDRS Charts In Patients With Visual Field Loss From Inherited Retinal Degenerations. *British Journal of Ophthalmology* 2019 doi: 10.1136/bjophthalmol-2019-315124 242
A2.3 **Jolly JK.** Rod-cone dystrophies: a guide to genetics and management. Optometry Today continuing education article December 2019 242
A3.1 **Jolly JK**, Xue K, Edwards TL, Groppe M, MacLaren RE. Characterizing the natural history of visual function in choroideremia using microperimetry and multimodal retinal imaging. Investigative Ophthalmology and Vision Science 2017; 58(12): 5575-83. DOI: 10.1167/iovs.17-22486 243
A3.2 **Jolly JK**, Edwards TL, Moules J, Groppe M, Downes SM, MacLaren RE. A qualitative and quantitative assessment of fundus autofluorescence patterns in patients with choroideremia. Investigative Ophthalmology and Vision Science 2016; 57:4498-4503. DOI: 10.1167/iovs.15-18362 243
A3.3 **Jolly JK**, Groppe M, Birks J, Downes S, MacLaren RE. Functional Defects in Colour Vision in Choroideremia. American Journal of Ophthalmology 2015; 160(4): 822-31. DOI: 10.1016/j.ajo.2015.06.018 243
A3.4 Han RC, **Jolly JK**, Xue K, MacLaren RE. The effects of pupil dilation on MAIA microperimetry. Clinical and Experimental Ophthalmology 2017; 45(5): 489-495. DOI: 10.1111/ceo.12907 244

A3.5 Han RC, Gray J, Han J, MacLaren RE, **Jolly JK**. Optimisation of dark adaptation time required for mesopic microperimetry. British Journal of Ophthalmology 2019; 103: 1092-98. doi: 10.1136/bjophthalmol-2018-312253.....244

A3.6 Talib M, **Jolly JK**, Boon CJF. Measuring Central Retinal Sensitivity Using Microperimetry. Methods in Molecular Biology (In book: Retinal Gene Therapy, pp.339-349). 244

A3.6 Edwards TL, **Jolly JK**, Groppe M, Barnard AR, Cottriall CL, Tolmachova T, Black GCM, Webster AR, Lotery AJ, Holder GE, Xue K, Downes SM, Simunovic MP, Seabra MC, MacLaren RE. Long term improvement in visual acuity after retinal gene therapy for choroideremia. New England Journal of Medicine 2016; 374:1996-8. DOI: 10.1056/NEJMc1509501.....244

A3.7 Xue K, **Jolly JK**, Barnard AR, Rudenko A, Patricio MI, Edwards TL, Groppe M, Tolmachova T, Black GC, Webster AR, Lotery AJ, Holder GE, Downes SM, Seabra MC, MacLaren RE. Retinal Gene Therapy for Choroideremia in a Multicentre Dose Escalation Phase I/II Clinical Trial. Nature Medicine 2018; 24(10): 1507-12. DOI: 10.1038/s41591-018-0185-5.....244

List of Figures

Figure 1-1: Anatomy of the human retina. Light enters the eye at the top of the image and travels through the circuitry to be detected by the photoreceptors. Specific features of the photoreceptors are labelled on the right. Figure created in BioRender.com. _____ *20*

*Figure 1-2: Photoreceptor density maps of the retina. Figure provided with permission from C Curcio. Adapted from Curcio, Sloan, Kalina, Hendrickson 1990, Human photoreceptor topography, J Comp Neurol 292; 497-523. Photoreceptor topography in the human retina. Colour scale: 0-200,000 cells/ mm2 in increments of 12,500 cells/ mm^2. Cones are presented on a log scale and rods on a linear scale. The black dot is the optic nerve head (blind spot).*_____ *21*

*Figure 1-3: Layers of the retina visible with ocular coherence tomography imaging.*_____ *25*

Figure 1-4: Impact of a change in focusing on threshold measurements with microperimetry. The top image shows the focussing of the image at the start. The bottom images shows the corresponding test result. Black points were not seen, red and orange indicate low threshold and green shows normal threshold. The number of black points is higher and the number of green points is lower on the poorly focussed (retinal island not clearly visible) image on the left. _____ *27*

Figure 1-5: T1-stuctural weighted scan of the brain. (A) Visual white matter tracts between the eye and the primary visual cortex on axial view. (B) The arrows show the calcarine sulcus in a sagittal view of the brain. The sulcus represents the gap between the superior and inferior calcarine gyri of the primary visual cortex. _____ *29*

Figure 1-6: (A) Patient presenting with small central islands of vision only and functioning very well. (B) Patient presenting with preserved central vision and additional temporal preservation of vision but a great deal of difficulty with mobility. _____ *32*

Figure 1-7: Biological basis of action of genetic mutations. Genes listed on the left of the rod cell are expressed in rods only. Genes listed between the rods and cones are expressed in both and the level of the listing relates to localisation within the photoreceptor cells. The genes listed under the RPE are expressed in this tissue. These diagrams were created from information in the Online Mendelian Inheritance in Man database (OMIM #268000). _____ *36*

Figure 1-8: (A) Fundus photograph of typical case of choroideremia. (B) View of the Oxford Bridge of Sighs (C) Simulated reduced visual field of eye A on scene B. (D) Autofluorescence image of a normal eye. (E) Autofluorescence image of eye A showing the well preserved central island. (F) Autofluorescence image of a female carrier. _____ *38*

Figure 1-9: (A) Autofluorescence image typical of an eye with RPGR related X-linked retinitis pigmentosa showing a ring of hyperfluorescence with peripheral hypofluorescence (yellow arrow). (B) Infrared image of the same eye showing the location of the OCT slice (green line). (C) OCT image showing central preservation of the outer retina (blue arrow) with peripheral degeneration (red arrow). Scale bars, 200 µm in A, B and C. _____ *39*

Figure 1-10: Summary of details found for gene therapy human clinical trials detailing location, indication and trial phase (as of October 2018). 43

Figure 1-11: (A) Histogram to show the number of additional outcome measures reported by 79% of trials with peer-reviewed publications. (B) Range of visual function tests currently used as secondary outcome measures in reported ocular gene therapy trials from Table 1.1. 50

Figure 2-1: Effect of visual field loss on reading ability on ETDRS charts. (A) Microperimetry of the remaining central visual field in one eye with advanced choroideremia. The coloured areas indicate the seeing parts of the retina. (B) ETDRS chart for measuring visual acuity. (C) A simulation of the appearance of the chart in B to the eye in A, making it difficult to track across the letters and obtain an accurate measure of visual acuity. (D) E-ETDRS presentation with single letter on the centre of the screen. (E) EVA-SL presentation with a single line of letters across the centre of the screen. (F) Simulation of visual field loss on EVA, the patient can more easily search around the letter as it stays within a limited area. 57

Figure 2-2: Presentation paradigm for single line method of measuring visual acuity using the Electronic Visual Acuity (EVA) system. 59

Figure 2-3: Genetic diagnosis of patient participants enrolled. N/A denotes genetic confirmation not available. The genes responsible for the inherited retinal degeneration are listed below the pie chart. 61

Figure 2-4: Figures A and B refer to the healthy group. Other figures are based on patient data. (A) Box and whisker plot showing mean, standard deviation and range of data points in healthy volunteer participants with outliers identified. (B) Bland-Altman plot comparing ETDRS charts and the two EVA presentation paradigms of the automated E-ETDRS and single line presentation (EVA-SL) in healthy volunteer group. The dashed lines represent mean difference and the dotted lines show the limits of agreement. (C) Box and whisker plot showing mean, standard deviation and range of data points in patient participants with outliers identified in the rod-cone dystrophy patient group. (D) Bland-Altman plot comparing ETDRS charts and the E-ETDRS paradigm in the patient group. (E) Bland-Altman plot comparing ETDRS charts and single line presentation (EVA-SL) in the patient group. (F) Bland-Altman plot comparing E-ETDRS and EVA-SL. The dashed lines in the Bland-Altman plots represent mean difference and the dotted lines show the limits of agreement. 63

Figure 2-5: Bland-Altman plot from figure 3B with adjusted X-axis to allow viewing of the scatter of points in the control group. 64

Figure 2-6: Representative microperimetry examples of (A) Non-seeing eye showing a maximum of 1 seeing point in the central visual field. (B) Seeing eye with all central points having a measurable threshold. (C) Correlation in non-seeing eyes using difference between charts and electronic test and distance to nearest seeing point. (D) Correlation in seeing eyes using difference between charts and electronic test and central microperimetry threshold. (E) Correlation in seeing eyes using difference between charts and electronic test and width of vision at the fovea. 66

Figure 2-7: Scatter graph of visual acuity (VA) over 5 visits for 14 eyes with ETDRS results represented with solid lines and electronic (E-ETDRS) results represented with dashed lines. _____ *67*

Figure 2-8: Cone opponency demonstrated by cone inputs into the bipolar cell and the resultant opponent system at the end of the circuit. The blue cone cell represents the S cone. The red cones represents the L cone and the grey cone cell represents the M cone. (A) shows the blue-yellow opponency with the blue contribution from S-cones, and yellow created by mix of input from L and M cones. (B) ON centre receptive field showing the additive effect of L and M-cones. (C) OFF centre receptive field showing the opposite input of the L and M-cones. _____ *72*

*Figure 2-9: (A) Farnsworth-Munsell 100 Hue colour vision test. (B) Simulation of visual field loss restricting the view of the test resulting in slow test times. (C) Cambridge colour test (CCT) target. (D) Low vision version of the CCT showing 4 circles across the screen, providing an easier target for patients with low vision and reduced visual field. (E) Example output from full CCT version, producing an ellipse in colour vision function in colour space. (F) Example output from trivector test showing outputs for the protan, deutan and tritan axes.*_____ *74*

*Figure 2-10: Example healthy pattern electroretinogram (PERG) recorded with the Espion system for right (OD) and left (OS) eyes. The P50 and N95 components are the key features for disease monitoring. The normal P50 component occurs at 50 ms and has an amplitude of > 4 µV on the standard PERG. The N95 component occurs at 95 ms and has a larger amplitude than the P50 with a resultant P50:N95 ratio of greater than 1:1.*_____ *77*

*Figure 2-11: Summary of colour vision results. (A) Spread of individual datapoints in all three test groups. Each line represents a composite of protan, deutan and tritan thresholds on the X, Y and Z axes respectively. The angle of the line shows the direction of the defect and the length of the line indicates the extent of the defect. The coloured shadows indicate the spread of the data for each group; green for controls, red for choroideremia preserved VA and blue for choroideremia reduced VA. (B) Pirate plot of group differences. The outer envelope shows the spread of the raw data with the widest point representing the median. Inside the envelope is a small boxplot showing the summary with mean and standard deviation. Additionally, dots represent each raw data measurement point.*_____ *80*

Figure 3-1: Rod visual cycle detailing the genes coding key elements at different stages of the process. _____ *90*

Figure 3-2: Details of the rod circuits showing multiple stages of convergence and divergence and parallel processing. _____ *91*

Figure 3-3: Defining features of the typical dark adaptation curve. The top orange curve represents cone recovery from the bleaching light. The rod-cone break (α point) signals the transition point to the rod recovery which is a slower process and consists of two primary components, S2 and S3. _____ *95*

Figure 3-4: Dark adaptation patterns seen in patients with choroideremia. (A) Dark adaptation curve from a control eye for reference. (B) Stepwise increase in sensitivity with increased time in the dark. (C) Normally shaped dark adaptation curve with a reduced endpoint found in mild disease. (D) Slowed and reduced rod function

observed in moderate disease. (E) Cone only curve with no or little evidence of rod adaptation recorded in severe disease. _____ *98*

Figure 3-5: (A) Pearson correlation between the final dark adaptation threshold and FST result. (B) FST results in the eyes shown in the groups from Figure 3.4 with the addition of a control group (group 4) for reference. Lines and stars denote statistically significant differences (P ≤ 0.05. (C) Relationship of white FST measurement with the difference between blue and red sorted by group (colours). The dotted line indicates the change from a rod mediated response to a mixed rod – cone response. Values below the line are rod mediated. (D) FST results in female carriers with a pictorial representation of the correlation with phenotype. _____ *101*

Figure 3-6: (A) Relationship between remaining log retinal % area as measured on blue fundus autofluorescence (AF) and FST measurement. The grey dotted straight line denotes the lower limit of normal for FST. The dashed lines are the 95% confidence intervals around the solid regression line. (B) Examples of eyes with the same preserved AF area (11%) showing differing FST outputs and differing patterns of AF preservation. _____ *102*

Figure 3-7: Flowchart of study assessments. _____ *108*

*Figure 3-8: (A) Raw VA measures for each individual in the control and patient groups. Boxplots of mesopic microperimetry threshold (B) and FST threshold (C) showing median, interquartile range and full maximum and minimum of datasets. (D) shows the mean of each S-MAIA test conducted with cyan and red stimuli with the difference between the tests shown for each group. * denotes statistically significant difference between groups (P < 0.01).* _____ *110*

Figure 3-9: Typical results from the S-MAIA for an example control (left) and patient (right) eye. (A) Mesopic microperimetry is normal in the control eye, small central island of remaining vision in the patient eye. (B) Scotopic cyan testing (505 nm). A small rod free zone can be seen in the control eye, patches of remaining rod function are present in the patient eye. (C) Scotopic red testing (627 nm) shows patches of function in the patient eye. (D) Difference between cyan and red shows rod free zone in the centre in the control eye. The patient eye has patches that are rod dominated (blue) and have rod degeneration (red). The brown areas can be balanced between rods and cones, or show areas with loss of both. _____ *111*

Figure 3-10: Pointwise averages represented as microperimetry spatial maps. The colour bar represents the threshold colour scale (dB) for each plot. Control group represented on the left and patient group represented on the right. (A) Mesopic microperimetry. (B) Scotopic cyan testing (505 nm). (C) Scotopic red testing (627 nm). (D) Difference between cyan and red. _____ *114*

Figure 4-1: Indication of the cells likely contributing to each OCT layer. Image created from figure 1.1 and https://www.heidelbergengineering.com/int/news/know-your-retinal-layers-33401465/ _____ *120*

Figure 4-2: (A) Layer definitions used for further analysis. 1 = total retinal thickness; 2 = inner retina; 3 = photoreceptor complex. (B) Demonstration of method used for eccentricity calculations. Each dot represents a

thickness measurement at each pixel. The circles represent zones used for calculation of average thickness at 2 different eccentricities. _____ *124*

Figure 4-3: Demonstration of retinal remodelling. Sample thickness measurements from representative eyes from the control, mild and severe disease groups. Thickness measurements are shown for total thickness, inner retina and the photoreceptor complex. _____ *126*

Figure 4-4: Summary of thickness measurements from table 4.2 for total thickness, inner retinal thickness and photoreceptor complex thickness at different eccentricities. Patient group in darker colours and control group in lighter colours. The right eye (OD) is represented by plain filled bars and left eye (OS) represented by the bars containing lines. The error bars show standard deviation. _____ *128*

Figure 4-5: (A) Correlation between microperimetry threshold and retinal thickness. Solid lines show the regression lines with 95% confidence intervals presented by the dashed lines. A positive correlation is present between microperimetry threshold and both photoreceptor complex thickness and inner retinal thickness. (B) Microperimetry results overlaid on the photoreceptor outer segment map for subject 007 shown in figure 4.2. 129

Figure 5-1: (A) Sagittal view of the inferior longitudinal fasciculus (ILF). (B) Sagittal view of the superior longitudinal fasciculus (SLF) 1 and 2. (C) Coronal view of the vertical occipital fasciculus (VOF). _____ *138*

Figure 5-2: Mechanism of diffusion MRI. The circles represent free flowing water molecules in the cerebrospinal fluid and grey matter. The elongated oval represents movement water molecules constrained by the axons of white matter. _____ *140*

Figure 5-3: (A) Locations of stimuli presented with original Esterman test (red triangles) and the new modified test (yellow circles) to show differences between them. The new test covers a larger area of the visual field with a more even spread. (B) Example output from the test. The green triangles represent seen points and red circles not seen. Both symbols overlaid indicate that the point was seen on one presentation but not on the other. _____ *147*

Figure 5-4: All data are presented as a sagittal view on the left and axial view on the right. (A) White matter tracts for the control participant group displaying the collective results across the group and registered to a standard template displayed against the MNI standard brain. (B) Same view for the choroideremia participants. Scale bar applies to images C-E. Probability maps for FA differences incorporating visual function as a covariate. The colours show voxels with a significant relationship between white matter pathways and visual function. (C) Visual acuity. (D) Microperimetry threshold of the central visual field. (E) Octopus periphery score. _____ *150*

Figure 5-5: Group average representations of the optic radiations representing macular fibres in blue (central 5 degrees of vision), and peripheral vision fibres in pink (7-90 degrees of vision). Both peripheral and macular fibre bundles had lower fractional anisotropy (FA) in the patient group compared to the control group. Underneath are the average microperimetry results for the group with right and left eyes combined. (A) Control group and (B) Choroideremia group. _____ *153*

Figure 5-6: Tract profiles in choroideremia (blue) and control (green) groups showing FA values across the tracts. The top row shows tracts in the right hemisphere and bottom row shows tracts in the left hemisphere. The columns show tract profiles for the macular and peripheral bundles respectively. The shaded area around the bars represents the standard deviation, created by Rob Campbell (2020). raacampbell/shadedErrorBar (https://www.github.com/raacampbell/shadedErrorBar), GitHub. _____ 154

Figure 5-7: Summary of group measures with green representing control group and blue representing choroideremia patient group. Error bars show the standard deviation. Visual field results are presented in the left with combined right and left microperimetry threshold at different eccentricities and a global octopus score. On the right, the FA scores are presented in each bundle. Underneath OCT thickness measures are shown at 1,3,5, and 7 degrees eccentricity for each eye separately._____ 155

Figure 5-8: Summary statistics comparing choroideremia (black bars) and control (grey bars) groups. Plots show visual acuity, microperimetry threshold, OCT thickness within the central 1 degree and a ring located around 7 degrees from the fovea, and tract measurement with FA on the right Y axis (solid shading) and MD on the left Y axis (patterned bars). Both FA and MD show a reduction in the disease population. The error bars represent standard deviation. Stars represent a significant difference between the groups._____ 157

Figure 5-9: Correlation between tract measures and microperimetry threshold. A positive correlation was seen between microperimetry threshold and FA (top row) in both the ILF (left hand side) and VOF (right hand side). A negative correlation is present between threshold and MD (bottom row). _____ 158

Figure 5-10: Tract profiles in choroideremia (blue) and control (green) groups showing FA values across the tracts. The top row shows tracts in the right hemisphere and bottom row shows tracts in the left hemisphere. The columns show tract profiles for the ILF, SLF, and VOF respectively. The stars by the tract name show which tracts were significantly different between the patient and control disease states. The shaded area around the bars represents the standard deviation._____ 159

Figure 5-11: Tract profiles in choroideremia (blue) and control (green) groups showing MD values across the tracts. The top row shows tracts in the right hemisphere and bottom row shows tracts in the left hemisphere. The columns show tract profiles for the ILF, SLF, and VOF respectively. The stars show which tracts were significantly different between the patient and control disease states. The shaded area around the bars represents the standard deviation. _____ 160

List of Tables

Table 1-1: Comparison of clinical trials record and published outcomes in ocular gene therapy trials. AF = fundus autofluorescence; AMD = age-related macular degeneration; ERG = electroretinogram; FST = full-field stimulus threshold; IOP = intraocular pressure; OCT = ocular coherence tomography; RNFL = retinal nerve fibre layer; VA = visual acuity; VEP = visual evoked potential. _____ *47*

Table 2-1: Summary of participant demographics and summary of test results. _____ *62*

Table 2-2: Summary of modified Bland-Altman results for participants comparing ETDRS charts (ETDRS), electronic ETDRS testing paradigm (E-ETDRS), and electronic single line presentation (EVA-SL). Final patient subgroup analysis is based on classification of how many of the central foveal points on microperimetry were seeing or non-seeing. _____ *65*

Table 2-3: Longitudinal measurements with ETDRS charts and automated ETDRS (E-ETDRS) charts. Px = patient. _____ *68*

Table 2-4: Summary characteristics of patient groups. All data is presented as mean ± standard deviation. ___ *78*

Table 2-5: Classification of eyes as normal or abnormal when tested with the 100 Hue and Cambridge Colour Test (CCT). _____ *81*

Table 3-1: Patient demographics and summary initial results for populations tested. FST = full field stimulus testing. DA = dark adaptation. AF = fundus autofluorescence. Data are presented as mean ± standard deviation or mean and [range]. _____ *97*

Table 3-2: Dark adaptometry measures in patient and control eyes. Data are presented as mean ± standard deviation. _____ *99*

Table 3-3: Subject demographics and summary results, including repeatability analysis. Data are presented as mean [range] or mean ± standard deviation. BA = Bland-Altman. _____ *109*

Table 4-1: Subject demographics. All values are presented as mean with the range in brackets. _____ *125*

Table 4-2: Summary of layer thickness measures (µm) across different eccentricities of the retina. _____ *127*

Table 5-1: List of all the apps used from the Brainlife.io platform to process the dMRI data. _____ *146*

*Table 5-2: Summary measures of ventral and dorsal tracts and ocular data. Data are presented as mean ± SD. The * denotes the measures that are statistically different between groups.* _____ *156*

List of Abbreviations

ACT Anatomically-constrained tractography

AF Fundus autofluorescence

AMD Age-related macular degeneration

ANOVA Analysis of variance

ART Automatic real-time averaging

BA Bland-Altman analysis

CCT Cambridge colour test

CR Coefficient of repeatability

dMRI Diffusion-weighted MRI

ERG Electroretinogram

FA Fractional anisotropy

FDA Food and drug administration

fMRI Functional MRI

FST Full field stimulus threshold

GEE Generalised Estimating Equations

ILF Inferior Longitudinal Fasciculus

IOP Intraocular pressure

IRD Inherited retinal degeneration

ISCEV International Society for Clinical Electrophysiology

JND Just noticeable difference

LCA Leber Congenital Amaurosis

LGN Lateral geniculate nucleus

LHON Leber Hereditary Optic Neuritis

MAIA The Macular Integrity Assessment device

MD Mean diffusivity

MRI Magnetic resonance imaging

OCT Ocular coherence tomography

PERG Pattern electroretinogram

PIT Posterior inferior temporal region

pRF Population receptive fields

RdCVF Rod-derived cone viability factor

REP1 Rab escort protein-1

RNFL Retinal nerve fibre layer

ROI Region of interest

RP Retinitis pigmentosa

RPE Retinal pigment epithelium

RPGR Retinitis Pigmentosa GTPase Regulator

S-MAIA Scotopic MAIA

SLF Superior Longitudinal Fasciculus

SOP Standard Operating Procedure

TBSS Tract based spatial statistics

V1 Primary visual cortex

VA Visual acuity

VEP Visual evoked potential

VOF Vertical Occipital Fasciculus

Chapter 1: Introduction

Papers arising:

Jolly JK, Bridge H, MacLaren RE. Outcome Measures Used in Ocular Gene Therapy Trials: A Scoping Review of Current Practice. *Frontiers in Pharmacology* 2019 doi: 10.3389/fphar.2019.01076

Jolly JK. Rod-cone dystrophies: a guide to genetics and management. Optometry Today continuing education article December 2019.

My contributions to this chapter: The design, conduct and writing of the scoping review was my original work and conducted over a 6 month period.

Contributions to this chapter: Robert MacLaren and Holly Bridge reviewed the scoping review manuscript before publication.

1. Introduction

1.1 Introduction to the visual system

The two key components of the visual system are the eye and the brain, and these are connected by the optic nerve and optic tracts. While the eye is essential for the detection of light that leads to vision, the brain is critical for the interpretation of the retinal output. The eyes are intimately connected to the brain with both parts being necessary for vision. Both structures share many of the same neurotransmitters including glutamate, GABA, acetylcholine, and brain-derived neurotrophic factor (Kolb, Ralph, and Eduardo 1995; Afarid, Torabi-Nami, and Zare 2016). This is not surprising as both the eye and the brain develop from the foetal neural ectoderm (Heavner and Pevny 2012).

1.2 The eye

The eye is the primary organ of sight. The key light sensitive structure is the retina, found at the back of the eye. The retina consists of several cell types critical for vision and capturing photons of light (Figure 1.1). Complex circuitry then processes the input.

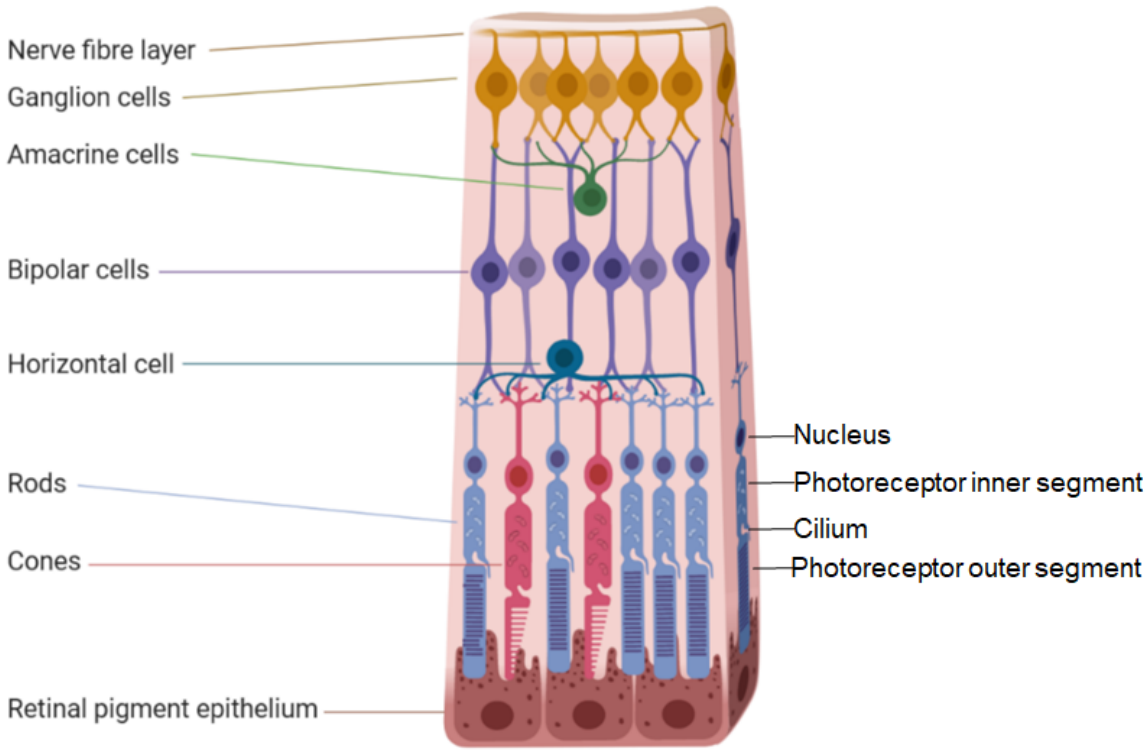


Figure 1-1: Anatomy of the human retina. Light enters the eye at the top of the image and travels through the circuitry to be detected by the photoreceptors. Specific features of the photoreceptors are labelled on the right. Figure created in BioRender.com.

1.2.1 Retina

1.2.1.1 Photoreceptors

There are two photoreceptor classes. The rod system is optimised for low light vision. The cone system has greater resolution and provides colour vision. Rods vastly outnumber cones in order to provide the necessary increased sensitivity (Figure 1.2) (Curcio et al. 1990). However, there is significant interaction between the rod and cone systems, particularly in low light levels (Zele, Maynard, and Feigl 2013).

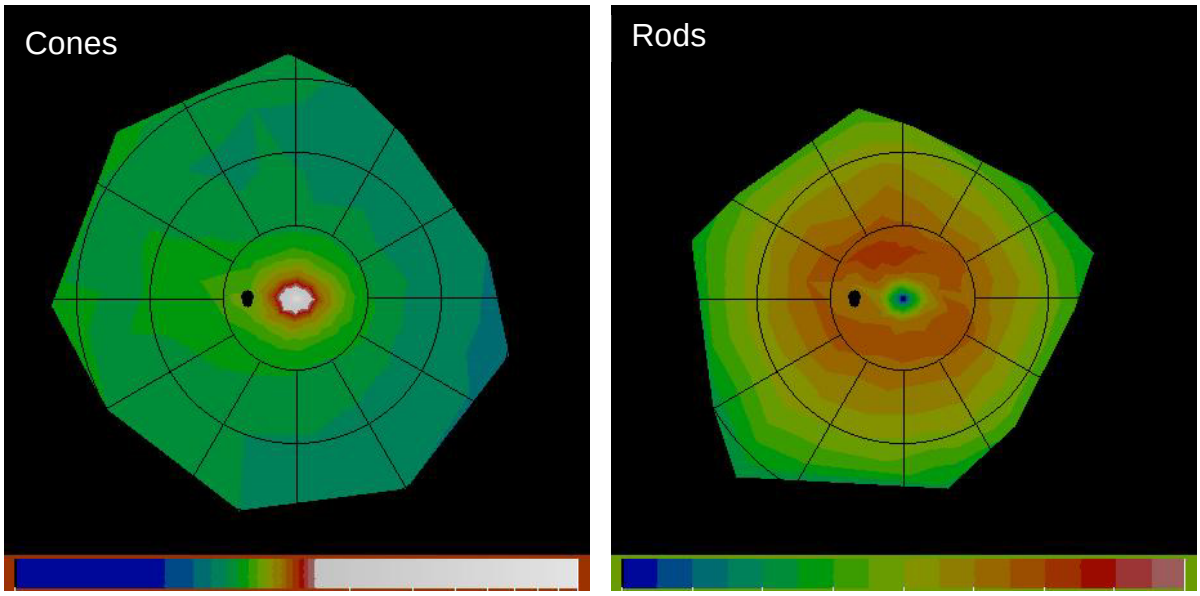


Figure 1-2: Photoreceptor density maps of the retina. Figure provided with permission from C Curcio. Adapted from Curcio, Sloan, Kalina, Hendrickson 1990, Human photoreceptor topography, J Comp Neurol 292; 497-523. Photoreceptor topography in the human retina. Colour scale: 0-200,000 cells/ mm2 in increments of 12,500 cells/ mm^2. Cones are presented on a log scale and rods on a linear scale. The black dot is the optic nerve head (blind spot).

Photoreceptors consist of two parts: inner and outer segments connected by the cilium. The inner segment contains the nucleus and cell machinery. At the end of the inner segment is a synaptic terminal to connect to the bipolar cells. The cell bodies form the outer nuclear layer. At the other side, photoreceptors connect with retinal pigment epithelium (RPE), which have a supportive role, particularly for rods.

Photoreceptors contain opsins, which are the light sensitive chemicals and differ in rods and each of the three cone types. These are generated in the inner segment and passed through the cilium into the outer segments. The other critical component is retinal, which is created in the interphotoreceptor matrix, surrounding the photoreceptors, and transported in. The outer segments have stacks of membranes embedded with the opsin molecule. The stacks are created by outpouchings from the cell membrane. In rods, these detach from the membrane and become free floating discs. These are shed and restored on a daily basis. When a photon of light is absorbed, the 11-cis form of the opsin is converted to the all-trans form, setting off the

phototransduction cascade, a complex series of chemical processes that convert the light to an electrical signal. Rods are thinner than cones but both their shape and size vary with retinal location. The seminal work conducted by Christine Curcio shows the pattern of photoreceptor density across the retina for both rods and cones (Curcio et al. 1990, 1993).

1.2.1.2 Retinal circuits

Measurements of visual function will be the summation of different cell contributions to the retinal circuitry, and not just rods and cones (Curcio et al. 1993). Photoreceptors directly connect to bipolar and horizontal cells. These are then connected to ganglion cells, with amacrine and horizontal cells modulating the signal (Figure 1.1).

There are multiple types of bipolar cells, allowing a variety of combinations of connections to the rods and cones separately or by mixing the signals, as well as differential handling of the photoreceptor signal in parallel (Field and Chichilnisky 2007). The cells are each either ON- or OFF- bipolar cells, thereby introducing the presence of receptive fields. Midget bipolar cells at the fovea allow connections with single cone cells, allowing the discrimination of fine detail. Conversely the ON-bipolar pathway is essential for night vision by maintaining a positive potential in the presence of light (Kolb, Ralph, and Eduardo 1995).

Horizontal cells are involved in feedback signals to adjust gain of response by having both post and pre-synaptic connections and inverting synapses, particularly with cones (S. Wu 1991). Two morphologies of horizontal cells have been noted which connect with either rods or cones. However, response kinetics of the signals also allow separation of the rod and cone signals. By creating lateral connections, spatial opponency from cones is created in the bipolar cells (Kolb, Ralph, and Eduardo 1995; Field and Chichilnisky 2007). The response characteristics change in different light levels (S. Wu 1991).

Amacrine cells release dopamine, a neuromodulator which is taken up by RPE, photoreceptors, bipolar, horizontal, gabaergic amacrine cells and ganglion cells. This is thought to balance the rod and cone inputs, altering sensitivity and maintaining a retinal circadian rhythm (Witkovsky 2004). The complete role of amacrine cells is not yet well understood, however they have the largest variety of subtypes and form the largest numbers of synapses in the retina. The use of both horizontal and vertical connections allows not only lateral connections for receptive field function, but may also allow the cells to contribute to the temporal kinetics of the responses in the retina. By synapsing with other amacrine, bipolar and ganglion cells, and connecting across different levels in the retina, amacrine cells contribute to the organisation of specialised circuits (Field and Chichilnisky 2007).

Retinal ganglion cell axons exit the eye via the optic nerve head and terminate primarily in the lateral geniculate nucleus (LGN) (Kolb, Ralph, and Eduardo 1995). Ganglion cells represent the interface between the retina and the central nervous system. The chemical messages from the other neural cell types are integrated by the ganglion cells and output as a nerve spike, the language of the brain. By combining the information from the other neural cell types, ganglion cells represent different aspects of the visual scene which are then processed further in the brain. The receptive field size of the retinal ganglion cells changes with eccentricity across the retina, with regular sampling across visual space (Field and Chichilnisky 2007).

1.2.2 Structural analysis of the retina

1.2.2.1 Fundus autofluorescence

Fundus autofluorescence (AF) is produced by retinoid byproducts of the visual cycle that accumulate in the RPE (Schmitz-valckenberg et al. 2008). Although the majority of fundus blue AF originates from the RPE (Ruickmann, Fitzke, and Bird 1995), photoreceptors have been shown to contribute to the AF signal (Flynn et al. 2014; Ach et al. 2014). Autofluorescence

imaging assists in the diagnosis of a wide range of retinal and RPE disorders, including age-related macular degeneration (AMD) and Stargardt disease, and can be a valuable independent marker of anatomic disease progression (Fleckenstein et al. 2014; Burke et al. 2014; Delori, Goger, and Dorey 2001). Reduced AF signal is commonly associated with retinal damage or cell death, as demonstrated by electrophysiology and perimetry studies (Lois et al. 2004); for example, a decrease in signal corresponds to visual field loss in patients with retinitis pigmentosa and cone–rod dystrophies (Lois et al. 2004; Ogura et al. 2014). An increase in signal tends not to accompany visual field loss (Ogura et al. 2014) but may be associated with a reduction in central sensitivity (Oishi et al. 2013). Increased autofluorescence is believed to indicate regions of defects in photoreceptor outer segment disc shedding and phagocytosis, while decreased autofluorescence may signify disordered RPE with deposition of abnormal material or atrophy of the underlying RPE and photoreceptors (Fleckenstein, Issa, and Holz 2014).

1.2.2.2 Ocular coherence tomography (OCT)

Ocular coherence tomography (OCT) allows us to delve deeper by visualising individual layers in the retina (Figure 1.3). Infrared interferometry is used to obtain high resolution cross-sectional images. The anatomy is then derived from the reflectivity bands. The automatic segmentation software which separates the layers has been shown to have poor performance in diseased eyes (Costa et al. 2006). For this reason, much time has been spent on producing an optimised pathway for this process and therefore accurate layer analysis.

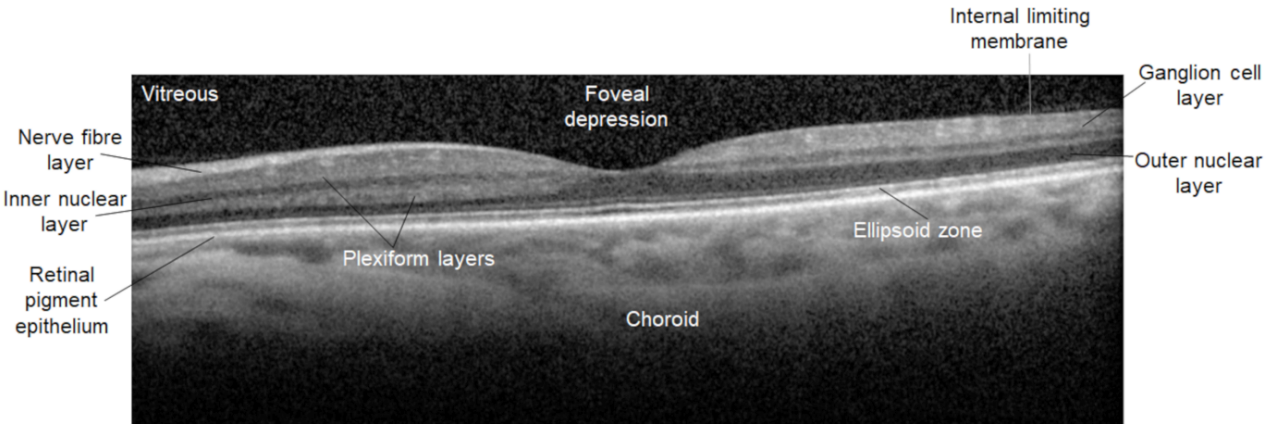


Figure 1-3: Layers of the retina visible with ocular coherence tomography imaging.

1.2.3 Visual functional measures

The measurement of visual function is an essential part of ophthalmic examinations. It provides an insight into how an individual perceives the world around them. Multiple tests have been designed to elucidate different aspects of vision, under different conditions. The visual system performs differently under photopic, mesopic, and scotopic conditions as the interaction between rods and cones alters (Hwang et al. 2013), so it is important to consider these differences when interpreting any tests. A sample of tests probing aspects of visual function are reported in more detail in chapters 2 and 3. An assessment used frequently throughout all projects is microperimetry.

1.2.3.1 Microperimetry

Microperimetry is fundus-controlled perimetry, allowing the measurement of retinal sensitivity and fixation stability. The machine utilised for this work is the MAIA (Centervue, Padova, Italy). It has a scanning laser ophthalmoscope camera to monitor fixation and provide an image of the fundus, refreshing at a rate of 25Hz. This property makes it possible to carry out precise structure function correlations, particularly in disease (Montesano et al. 2020). Background illumination

is set to 1.27cd/m^2 with a Goldmann size III (0.43^o) stimulus. The choice of the MAIA is based on the wide dynamic range of 36dB, so no ceiling effect is present (Pfau, Lindner, Fleckenstein, et al. 2017). The Maxwellian setup allows microperimetry to be conducted with or without dilation making it a versatile tool for studies (Han et al. 2017). Microperimetry is also a recognised outcome measure for clinical trial approval by the Food and Drug Administration (FDA) (Csaky et al. 2017).

The dB scale employed is similar to that utilised in other forms of perimetry. The maximum stimulus intensity (0dB) in the MAIA is 318 cd/m^2. According to Weber's law, the just-noticeable difference (JND), the smallest change in stimulus that can be perceived, is proportional to the initial stimulus intensity. Fechner's law states that the subjective sensation is proportional to the logarithm of the stimulus intensity, assuming all JND steps are perceptually equal to each other. In visual field testing, the logarithmic scale of the decibel represents the luminance difference between background and stimulus (Schwartz 2010). Threshold can then be probed at each point using a staircase algorithm. In the case of the MAIA this follows a 4-2 pattern. Mesopic microperimetry is considered a reflection of central cone function (Han et al. 2018; Crossland et al. 2012) and has been used in the investigation of a number of diseases (Jolly et al. 2017; Yusuf et al. 2018; Ratnarajan et al. 2018; Z. Wu, Ayton, et al. 2015; Sassmannshausen et al. 2018). Good practice guidance for the conduct of microperimetry has previously been published and formed the basis of test protocols used in the studies presented within this thesis (Talib, Jolly, and Boon 2018). Some key principles were taken into account when evaluating the reliability of the microperimetry tests conducted.

1) I included learning trials (Z. Wu et al. 2013b; Jolly et al. 2017).

2) Adaptation time prior to testing was only incorporated when necessary for comfort or accurate sensitivity measurement (Han et al. 2018).

3) Adequate time and care was spent on both instruction (Glen, Baker, and Crabb 2014) and set up, ensuring not only patient comfort but also accurate focusing.

4) If the focus is not set correctly, this can impact the final threshold measured due to a change in the plane of measurement (Figure 1.4). Focus of the image was therefore inspected carefully.

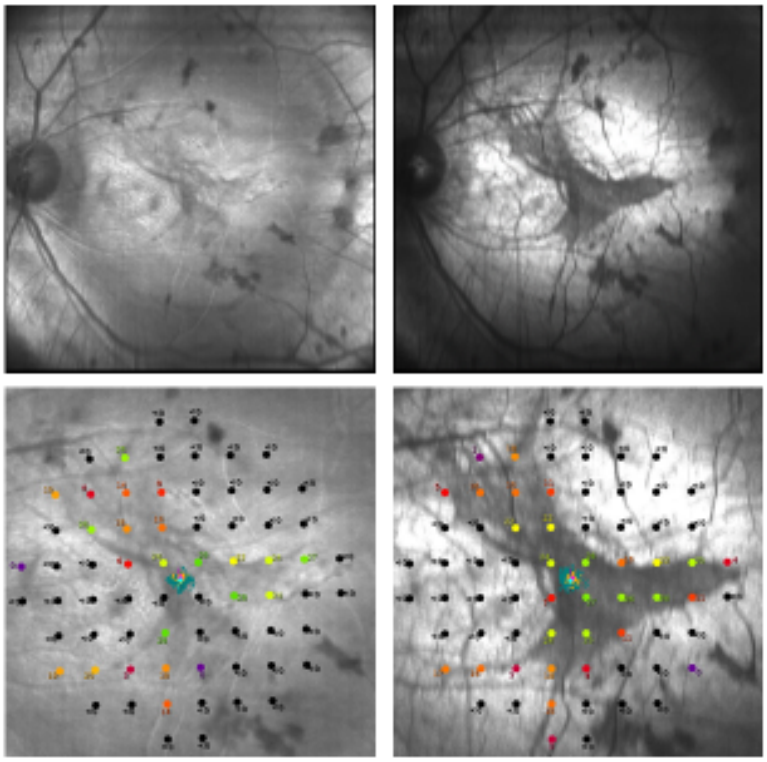


Figure 1-4: Impact of a change in focusing on threshold measurements with microperimetry. The top image shows the focussing of the image at the start. The bottom images shows the corresponding test result. Black points were not seen, red and orange indicate low threshold and green shows normal threshold. The number of black points is higher and the number of green points is lower on the poorly focussed (retinal island not clearly visible) image on the left.

1.2.3.2 Gaps in knowledge

There are a number of other assessments used to probe visual function such as visual acuity and colour vision assessment. These are detailed further in subsequent chapters. Traditional clinical measures are not always suitable for the assessment of patients with inherited retinal degenerations for several reasons. Firstly, many were not designed for clinical monitoring of retinal diseases but rather as general screening tools. Secondly visual field loss can impact on

the ability to undertake the tests and the accuracy with which the tests can be completed. Thirdly it is not always clear what is precisely being measured. The following chapters aim to begin the process of tackling these gaps.

1.3 The Visual Brain

1.3.1 The visual pathway

Information from the retina is projected via the nerve fibre layer along the optic nerves to the optic chiasm. At the chiasm, the nasal fibres crossover but the temporal fibres remain ipsilateral. This reconfiguration of the visual information ensures each optic tract carries information from both eyes, representing the full contralateral hemi-field of vision. The optic tracts terminate in the LGN before projecting via the optic radiations to the primary visual cortex (Figure 1.5 A). The optic radiations are around 98 mm in length. Visual field representation is preserved in the distribution of the optic radiation fibres (Peltier et al. 2006). The primary visual cortex is situated alongside the calcarine sulcus in the occipital cortex in both hemispheres (Figure 1.5 B).

1.3.2 Preservation of the visual field along the visual pathway

The visual field is preserved along the visual pathway from the eye to the brain. This property is manipulated in the clinical diagnosis of various disorders along the visual pathway through the use of visual field testing. Preservation of spatial information is critical as it cannot be reconstructed through other means. For this reason, visual field maps are represented at several levels in the cortical circuitry (Wandell, Dumoulin, and Brewer 2007).

The ganglion cell axons are carefully arranged according to visual field representation along the optic nerves and this is preserved along the tracts and LGN (Aebersold et al. 1981; Kupfer, Chumbley, and Downer 1967) with differential paths for crossed and uncrossed fibres (Hoyt

1962). The macular fibres spread out as they pass through the white matter tracts taking up a large area of the tracts and the bulk of the chiasm (Hoyt 1962). The fibres representing the central visual field are embedded centrally along the optic radiations as can be seen by diffusion MRI imaging (Yoshimine et al. 2018).

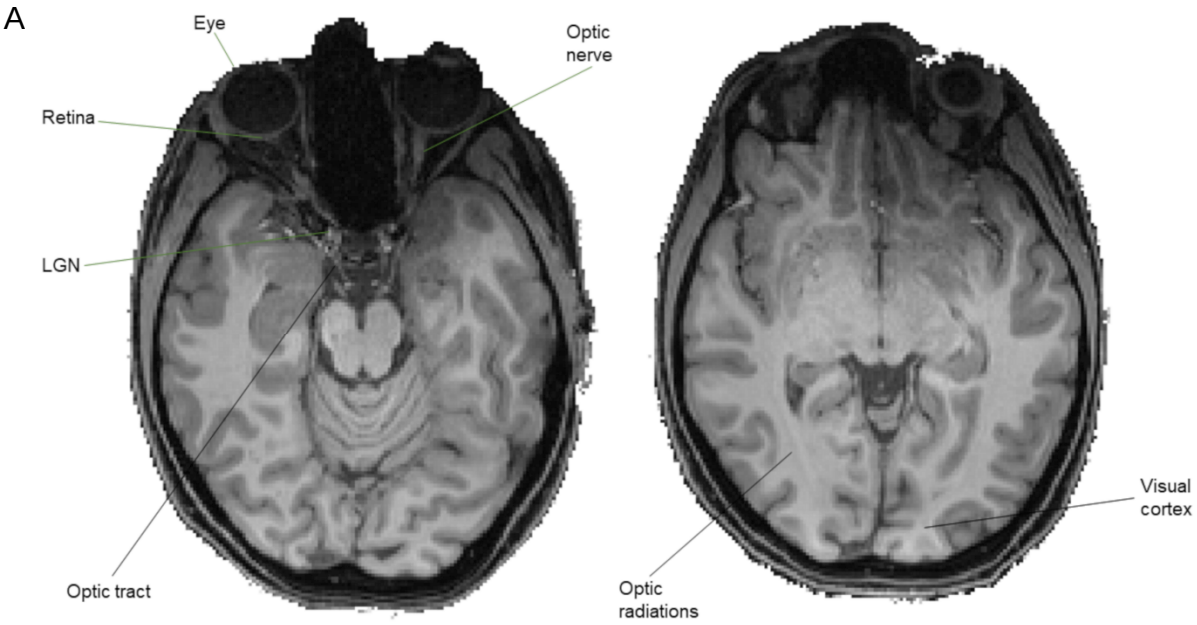


Figure 1-5: T1-stuctural weighted scan of the brain. (A) Visual white matter tracts between the eye and the primary visual cortex on axial view. (B) The arrows show the calcarine sulcus in a sagittal view of the brain. The sulcus represents the gap between the superior and inferior calcarine gyri of the primary visual cortex.

The earliest evidence for visual field representation in the visual cortex came from reports of injured soldiers presenting with localised wounds and associated visual defects in the First World War. This work showed that the most central areas of visual field are represented in the posterior part of the visual cortex. The upper visual field is represented in the ventral portion of the cortex (lower arrow Figure 1.5 B) and the inferior visual field is in the dorsal part of the calcarine sulcus (upper arrow Figure 1.5 B). The dorsal, ventral pattern is also noted in the optic radiations (Holmes 1918).

In addition the visual field preservation has been noted in the visual cortex in both the primary visual cortex and higher areas (Wandell, Dumoulin, and Brewer 2007; Wandell and Winawer 2011; Kolster et al. 2009). Although the visual field representation is preserved, the brain does change the sensitivity to different areas of the visual field by altering the weighting of the visual field maps, making it an important factor when considering diseases that cause visual field loss (O'Connell et al. 2016). Cortical magnification of the central area results in a greater cortical area being devoted to processing information from the macular area compared to the periphery (Holmes 1918; Horton and Hoyt 1991; Yoshimine et al. 2018). However the level of cortical magnification varies in different areas (Gattass et al. 2005) and between individuals (Horton and Hoyt 1991), so defining it mathematically is very challenging. An understanding of this organisation is important when considering diseases that cause visual field loss (O'Connell et al. 2016).

1.3.3 Brain adaptability

The brain is more adaptable in adulthood than originally thought. Amblyopia is the presence of reduced visual acuity in one eye as a result of unequal visual input from the eyes to the developing brain, which is not treatable by refractive correction. It was previously thought that amblyopia could only be treated within the developmental period. There is recent evidence that

amblyopia treatment can be successful long after the traditionally defined developmental period (Wong 2012; Li et al. 2011). Additionally there have been several case studies and anecdotal reports of patients recovering from amblyopia following the loss of vision in the non-amblyopic eye (Rabin 1984; Kaarniranta and Kontkanen 2003). Adults are capable of learning new skills, with the pathways in the brain developing to aid this process (Sampaio-Baptista et al. 2014, 2015). From my own personal experience of working in low vision clinics and with low vision patients, I have observed large differences in patients' ability to cope with their visual loss. Some of this may be personality based but there does seem to be a deeper mechanism at play. This thought was brought into deep focus for me and sparked my interest in this area after seeing the two patients presented in Figure 1.6 and observing their contrasting behaviour in the same year. For example, the patient with retinitis pigmentosa (RP) in Figure 1.6 A was able to walk around confidently without bumping into objects despite very small visual fields. The patient in Figure 1.6 B however, was very reliant on his white cane and frequently bumped into objects despite larger visual fields. Personality may explain the difference in confidence but cannot entirely explain the difference in the objective measure of bumping into objects. This observation has recently been supported by simulation of visual defects, which showed decrease in visual field did not account for decrease in function reported by the patient (Chow-Wing-Bom, Dekker, and Jones 2020). Alterations in the brain pathways as a result of vision loss are likely to be different across individuals and may contribute to the altered adaptation in response to visual deficits.

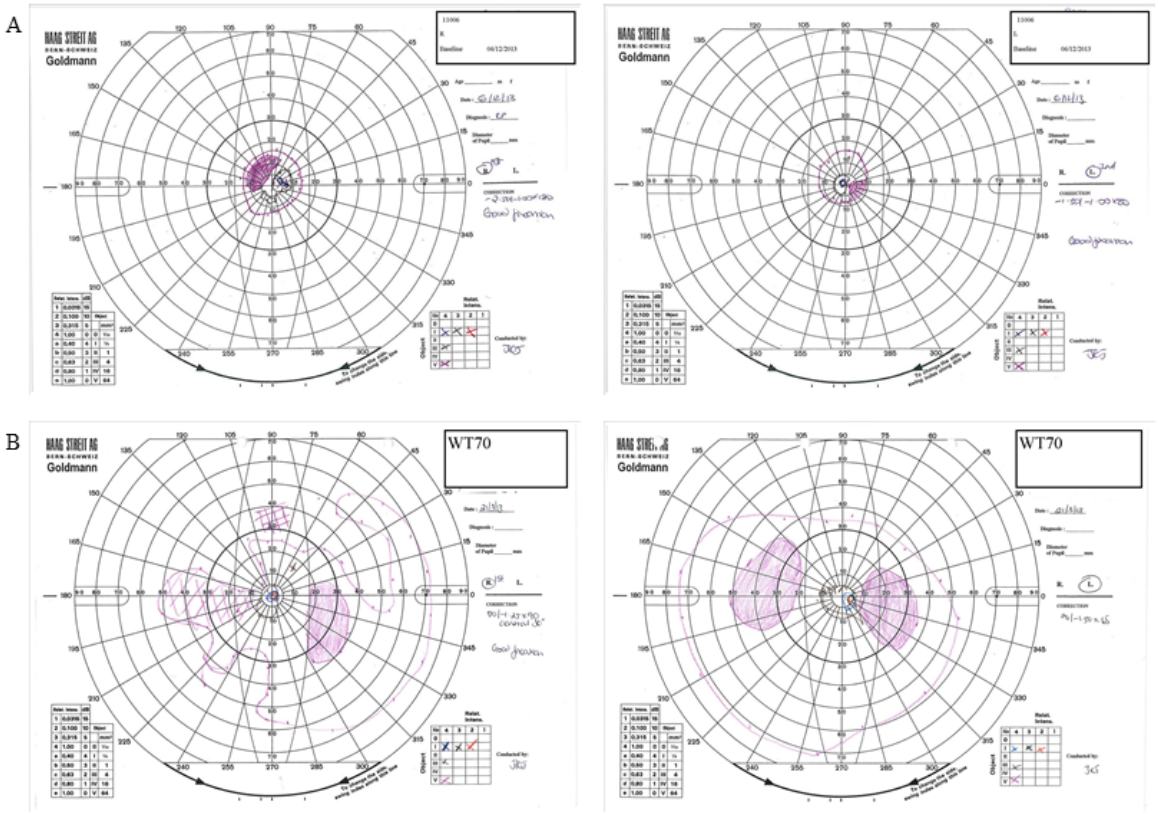


Figure 1-6: (A) Patient presenting with small central islands of vision only and functioning very well. (B) Patient presenting with preserved central vision and additional temporal preservation of vision but a great deal of difficulty with mobility.

There is a growing body of evidence that retinal disease has downstream effects in the visual brain (H. Brown et al. 2016). The presence of secondary degeneration in the visual brain following retinal degeneration could potentially impose limits on the improvement in vision following treatment of the retina. Indeed, there is a growing body of evidence that retinal disease has downstream effects in the visual brain (H. Brown et al. 2016; Rokem et al. 2017). Magnetic resonance imaging (MRI) white matter structural changes have been reported in a range of visual disorders. In glaucoma MRI has indicated smaller optic nerve diameter, smaller LGN, and white matter changes along the whole visual pathway. Juvenile macular degeneration and age-related macular degeneration have shown both grey and white matter changes in the visual areas including the occipital lobe and the optic radiations. Juvenile macular degeneration has also been

associated with changes in the LGN. Both conditions have demonstrated functional changes in the macula region (H. Brown et al. 2016). Retinitis pigmentosa has been associated with cortical thickness differences and functional changes in the part of the early visual cortex associated with peripheral vision (Sabbah et al. 2017; Sanda et al. 2018). The changes reported in these studies have been attributed to a variety of processes including cortical plasticity, synaptic reorganisation, and changes in both directions from both feedback and feedforward mechanisms. However, these studies are based on small cohorts of patients and the results have not been systematically related to the degree of eye disease present or type of visual field loss caused by the ophthalmic disease. In addition, few studies have gone beyond the primary visual cortex, which is a key component of understanding the complete visual system. The work presented in this thesis aims to begin to fill this gap.

1.3.4 Assessment of the visual brain

There are multiple types of MRI available to probe both structural and functional aspects of the brain, as well as neurotransmitter levels. This work will focus on the structural measurement of the visual brain. Briefly, T1-weighted structural MRI provides a high-resolution image of the brain to calculate changes in grey matter volume and cortical thickness over time. Diffusion-weighted imaging provides a measure of white matter structure in the brain. This imaging measures the movement of water molecules in the brain, and can be used to measure how they move along the axons of neurons. The main metrics are fractional anisotropy and mean diffusivity, which indicate the structural integrity of white matter pathways. If the pathways are damaged or degenerate, water molecule movement becomes less ordered, and this can be quantified with diffusion imaging. Specifically of interest are the optic radiations taking information to the primary visual cortex (V1), but the pathways within the cortex are also of

interest to determine whether the effects of visual field loss extend beyond the early areas (H. Brown et al. 2016).

1.4 Rod-cone dystrophies

1.4.1 General introduction

Rod-cone dystrophies describe genetic retinal degeneration characterised by a primary loss of rods with secondary cone involvement as defined by electrophysiological findings. Retinitis pigmentosa (RP) is the most well-known and describes a group of genetically heterogeneous retinal dystrophies. They present with rod photoreceptor loss and progress to impact cone function but the rate of progression is very variable depending on the precise genetic defect and the individual. Exposure to risk factors such as light exposure will also impact progression rate. Rod-cone dystrophies are currently being investigated in a number of gene therapy clinical trials and therefore present the more immediate need for investigation.

RP is estimated to affect up to one in 3000 people but can be caused by over 80 different genes (Dias et al. 2018; Verbakel et al. 2018). These cause relatively consistent clinical presentations, known as phenotypes, depending on the mechanism of action of the gene as well its interaction with other factors. RP shows different modes of inheritance. The most common include autosomal recessive, dominant, X-linked or mitochondrial. Most people have 22 sets of autosomal chromosomes, with a copy from each parent, and one pair of sex chromosomes. The sex chromosomes are XX for females and XY for males. The Y chromosome is smaller than the X chromosome and contains less genetic material. Autosomal dominant inheritance in its simplest form arises from defects on a gene on one of the autosomal chromosomes. Autosomal recessive inheritance occurs when there is a defect on both copies of a gene on one of the autosomal chromosomes. X-linked inheritance occurs on the X chromosome so affects males more than females. Female carriers of X-linked diseases can also present with fundal

abnormalities, but these do not always cause vision loss. Some female carriers can also present with male pattern disease (Edwards et al. 2015; Nanda et al. 2018). Each cell in the female body randomly switches off one X chromosome, known as X inactivation. If the number of cells switching off the healthy X chromosome is high, this is considered skewed X inactivation. The balance of normal *versus* abnormal X chromosomes switched off will determine how affected a female will be. Syndromic RP is associated with problems in other parts of the body. The most common genes causing RP are rhodopsin, RPGR and USH2A (Berson 2007).

Patients with RP present with nyctalopia (poor night vision), reduced peripheral vision as a result of photoreceptor loss, photophobia, and glare. Night vision abnormalities can remain unnoticed in patients living in well-lit urban environments so careful questioning during history is often required. Visible fundus abnormalities are typically 'bone spicule' pattern pigment changes, attenuation of the retinal vessels, and a waxy pale optic nerve head. RP typically presents from the late teens onwards and is progressive. However, age of onset can be very variable and can range from childhood to the sixth decade of life (Verbakel et al. 2018). The specific presentation is related to the underlying genetic defect as the genes implicated in rod-cone dystrophies are expressed in a variety of tissues as recorded in the Online Mendelian Inheritance in Man database (Figure 1.7).

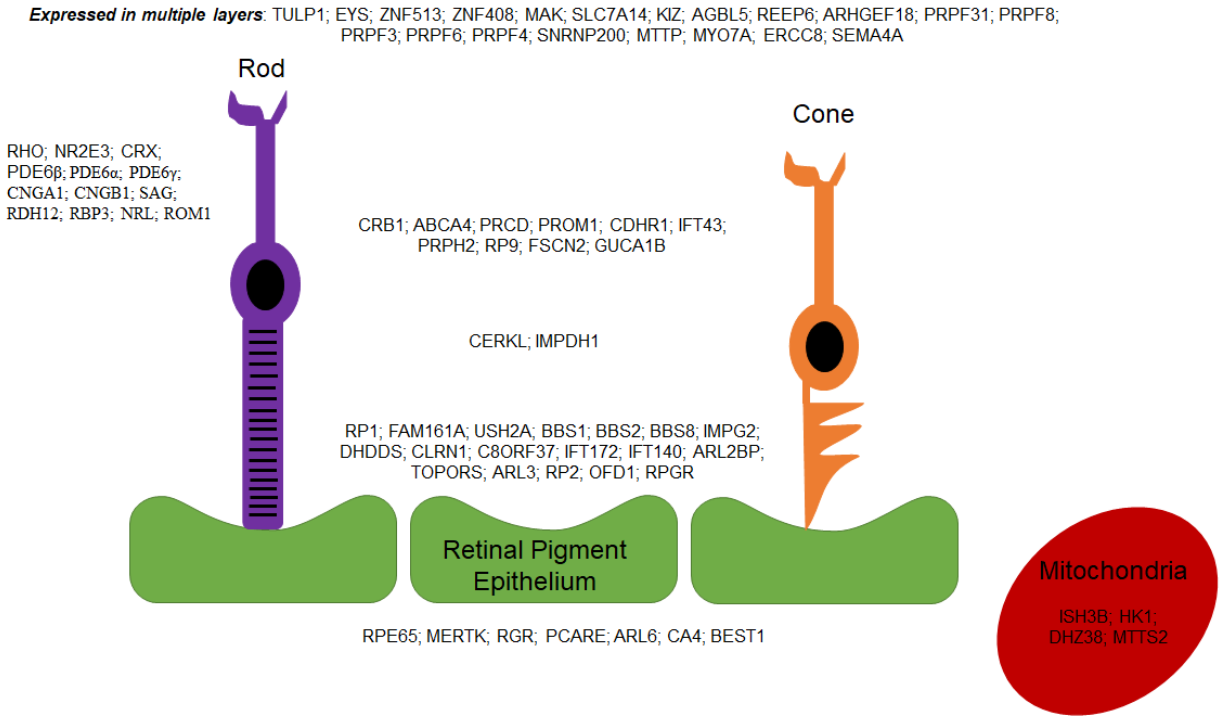


Figure 1-7: Biological basis of action of genetic mutations. Genes listed on the left of the rod cell are expressed in rods only. Genes listed between the rods and cones are expressed in both and the level of the listing relates to localisation within the photoreceptor cells. The genes listed under the RPE are expressed in this tissue. These diagrams were created from information in the Online Mendelian Inheritance in Man database (OMIM #268000).

There is a high incidence of low mood, frustration and loneliness in patients with RP, which can often be worse in younger patients and acknowledgement of this with appropriate support is important (Latham et al. 2015). When evaluating the cost effectiveness of retinal gene therapies, economic modelling does not include assessment of the negative emotional aspects of disease and positive emotional impact of therapy. However, gene therapy still presents a valuable treatment option, particularly as there are currently no established treatments (Halioua-Haubold et al. 2019). In order to achieve regulatory approval, it is essential to understand the tests being used and then use the correct tests to reflect the genetic defect. By using the most appropriate tests as outcome measures, efficacy can be demonstrated. Currently established clinical tests are not always the most appropriate to achieve this. For this reason, for some of the subsequent studies presented, a particular disease will demonstrate the utility of the measure being evaluated. A brief introduction to the models used is provided.

1.4.2 Choroideremia

Choroideremia is a progressive X-linked inherited retinal degeneration affecting the RPE, choroid and photoreceptors. It is caused by a mutation in the *CHM* gene, which codes for the Rab escort protein-1 (REP1), a key mediator of membrane trafficking in the photoreceptors and RPE (Seabra, Brown, and Goldstein 1993; Tolmachova et al. 2010). Early symptoms include nyctalopia and reduced peripheral vision, which typically proceeds to loss of visual acuity (VA) and legal blindness as early as the third or fourth decade (MacDonald, Russell, and Chan 2009). The natural history of choroideremia has been well characterised in terms of both structure and function, making it a good model for the study of new outcome measures (Jolly et al. 2017; Xue et al. 2016; Jolly et al. 2016). Additionally, advanced choroideremia is characterised by well-defined retinal islands allowing precise measurement of the remaining retinal structures (Figure 1.8). Although choroideremia is inherited on the X-chromosome and affects mostly males, female carriers can be affected to differing degrees due to variable X-inactivation (Edwards et al. 2015). The variability in the female phenotype can provide additional information about the degree of retinal preservation required for aspects of vision. Gene therapy for choroideremia has completed phase 1 trials (NCT01461213) and is currently in phase 2 (NCT02553135, NCT02671539, NCT02407678) and 3 trials (NCT03507686, NCT03496012) around the world (Xue et al. 2018; Dimopoulos, Hoang, et al. 2018; Lam et al. 2019; Fischer, Ochakovski, et al. 2020).

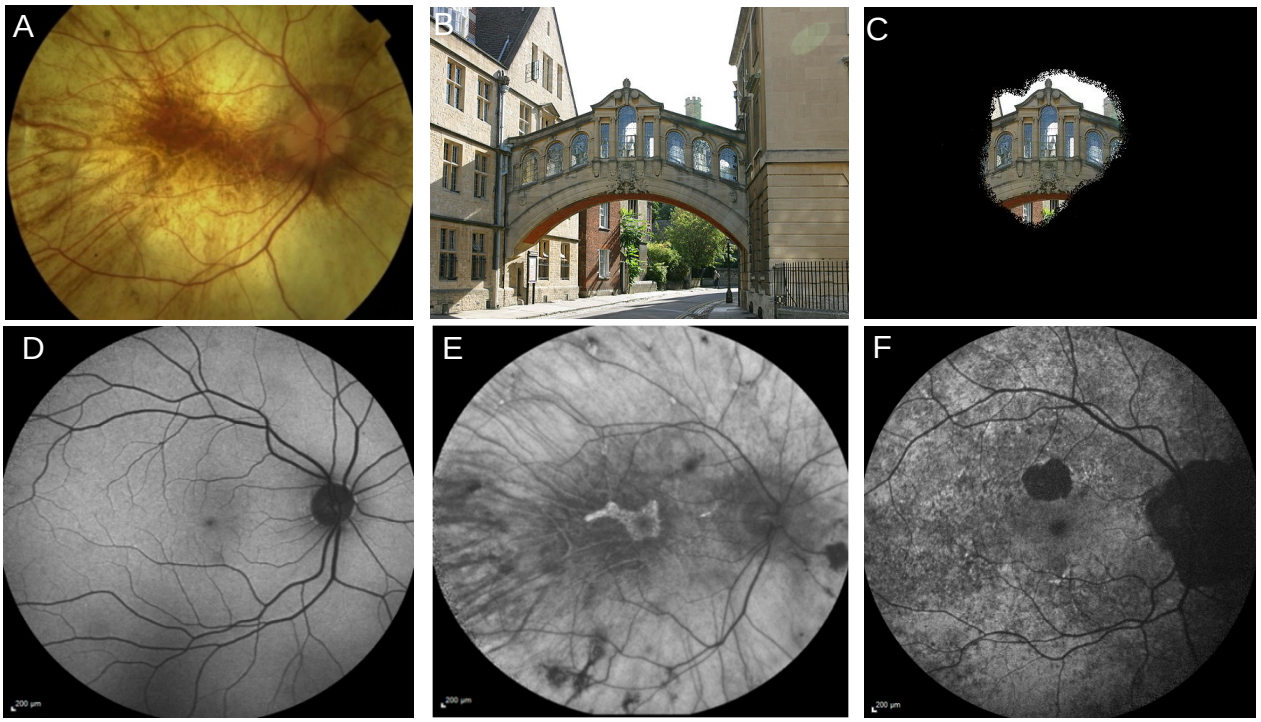


Figure 1-8: (A) Fundus photograph of typical case of choroideremia. (B) View of the Oxford Bridge of Sighs (C) Simulated reduced visual field of eye A on scene B. (D) Autofluorescence image of a normal eye. (E) Autofluorescence image of eye A showing the well preserved central island. (F) Autofluorescence image of a female carrier.

1.4.3 RPGR retinitis pigmentosa

RPGR associated RP is the commonest form of X-linked retinitis pigmentosa and also presents with specific characteristics in female carriers (Nanda et al. 2018). It is a progressive rod-cone dystrophy presenting in a similar fashion to choroideremia, with earlier presentation and faster progression (Figure 1.9) (Sandberg et al. 2007; Menghini et al. 2020). Mutations affecting the Retinitis Pigmentosa GTPase Regulator (RPGR) gene affects function of the protein in the photoreceptor cilia connecting the inner and outer segments. It has a role in regulating and moving membrane proteins between the inner and outer photoreceptor segments (Megaw, Soares, and Wright 2015). RPGR RP represents a model of photoreceptor disease and is used in studies where this is a useful property. *RPGR* gene replacement therapy is currently in phase 1 trials NCT03116113 (Cehajic-kapetanovic et al. 2020). The natural history of RPGR has been characterised (Talib et al. 2019; Buckley et al. 2020).

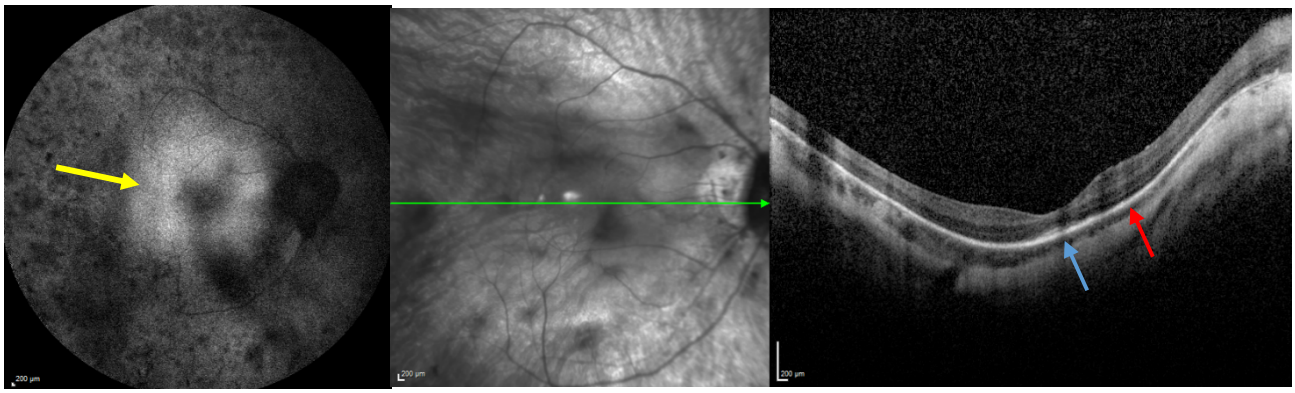


Figure 1-9: (A) Autofluorescence image typical of an eye with RPGR related X-linked retinitis pigmentosa showing a ring of hyperfluorescence with peripheral hypofluorescence (yellow arrow). (B) Infrared image of the same eye showing the location of the OCT slice (green line). (C) OCT image showing central preservation of the outer retina (blue arrow) with peripheral degeneration (red arrow). Scale bars, 200 µm in A, B and C.

1.5 Gene therapy outcome measures: Current practice

1.5.1 Introduction to gene therapy

The eye presents the perfect organ for gene therapy. It is an immune privileged site, which is protected by the blood retinal barrier. The target cells, such as photoreceptors and retinal pigment epithelium are frequently non-dividing, meaning any intervention is likely to last for life. The different structures in the eye can be visualised due to the optical clarity inherent in the eyeball or can be imaged with well documented techniques (Fleckenstein, Issa, and Holz 2014; Zysk et al. 2007). The structures in the eye can be targeted by various surgical procedures. Finally, many disease processes have a degree of symmetry. This means that when treating one eye, the other eye can act as a control for comparison. For these reasons, ocular gene therapy is being trialled as an experimental treatment for an increasing number of conditions. There are established techniques to measure both structural and functional changes, with work ongoing in this field to evaluate the different diseases being treated. The success of gene therapy can be determined by the pattern of change seen in visual function measurement compared to the control or natural

history. Since visual function is the major marker for success of gene therapy, it is critical to establish guidelines for best practice. The first ocular gene therapy (for RPE65 mutations) was approved by NICE in November 2019 for clinical use in NHS patients. Any guidance developed can therefore be applied to clinical practice as well as research trials.

Gene therapy can follow several different strategies. Most commonly, it is the supplementation of a defective gene with a working copy in affected target cells, as has been used in treating achromatopsia and choroideremia. However, in some cases, such as with neovascular age-related macular degeneration, the gene expression may introduce a factor to help dampen the disease response. The mode of action is less important than the disease being investigated in determining the appropriate measures to use for trial monitoring. The Monaciano Symposium identified the measurement of treatment outcome as an area requiring priority review in order to aid the robustness of clinical interventional trials (Thompson et al. 2015). It calls for the investigation into appropriate outcome measures for each disease to measure structure and function without adding an unreasonable burden on the patient. They propose a standardisation of testing protocols and data analysis. The reproducibility and reliability of tests should also be pre-defined.

With the increase in the number of trials using ocular gene therapy, the importance of adequate outcome measures is gathering support. The success of gene therapy relies on three key aspects. Firstly, the viral vector is developed over several years and optimized in animal models before reaching human trials (Patrício et al. 2017; Koilkonda et al. 2014). Much work has been conducted on optimising the delivery of the therapeutic vector (Xue et al. 2017; Salvetti et al. 2017). Another component required for success of clinical trials is the adequate measurement of therapeutic impact. This requires a combination of the evaluation of ocular structure via imaging, and measurement of visual function. Standardised clinical visual function measures were largely developed for use in a clinical setting rather than for the assessment of novel interventions and may not always be adequate for measurement of a therapeutic effect. For example the 100-Hue test for colour vision has wide normative ranges, making interpretation of longitudinal data

difficult (Kinnear and Sahraie 2002). The relationship of the outcome measures to disease progression and therefore the therapeutic window should also be better understood to interpret clinical trial findings. In addition, disease features such as visual field loss may make the conduct of the test difficult.

A systematic review of gene therapy for retinal disease has been registered on the PROSPERO database (CRD42017056500) by London City University, but not yet completed. This specifies visual outcome as the outcome measure for assessing the success of trials, but the type of vision measure being looked at is not detailed, demonstrating the importance of providing further guidance on this topic. Additionally as bilateral gene therapy will become more common, there will no longer be a control eye to provide a comparison as is done in many phase 1 trials, making vision outcome measures even more critical (MacLaren 2016). Visual function is a combination of many aspects of vision, including detail, colour, contrast, speed of vision and night vision. The objective of this review is to review the outcome measures listed and published for registered gene therapy trials in order to establish current practice, and to consider the scope for development of relevant and specific outcome measures.

1.5.2 Scoping review methodology

All clinical interventional trials should be registered on a publicly available database. The databases on Clinicaltrials.gov (RRID:SCR_002309), EU clinical trials register (RRID:SCR_005956), and the NIH clinical trials register were searched for all registrations until the end of October 2018, using the following search terms: gene therapy; subretinal injection, intravitreal injection, STX eye trial, Nightstar, Applied genetic, MeiraGTx, Hemera, Oxford Biomedica, Sanofi, Spark, ProQR, GenSight, Genzyme.

Duplicate records were omitted from analysis. Natural history studies, or studies specifically for long-term follow up of patients in a previous trial were also excluded in order to focus on the

primary interventional trials. I then searched for any results from studies with a registered start date of greater than 12 months before October 2018. This was done via PubMed, study group websites and Scopus. Searches were conducted using the investigator details and registered study name. Publications for the same study were grouped together and analysed as an integrated dataset, with discrepancies between the primary outcome measure on the clinical trials record versus the final publications being noted.

1.5.3 Scoping review results

1.5.3.1 Listed outcome measures

I identified 50 unique clinical trials on the registers for 17 ophthalmic indications (Figure 1.10). Leber Congential Amaurosis (LCA), Leber Hereditary Optic Neuritis (LHON) and choroideremia are the only conditions that have so far reached phase 3 trials, with LCA now an approved treatment. Outcome measures were analysed according to clinical trial phase and were separated into four categories: safety, validated tests, novel test methods and non-specific (Supplementary Table 1).

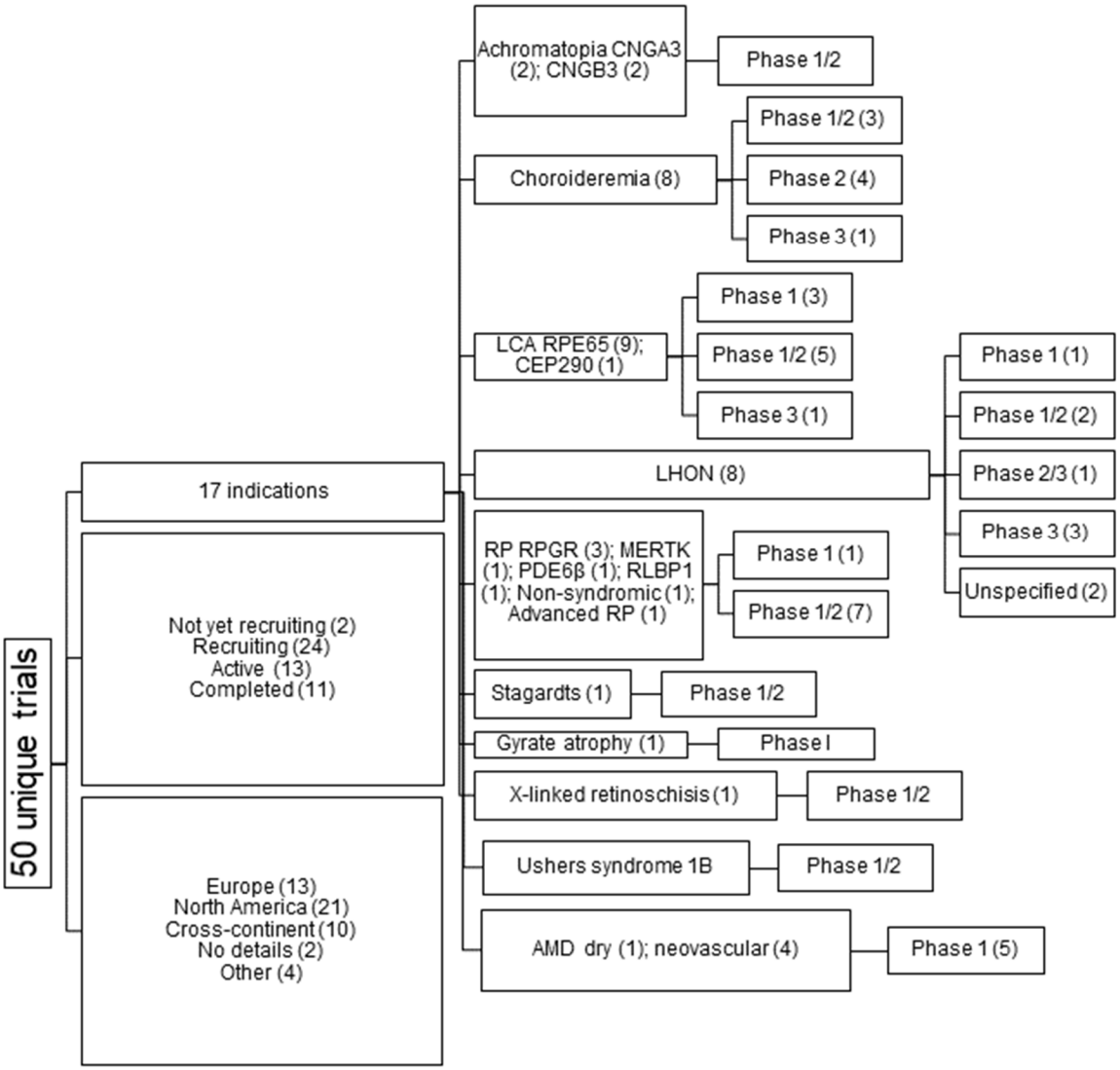


Figure 1-100: Summary of details found for gene therapy human clinical trials detailing location, indication and trial phase (as of October 2018).

Study ID (clinicaltrials.gov), disease and gene therapy delivery method	**Phase; Full/prelim**	**Pre-specified primary outcome**	**Reported primary outcome**	**Pre-specified secondary outcome**	**Reported secondary outcome**
NCT01024998 Neovascular AMD AAV intravitreal (Heier et al. 2017)	I ; Full	Adverse events, maximum tolerated dose.	Adverse events, change in VA and vector DNA concentration in biological samples.	Decreased retinal thickness.	Transgene expression in aqueous fluid and OCT thickness.
NCT01494805 Neovascular AMD AAV subretinal (Rakoczy et al. 2015; Constable et al. 2017)	I/II ; Both	Adverse events and laboratory measures.	Adverse events and laboratory measures.	VA, foveal thickness, and CNV lesion.	VA, retinal thickness, and standard injection retreatments.
NCT01301443 Neovascular AMD lentivirus subretinal (Campochiaro et al. 2017)	I ; Full	Adverse events.	Adverse events, change in VA, ocular inflammation, IOP, laboratory measures.	OCT intraretinal fluid.	Transgene expression, OCT macular thickening, lesion measures on fluorescein angiography, VA.
NCT01461213 Choroideremia AAV subretinal (MacLaren et al. 2014; Edwards et al. 2016a)	I/II ; Prelim	VA.	VA.	Microperimetry, OCT and AF.	Microperimetry threshold, OCT thickness, AF area.

NCT02553135 Choroideremia AAV subretinal	II ; Full	Adverse events.	VA, adverse events.	Macular autofluorescence, microperimetry.	Microperimetry, contrast sensitivity, color vision, autofluorescence area, OCT ellipsoid zone and choroidal thickness assessments, safety.
NCT02671539 Choroideremia AAV subretinal	II ; Full	VA.	VA.	Adverse events, autofluorescence, microperimetry, contrast sensitivity, colour vision.	Microperimetry, autofluorescence area, OCT ellipsoid zone and choroidal thickness, safety.
NCT02077361 Choroideremia AAV subretinal	I/II ; Full	Adverse events.	Safety including adverse events.	Microperimetry, Goldmann visual field, multifocal ERG, FST, OCT, photos and autofluorescence.	VA, autofluorescence area, OCT ellipsoid zone, microperimetry, quality of life questionnaire.
NCT01482195 MERTK AAV subretinal (Ghazi et al. 2016)	I ; Full	Adverse events and laboratory measures.	Safety measures.	VA and FST.	VA, FST, OCT thickness.
NCT01267422 LHON AAV intravitreal (Wan et al. 2016)	Not given ; Prelim	VA, laboratory measures.	VA, laboratory measures.	IOP, neutralising antibody assay, OCT RNFL thickness, computerised visual field mean deviation and visual field index, VEP, ERG, liver and kidney function.	Visual field index and mean deviation, VEP, OCT RNFL thickness, and blood tests.
NCT02161380	I ; Prelim	Toxicity	Loss of VA.	None	OCT RNFL thickness, pattern ERG, and adverse events.

LHON AAV intravitreal (Feuer et al. 2016)					
NCT01496040 LCA AAV subretinal (Le Meur et al. 2018)	I/II ; Full	Biodistribution in urine and nasal samples.	Adverse events and bio-distribution.	ERG, questionnaire, distance VA, near VA, colour vision, pupillometry, microperimetry and, dark adaptation.	Chorioretinal imaging, OCT thickness, undefined questionnaire, distance VA, nystagmus measures, visual field, microperimetry, fMRI, ERG, pupillometry and, mobility test.
NCT00749957 LCA AAV subretinal (Weleber et al. 2016)	I/II ; Full	Adverse events.	Adverse events.	Static perimetry and VA.	VA, static perimetry hill of vision, kinetic perimetry hill of vision, ERG, OCT, photography and quality of life questionnaire.
NCT00481546 LCA AAV subretinal (Hauswirth et al. 2008; Cideciyan et al. 2008, 2009; Jacobson et al. 2012; Cideciyan et al. 2015)	I ; Both	Toxicity, symptoms and, adverse events.	Laboratory measures, symptoms and, adverse events.	Visual function.	VA, FST, dark adaptation kinetics, chromatic stimuli sensitivity, kinetic perimetry, OCT thickness, fixation analysis, pupillary light reflex, mobility testing, eye movements and, fMRI.
NCT00516477 LCA AAV subretinal (Maguire et al. 2008, 2009; Ashtari et al. 2011; Testa et al. 2013)	I ; Both	Safety and tolerability.	Adverse events.	Change in visual function psychophysical and objective measures.	Pupillary light reflex, nystagmus testing, kinetic perimetry, microperimetry, OCT, AF, FST, ERG, mobility testing and fMRI.

NCT01208389 LCA 2nd eyes (Bennett et al. 2016)	I/II ; Prelim	Adverse events.	Adverse events.	VA, VF, pupillary light response, mobility testing, FST and, contrast sensitivity.	FST, kinetic perimetry, VA, pupillary light reflex, mobility and fMRI.
NCT00643747 LCA AAV subretinal (Bainbridge et al. 2008, 2015; Ripamonti et al. 2015)	I/II ; Both	Inflammation	Adverse events.	Visual function.	Laboratory measures, VA, kinetic perimetry, microperimetry, dark-adapted perimetry, mobility, contrast sensitivity, colour vision, spectral sensitivity, retinal imaging and, ERG.
NCT00999609 LCA AAV subretinal (Russell et al. 2017)	3 ; Full	Multi-luminance mobility testing bilateral.	Multi-luminance mobility testing bilateral.	FST, multi-luminance mobility testing monocular and, VA.	FST, multi-luminance mobility testing monocular, VA, kinetic perimetry, Humphrey static visual fields, contrast sensitivity and, pupil light reflex.
NCT02317887 XLRS AAV intravitreal	1 ; Full	Adverse events, retinal structure, ocular structure.	Adverse events, inflammation	Visual function, OCT, ERG, AAV antibodies.	VA, microperimetry, ERG, OCT macular thickness, AAV antibodies.

Table 1-1: Comparison of clinical trials record and published outcomes in ocular gene therapy trials. AF = fundus autofluorescence; AMD = age-related macular degeneration; ERG = electroretinogram; FST = full-field stimulus threshold; IOP = intraocular pressure; OCT = ocular coherence tomography; RNFL = retinal nerve fibre layer; VA = visual acuity; VEP = visual evoked potential.

Visual acuity (VA) was included in almost all studies as either a primary or a secondary measure. Various forms of perimetry also featured highly in the outcome measures list. Out of the 50 trials, 16 used broad descriptors which did not make clear what data were being collected or how it was going to be used. Other used descriptors such as visual function or specifying imaging techniques with no details of the aspect of the images to be examined. One did not specify any outcome measures.

1.5.3.2 Published trials

One trial marked as completed has not yet been published (NCT00001735). Eighteen trials have associated results in the peer-reviewed literature. Table 1.1 details the correlation between the trial register record and the outcomes reported in the peer reviewed papers. Where primary and secondary outcomes were explicitly stated in the paper, these were recorded if also reported in the results. Anything not reported in the results or supplemental sections was not counted. In reports where primary or secondary was not made clear, all measures reported were recorded and primary versus secondary was inferred from emphasis and context.

There was 100% compliance with reporting on the pre-specified primary outcome measures. Sixteen trials pre-specified one or more secondary outcome measures. These were met in full by 61% (11) trials. Five trials did not meet all of the outcome measures but did meet some of them. In addition, 83% (15/18) trials reported additional outcome measures, including a range of features, such as retinal imaging, aspects of visual function and functional MRI (fMRI) imaging. Figure 1.11 A demonstrates the number of additional secondary outcomes carried out in the published literature but not originally included in the register as a histogram. Figure 1.11 B shows the array of the visual function tests reported. VA was the most commonly used assessment of visual function. Perimetry was also commonly used but could take several different forms, each of which are targeting different areas of the visual field. Mobility testing is not standardized and

appears in almost half the published trials. Electroretinograms are measured in a similar number of trials but are standardized due to ISCEV standards. The tests listed in low number of trials, are generally non-standardised exploratory techniques such as fixation analysis and dark-adapted perimetry.

1.5.4 Justification of thesis

Adverse events are a key part of phase 1 trials as would be expected. VA is also a frequent factor in determining treatment effects and is reported in 94% of trials. It is a widely accepted measure, both clinically and by medical regulatory authorities. VA has been reported to have higher variability in low vision patients so strategies to optimise VA measurements in patients with disease need to be better established (Kiser et al. 2005).

Even within trials for the same disease, visual outcome measures differ across sites, making direct comparison difficult. This is especially problematic due to the small numbers of patients involved in these highly specialised trials. The ideal way forward would be to conduct formal natural history studies and additional validation studies of novel outcome measures where existing measures are not sufficient or appropriate. The length of natural history studies should be determined by the nature of the disease being investigated. Fast progressing conditions will require a shorter follow up period of one or two years. Slower progressive conditions should ideally have a longer follow up period. An initial audit of imaging and functional data collected in the clinical environment can provide guidance on the speed of progression as a starting point such as conducted by Jolly et al 2016 and 2017 in choroideremia (Jolly et al. 2016, 2017). Combining structural and functional data will be helpful in better understanding the disease process as well as treatment impact in both natural history trials as well as in final outcome measures chosen.

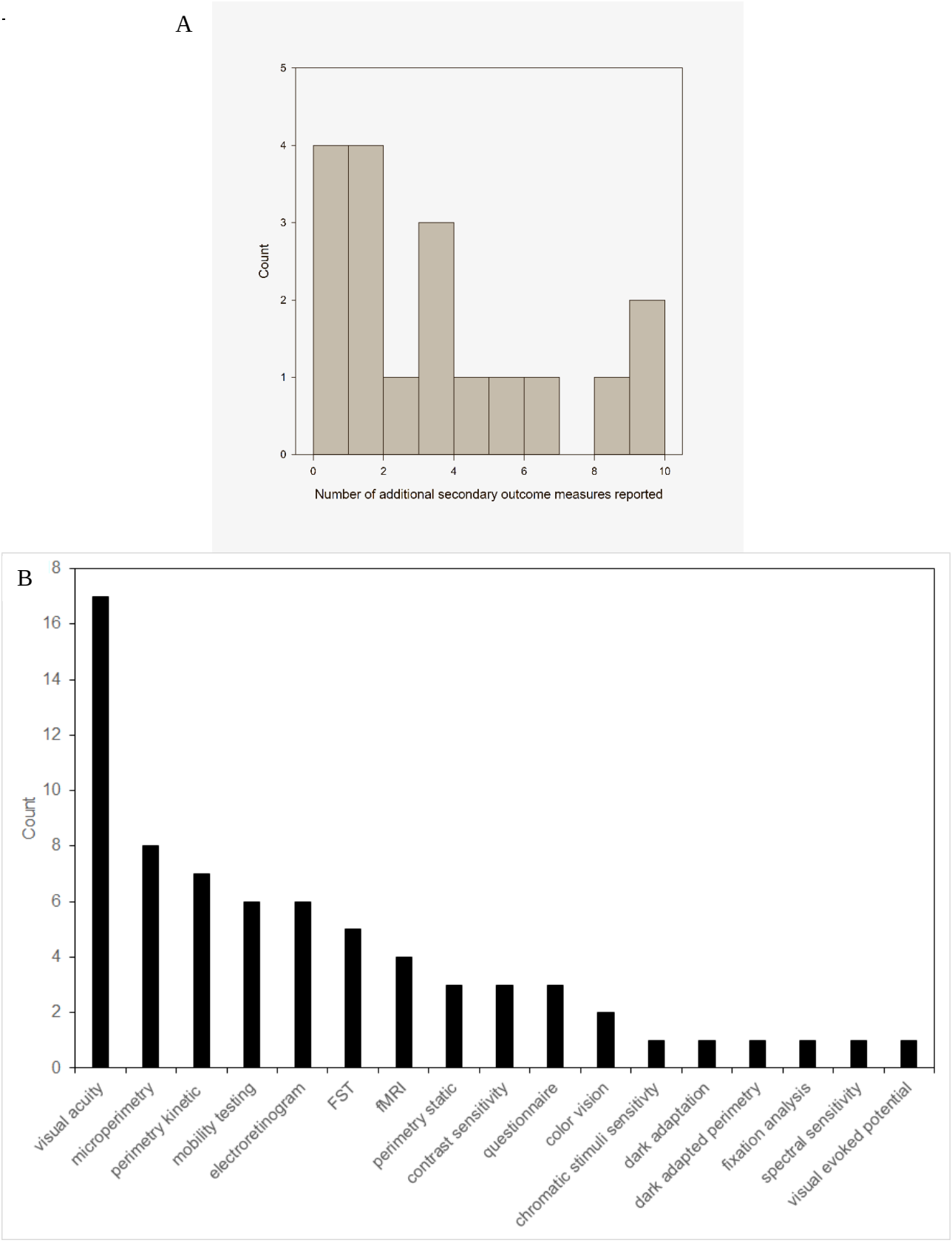


Figure 1-11: (A) Histogram to show the number of additional outcome measures reported by 79% of trials with peer-reviewed publications. (B) Range of visual function tests currently used as secondary outcome measures in reported ocular gene therapy trials from Table 1.1.

Patient quality of life is highly dependent on their perception of the world. Subjective assessment using validated instruments can provide insights into visual perception from the patients' perspective and can be considered as part of the battery of outcome measures (de Boer et al. 2004). Defining success based on clinical (such as repeatability) and patient (such as improvement required for greater quality of life) factors will make a stronger case for the success of therapy, particularly for phase 2 and 3 trials (Mcglothlin and Lewis 2014). Although questionnaire results may be considered biased due to the patients' motivation, the subjective feedback can provide very powerful evidence for the real-world impact of any therapy in a way that clinical measures are unable to achieve. Many funding bodies in the United Kingdom encourage the use of patient and participant involvement in research as the insights they can provide can have an influence on guiding researchers to improved clinical trial design, as well as impact when reporting results (Boote, Baird, and Sutton 2011).

Despite visual function being highlighted as an important factor in the success of gene therapy trials, little progress has been made on developing a coherent approach worldwide (Thompson et al. 2015). Other medical fields have highlighted similar issues in terms of the need to develop appropriate outcome measures for gene therapy (Lähteenvuo and Ylä-Herttuala 2017). As more diseases are targeted by a gene therapy approach, and trials progress to phase 2 and 3, this will become ever more important. Cataract formation is a side effect of the invasive vector delivery techniques (Gupta et al. 2007; Hasler et al. 2015). Moreover, patients are followed up over long periods of time, increasing the chance of age-related cataract formation. Thus, it is necessary to account for the effect of cataract on visual function measures to ensure that any deficits do not interfere with determining the impact of gene therapy. Otherwise, results may be skewed in a negative way masking the therapeutic effect. Greater investment is needed in exploring disease parameters in more detail in order to complete gene therapy trials in an effective, timely and cost-effective manner. This review provides an important starting point for clinical trial design and the justification for the work presented in this thesis.

1.6 Scope of the thesis

With the rise in the development of novel therapies for inherited retinal conditions, the outcome measures used for the assessment of these therapies and subsequently to monitor treatment effect if approved, is important to establish at this stage. Any outcome measures utilised must balance acceptance by the regulatory authorities with being scientifically rigorous in investigating the aspect they are probing. In addition, the tests must be practical for both patients and practitioners across different centres to implement. The visual system is highly co-ordinated and integrated and cannot be considered in isolation. In order to understand the full impact of disease, the visual system should be considered as a whole entity. Inherited retinal degenerations present with visual field loss in the periphery which gradually encroaches on the centre. This presents unique challenges on a practical level when assessing the patients. In addition, the loss of visual field may cause downstream impact within the circuits of the visual system. The aim of this thesis is to:

1) Optimise the measurement of visual acuity in the presence of visual field loss, as visual acuity is the most widely accepted measured of visual function.
2) Probe different aspects of visual function, taking into account the impact of visual field loss. Investigate the repeatability of these measures as well as understanding what exactly they represent of the retinal circuits.
3) Examine the visual brain in the presence of visual field loss.

1.7 Colour schemes used

Colour schemes for figures have not been used consistently through this thesis. Colour can be used very effectively to impart information but can also cause problems for readers who have a colour vision deficiency (Rougier, Droettboom, and Bourne 2014). This often includes the outputs from clinical tests and established imaging techniques. Where the information is

maximally relevant to a clinical audience, the colour schemes used reflect the outputs of the clinical assessments. The neuroscience chapters have utilised colour schemes that have optimised luminance and colour profiles for all readers

Chapter 2: Photopic Function

Papers arising:

Jolly JK, Juenemann K, Boagey H, Nadsady M, Bridge H, MacLaren RE. Validation of Electronic Visual Acuity (EVA) Measurement Against Standardised ETDRS Charts In Patients With Visual Field Loss From Inherited Retinal Degenerations. *British Journal of Ophthalmology* 2019 doi: 10.1136/bjophthalmol-2019-315124

My contributions to this chapter: I designed, obtained ethics, and conducted both studies. I carried out all data analysis and interpretation. Data collection for the EVA study took place between May 2017 and July 2018. Data collection for the colour vision study took place 7 months in 2017.

Other contributions to this chapter: Heather Boagey and Marie Nadsady contributed to EVA data collection as part of supervised undergraduate projects. Kristin Juenemann contributed to EVA data collection as part of a supervised masters project and conducted some of the preliminary repeatability analysis. Holly Bridge and Robert MacLaren reviewed the final paper. Statistical advice was provided by Joanna Moschandreas, Centre for Medical Statistics. The writing of the published article was my original work.

2. Photopic Function

2.1 Optimisation of visual acuity measurement in the presence of visual field loss.

2.1.1 Abstract/Summary

With the increase in clinical trials evaluating the efficacy of a therapy for retinal disease, there is a need to ensure that outcome measures are both accurate and standardized. The US Food and Drug Administration favours the use of visual acuity (VA) measured using ETDRS logMAR charts. The loss of visual field can interfere with visual tracking across the charts, leading to increased variability of measurements. Electronic visual acuity (EVA) presents the optotype on the centre of a screen, thereby removing the tracking element of the task, and may provide a more precise measurement. The aim of this study was to establish whether the use of electronic visual acuity measurement, could reduce the variability of VA measurement. Visual acuity was measured twice per chart type using ETDRS charts, EVA automated single letter (E-ETDRS) and EVA single line (EVA-SL) presentation (EMMES, USA). Patients underwent microperimetry (MAIA, Centervue, Italy) to determine visual field. Eyes with the visual field defect encroaching on the foveal centre benefitted most from use of the EVA system. Electronic measurement of visual acuity should be considered in future interventional clinical trials.

2.1.2 Importance of visual acuity measurement

Visual acuity (VA) is a key part of any ophthalmic assessment in both clinical practice and clinical research. There are a range of VA measurement types probing different aspects of vision including distance vision and near vision (Bailey and Lovie-Kitchin 2013; Jolly, Couldridge-Smith, et al. 2019). VA measurement can also be conducted in the very low vision population (Jolly, Gray, et al. 2019) or can be made more sensitive with the addition of filters (Wood et al. 2020). It is an assessment of the ability to see fine detail and, as a basic measure, is well

understood by clinicians. Measured in minutes of arc, VA is calculated as the reciprocal of the minimum angle of resolution (MAR), and is most commonly assessed with logMAR charts. Despite the popularity of these charts, clinical change can only be said to be detected significantly when VA alters more than 0.2 logMAR (2 lines on the chart), due to the test-retest variability (Rosser et al. 2003). Moreover, the variability in low vision patients is even greater than reported in control and mild disease populations (Kiser et al. 2005; Bittner et al. 2011). New strategies are therefore required to reduce the variability in the low vision population to better quantify therapeutic effects.

When novel interventions are trialled for ophthalmic indications, VA is often defined as a key outcome measure (Jolly, Bridge, and MacLaren 2019). It is a well-accepted measure by the Food and Drug Administration (FDA) and other regulatory authorities (Kaiser 2009). Standardised charts are highly regulated with control over the font type, spacing across and between lines, size progression and legibility of letters used (Bailey and Lovie-Kitchin 2013). Any new presentation or scoring methods must therefore meet the scientific rigours of the established Early Treatment Diabetic Retinopathy Study (ETDRS) charts. New tests must also be validated against the ETDRS charts in both healthy controls and patient populations to ensure equivalency of the tests. This can be done using Bland-Altman comparison.

One possible reason for the reduced precision in the low vision population is the impact of visual field loss on the ability to track across the letters on the chart as demonstrated in Figure 2.1. In the presence of visual field loss, once patients lose their place on the chart it can be very difficult for them to pick up and continue to read. VA testing therefore becomes a test of localisation and tracking of the position of the letters on the chart, as well as acuity. A group of patients with choroideremia, a rod-cone dystrophy, participating in a focus group to discuss visual testing, confirmed experiencing this difficulty. The aim of this study was to measure the impact of using an electronic VA testing system on VA measurement. This system reduces the requirement for letter localisation due to presentation of the letters on the centre of the screen. VA testing was

performed in a group of healthy volunteers to investigate equivalence of the electronic systems and ETDRS charts. We also tested a group of patients with rod-cone dystrophies in order to determine the relationship between visual field loss, VA performance and type of test.



Figure 2-1: Effect of visual field loss on reading ability on ETDRS charts. (A) Microperimetry of the remaining central visual field in one eye with advanced choroideremia. The coloured areas indicate the seeing parts of the retina. (B) ETDRS chart for measuring visual acuity. (C) A simulation of the appearance of the chart in B to the eye in A, making it difficult to track across the letters and obtain an accurate measure of visual acuity. (D) E-ETDRS presentation with single letter on the centre of the screen. (E) EVA-SL presentation with a single line of letters across the centre of the screen. (F) Simulation of visual field loss on EVA, the patient can more easily search around the letter as it stays within a limited area.

An electronic VA measurement system (EVA) was devised to promote greater standardisation of ETDRS visual acuity measurement (Beck et al. 2003). This has been commercialised by the EMMES Corporation (EMMES, Rockville, USA) and is FDA approved. The EVA is able to display single letters on the centre of a computer screen surrounded by crowding bars with automated scoring (E-ETDRS). The automated algorithm resembles standard ETDRS testing with 5 letters tested at each size. Testing continues until the smallest line with no letters seen is

reached (Beck et al. 2003). In addition, manual scoring can be conducted with presentation of single letters or single lines in the centre of the computer screen. All these presentation methods can be set to use Sloan letters in order to resemble ETDRS charts as closely as possible. The automated single letter presentation (E-ETDRS) and manual single line (EVA-SL) presentation methods were investigated here.

2.1.3 Methods

Ethical approval for this study was granted by the UK Health Regulatory Authority (reference 17/NS/0036) and it was conducted in accordance with the Declaration of Helsinki. All participants gave informed consent to take part. The study population consisted of two groups, non-visually impaired volunteers and patients with a confirmed diagnosis of rod-cone dystrophy from the outpatient clinics at the Oxford Eye Hospital, United Kingdom. Forty-one volunteers were recruited through accompanying persons in the eye clinics and age-matched to the patient group. VA is not significantly affected by gender or fully corrected refractive error in a clinically significant way so this was not controlled between groups (B. Brown and Yap 1995; R. Klein et al. 1991). Sixty-five consecutive patients, with a diagnosis of rod-cone dystrophy, were included in the study. Patients underwent VA testing with ETDRS charts, E-ETDRS automated paradigm and the EVA single line presentation (EMMES Corporation, USA) with optimal refractive error as determined by a subjective refraction in place. Each test was performed twice on the right eye of each participant. All tests were completed once and then repeated in a random order. The patient group underwent visual field testing with microperimetry on the MAIA using the 10-2 test grid centred over the fovea (Centervue SpA, Padova, Italy).

ETDRS charts were presented at 4m in a backlit frame. Chart R was used for refraction, chart 1 was presented to the right eye and chart 2 presented for the second test. Both eyes were covered during changeover of the charts to prevent any letters being memorised. If fewer than 20 letters

were read at 4m, the chart was moved to 1m to test the top 6 lines, and the final score was the sum of the number of letters read at both distances. If more than 20 letters were read at 4m, 30 letters were added to the letter score as the assumption was made that all letters would be read at 1m. The EVA system was set at 3m. The E-ETDRS presented the examiner with instructions on the iPod used to control the test stimuli and followed scoring previously described by Beck et al (Beck et al. 2003). Results were displayed on the iPod screen on completion and recorded on the case report form. The EVA single line (EVA-SL) presentation followed ETDRS parameters as closely as possible with the 20/200 line being presented in the first instance. The presentation of stimuli followed the procedure outlined in Figure 2.2. Room lights were switched off for the duration of all three tests. Detailed SOPs are provided in Appendix 1.

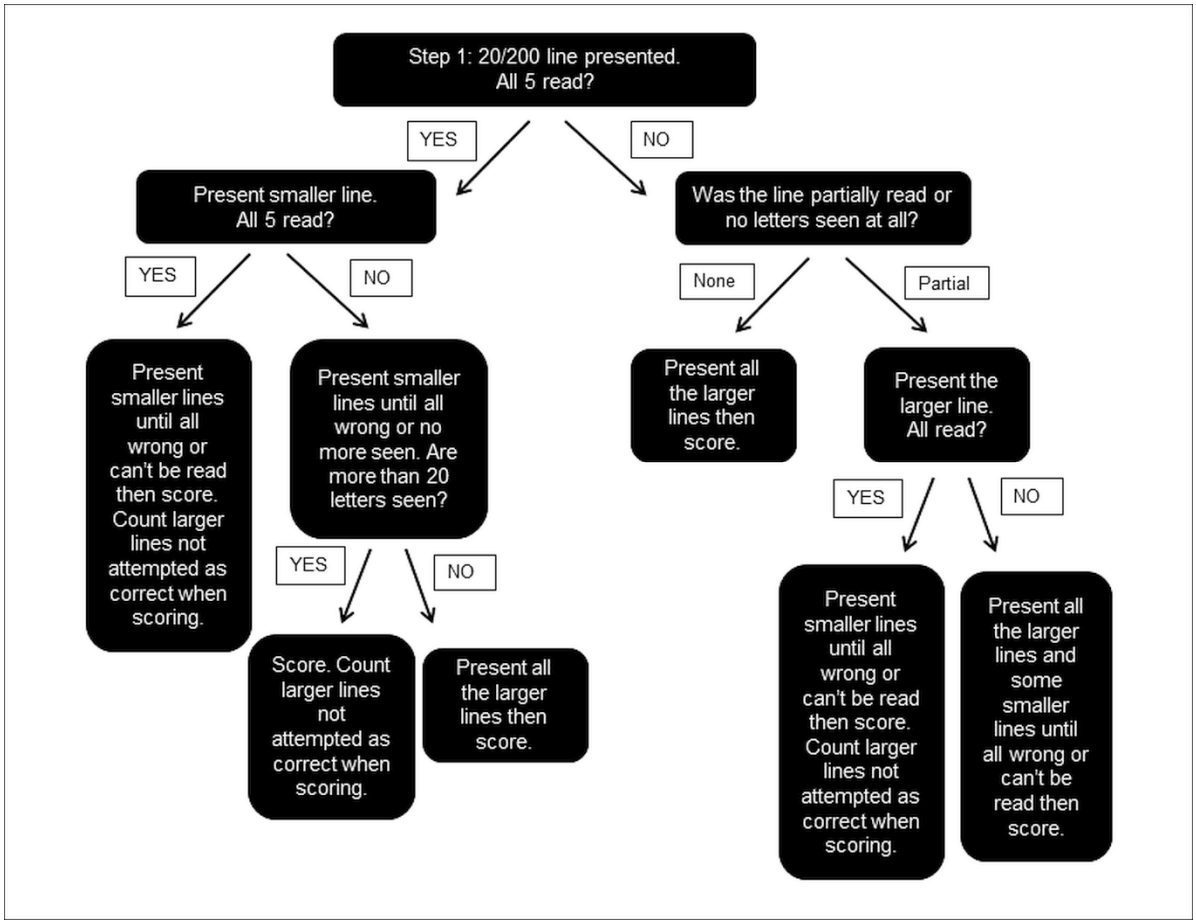


Figure 2-2: Presentation paradigm for single line method of measuring visual acuity using the Electronic Visual Acuity (EVA) system.

Based on previous work, the standard deviation of the differences between the visual acuity assessments methods was estimated to be 0.08logMAR, translating to 4 letters (Bailey and Lovie-Kitchin 2013). With a sample size of 50, this equates to a 95% CI for each of the Bland-Altman limits of agreement of +/- 1.9 letters (using $1.71SD/\sqrt{n}$). A sample size of 50 is the minimum recommended sample size for method agreement studies (Altman 1990). The extended Bland-Altman method, appropriate for repeated measurements, was used to assess agreement between the charts for each group of participants by calculating 95% limits of agreement. This method is also robust to non-normal data (Bland and Altman 1999). The coefficient of repeatability (CR), the difference within which repeat readings are expected to be for 95% of participants, was calculated as $1.96\sqrt{2}$ times the within subject standard deviation using one-way ANOVA (within subject standard deviation calculated from the square root of the residual mean square) under the assumptions of i) true replicates (no systematic difference between the samples) and ii) no relationship between difference and mean, tested using plots (Bland and Altman 1996; Bland and Altman 1996b). The eyes were split into "seeing" and "non-seeing" foveas based on microperimetry measurements. Non-seeing does not relate to the visual function of the eye but to the central fovea only for the rest of the manuscript. In order to differentiate patients with advanced loss of peripheral visual field from those who had lost central fixation and were using eccentric viewing, eyes were classified as foveal seeing or non-seeing based on the proportion of central microperimetry points seen (Figure 2.6 A and B). If two or more of the central four points had a threshold > 1dB, the eye was classed as seeing centrally (n=25), otherwise the eye was classified as non-seeing centrally (n=37). The distance to the edge of the nearest seeing point on the microperimetry plot was calculated in degrees (the minus sign on Figure 2.6 C denotes the point was on non-seeing retina). The pairwise difference between tests were correlated (using Spearman's rank correlation coefficient) with the horizontal and vertical distance to the nearest seeing point in the non-seeing fovea group and with the central threshold

and central island diameter in the seeing fovea group. Statistical analysis was conducted with SPSS (version 25.0, IBM Software, New York, USA).

2.1.4 Results

2.1.4.1 Patient demographics

Participant demographics and summary results for the right eye are presented in Table 2.1. A range of genetic diagnoses were represented within the patient group, with 51% of participants having choroideremia, 18% having RPGR, 6% with USH2A mutations, 18% without a confirmed genetic mutation and 7% having other mutations (Figure 2.3).

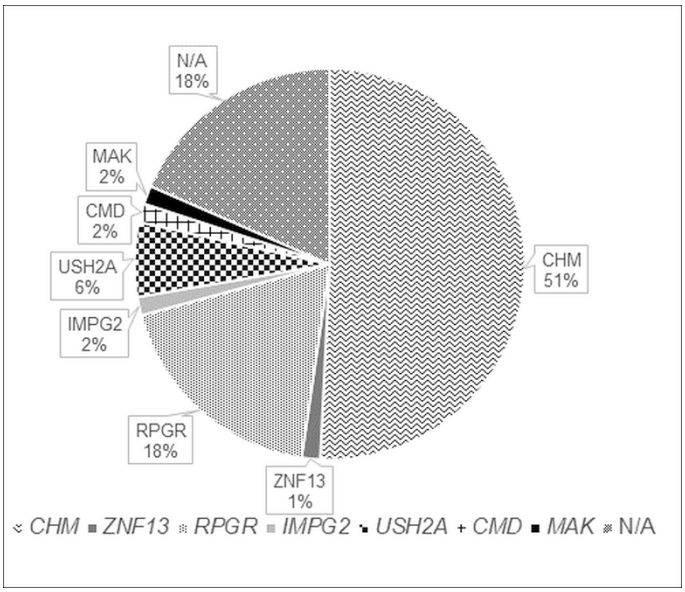


Figure 2-3: Genetic diagnosis of patient participants enrolled. N/A denotes genetic confirmation not available. The genes responsible for the inherited retinal degeneration are listed below the pie chart.

Factor	Healthy volunteers	Patient participants
N (people)	42	65
Age (years) mean [range]	46.1 [20.1 – 75.2]	51.2 [22.9 – 81.1]
Male / Female	26 / 16	54 / 12
ETDRS VA (letters) mean ± SD 1st attempt	87 ± 5	48 ± 29
ETDRS VA (letters) mean ± SD 2nd attempt	87 ± 5	51 ± 28
E-ETDRS (letters) mean ± SD 1st attempt	90 ± 6	51 ± 29
E-ETDRS (letters) mean ± SD 2nd attempt	90 ± 6	52 ± 30
EVA-SL (letters) mean ± SD 1st attempt	89 ± 6	52 ± 28
EVA-SL (letters) mean ± SD 2nd attempt	89 ± 6	53 ± 27

Table 2-1: Summary of participant demographics and summary of test results.

2.1.4.2 Visual acuity measurement in healthy volunteers

The boxplot in Figure 2.4 A shows the spread of the data on each test. The coefficient of repeatability was 6 letters in the ETDRS charts, 5 letters on the E-ETDRS protocol and 5 letters on the EVA-SL presentation. On average, volunteers read 2-3 letters more on both electronic versions of the test compared to the ETDRS charts with 95% CIs from -4 (-4 to -5) to 10 (10 to 10) and -5 (-5 to -5) to 9 (9 to 9) (for ETDRS vs E-ETDRS and EVA-SL respectively (Figures 2.4 B dashed lines on Bland-Altman plots). The agreement of the tests was assessed using a modified Bland-Altman analysis of the differences between tests using the right eye data incorporating repeat measures (Bland and Altman 1999). The results are shown in Table 2.2 and Figure 2.4 B Bland-Altman plots, which plot difference between tests against the mean of the measures. The dashed line showing the mean difference between the tests and the dotted lines showing the limits of agreement between tests. Figure 2.5 shows this data in more detail by altering the X-axis scale to a minimum of 75 letters (equivalent to 6/9.5).

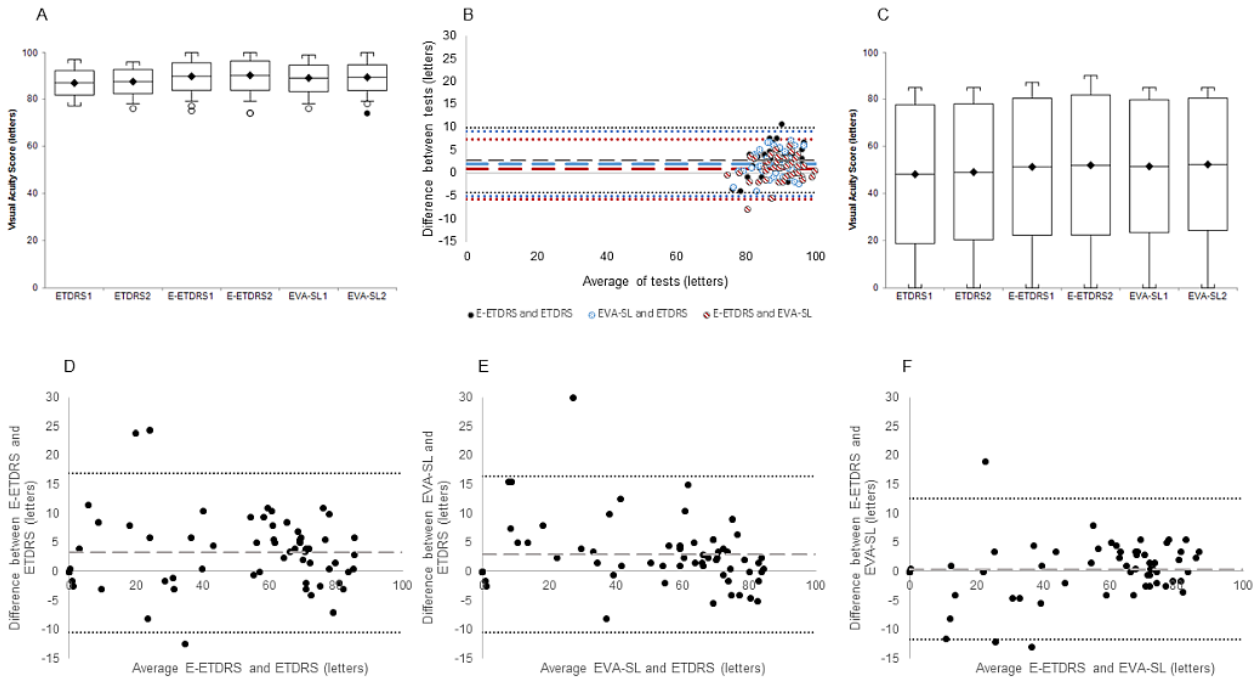


Figure 2-4: Figures A and B refer to the healthy group. Other figures are based on patient data. (A) Box and whisker plot showing mean, standard deviation and range of data points in healthy volunteer participants with outliers identified. (B) Bland-Altman plot comparing ETDRS charts and the two EVA presentation paradigms of the automated E-ETDRS and single line presentation (EVA-SL) in healthy volunteer group. The dashed lines represent mean difference and the dotted lines show the limits of agreement. (C) Box and whisker plot showing mean, standard deviation and range of data points in patient participants with outliers identified in the rod-cone dystrophy patient group. (D) Bland-Altman plot comparing ETDRS charts and the E-ETDRS paradigm in the patient group. (E) Bland-Altman plot comparing ETDRS charts and single line presentation (EVA-SL) in the patient group. (F) Bland-Altman plot comparing E-ETDRS and EVA-SL. The dashed lines in the Bland-Altman plots represent mean difference and the dotted lines show the limits of agreement.

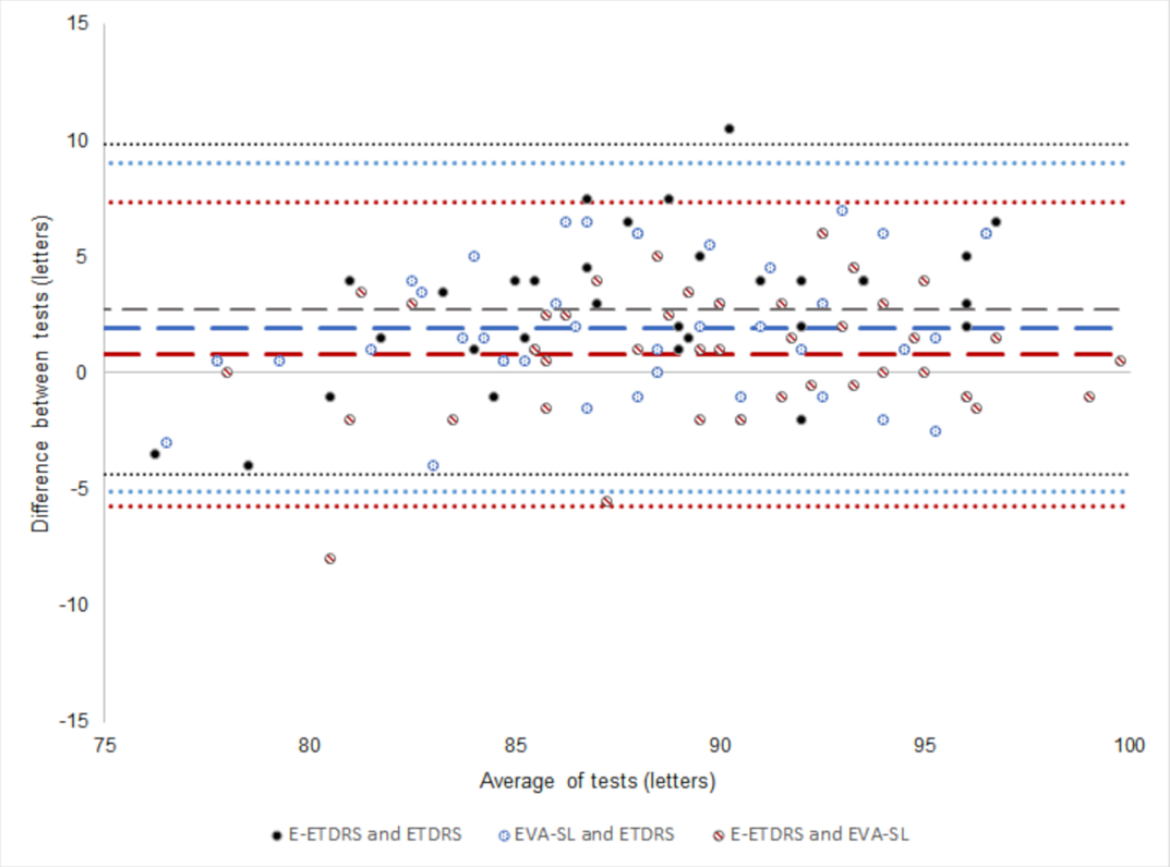


Figure 2-5: Bland-Altman plot from figure 3B with adjusted X-axis to allow viewing of the scatter of points in the control group.

2.1.4.3 Visual acuity measurement in patient group

The boxplot in Figure 2.4 C shows the spread of the data. The coefficient of repeatability was 7.5 letters in the ETDRS charts, 7.3 letters on the E-ETDRS protocol and 7.9 letters on the EVA-SL presentation. On average, patients read 3 letters more on both electronic versions of the test compared to the ETDRS charts with 95% CIs from -10 (-10 to -11) to 17 (17 to 17) and -10 (-10 to -11) to 16 (16 to 17) for ETDRS vs E-ETDRS and EVA-SL respectively (Figures 2.4 D-F dashed lines on Bland-Altman plots). The comparability of the tests was assessed using a modified Bland-Altman analysis of the differences between tests using the right eye data incorporating repeat measures. The results are shown in Table 2.2 with tighter agreement between the two electronic tests. The dashed line shows the mean difference between the tests and the dotted lines show the limits of agreement between tests.

Volunteer participants						
Letters	**E-ETDRS vs ETDRS**		**EVA-SL vs ETDRS**		**E-ETDRS vs EVA-SL**	
Mean Difference (95% CI)	3 (2 to 4)		2 (1 to 3)		1 (0 to 2)	
Lower limit of agreement (95% CI)	-4 (-5 to -4)		-5 (-5 to -5)		-6 (-6 to -5)	
Upper limit of agreement (95% CI)	10 (10 to 10)		9 (9 to 9)		7 (7 to 8)	
Patient participants complete group						
Mean Difference (95% CI)	3 (2 to 5)		3 (1 to 5)		0 (-1 to 2)	
Lower limit of agreement (95% CI)	-10 (-11 to -10)		-10 (-11 to -10)		-12 (-12 to -11)	
Upper limit of agreement (95% CI)	17 (17 to 17)		16 (16 to 17)		13 (12 to 13)	
Patient participant subgroup analysis						
Subgroup	Non-seeing	Seeing	Non-seeing	Seeing	Non-seeing	Seeing
Mean Difference (95% CI)	5 (2 to 7)	2 (-1 to 4)	4 (3 to 10)	2 (0 to 5)	1 (-1 to 3)	-1 (-3 to 2)
Lower limit of agreement (95% CI)	-9 (-10 to -8)	-11 (12 to -10)	-12 (-12 to -11)	-9 (-10 to -8)	-11 (-12 to -11)	-11 (-12 to -11)
Upper limit of agreement (95% CI)	18 (17 to 19)	14 (14 to 15)	19 (18 to 19)	13 (13 to 14)	13 (13 to 14)	10 (9 to 11)

Table 2-2: Summary of modified Bland-Altman results for participants comparing ETDRS charts (ETDRS), electronic ETDRS testing paradigm (E-ETDRS), and electronic single line presentation (EVA-SL). Final patient subgroup analysis is based on classification of how many of the central foveal points on microperimetry were seeing or non-seeing.

2.1.4.4 Relationship to visual field

Three patients were unable to perform reliable microperimetry. A modified Bland-Altman analysis was conducted on the non-seeing and seeing eye subgroups. The non-seeing eyes showed wider limits of agreement and larger coefficient of variation than the seeing eyes as shown in Table 2.2. The CR of repeatability in the non-seeing group was 8 letters for ETDRS charts, 7 letters for the E-ETDRS protocol and 8 for EVA-SL. In the seeing group, CR was 5, 7 and 8 letters respectively for the ETDRS, E-ETDRS and EVA-SL respectively. We explored the

factors affecting the spread of the data to understand what role visual field played in the measurement of VA.

For eyes with a non-seeing fovea, Spearman correlation of the difference in visual acuity measurement between ETDRS charts and E-ETDRS score, and the distance to the edge of the nearest seeing point was not significant (r=0.09, P=0.31) (Figure 2.6 C). In the seeing eyes, the threshold measured at the central four points was averaged. Neither central threshold (r=-0.12, P=0.28), nor central island diameter at the fovea (r=0.09, P=0.32) predicted the difference in visual acuity measurement between ETDRS charts and E-ETDRS measurement (Figure 2.6 D and E).

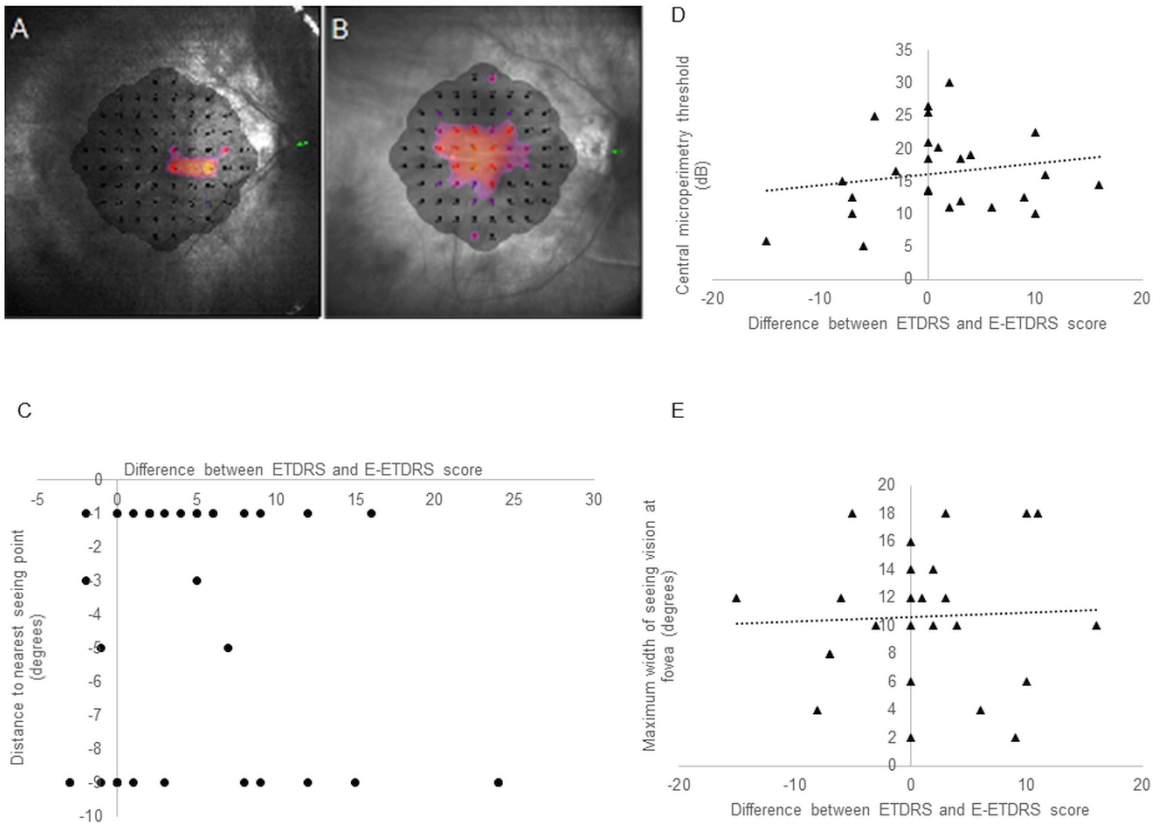


Figure 2-6: Representative microperimetry examples of (A) Non-seeing eye showing a maximum of 1 seeing point in the central visual field. (B) Seeing eye with all central points having a measurable threshold. (C) Correlation in non-seeing eyes using difference between charts and electronic test and distance to nearest seeing point. (D) Correlation in seeing eyes using difference between charts and electronic test and central microperimetry threshold. (E) Correlation in seeing eyes using difference between charts and electronic test and width of vision at the fovea.

2.1.4.5 Longitudinal VA measurement

A further subset of 14 patients with a variety of visual defects underwent assessment with ETDRS and E-ETDRS at five visits over 6 months in order to confirm the stability of measurements. These are shown in Figure 2.7. Visual analysis of the graph shows straighter lines indicating more stable measurement with the E-ETDRS paradigm. This appears to be more marked as the VA reduces. However, the Levene's test of equality of variances (one-way ANOVA) did not show any significant differences (F=1.18, P=0.28). The raw data are shown in Table 2.3.

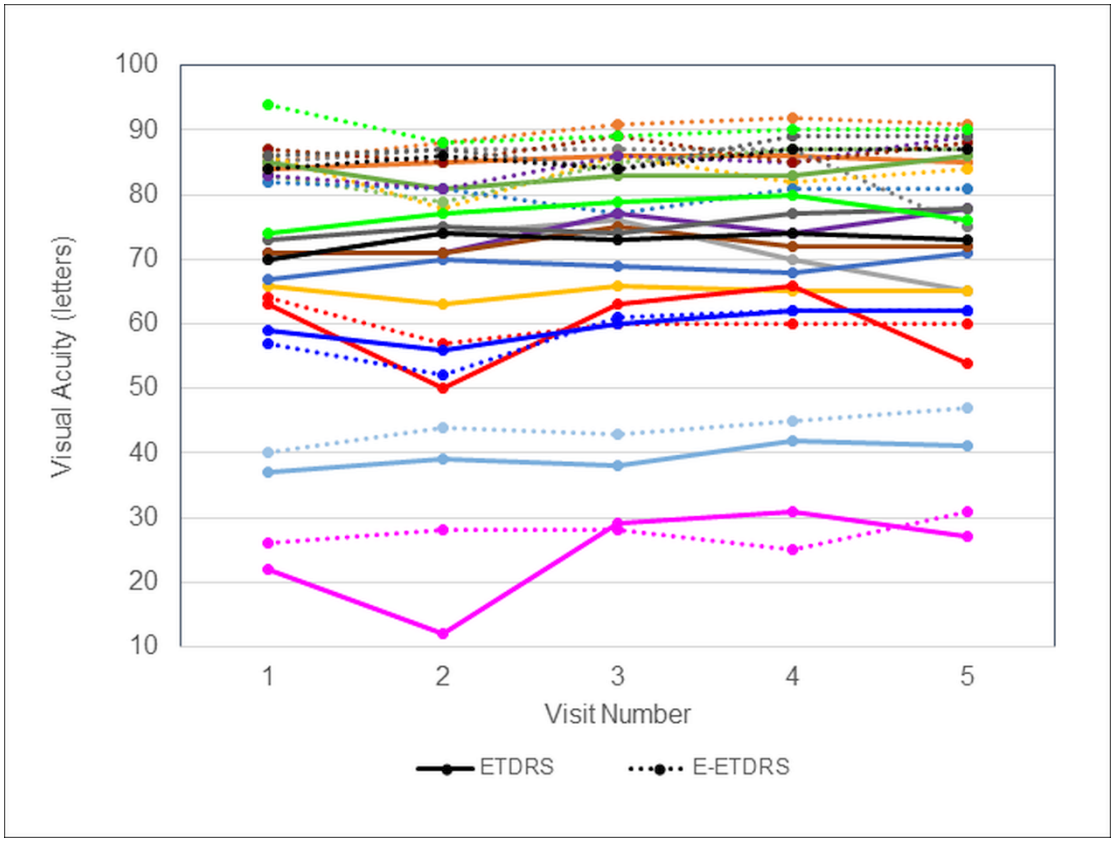


Figure 2-7: Scatter graph of visual acuity (VA) over 5 visits for 14 eyes with ETDRS results represented with solid lines and electronic (E-ETDRS) results represented with dashed lines.

	ETDRS						E-ETDRS				
Px	Screen	Day7	Month1	Month3	Month6	Px	Screen	Day7	Month1	Month3	Month6
	1	2	3	4	5		1	2	3	4	5
1	84	85	86	86	85	1 E	85	88	91	92	91
2	70	74	76	70	65	2 E	85	87	87	87	75
3	66	63	66	65	65	3 E	86	78	86	82	84
4	85	81	83	83	86	4 E	83	79	85	87	87
5	67	70	69	68	71	5 E	82	81	77	81	81
6	71	71	77	74	78	6 E	83	81	86	85	89
7	71	71	75	72	72	7 E	87	85	89	85	88
8	73	75	74	77	78	8 E	86	87	84	89	89
9	74	77	79	80	76	9 E	94	88	89	90	90
10	70	74	73	74	73	10 E	84	86	84	87	87
11	63	50	63	66	54	11 E	64	57	60	60	60
12	37	39	38	42	41	12 E	40	44	43	45	47
13	22	12	29	31	27	13 E	26	28	28	25	31
14	59	56	60	62	62	14 EVA	57	52	61	62	62

Table 2-3: Longitudinal measurements with ETDRS charts and automated ETDRS (E-ETDRS) charts. Px = patient.

2.1.5 Discussion

The vision measured with the electronic charts is equivalent to traditional ETDRS charts in healthy participants and the tests can be used interchangeably. The limits of agreement in the patient population are larger than the 10 line cut off for variability in the rod-cone dystrophy patient population, particularly with the non-foveal seeing eyes. Therefore, the decision about whether to use standard charts or electronic presentation should be carefully considered for each study. Electronic presentation of optotypes on the centre of a computer screen may provide more precise measures of visual acuity than traditional ETDRS charts in patients with visual field loss affecting the central fovea. The ability to see with the central foveal area appears to be the only determinant of whether the electronic charts are beneficial as neither distance of the seeing points from the fovea of threshold in the centre were factors in explaining the results. The wider limits of agreement in the patient group is as expected, and the variability is largely explained by the non-seeing foveal eyes with the larger limits of agreement and larger CR as compared to the

foveal seeing eyes. The two electronic display paradigms are closely related as shown by the comparison of the 95% confidence intervals for the means. Interestingly, the limits of agreement in the foveal non-seeing eyes are narrower and comparable to the foveal seeing eyes when comparing both electronic charts, indicating a higher degree of precision by the electronic charts when comparing the tests. The coefficient of repeatability was similar across test paradigms and remained within the 10 letters (2 lines) previously reported in the control group and the patients with seeing eyes using both electronic charts, indicating any of the tests can be used for measurement of VA in a clinical trial setting. The largest CR was in the eyes where foveal vision was affected, indicating this group accounts for the bulk of the variability seen in patients.

The electronic charts have two known advantages over the physical chart format. Firstly, the localisation element is removed. Secondly all VA sizes can be measured without adjustment of the screen. For VA measurement below 6/60, the ETDRS charts must be moved to 1m in order to continue testing which may introduce error due to change in the accommodative demand. Furthermore, in those with visual field loss, changing the distance of the charts will affect where the letters fall on the remaining visual field. By removing this requirement to move the chart, more consistent measurements can be obtained and may explain why the VA measurements appear to be more stable over time with the EVA system, particularly for those with low VA. With small visual fields, larger letters can be too big to fit within the seeing area, causing discrepancies between VA measurements on large versus small letters. By projecting a single letter on the centre of the screen, the patient can more easily scan around the letter to identify it and not fear losing their place on the chart. Further testing on a larger sample size with a larger number of lower vision patients is required to confirm this trend.

Although tracking abilities are an important factor in day to day vision, clinical trials and clinical service measurement of vision will have different priorities. In clinical trials defining visual acuity as a key endpoint, the absolute acuity will be the critical measure. In this situation, removing the error introduced by tracking will be important. However, in paediatric clinics, the

assessment of real-world ability is a greater priority so this may not be the best approach to use. With low vision monitoring, the goals of the patient and practitioner will influence whether electronic VA or chart based VA measurement is most appropriate.

2.1.6 Conclusion

We have validated two testing paradigms on the commercially available and FDA approved EVA system against ETDRS charts in a group of healthy participants. In patients with rod-cone dystrophy we have shown equivalence of VA measurement in the short and long term using electronic VA measurement, with possible increased precision when the visual field loss affects the fovea. We suggest larger studies comparing EVA to ETDRS in a range of disease types would be helpful to confirm these findings.

2.1.7 Implications for clinical practice

I propose that future trial protocols should consider the use of electronic VA in patients with visual field loss, particularly encroaching on the fovea, in situations where an accurate measure of ocular resolution rather than function is required.

2.2 Colour vision in rod-cone dystrophies

2.2.1 Abstract/Summary

Colour vision is considered a marker of cone function beyond the fovea. Colour vision defects, particularly in the tritan axis are seen early in choroideremia, independent of visual acuity and pattern electroretinogram function. The Cambridge colour low-vision version trivector test is able to determine information about the protan, deutan and tritan axes more reliably than the

current gold standard for clinical trials of the Farnsworth Munsell 100 Hue. The rod and cone systems are not independent pathways and the results may indicate the interplay between them.

2.2.2 Introduction to colour vision

Whilst visual acuity is a useful measure of cone function in the fovea, cones are present across the retina. Colour vision is a key function of cone photoreceptors and can therefore be used to monitor cone related changes across a wider region. The basis of colour vision is cone photoreceptor response to photons of light, known as the trichromatic theory of colour vision, followed by post-receptor and brain processing of the responses, known as the theory of colour opponency.

The first stage of colour vision involves responses from three classes of cone photoreceptors; L, M and S cones (denoting long, medium and short wavelengths respectively). L and M cones form the bulk of cone photoreceptors in the retina and occur in different ratios across individuals. They are most concentrated centrally and reduce in density with increasing eccentricity. The spectral sensitivity of each of these cone types peaks around 558, 531 and 419 nm respectively but there is significant overlap in spectral sensitivity, particularly between L and M cones. The opsin content spectral sensitivity determines the likelihood of each cone responding to incident light but these responses alone cannot provide information about the colour composition of the scene (Brainard 2015; Simunovic 2016).

The second stage of colour vision processing therefore is computational beginning at the level of the bipolar cells. S-cone responses are contrasted to M and L-cone responses. There are additionally receptive fields containing information from L-cones against M-cones. Therefore the cone opponent systems are (L+M), (L-M), and (S-(L+M)) shown in Figure 2.8 (Simunovic 2016). Modulation of the signal occurs in the brain to balance out unevenness in the signal within

and across individuals. The retinal circuits processing signals from the cone photoreceptors must account for the interleaved cone mosaics (Brainard 2015).

Although the *REP1* gene does express in both rods and cones, choroideremia is a primary rod degeneration (MacDonald, Russell, and Chan 2009). Rods appear to have a role in cone survival by the excretion of trophic factors that have a protective effect on cones. This is thought to be the cause of secondary cone degeneration in rod-cone dystrophies. The key protective trophic factor has been termed rod-derived cone viability factor (RdCVF) which is not produced by defective rods (Narayan et al. 2016). Although other mechanisms have been proposed for the secondary cone degeneration, RdCVF has been used in preclinical gene therapy trials to prevent secondary cone loss (Byrne et al. 2015). This shows how closely the rod and cone systems are intertwined.

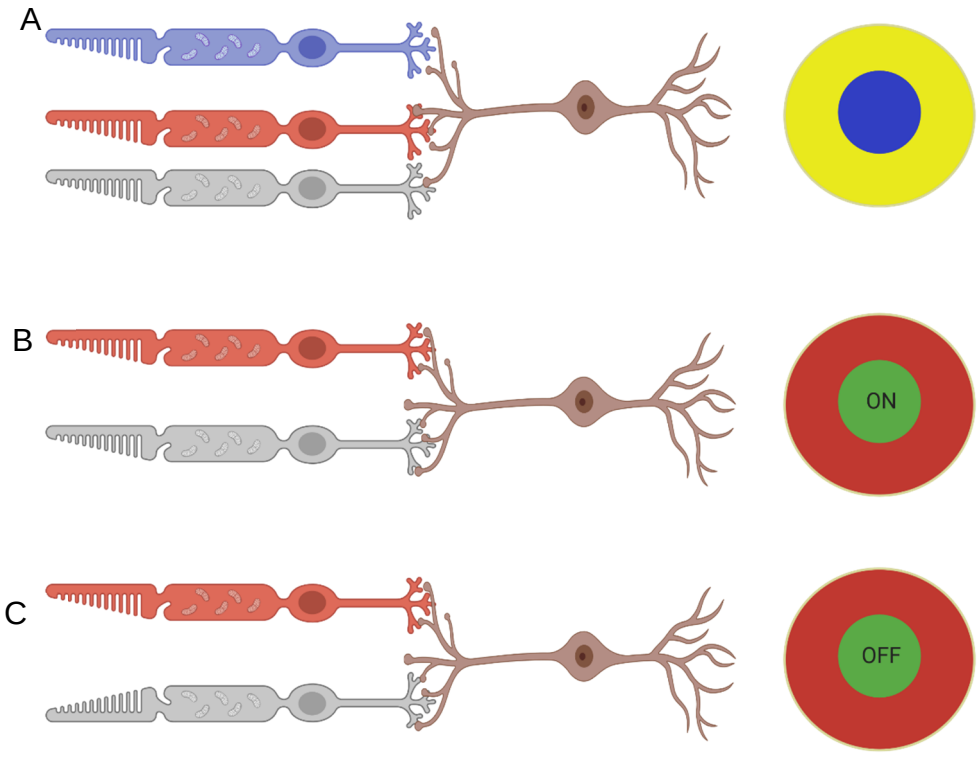


Figure 2-8: Cone opponency demonstrated by cone inputs into the bipolar cell and the resultant opponent system at the end of the circuit. The blue cone cell represents the S cone. The red cones represents the L cone and the grey cone cell represents the M cone. (A) shows the blue-yellow opponency with the blue contribution from S-cones, and yellow created by mix of input from L and M cones. (B) ON centre receptive field showing the additive effect of L and M-cones. (C) OFF centre receptive field showing the opposite input of the L and M-cones. Image created using BioRender.com

Colour vision testing can be performed via a number of different tests. The preferred test by the FDA for investigation of acquired colour vision loss is the Farnsworth-Munsell 100 Hue test (Figure 2.9 A) due to its longstanding history for colour functional assessment (Seitz et al. 2018). It consists of 85 caps across four boxes that must be arranged in order by the participant. Each cap measures 13 mm in diameter and the hues are arranged in perceptually equal steps. The degree of error is calculated from the arrangement of the caps. One drawback of the test is the large number of artefacts during analysis (Simunovic 2016). Additionally, there is a high degree of test variability, making reliable quantitative analysis difficult due to the large normative ranges. Large changes are needed between visits to establish a true change (Kinnear and Sahraie 2002). An alternative format for colour vision testing has been commercialised by Cambridge Research Systems (Figure 2.9 C) and is known as the Cambridge Colour Test (CCT). A low vision version of the CCT (Figure 2.9 D) has been used in clinical trials aiming to enhance cone function (Zein et al. 2014; Fischer, Michalakis, et al. 2020). The test is based on a previously developed protocol. It can be used in patients with poor visual acuity and reduced visual fields making it very useful for clinical disease populations (Simunovic et al. 1998). The trivector algorithm allows the investigation of L, M and S cone function, allowing it to be conducted in a shorter time frame than the 100 Hue whilst providing more targeted information (Figure 2.9 F).

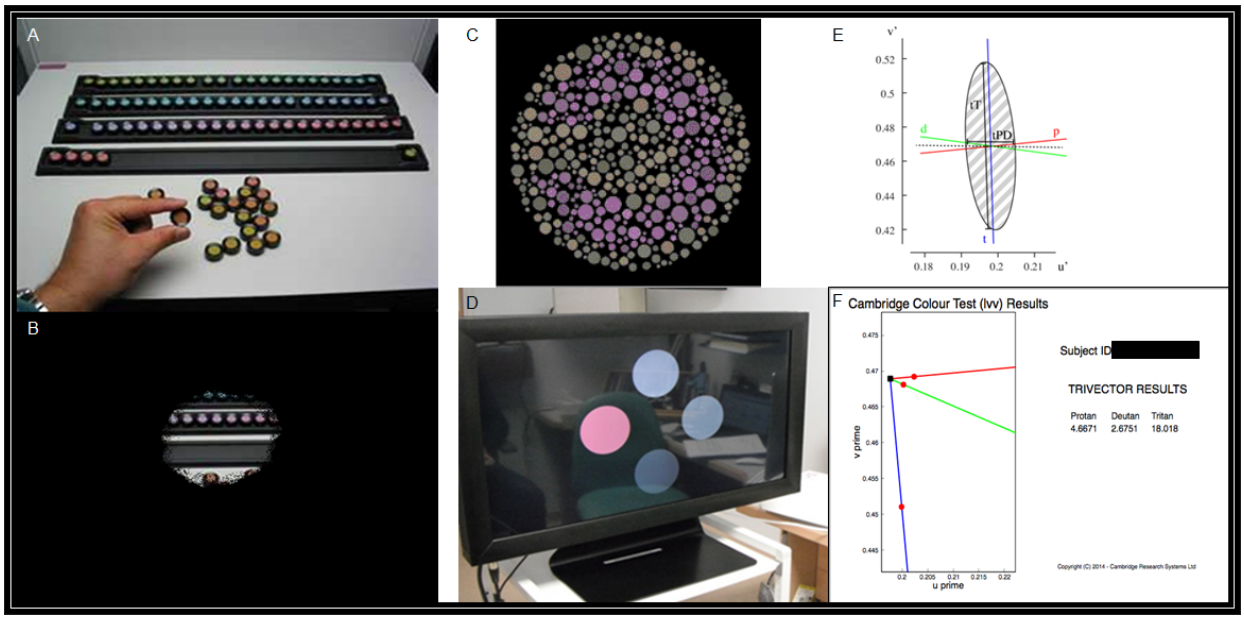


Figure 2-9: (A) Farnsworth-Munsell 100 Hue colour vision test. (B) Simulation of visual field loss restricting the view of the test resulting in slow test times. (C) Cambridge colour test (CCT) target. (D) Low vision version of the CCT showing 4 circles across the screen, providing an easier target for patients with low vision and reduced visual field. (E) Example output from full CCT version, producing an ellipse in colour vision function in colour space. (F) Example output from trivector test showing outputs for the protan, deutan and tritan axes.

Choroideremia presents with early colour vision defects which have been difficult to characterise with standard clinical tests (Jolly et al. 2015; Heon et al. 2016). The investigation of colour vision has been recommended in the battery of tests to investigate the disease but a better test is required to determine the driver of this colour vision loss. The standard version of the CCT was investigated in choroideremia and showed a defect skewed towards the tritan axis. This test is a demanding task and may not be suitable for all clinical trials participants if vision is low (Seitz et al. 2018). Additionally, the ellipses (Figure 2.9 E) are time consuming to measure compared to the trivector test due to the number of colours being probed. Colour vision loss is not thought to be influenced by visual field loss, despite the challenges visual field loss presents in conduct of the tests as demonstrated in Figure 2.9 B (W. Swanson, Birch, and Anderson 1993; Jolly et al. 2015). This study aims to investigate the low vision CCT trivector test in order to characterise colour vision loss in choroideremia as an outcome measure for clinical trials. In addition, factors will be investigated to understand the nature of the colour vision loss seen.

2.2.3 Methods

2.2.3.1 Assessments and statistical analyses

Patients were examined as part of the screening process for an ongoing retinal gene therapy trial for choroideremia (NCT02407678) and provided informed consent for all assessments. Control participants were recruited from accompanying persons and staff members. Informed consent was obtained and the work adhered to the Declaration of Helsinki. All participants underwent VA testing with ETDRS charts and colour vision testing with the Metropsis (Cambridge Research Systems, Cambridge, UK). Individuals with visible media opacities or congenital colour vision abnormalities were excluded.

The trivector test low vision version was optimised for the testing of L, M and S-cones in CIE 1976 L*u*v* colour space with the white point set to D65. Colours were set on the Azimuth system with values of 5.9852, 4.8387 and 0.0667. Defects measured are known as protan, deutan and tritan from this point forward. Four discs were displayed on the screen with the centre of each disc set at 4.3 degrees from the centre. Each disc was presented at a size of 2 degrees with the screen set at 1.5 m from the line of sight. The stimuli were presented for a maximum of 20 seconds to allow participants time to look around the screen and observe all discs even in the presence of severe visual field loss. An auditory signal accompanied presentation of the stimulus in order to alert patients to the stimulus in case they were looking at an area outside of their visual field. Three discs were presented with varying brightness of grey and one was presented with the colour under investigation so that luminance clues could not be used by the participant. The participant was instructed to choose which disc contained a colour through the use of an attached button box. Thresholds were established through the use of interleaved staircases. Each staircase involved a decrease rate of 50% hue saturation before the 1st reversal and 12.5% after the 1st reversal, and an increase rate of 25%. Threshold determination required six out of seven reversals to be used for threshold determination. However, five negative responses aborted the

test, setting the threshold at maximum saturation. The patients were given a training run before running the actual test to allow for a learning effect. Due to unequal variances, post-hoc analysis was conducted with Games-Howell comparisons. Detailed SOPs are provided in Appendix 1.

Patients were divided into two groups for the group analysis: preserved VA (≥ 80 letters based on population studies defining the upper limit of normal (B. Brown and Yap 1995)) and reduced VA (< 80 letters) as reduced vision associated with loss in M-L mechanism and would not provide as much information about the disease specific colour loss (Simunovic 2016). Therefore, examining patients with preserved VA allowed examination of the earliest defects. Results for protan, deutan and tritan axes were compared between groups separately using a one-way ANOVA following log transformation of the colour vision results.

A subset of patients conducted both the 100 Hue and CCT. The 100 Hue was set at 50 cm and took place within a cabinet with standard illuminant C lighting. The 100 Hue set was less than two years old and had been certified for colour accuracy. Caps were randomised by the examiner prior to testing and placed back in the tray. The participant was instructed to arrange the caps in smooth progression between the end caps. The order of the caps was input into the accompanying customised software in order to calculate the total error score. The tests were subsequently classified as normal or abnormal based on published values for the 100 Hue (Kinnear and Sahraie 2002), and calculated values for the upper 95% confidence limit of normal from the normative data collected above. Although colour vision is known to change with age, insufficient data exists to provide normative data for the CCT test used across ages (Paramei and Oakley 2014). Additionally, the reported variation across the age range represented by our cohort is small. A kappa agreement between tests was calculated.

This subset also underwent testing with the pattern electroretinogram (PERG) with both standard (15 degrees) and large field (30 degrees) grids using a gold foil electrode to understand the functional changes in macular function and impact on colour vision. Testing was performed as

per the ISCEV protocol using the Espion system (Diagnosys LLC, Lowell, MA) (Bach et al. 2013). The key features of the PERG are P50 peak time and amplitude as markers of macular dysfunction. Additionally, N95 is indicative of ganglion cell dysfunction (Figure 2.10). The colour vision results for each axis were treated as Cartesian co-ordinates and a combined vector calculated with $||CV|| = \sqrt{(protan^2 + deutan^2 + tritan^2)}$, where ||CV|| is the absolute colour vision vector length. A regression model examined the relationship between the PERG and the colour vision vector.

All results are reported for the right eye only. All statistical analyses were conducted in SPSS (version 25.0, IBM Software, New York, USA).

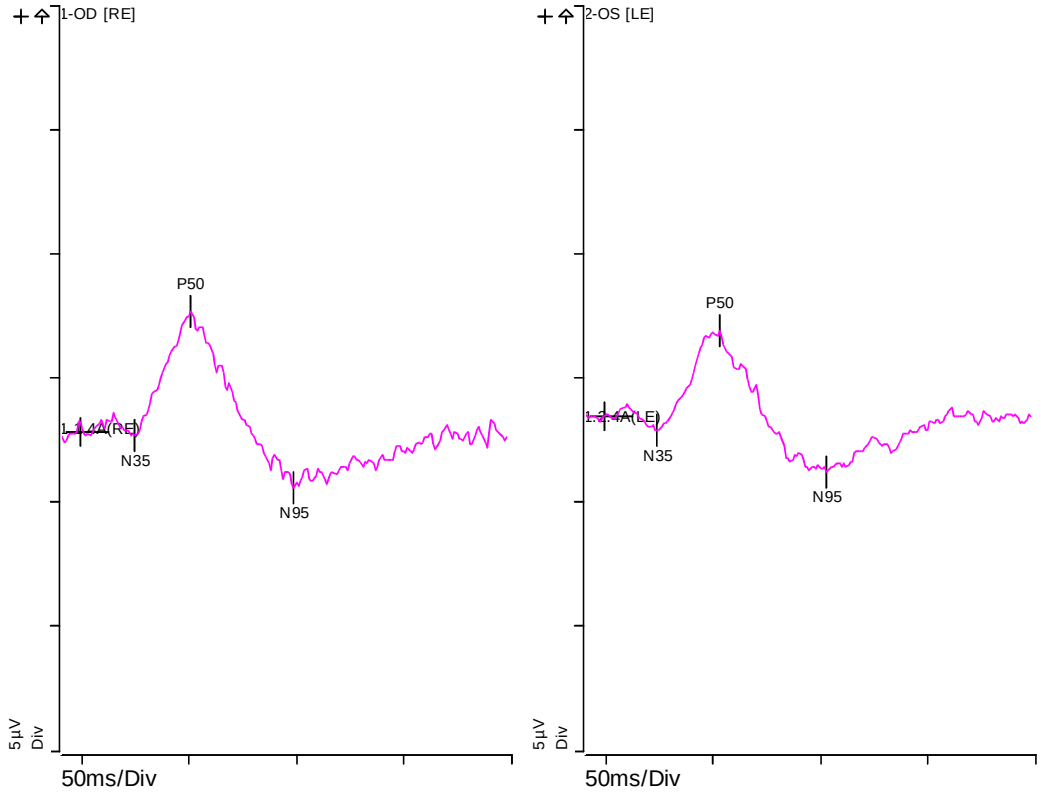


Figure 2-10: Example healthy pattern electroretinogram (PERG) recorded with the Espion system for right (OD) and left (OS) eyes. The P50 and N95 components are the key features for disease monitoring. The normal P50 component occurs at 50 ms and has an amplitude of > 4 µV on the standard PERG. The N95 component occurs at 95 ms and has a larger amplitude than the P50 with a resultant P50:N95 ratio of greater than 1:1.

2.2.3.2 Participants

The full cohort consisted of 21 control participants (age range 20 to 46 years), 35 choroideremia patients with VA ≥ 80 letters (equivalent to 0.10 logMAR, age range 14 to 55 years), and 18 choroideremia patients with reduced VA (age range 17 to 71 years). The subset of 30 patients that underwent additional testing had a mean age of 32 years, with a range of 17 to 55 years. Summary statistics are shown in Table 2.4.

Group	N (eyes)	Age	VA	Protan threshold	Deutan threshold	Tritan threshold
Control	21	31 ± 6	91 ± 4.8	3.982 ± 2.353	4.559 ± 3.151	6.725 ± 2.467
Preserved VA	35	31 ± 9	86 ± 3.8	13.814 ± 20.334	9.872 ± 10.447	20.813 ± 27.983
Reduced VA	18	34 ± 15	72 ± 9.6	17.519 ± 19.946	14.401 ± 18.283	27.602 ± 25.803
Patient subset	30	32 ± 9	83 ± 5.4	3.453 ± 7.455	3.246 ± 6.114	6.673 ± 10.808

Table 2-4: Summary characteristics of patient groups. All data is presented as mean ± standard deviation.

2.2.4 Results

2.2.4.1 Comparison between groups shows early tritan loss

Figure 2.11 A shows the spread of the raw data, with the worst threshold (highest number) along the tritan axis in all three groups as shown by the longest vector lines aligned with the vertical axis. The spread of the values across individuals is smaller in the control group compared to the patient groups. Group averages are shown in Figure 2.11 B. There was a statistically significant difference between groups as determined by one-way ANOVA for protan ($F(2,53) = 9.09$, $P < 0.01$), deutan ($F(2,53) = 6.44$, $P < 0.01$), and tritan ($F(2,53) = 19.54$, $P < 0.01$). A Games-Howell post hoc test revealed that the colour vision scores were statistically significantly lower in both the preserved and reduced VA cohorts compared to the control group for all three cone types (P

≤ 0.05). The two patient groups were not significantly different for any of the cone classes (P > 0.05). In order to match the VA average of the control group, qualitative assessment of the five patient eyes with a VA of 90 (equivalent to -0.10 logMAR) or greater showed that only one had a normal CCT colour score in all three axes. Two eyes had a defect in the tritan, one had a protan defect, and one across all three axes.

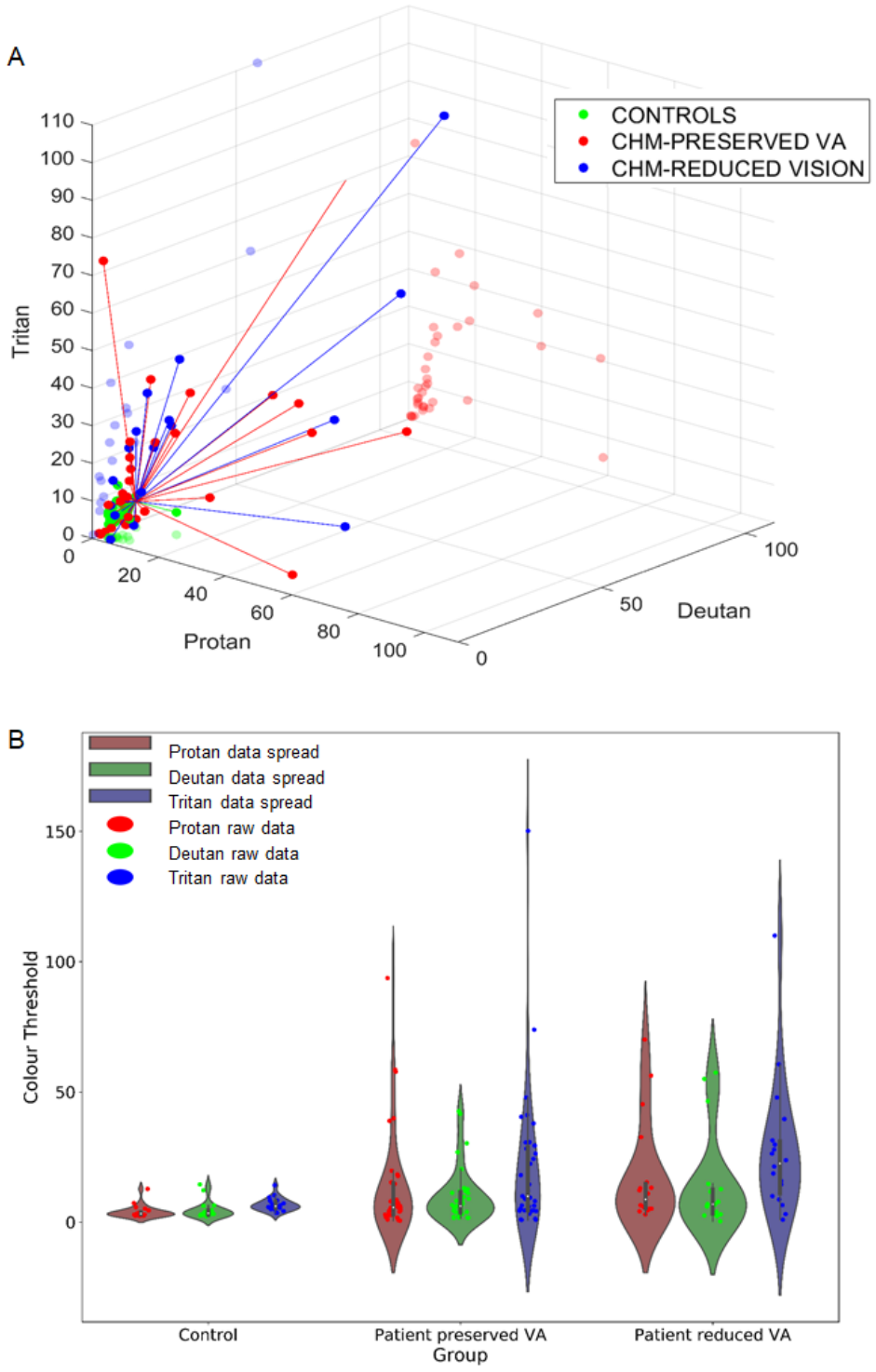


Figure 2-11: Summary of colour vision results. (A) Spread of individual datapoints in all three test groups. Each line represents a composite of protan, deutan and tritan thresholds on the X, Y and Z axes respectively. The angle of the line shows the direction of the defect and the length of the line indicates the extent of the defect. The coloured shadows indicate the spread of the data for each group; green for controls, red for choroideremia preserved VA and blue for choroideremia reduced VA. (B) Pirate plot of group differences. The outer envelope shows the spread of the raw data with the widest point representing the median. Inside the envelope is a small boxplot showing the summary with mean and standard deviation. Additionally, dots represent each raw data measurement point.

2.2.4.2 Comparison with 100 Hue reveals the Cambridge Colour Test is more discerning

The majority of patients showed abnormal results on both tests (Table 2.5). The 100 Hue was not able to classify a clear axis of defect in any of the eyes. Out of the 19 eyes classified as abnormal by the CCT, 26% were classified as having a clear tritan defect, 11% as having a protan defect, 16% as having a deutan defect and 47% as having a defect in multiple cone classes. The tritan was affected in all situations affecting multiple cone classes. There was no relationship to VA as eyes with reduced VA were classified as having normal colour vision, and normal VA could be associated with any type of colour vision loss. The Kappa agreement was low at k = 0.3878, P = 0.03, showing poor agreement between tests.

	CCT abnormal	CCT normal
100 Hue abnormal	17	6
100 Hue normal	2	5

Table 2-5: Classification of eyes as normal or abnormal when tested with the 100 Hue and Cambridge Colour Test (CCT).

2.2.4.3 Relationship with PERG indicates colour vision is not just related to macular function

In order to look at macular function as a whole, PERG was conducted. In response to the standard field PERG stimulus, the P50 and N95 were measurable in 26 out of 30 eyes, with the remaining 4 showing a flat line response. Mean P50 peak time for the cohort was 56.4 ± 12.7 ms with a P50 amplitude of 0.77 ± 0.49 µm. These indicate a marked impairment in macula function. The N95 amplitude for the cohort was 1.89 ± 1.17 µm, showing a preserved P50:N95 ratio indicating preserved ganglion cell function. The multiple regression model indicated no significant relationship between any of the PERG parameters with ||CV|| (R = 0.16, P = 0.91). Coefficients were -1.2 [-10.4 to 8.0], P = 0.79 for P50 peak time, 44.6 [-260.7 to 349.8], P = 0.77 for P50 amplitude, and 20.2 [-103.5 to 143.8], P = 0.74 for N95 amplitude.

In response to the large field PERG stimulus, amplitudes should be approximately double the standard PERG and peak times should remain unchanged. The P50 and N95 were measurable in 27 out of 30 eyes, with the remaining 3 showing a flat line response. Mean P50 peak time for the cohort was 53.1 ± 19.0 ms with a P50 amplitude of 1.10 ± 0.73 µm. These indicate a marked impairment in macula function persists despite the larger stimulus. The N95 amplitude for the cohort was 3.07 ± 5.80 µm. The multiple regression model indicated no significant relationship between any of the PERG parameters with ||CV|| (R = 0.36, P = 0.29). Coefficients were -7.5 [-16.5 to 1.5], P = 0.10 for P50 peak time, 26.0 [-212.1 to 264.1], P = 0.82 for P50 amplitude, and -1.0 [-25.8 to 23.8], P = 0.94 for N95 amplitude.

2.2.5 Discussion

In summary the CCT was more discerning in the ability to classify the type of colour deficit compared to the current gold standard of the 100 Hue (with which it showed poor agreement). In addition, it was a shorter test taking approximately 5 minutes per eye as opposed to 30 minutes for the 100 Hue. The patients with choroideremia developed colour vision defects from an early stage, even in the presence of normal VA, indicating cone dysfunction. Defects did not appear to worsen with decreasing VA. The majority of colour vision defects were noted to include the tritan axis in keeping with previous reports in rod-cone dystrophies (Seitz et al. 2018; W. Swanson, Birch, and Anderson 1993).

There are numerous differences in S cones compared to L and M cones. S cones are fewer in numbers, forming around 7% of the cone cells in the retina. They are not present in the foveal rod-free zone and appear around the same eccentricity as the rods appear in the retina, so the highest density of S cones does not coincide with the highest density of L and M cones. S cones have a more regular mosaic than do L and M cones, with less variability in the periphery. They are still prevalent within the macular area but the mosaic of S cones is independent of the L and

M cones (Curcio et al. 1991). However, evolutionarily S cones predate M cones so it is reasonable to expect that the retinal circuits have adapted for the mosaic and density, making it unlikely that the paucity and location of S cones is a cause for the tritan loss seen.

In addition, due to the sensitivity profile of the S cones to short wavelength light, they are susceptible to the harmful effects of the increased scatter seen in short wavelengths. One function of the RPE is to absorb stray light (Strauss 2005). Loss of the RPE as found in choroideremia may increase damage to short wavelength cones by the lack of shielding from harmful light.

There are a number of structural differences between the cone classes. The inner segments are more cylindrical in shape as are rod outer segments. Central S cones are smaller than L and M cones but increase in diameter towards the periphery (Curcio et al. 1991). Some of these differences can be explained by genetics. The OPN1SW gene, found on chromosome 7, is the basis for S cones. Genes for both the L and M cones are found on the X chromosome. The amino acid sequence encoding the opsin pigments show 96% homology between the L and M cones but only 43% homology between the L/M cones and the S cones. The S cones and rhodopsin have 75% homology (Nathans, Thomas, and Hogness 1986).

Morphological similarities between S cones and rods also include the lack of carbonic anhydrase activity, which is present in the other cone classes. Another difference is the presence of the S-antigen on both S cones and rods, a protein involved in the recovery phase of the light transduction cascade (Nork et al. 1990). These differences will have an impact on the functioning of the S cones. S cones are slower to respond than L and M cones (Nork et al. 1990). This difference in kinetics is likely as a result of differences in membrane hyperpolarization. L and M cones have membrane voltage-gated ion channels which change responses depending on the nature of stimulation, not found in S cones. This causes slower light adaptation in S cones, as well as reduced ability to respond over a wide range of contrast and luminance combinations (Howlett, Smith, and Kamermans 2017). S cones have evolved a different function in the visual

system compared to the L and M cones. S cones do not contribute to high detail spatial vision (Curcio et al. 1991). S cones also contribute to non-visual circuits so have different circuits compared to the L and M cones (Patterson et al. 2020). The slower kinetics and less easily modulated response of the S cones may have a role in their contribution to the circadian rhythm as the result is a more stable percept over time.

S cones have been reported to be more susceptible to metabolic damage (Hood and Greenstein 1988). There is an increase in the inflammatory response following rod death which has a larger effect on S cones compared to L and M cones (Di Pierdomenico et al. 2020). Cones cells have access to an alternative visual pathway via Műller cells to reduce reliance on the RPE. Műller cells have a lower association with S cones compared to other cone types (Lindenau et al. 2019). In view of the differences between S cones and other cone types, and simultaneous similarities with rods, it is possible that S cones may be affected by primary rod disease, either via inflammatory processes or structural impacts.

L, M and S cones do not work independently. L and M cone signals have been shown to modulate the S cone mosaic and influence the percept created by the filling in process in the brain (Brainard 2015). Conversely, the S cones have been shown to influence the response characteristics of M cones, altering the stimulus perception. This is thought to occur by altering post-receptor processing (Schmidt et al. 2018; Kling et al. 2019). It is possible that tritan defects reflect damage in all three cone types but manifest as they do due to the interaction between the cone classes. Due to the large targets used, fixation changes are unlikely to play a role in the findings.

An additional factor is the interplay between rods and the chromatic pathway due to sharing of post-receptor pathways. Rod input is larger into the S cone pathway compared to the L and M cone pathway in mesopic conditions (Cao et al. 2008). Rods have greater interaction with the S cone pathway. Balance of the two systems changes with both illumination and with disease so this relationship may also be changing (Zele, Maynard, and Feigl 2013). Rods and cones are

connected directly by horizontal cells and indirectly through bipolar cells. Interactions change with changing circumstances in ways that are not fully understood (Grimes, Songco-Aguas, and Rieke 2018). As the amount of functioning retina decreases, it is possible that overall response to retinal illumination decreases, altering the balance of light sensed in the eye and disrupting the interaction between rods and cones.

Colour vision loss occurred prior to VA loss in many patients and appeared to be independent to spatial visual processing pathways. The spatial and chromatic pathways appear to operate in parallel. Yet the visual system seamlessly combines these to form a coherent image (Kling et al. 2019). In choroideremia, foveal architecture is disrupted before VA loss occurs making it important to evaluate other measures such as colour vision to assess the functional impact (Jacobson et al. 2006).

The macular function shows a marked abnormality in the patient cohort reported here, including those with preserved VA as shown by the PERG. However, this does not appear to influence the colour vision results in keeping with previous findings (Falcao-Reis et al. 1991). PERG and psychophysical results have been reported to be discordant and this may reflect the different areas served by the two modes of testing (Ciavarella et al. 1997). I have previously shown a relationship between colour vision defect with microperimetry (Jolly et al. 2015). Microperimetry is likely reflective of cone function in the area tested so is more likely probing similar function (Han et al. 2018; Simunovic, Moore, and MacLaren 2016). Additionally autofluorescence area of preservation appeared to play a role in explaining colour vision, indicating a wider area of retina is likely to be involved in processing colour as opposed to spatial discrimination. Cones have been found to exist beyond the edges of autofluorescence islands (Foote et al. 2019). The next stage of analysis is to examine the OCT ellipsoid zone across the region in order to examine how much of the retina should remain intact to explain colour vision defects.

In summary, tritan defects are seen early in rod-cone diseases. It is not clear whether this reflects the interaction of defective rods in the cone system or degeneration in cone photoreceptors. The rod and cone systems are closely intertwined in the post-receptor processing of the signals and cannot be easily teased apart using standard clinical tests.

2.2.6 Future directions

Anecdotally a number of patients treated with gene therapy have reported improvements in their perceived colour vision so this is an important area of investigation. Working with laboratory based scientists who can examine the S cones directly may be the only way to determine whether the S cone loss is a direct or indirect result. Silent substitution techniques have been developed to examine each photoreceptor class individually and, may also prove a valuable tool in understanding differential effects of rod disease on L/M versus S cones.

2.2.7 Novel findings

The CCT low vision trivector test presents an effective colour vision test to isolate L, M and S cone function. S cone abnormalities occur in rod-cone dystrophies and should be monitored.

2.2.8 Implications for clinical practice

The CCT is very useful in situations requiring monitoring of the individual photoreceptors, such as in interventional clinical trials. Other computerised tests, or the full CCT protocol can provide information about general colour vision function.

Chapter 3:
Scotopic Function

Papers arising: In preparation

My contributions to this chapter: I designed, obtained ethical approval, and conducted data collection for both studies. I conducted the data analysis and interpretation. Data collection for the dark adaptation study took place over a 3 year period (each assessment took 3 hours). The scotopic MAIA study data collection took place over a 12 month period (each assessment took 3-4 hours).

Contributions to this chapter: Anika Nanda contributed to data collection for the scotopic MAIA project. Matt Gabel created the custom colour schemes for MATLAB for the analysis in section 3.4.4.3, in order to match the raw data.

3. Scotopic Function

3.1 Introduction to scotopic vision

Although the largest influence on quality of life is central vision, low light vision has a contributory factor (Owsley et al. 2006). In conditions affecting the rod photoreceptors, such as rod-cone dystrophies, night vision problems present as one of the earliest symptoms of disease. Establishing methods for analysis is therefore critical when assessing this group of patients. Scotopic function has been recorded to reduce with age. Rod density decreases with increasing age, beginning in the inferior retina and spreading across the central retina, with maximal effect 0.5 to 3mm eccentricity. Rod density loss is lower in the far periphery in later stages of life. Anatomical studies show that rod inner segments expanded to fill the gaps caused by the cell loss resulting in a normal looking mosaic (Curcio et al. 1993). Rhodopsin content of adult eyes does not change with age (Fulton et al. 1999). When these results are taken together, the change in scotopic sensitivity changes with age is likely related to the scotopic circuits and shows the importance of considering circuits as well as rod photoreceptors when discussing scotopic function. Scotopic function does vary at different locations of the retina, so the use of a global versus a local measure of function provides an additional consideration (Tahir et al. 2017).

3.1.1 Rod photoreceptors

The total number of rods in the human retina ranges from 77.9 to 107.3 million (Curcio et al. 1990). Rods have greater sensitivity than cones due to opsin difference (rhodopsin), neurotransmitter differences and faster rate of activation with slower inactivation as a result of differences in the phototransduction cascade from cones (Sampath et al. 2005; Morshedian and Fain 2017). The rhodopsin molecules are in the rod outer segment disc membranes and move freely. The dense packing of the molecules and the high diffusion coefficient of the molecule

increases the probability of absorption of a photon of light. The retinoid cycle which involves the conversion of 11-*cis* retinal, a chromophore that binds to rhodopsin, to the trans form and back again takes place across the rods and RPE, revealing a close relationship between the two structures. This is part of the phototransduction cascade, which triggers an electrical response to light. Retinal is a vitamin A derivative and human eyes contain a large reserve in the RPE under normal conditions (Lamb and Pugh 2004). In rods, the phototransduction cascade follows a different pathway and utilises different components compared to cones (Ingram, Sampath, and Fain 2016).

A bright light will activate opsins in the photoreceptors. When a substantial proportion of rhodopsin in rod outer segments has been exposed to light, rods lose sensitivity. This process is known as bleaching (Corson et al. 1990). After rods have been fully bleached with intense light, the recovery process can be studied to better understand rod function. This is known as dark adaptation and the time taken corresponds well to the regeneration time of rhodopsin with the transfer to 11-*cis* retinal between the RPE (Lamb and Pugh 2004). A number of genes have been identified to be involved in the phototransduction cascade and associated pathways (Figure 3.1).

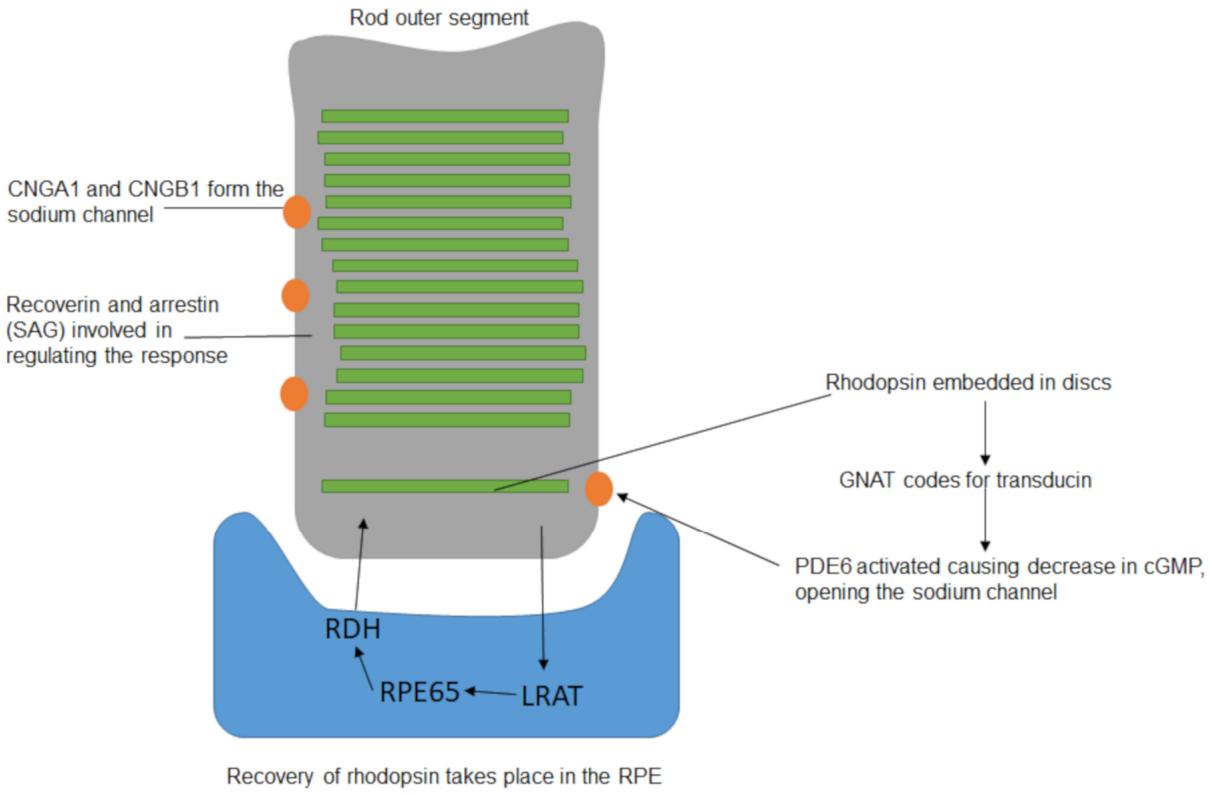


Figure 3-1: Rod visual cycle detailing the genes coding key elements at different stages of the process.

3.1.2 Retinal circuits for the rod

Both the rod photoreceptors and their circuits (shown in Figure 3.2) have been optimised for images with a low signal to noise ratio. The phototransduction cascade in rods is able to respond to single photon stimulations. The side effect of having such an exquisitely sensitive system is the susceptibility to noise in the system. Nonlinear pooling of the rod responses and multiple stages of convergence before parallel processing in the inner retina helps to reduce this noise, increasing the reliability of the low light signal (Field and Sampath 2016). Elements of the phototransduction cascade, such as recoverin, can modulate the downstream responses along the visual circuits. The mechanism of these changes is not fully understood (Sampath et al. 2005). Beyond the bipolar cells, amacrine cells modulate the signal, and retinal ganglion cells are able to alter their connectivity to bipolar cells as light levels change. There are differences in the way that the ON and OFF pathways encode information and this allows more information to be

extracted from the visual scene, especially in low light levels (Takeshita, Smeds, and Ala-Laurila 2017; Kolb, Ralph, and Eduardo 1995).

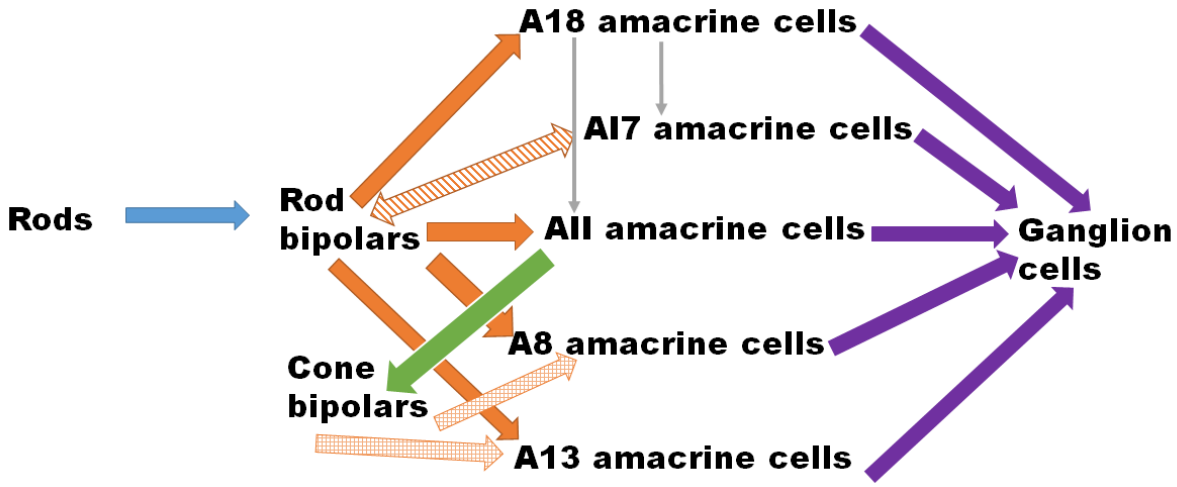


Figure 3-2: Details of the rod circuits showing multiple stages of convergence and divergence and parallel processing.

3.2 Measurement of scotopic vision

Rod function can be assessed with the use of electrophysiology (Johnson et al. 2019). Although this is an effective strategy providing an objective measure, the use of electrophysiology requires highly specialised staff and resources. Moreover, patients have useful residual function even in the absence of a measurable electroretinogram, particularly in rod-cone dystrophies. It is in these situations that psychophysical techniques become most useful. Dark adaptometry is the measurement of the dark adaptation process following bleaching with a bright light. The recovery of visual sensitivity is measured over time. The standard method for dark adaptometry has been the Goldmann-Weekers dark adaptometer, which presents an 11-degree achromatic stimulus. Luminosity of the stimulus is adjusted as threshold alters over time (Peters, Locke, and Birch 2000). This can present difficulties for a research setting as it is a paper-based system making it challenging to conduct sophisticated analyses. The reliability of the test is also dependent on the skill of the operator. Several newer techniques have been proposed for the

measurement of rod function including scotopic perimetry and full-field stimulus threshold (FST) testing as explored below. The FST defines absolute threshold by measuring the dimmest light that can be seen following a period of adaptation.

3.3 Investigation of global scotopic function

3.3.1 Abstract/Summary

Dark adaptation is a useful technique to probe how visual function adapts under scotopic conditions. The whole process can be measured following a period of light adaptation. Additionally, the final threshold can be measured independently using FST. Dark adaptation is slower and shallower in patient eyes compared to the control eyes. The degree of dark adaptation difficulty can be predicted from a single measure of FST with white light. However, the white light cannot elucidate how much of the response is derived from rods or cones individually.

3.3.2 Introduction to FST

The FST test was developed on the Espion system (Diagnosys LLC, Lowell, MA). The Espion is a well-established system used for electrophysiology. The FST was designed to fill the need of a test of rod function in the low vision population. This is particularly important with the rise in treatments being trialled for rod-mediated diseases as shown in chapter 1. The white light allows the characterisation of both rod and cone mediated retinae due to the large measurement range. These responses can also be tested separately using chromatic stimuli. The use of chromatic stimuli has been reported in a range of conditions, but it has not been established whether a single white light can be used to extrapolate the same information. The FST response was shown to be primarily driven by the rod photoreceptors and is reflective of the function of the remaining retina (Roman et al. 2005, 2007).

The FST is being used as an outcome measure in several recent and ongoing trials using both the white and chromatic forms (Jolly, Bridge, and MacLaren 2019). The test can be performed without good fixation as well as in the presence of nystagmus (Jacobson et al. 2017). It is feasible in very low vision patients when other tests such as electroretinograms or visual field testing cannot be conducted (M. Klein and Birch 2009; Messias et al. 2013; Stingl et al. 2019). This makes it potentially very useful for a wide array of patient populations. There is a suggestion that the central retina provides a greater input into the FST response despite the widespread presence of rods across the retina (Messias et al. 2013; Dimopoulos, Freund, et al. 2018). The density of rods is higher in the peripheral retina (Curcio et al. 1990). It is therefore feasible that larger numbers of rods synapse with individual bipolar cells in the periphery compared to central retina. This would potentially result in the loss of central rods having a greater influence on scotopic sensitivity.

3.3.3 Methods

Detailed SOPs are provided in Appendix 1.

3.3.3.1 Dark adaptation curves

Dark adaptation curves were recorded using the dark adaptation module on the Espion E2 Colordome (Diagnosys LLC, Lowell, MA), software version 6.61.12. This test illuminates the full retinal field, allowing all surviving retinal areas to be stimulated. Pupils were dilated using 1% tropicamide and 2.5% phenylephrine hydrochloride. The eye not being tested was occluded with the use of two layers of patching to prevent light leakage from that eye, room lights were switched off and the room was protected from external light exposure. In the interests of time, most subjects only had the right eye tested. Careful instructions were provided to warn subjects the light being presented was extremely faint, and responses should take this into account. The

stimulus consisted of a 6500 K white light with a presentation length of 200 ms and a 2000 ms response window. Auditory sounds were presented before and after a period of threshold determination at discrete time points. The pupil size was measured and input into the system as the light intensity presented was adjusted for pupil size. The operator was separated from the subject with a curtain and a red filter was placed over the computer screen operating the examination to reduce any light leakage influencing the results of the test.

The test started with a five minute bleaching period using light of 1000 cd/m^2 to get as close to 100% bleach as possible (Hecht, Haig, and Chase 1937). This was to ensure all participants underwent complete bleaching and started at the same point. Once bleaching was complete, the stimulus was presented and the subject was asked to push the button each time the stimulus was seen. A staircase method was used to find the threshold at each point tested, with threshold determined based on the last point seen. Testing occurred frequently in the period immediately following bleaching, decreasing in frequency as time went on to ultimately allow 23 seconds between trials after ten minutes. This allowed the subject to rest intermittently and reduce fatigue. I remained in the room monitoring the responses during testing to provide instructions and encouragement as needed. The test was stopped once I deemed that a final plateau had been reached. This involved a minimum of five points with no increase in sensitivity (reduction in threshold), though clinical judgement was used to evaluate this in view of the variability displayed during the examination. The test was run for a minimum of 25 minutes and could be extended beyond the default length of 45 minutes when required.

The dark adaptation curves were downloaded from Espion as tab delimited files analysed individually in Microsoft Excel (Microsoft, Redmond, USA). Due to technical problems before data download, two dark adaptation raw data files were corrupted and could not be analysed. The shape and critical portions of the dark adaptation curve are described by Patryas et al are shown in Figure 3.3 (Patryas et al. 2013). The key components recorded were the first threshold value immediately following the bleach period, the time to the α point denoting the rod-cone

break and threshold of this point, time to full dark adaptation as well as final threshold value. In addition, the S2 slope was calculated as a marker of 11-*cis* retinal concentration in the RPE. The slope of S3 was not quantified, as it was not well defined in many eyes and the significance of these portions is not well understood (Tahir et al. 2017). All statistical analyses were performed in SPSS (version 25.0, IBM Software, New York, USA).

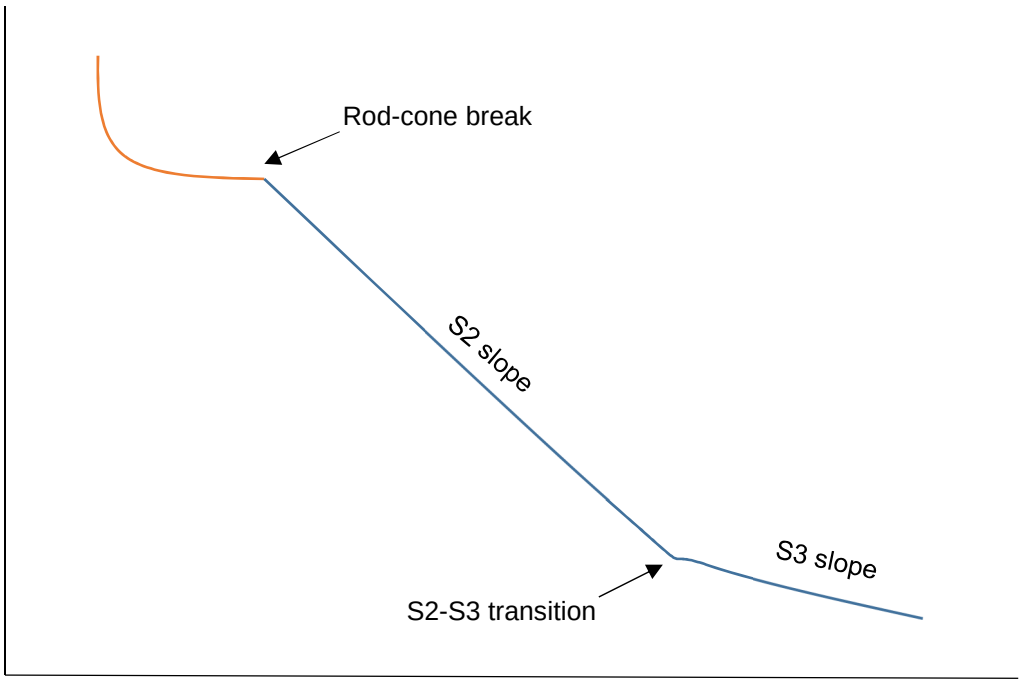


Figure 3-3: Defining features of the typical dark adaptation curve. The top orange curve represents cone recovery from the bleaching light. The rod-cone break (α point) signals the transition point to the rod recovery which is a slower process and consists of two primary components, S2 and S3.

3.3.3.2 Full field stimulus threshold testing

If dark adaptation had been performed, the subject was allowed a five minute rest period in the dark and then performed FST without further dark adaptation as the eye was deemed to be at peak sensitivity. If dark adaptation had not been performed, the subject was seated in the blacked out room in front of the Espion for 45 minutes with the eye not being tested being double patched. The participant sat forward at the end of the period and the inbuilt infrared camera allowed me to see whether the eye was in the right location and remained open during testing. The subject was presented with a forced choice paradigm. A beep denoted when a light was presented. The

subject had to press the right-hand button if the light was seen and the left button if the light was not seen. The orientation of the buttons was checked immediately before starting to ensure nothing had been moved during the dark adaptation period. Testing was performed with the white light with the 0 dB point being set to 0.01 cd/m^2. In order to provide training and save time, a short manual trial was conducted and the start intensity was set to be close to the point at which the light was reported as not seen. The stimulus was presented for 4 ms. Threshold determination was via a reversal staircase following a 4 dB decrease and 2 dB increase algorithm. The built-in two-parameter Weibull function was used to estimate the final threshold, determined by the 50% probability in detecting the stimulus intensity. A minimum of 2 tests was conducted with a minimum re-adaptation period of 3 minutes provided between tests. The final threshold values were used in the analysis.

3.3.3.3 Statistical analyses

The α point defined the rod-cone break. Dark adaptometry was compared between the patient and control group using MANOVA with initial threshold, time to α point, α point threshold, time to end point, final threshold and S2 slope. The assumptions of normality, equality of variance, absence of significant univariate outliers, and linearity were met. There was one multivariate outlier which was excluded. There was significant collinearity between the start, α, and final threshold so the last two measures were excluded from analysis. Pot hoc tests were conducted with Dunnett correction as covariance matrices had unequal variances between groups.

FST values were analysed comparing the groups described. All groups had a normal distribution but failed the test of equal variances. Kruskal-Wallis one-way ANOVA on ranks was performed with pairwise multiple comparisons using Dunn's method.

Autofluorescence area was measured on Heidelberg Eye Explorer (Heidelberg, Germany) and the percentage area remaining calculated as previously described (Jolly et al. 2016). This was

correlated with FST measurement. All statistical analyses were carried out with SPSS (version 25.0, IBM Software, New York, USA) and SigmaPlot (version 14.0, Systat Software, San Jose, USA).

3.3.3.4 Participants

This work was carried out in a group of patients with choroideremia and age-matched controls. Choroideremia was chosen for this study due to the well-defined islands visible on imaging, allowing for the areas with surviving rods to be well defined. Seventy-three patients with a clinically confirmed diagnosis of choroideremia underwent dark adaptometry and FST testing. In addition, 15 healthy control participants underwent dark adaptometry and 35 completed FST testing. Ten female carriers completed FST testing.

3.3.4 Results

Patient demographics are shown in Table 3.1.

Measure	**Male patient eyes**	**Female carrier eyes**	**Control eyes**	**Control eye subset with DA curves**
Age (years)	38.2 [13 – 70]	45.9 [17 – 74]	42.8 [20 – 70]	37.0 [20 – 63]
FST (dB)	-21.6 ± 14.0	-45.4 ± 9.5	-51.8 ± 4.2	-51.5 ± 5.1
FST (cd/m^2)	0.43 ± 2.31	0.000172 ± 0.00034	0.000012 ± 0.000018	0.000015 ± 0.000025
AF area (%)	9.5 ± 15.8	NA	NA	NA

Table 3-1: Patient demographics and summary initial results for populations tested. FST = full field stimulus testing. DA = dark adaptation. AF = fundus autofluorescence. Data are presented as mean ± standard deviation or mean and [range].

3.3.4.1 Dark adaptation patterns are reflective of disease severity

The full dark adaptation curves were analysed and three patterns of dark adaptation were identified in the patient population (Figure 3.4 C-E). The first pattern showed a normal shape to the dark adaptation curve, with a reduced endpoint indicative of mild disease (group 1, n = 16). The second pattern was slowed and reduced rod function observed in moderate disease (group 2, n = 34). The final pattern recorded in severe disease was a cone only curve with no or little evidence of rod adaptation (group 3, n = 23). In addition, in several patients, a stepwise increase in sensitivity was observed (Figure 3.4 B). Summary statistics are shown in Table 3.2.

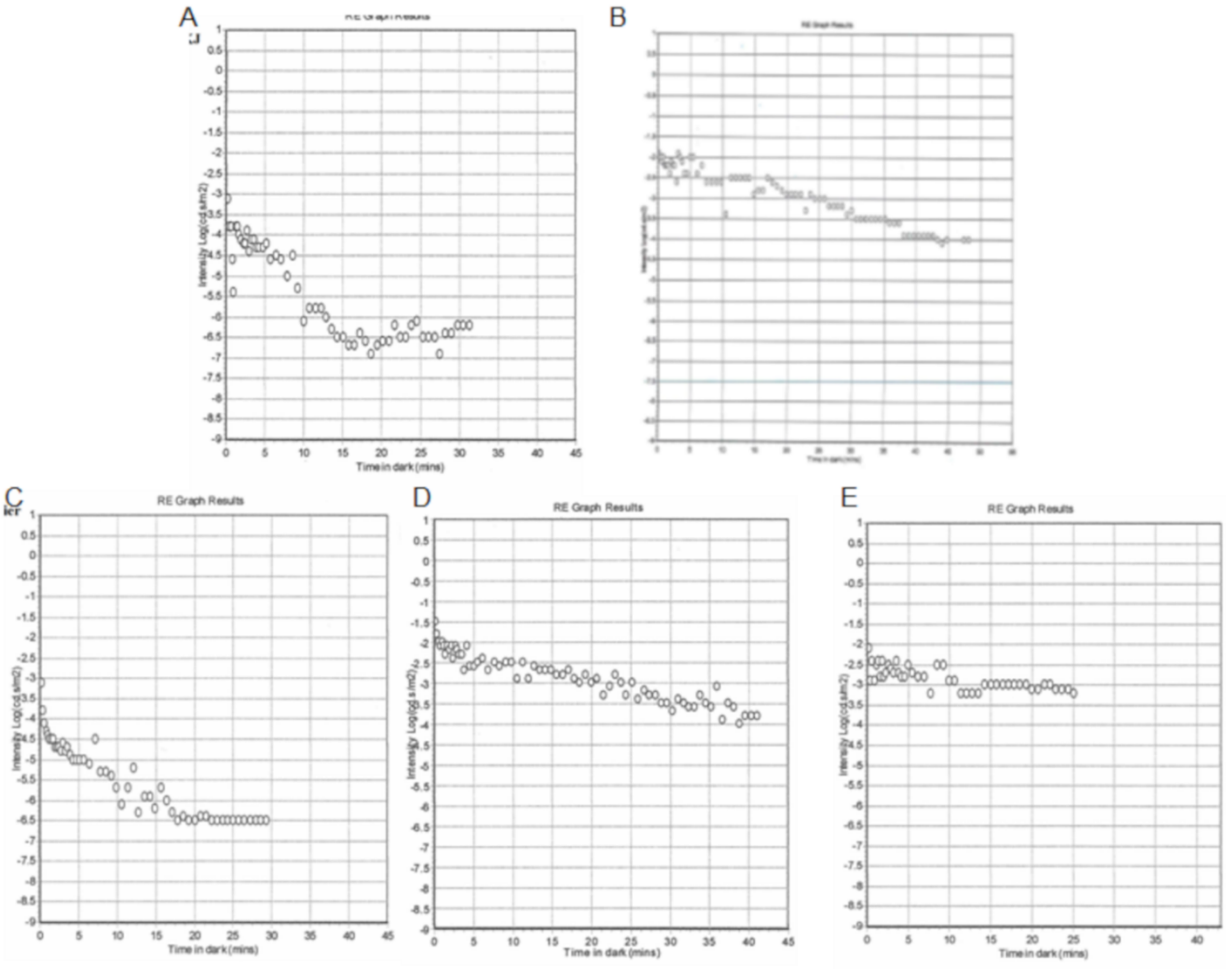


Figure 3-4: Dark adaptation patterns seen in patients with choroideremia. (A) Dark adaptation curve from a control eye for reference. (B) Stepwise increase in sensitivity with increased time in the dark. (C) Normally shaped dark adaptation curve with a reduced endpoint found in mild disease. (D) Slowed and reduced rod function observed in moderate disease. (E) Cone only curve with no or little evidence of rod adaptation recorded in severe disease.

Measure	Patient eyes	Control eyes
Initial threshold (dB)	-18.0 ± 0.7	-3.5 ± 0.5
Initial threshold (cd/m^2)	0.66 ± 1.2	0.5 ± 1.1
Time to α point (mins)	293.9 ± 103.0	223.1 ± 48.1
α threshold (dB)	-2.5 ± 0.6	-4.2 ± 0.5
α threshold (cd/m^2)	0.57 ± 1.2	0.05 ± 1.1
Time to final threshold (mins)	1595.9 ± 546.6	1301.7 ± 234.5
Final threshold (dB)	-3.8 ± 1.3	-6.9 ± 0.4
Final threshold (cd/m^2)	0.42 ± 1.3	0.2 ± 1.1
Slope S2 (log.cd/m^2 per minute)	-0.000086 ± 0.00065	-0.00265 ± 0.00062

Table 3-2: Dark adaptometry measures in patient and control eyes. Data are presented as mean ± standard deviation.

There was a statistically significant difference in dark adaptation features between the patient and control eyes, F (4, 79) = 42.7, P < 0.01. Post-hoc testing correcting for multiple comparisons shows all measures are significantly different between populations; lower initial threshold (F = 79.2; P < 0.01); longer time to α point (F = 6.8; P = 0.01); longer time to complete dark adaptation (F = 5.0; P = 0.03); and shallower S2 slope (F = 131.8; P < 0.01) in the patient population.

3.3.4.2 FST can provide information about the dark adaptation curve expected

There was a strong correlation between the dark adaptation final threshold and FST threshold of the full dataset (ρ = 0.90, P < 0.01) (Figure 3.5 A). The FST was found to be -6.4 ± 11.6 dB in group 1 (severe disease), -19.5 ± 1.5 dB in group 2 (moderate disease), -35.2 ± 8.5 dB in group 3 (mild disease), and -51.8 ± 4.2 dB in group 4 (control eyes). All three groups differed from controls (P < 0.01). Groups 1 and 2 did not differ significantly (P = 0.26), but groups 1 and 3 (P < 0.01) and groups 2 and 3 (P = 0.02) were significantly different (Table 3.2 and Figure 3.5 B).

This indicates a reduction in FST (less negative) early in the disease process, with a further decrease (positive shift) as disease state becomes severe.

The upper 95% limit of the FST in group 1 (displaying a cone dominated pattern of response) was -18 dB, equivalent to 0.016 cd/m^2. Previously, red and blue coloured lights have been used to probe rod and cone dark adapted function. A subset of 30 patients underwent additional FST testing with red and blue lights. The difference between the red and blue lights was calculated as previous work has indicated when the blue response is greater than 2.2 log units compared to red, it is indicative of a rod mediated response (Roman et al. 2005; Hwang et al. 2013). Out of the 30 eyes, six met this criterion for rod prevalence, distributed across all three dark adaptation groups (Figure 3.5 C).

Female carriers of choroideremia can present with a range of disease states, from mild speckling of the retinal appearance, to a male phenotype, depending on the degree of diseased cells and therefore the number of diseased cells in the eye. A classification system for female carriers has previously been described which grades the extent of disease visible in the eye (Edwards et al. 2015). FST results in these groups appears to reflect the degree of AF loss, as shown in Figure 3.5 D, further supporting the relationship between remaining retina and FST measurement.

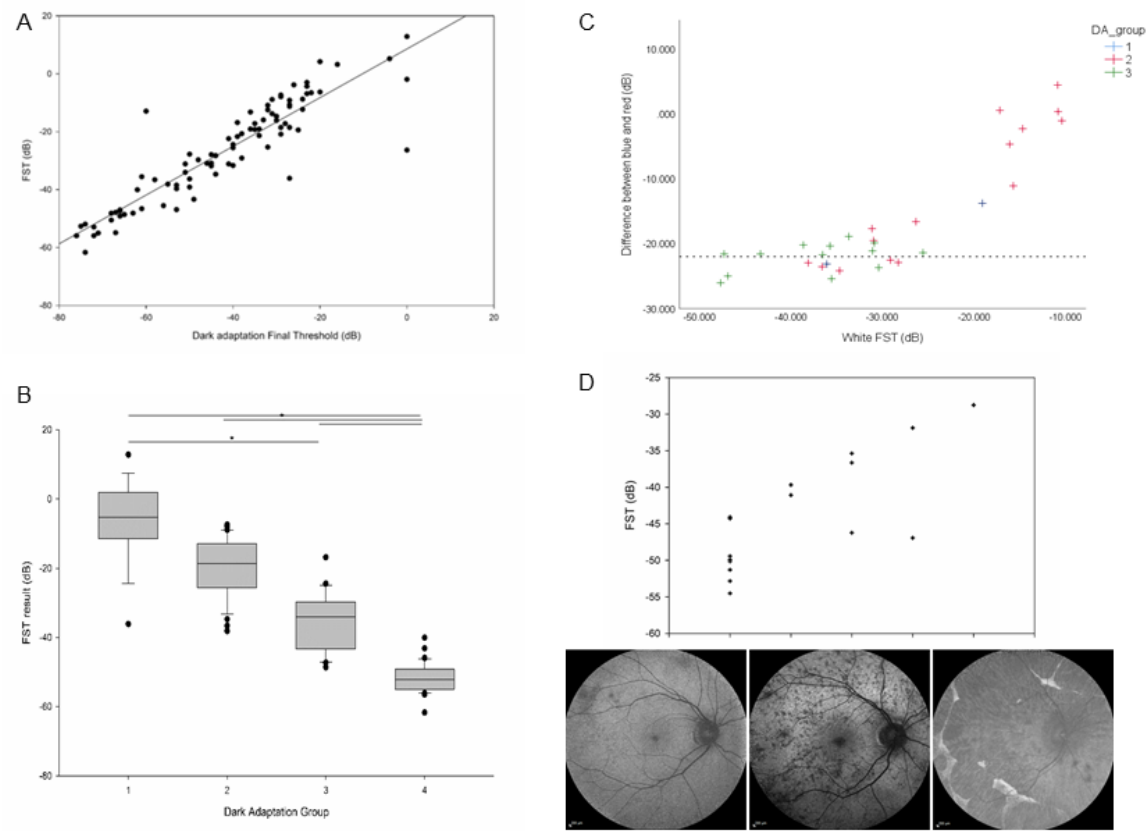


Figure 3-5: (A) Pearson correlation between the final dark adaptation threshold and FST result. (B) FST results in the eyes shown in the groups from Figure 3.4 with the addition of a control group (group 4) for reference. Lines and stars denote statistically significant differences ($P \leq 0.05$. (C) Relationship of white FST measurement with the difference between blue and red sorted by group (colours). The dotted line indicates the change from a rod mediated response to a mixed rod – cone response. Values below the line are rod mediated. (D) FST results in female carriers with a pictorial representation of the correlation with phenotype.

3.3.4.3 Retinal AF area influences FST measurement in disease

I probed the FST with AF area to understand the relationship of FST with the remaining retina (Figure 3.6 A). There is a strong regression with log area (R = 0.79, coefficient = -15.0 [-12.2 - -17.7], P < 0.01) indicating a 15 dB increase (drop in sensitivity) with each log unit reduction in retinal area. When examining the raw data, however, there were several examples of similar AF area associated with differing FST values (Figure 3.6).

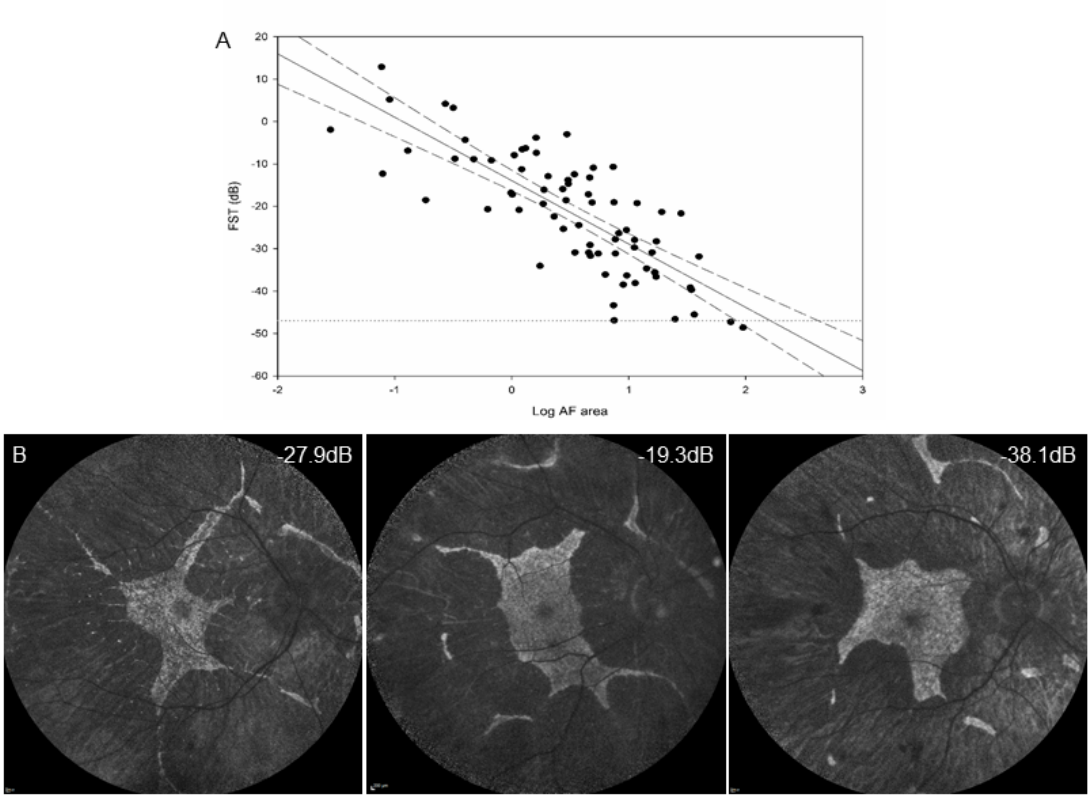


Figure 3-6: (A) Relationship between remaining log retinal % area as measured on blue fundus autofluorescence (AF) and FST measurement. The grey dotted straight line denotes the lower limit of normal for FST. The dashed lines are the 95% confidence intervals around the solid regression line. (B) Examples of eyes with the same preserved AF area (11%) showing differing FST outputs and differing patterns of AF preservation.

3.3.4.4 Factors affecting FST measurement

In order to understand the factors affecting the FST measurement, the control data were analysed for differences between males and females, as well as changes with age. There were 18 male controls and 17 female controls. An unpaired t-test did not show any difference between genders ($P = 0.85$). Regression analysis of FST results with age showed a decrease in sensitivity (increase in threshold) with age at a rate of 0.11 dB per year (95% confidence interval -0.06 – 0.11 dB per year). However, this relationship was not statistically significant ($r = 0.33$, $P = 0.06$).

3.3.5 Discussion

Dark adaptation following a light bleach becomes slower and shallower with disease severity. This process starts from the initial stages indicating a slowed response in cones as well as rods. The collinearity detected between the initial (cone adaptation), α (rod-cone break) and final threshold are indicative of the interconnectivity between photoreceptors within the retina. Cone and rod circuitry can modulate each other as shown in Figure 3.2. However, cones also appear to carry rod signals directly which may explain the link between all three thresholds (Schneeweis and Schnapf 1995). This may also explain how cones contribute to vision in low light without relaying colour vision information. The visual system adapts very quickly, reaching the ability to see in moonlight in around 3.5 minutes in control eyes, but longer in patient eyes.

Deviations from S2 shape indicate reduced levels of available 11-*cis* retinal, thereby altering the kinetics of the response (Lamb and Pugh 2004). Although the *REP1* gene is not a direct component of the phototransduction cascade, it does appear to have a disruptive effect on this process. The rods rely on RPE for this process. Although cones have an alternative pathway via Műller cells, the reduced sensitivity in the disruption in the primary pathway may be enough to disrupt sensitivity without affecting detailed vision (Ward et al. 2020).

FST is a good indicator of the severity of dark adaptation abnormalities and visual recovery under scotopic conditions, and allows classification of patients along the disease severity index. FST results in female carriers provide support for the degree of remaining retina influencing the FST measurement. Further evidence for the importance of the remaining retina comes from the strong relationship of FST to the AF island size in patients. However, the location of the remaining retina and hence density of remaining photoreceptors is also likely to have an influence on the measurement. Previous work on localised dark adaptometry within a rod rich region versus a cone rich region has shown the characteristics of the curves are different in these

regions, supporting this hypothesis (Tahir et al. 2017). I am exploring this further by looking at the location of the remaining retinal islands in addition to the size of them.

Measurement of FST with a white light is unable to tease apart the individual rod and cone components to the response. In order to do this, FST must be measured with red and blue lights separately. The response to white light does, however, provide information about function of the visual system as a whole, which may better reflect real world function. We know that cone function is affected early in the disease process (Jolly et al. 2015), and therefore night vision problems may be a reflection of combined rod and cone functional disturbance. In response to rod cell death, rod bipolar cells alter their synaptic tree and create aberrant connections with other photoreceptors (Wang et al. 2019). As shown in Figure 3.2, the rod and cone systems influence each other. The aberrant bipolar interactions may further confuse the network, resulting in rod disease impacting on cone function at a post synaptic level.

FST did not differ between males and females, nor show a significant change with age. The latter result is in contrast to previously reported changes in dark adaptation characteristics with age (Jackson, Owsley, and McGwin 1999). This could be because i) ageing changes are too subtle for detection with FST, ii) the age range of the participants was not wide enough, or iii) the sample size was too small. Age changes may need to be considered for long-term longitudinal studies.

3.3.6 Future directions

In order to answer the question about whether rod density is critical to the measurement of FST, work is currently ongoing to assess estimated density of remaining rods and cones within the remaining AF islands. This is using previously published histology data as a template in order to probe the relevance of AF island location as well as size to FST values measured, particularly in

view of the discussion around whether the FST response is driven by central or whole retinal areas (Roman et al. 2005; Collison et al. 2014).

3.3.7 Novel findings

The FST provides a useful marker of scotopic function following a period dark adaptation. It is able to predict the degree of difficulty of dark adaptation using a shorter, more user friendly test paradigm. The degree of FST reduction is reflective of the extent or functional retinal tissue loss.

3.3.8 Implications for clinical practice

The FST is a useful outcome measure for global scotopic function, particularly in low vision patients. It can be used as a proxy for the dark adaptation curve.

3.4 Scotopic visual fields

3.4.1 Abstract/summary

Scotopic microperimetry can be undertaken with the S-MAIA (Centervue, Padova. Italy) and allows assessment of localised changes to scotopic rod and cone function. This study forms an exploratory study to investigate the feasibility of use of the S-MAIA in a population of patients with rod-cone dystrophies and demonstrates the pattern of loss in both rod and cone function.

3.4.2 Introduction to scotopic perimetry

Dark adaptometry and FST measurement are useful as global measures of dark adaptation across the retina. In early disease or following interventional therapies it can be useful to understand the localised changes in the central retina. Two-colour perimetry has been used to investigate the

relative contributions of rods and cones under multiple light conditions (Simunovic, Moore, and MacLaren 2016; Jacobson et al. 1986; Massof and Finkelstein 1979; Fraser et al. 2016). These showed that to differentiate between rod and cone contributions to vision, both the stimuli and background need to be manipulated appropriately. Using spatial information allows the pattern of loss to be detected which can provide information into disease processes (Owsley et al. 2000).

The MAIA device has been updated and is now capable of performing scotopic testing in addition to mesopic testing, known as the S-MAIA (Centervue, Padova, Italy). For a clinical trial setting, the ability to use an existing FDA approved device makes it more likely that the results will be more widely understood and accepted. The S-MAIA utilises cyan stimuli (505 nm) and red stimuli (627 nm) with the difference calculated between them. The original version had a reduced dB range of testing under scotopic testing, but this has since been expanded to the full 36 dB in all conditions in order to remove ceiling effects. However, the dB scale used for scotopic tests is not directly comparable to the mesopic tests as it utilises the scotopic candela/m^2 scale. Both the cyan and red stimuli are thought to be rod-mediated in healthy observers outside of the central retina, which features the rod-free zone. The expected cyan-red-sensitivity difference would be 0 dB given the employed scale (Pfau, Lindner, Fleckenstein, et al. 2017). Since the dark-adapted cone sensitivity is close to the rod sensitivity for the red long wavelength stimulus, isolated rod-dysfunction is characterised by a predominant loss of scotopic cyan sensitivity, resulting in negative cyan-red sensitivity differences (Roman et al. 2005; Pfau, Lindner, Steinberg, et al. 2017; Heeren et al. 2019). The S-MAIA has been used in the investigation of age-related macular degeneration but has not to date been used in patients with rod-cone dystrophies (Pfau et al. 2019; von der Emde et al. 2019).

3.4.3 Methods

As this was an exploratory study, a group of patients with a clinical diagnosis of rod-cone dystrophies were recruited. The patients had a variety of genotypes and phenotypes. Patients had normal to mild VA loss to ensure they were able to conduct the test. The Health Regulatory Authority granted ethical approval for the study (REC reference 18/WM/0086). Each patient underwent ETDRS visual acuity testing, a training test under mesopic conditions, mesopic microperimetry using the scotopic testing grid with 5 minutes adaptation (Han et al. 2018), FST testing following 45 minutes dark adaptation and scotopic MAIA testing following a further 45 minutes dark adaptation. Breaks between periods of dark adaptation were provided to improve reliability. A dark adaptation period of 45 minutes was chosen based on the results of section 3.3.4.1 to allow the maximum number of individuals to reach peak sensitivity. The participants were randomised to FST or scotopic MAIA via a pre-set order to account for fatigue effects (Figure 3.7). S-MAIA (Centervue, Padova, Italy) testing employed cyan and red lights with wavelengths of 505 and 627 nm respectively. Cyan testing was completed three times followed by three red tests with a recovery period of at least 3 minutes between each test to allow calculation of repeatability. All follow up tests were conducted using the follow up function to ensure consistency of points being tested. The grid chosen consisted of 37 points and covered the central 10 degrees to include the region of retina where rod density begins to increase.

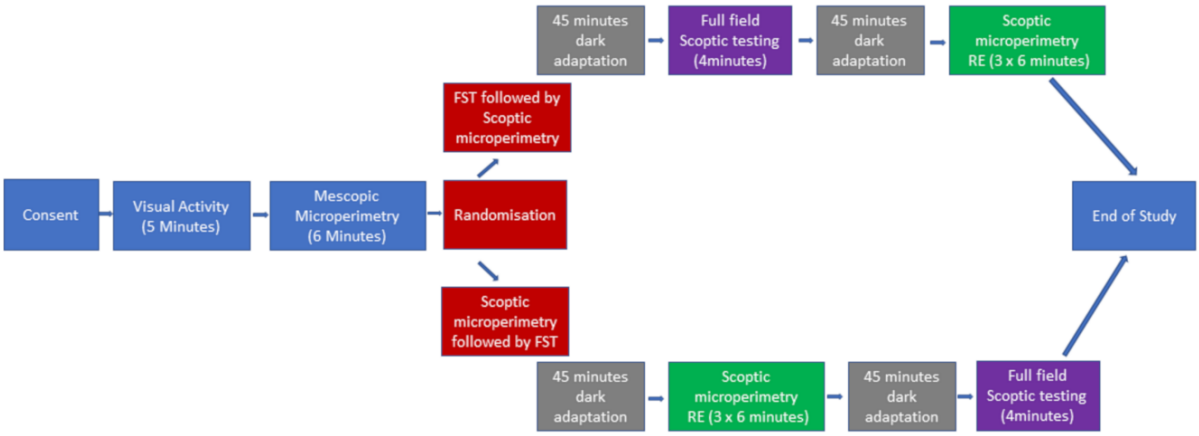


Figure 3-7: Flowchart of study assessments.

All assessments were conducted on the right eye only to avoid fatigue. Adjustment for bilateral testing was therefore not required. Detailed SOPs are provided in Appendix 1. A Bland-Altman analysis was conducted comparing test 1 and test 2 followed by test 2 and test 3. The groups were compared for each parameter using the Mann-Whitney U test with Bonferroni correction for multiple comparisons. All statistical analyses were conducted in SPSS (version 25.0, IBM Software, New York, USA). In order to explore the spatial patterns results were amalgamated across subjects in patient and control groups and interpolated plots created using MATLAB (version 2018a, The MathWorks, Natick, MA).

3.4.4 Results

Twenty patients with clinically confirmed rod-cone dystrophies and thirteen age-matched control participants were recruited. One patient could not perform any of the testing due to poor vision and was excluded from the cohort. Subject demographics and summary results of the participants completing the study are shown in Table 3.3. For cyan-red differences, a greater degree of negativity would point towards greater rod dysfunction.

Measure	Patient eyes	Control eyes
Age (years)	47.7 [27 – 77]	48.0 [26 – 81]
Female / male	7 /12	7 / 6
Visual Acuity (letters)	78 [48 – 90]	84 [76 – 93]
Mesopic MAIA threshold (dB)	11.7 ± 9.3	26.6 ± 1.5
Scotopic cyan threshold (dB)	6.1 ± 7.5	21.1 ± 4.9
Scotopic red threshold (dB)	9.2 ± 6.7	21.8 ± 3.4
Difference between cyan and red (dB)	-3.2 ± 4.9	-1.2 ± 1.1
Full field Stimulus Threshold (dB)	-27.3 ± 14.0	-51.7 ± 5.1
S-MAIA repeatability		
BA limits of agreement tests 1 & 2 cyan (dB)	4.89 to -4.86	2.13 to -0.85
BA limits of agreement tests 2 & 3 cyan (dB)	2.48 to -2.00	1.39 to -1.39
BA limits of agreement tests 1 & 2 red (dB)	5.71 to -3.67	1.89 to -1.25
BA limits of agreement tests 2 & 3 red (dB)	3.32 to -3.56	1.94 to -1.56

Table 3-3: Subject demographics and summary results, including repeatability analysis. Data are presented as mean [range] or mean ± standard deviation. BA = Bland-Altman.

3.4.4.1 Repeatability

Repeatability analysis of the mean threshold (Table 3-3) shows that the limits of agreement reduced between test 2 and 3 compared to the first two tests, indicating the first test acts as a learning experience for both colours. The limits of repeatability were wider in the patient population compared to the control population (Table 3.3). This difference appears to be clinically significant, particularly for the red stimulus.

3.4.4.2 Group comparisons

The data in each group are presented in Figure 3.8. The second S-MAIA values were used for statistical analyses. VA was not significantly different between groups (P = 0.07) but

microperimetry threshold for mesopic, cyan and red stimuli, as well as FST were significantly different between groups ($P < 0.01$).

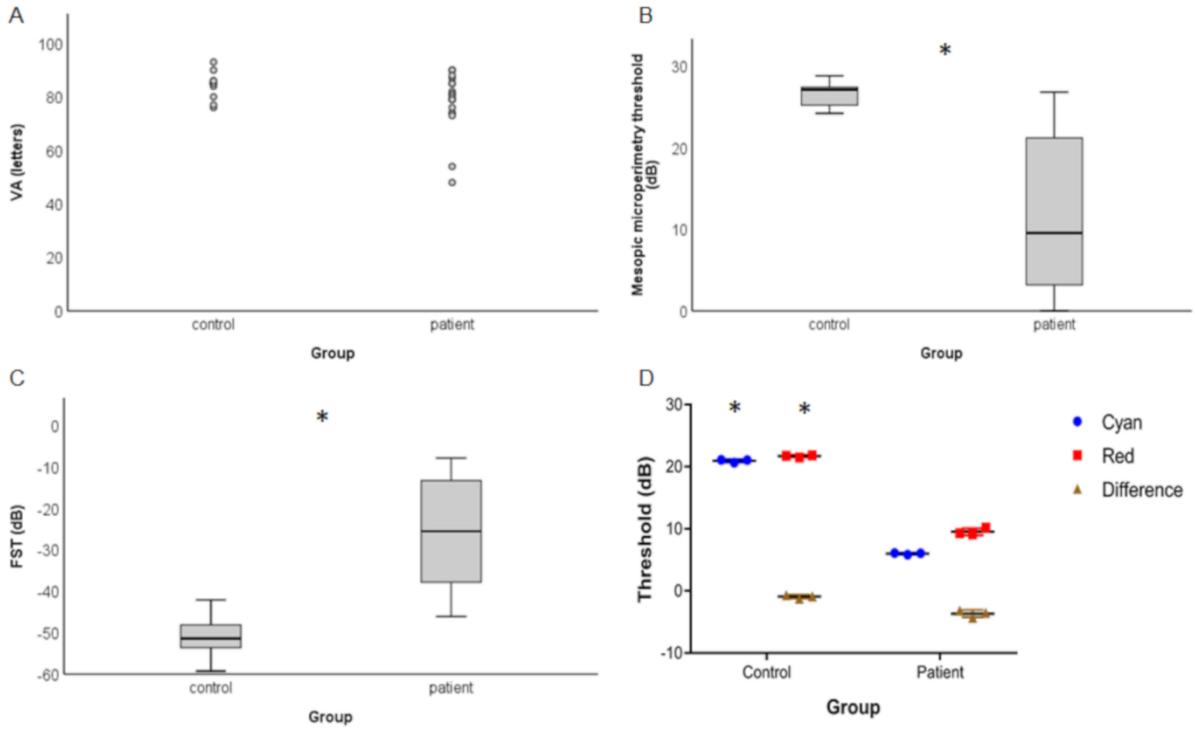


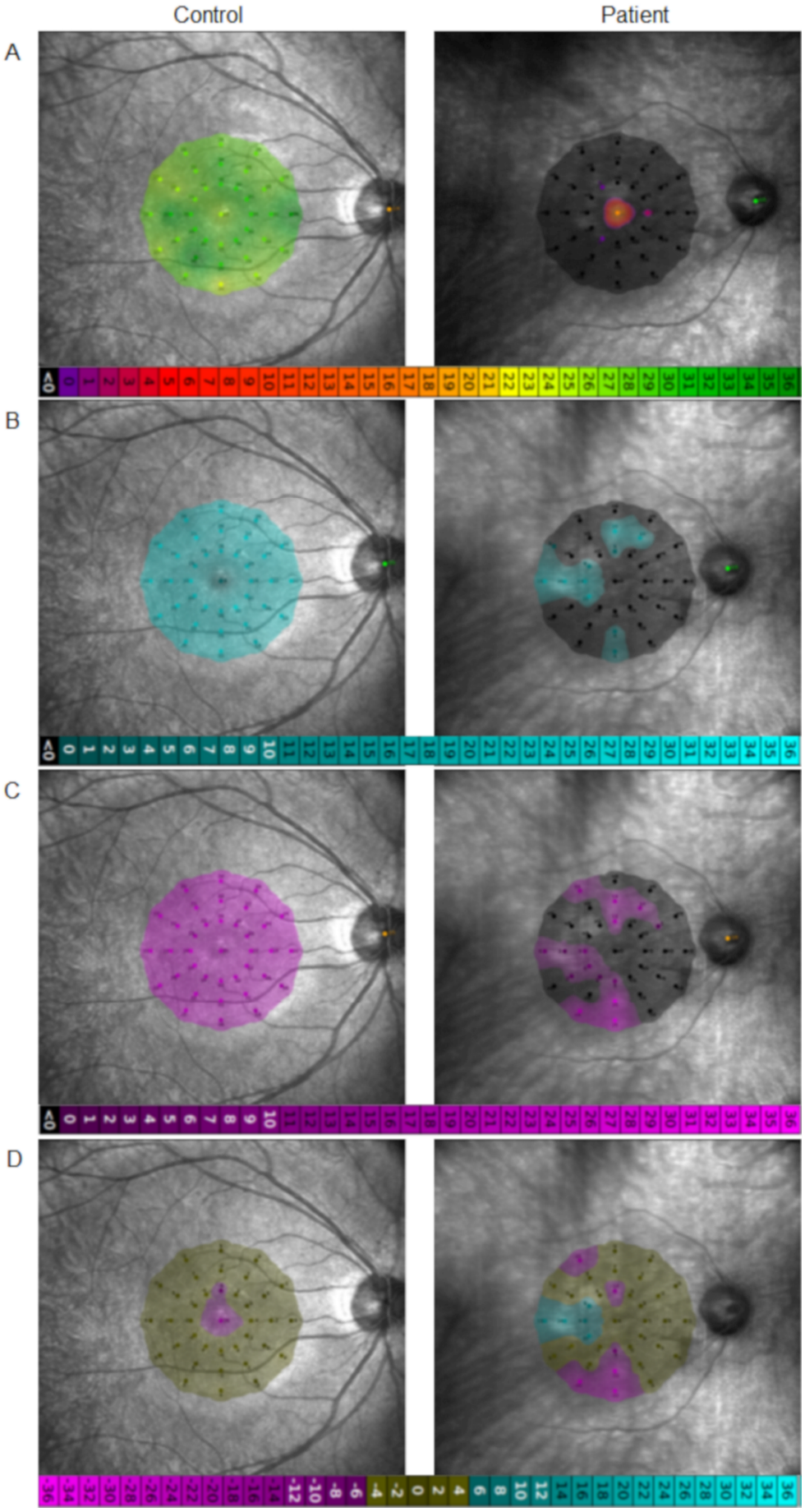
*Figure 3-8: (A) Raw VA measures for each individual in the control and patient groups. Boxplots of mesopic microperimetry threshold (B) and FST threshold (C) showing median, interquartile range and full maximum and minimum of datasets. (D) shows the mean of each S-MAIA test conducted with cyan and red stimuli with the difference between the tests shown for each group. * denotes statistically significant difference between groups ($P < 0.01$).*

3.4.4.3 Spatial differences

Typical examples of test results from a control (on the left) and patient (on the right) eye are shown in Figure 3.9. The mesopic maps show normal function across the field in the control eye compared to a small central island in the patient eye. The cyan map shows a central scotoma in the centre related to the rod free region. The patient eye shows several regions with no apparent rod function. On the red maps, the control eye shows a uniform ability across the visual field, whereas the patient eye has patchy loss of scotopic cone function, which does not match the cone function loss under mesopic conditions. The difference map shows a central cone dominated

region as would be expected due to the rod free foveal zone. The patient eye shows different areas of dominance for rods and cones. The brown can represent either total loss with both colours, or a healthy balance between rod and cone function.

Figure 3-9: Typical results from the S-MAIA for an example control (left) and patient (right) eye. (A) Mesopic microperimetry is normal in the control eye, small central island of remaining vision in the patient eye. (B) Scotopic cyan testing (505 nm). A small rod free zone can be seen in the control eye, patches of remaining rod function are present in the patient eye. (C) Scotopic red testing (627 nm) shows patches of function in the patient eye. (D) Difference between cyan and red shows rod free zone in the centre in the control eye. The patient eye has patches that are rod dominated (blue) and have rod degeneration (red). The brown areas can be balanced between rods and cones, or show areas with loss of both.


Control
Patient
A
B
C
D

Interpolated group averages were plotted against the original colour schemes for each test type (Figure 3.10). Mesopic testing shows all points within the normal range with highest sensitivity at the central foveal point. The patient results show a marked generalised depression across the visual field with relative central preservation. Scotopic testing with cyan stimuli (rod function) reveals a central depression denoting the rod free region in the control eyes. Sensitivity increased with increasing eccentricity. As expected, the patient population also showed the rod free zone. While function was depressed across the field, the greatest depression was in the periphery with relative preservation around 2.5 degrees. This coincides with the region in which rod density begins to sharply rise (Curcio et al. 1990). The difference plots reveal a cone mediated fovea in the control eyes surrounded by a balance between rod and cone mediated vision. The patient eyes have a larger zone of cone-mediated vision. Severe loss of both rod and cone function can result in a difference of 0 so the brown areas are uninformative in this case.

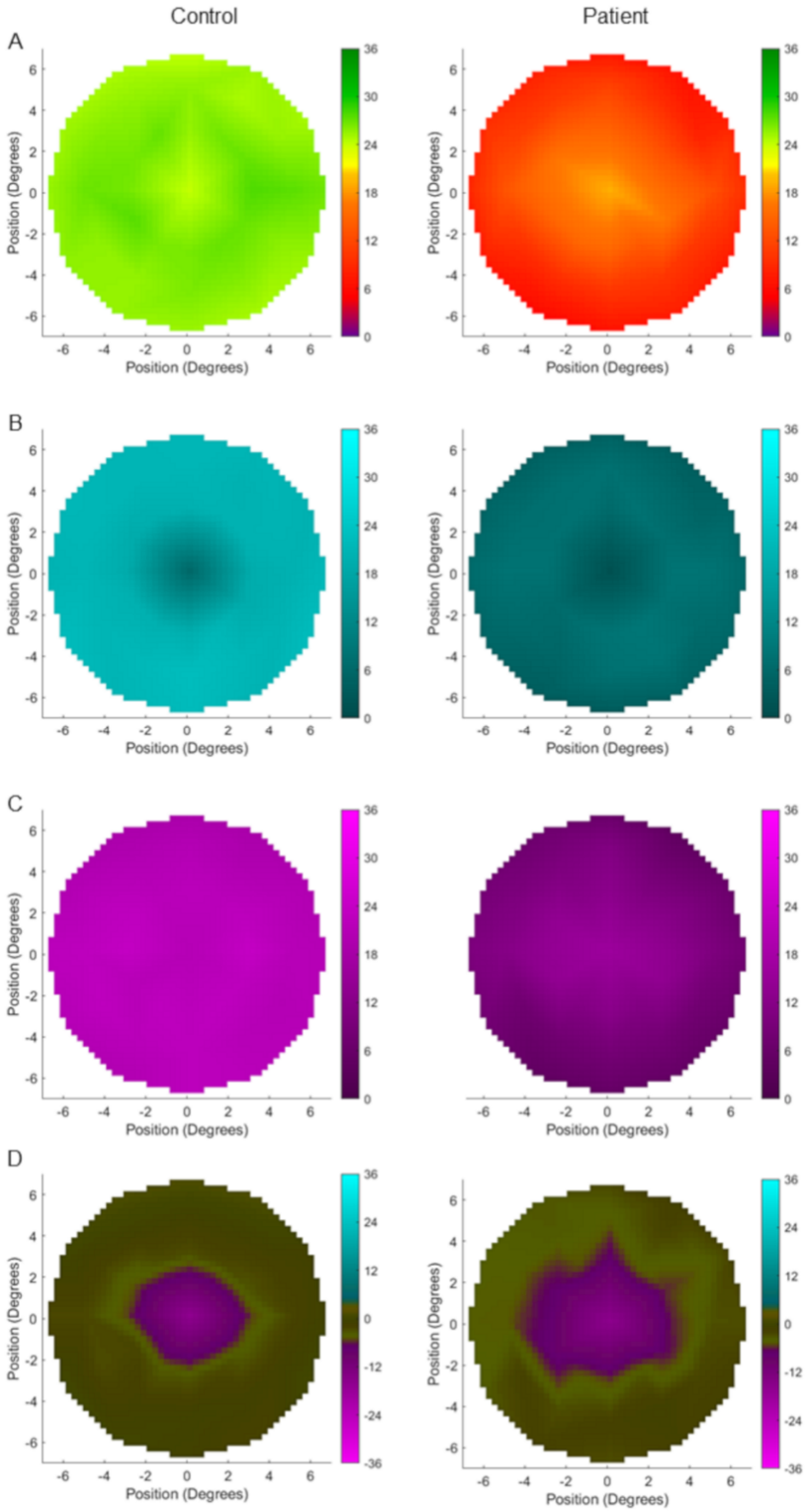


Figure 3-10: Pointwise averages represented as microperimetry spatial maps. The colour bar represents the threshold colour scale (dB) for each plot. Control group represented on the left and patient group represented on the right. (A) Mesopic microperimetry. (B) Scotopic cyan testing (505 nm). (C) Scotopic red testing (627 nm). (D) Difference between cyan and red.

3.4.5 Discussion

The repeatability assessment of the S-MAIA shows a larger coefficient of repeatability between test 1 and test 2 compared to between test 2 and test 3. This learning effect with the first test is in keeping with the pattern previously reported for mesopic microperimetry and indicates that the first test should be discarded (Z. Wu et al. 2013a). The repeatability measures reported here between test 1 and test 2 are lower than those reported previously (Pfau, Lindner, Fleckenstein, et al. 2017; Welker et al. 2018). However, many of the participants in this study were not perimetry naïve, thereby reducing the learning effect. Additionally, all participants underwent a training field under mesopic conditions prior to starting the study assessments.

All microperimetry assessments, as well as FST, were able to differentiate between the rod-cone dystrophy and control groups. The scotopic testing was able to provide information about the balance of rods and cones over the central 12 degrees using a 37 stimuli grid. This provided additional valuable information not provided by the FST, particularly in early disease. Examining S-MAIA in different types of genetic mutations may provide further information about how rod and cone loss occurs in these circumstances.

3.4.6 Future Directions

For this study a period of dark adaptation of 45 minutes was chosen based on previous dark adaptometry evidence. However, this proves an onerous test burden on both patient and examiner. For rod function testing in electrophysiology, 20 minutes is considered sufficient to obtain reliable results (McCulloch et al. 2015). In view of the relationship between start and finish threshold during dark adaptation, the shorter adaptation time of 20 minutes may be sufficient to obtain reliable results. This comparison is currently being undertaken.

I have planned studies to examine patients with different types of genetic mutations. For example, genes which are part of the phototransduction cascade are likely to have a different

pattern of loss compared to genes that express in both rods and cones. The S-MAIA will allow investigation of spatial patterns of central cell loss in different conditions.

3.4.7 Novel findings

The scotopic MAIA allows examination of localised changes in rod function in the central retina. This is the first time rod-cone dystrophy patients have been evaluated with the scotopic MAIA.

3.4.8 Implications for clinical practice

The scotopic MAIA is most useful in patients with reasonable VA due to the difficulty of the test. It is effective at monitoring regions of photoreceptor loss within the central retina.

Chapter 4:
Retinal Remodelling

Papers arising: Inner retinal thickening affects microperimetry thresholds in the presence of photoreceptor thinning in patients with *RPGR* X-linked retinitis pigmentosa.

In peer review

My contributions to this chapter: I developed the concept and analysis pipeline. I wrote the MATLAB code for analysis and conducted both image processing and statistical analysis. I wrote up the study and interpretation. Data analysis and code writing took 4 months 2019-20.

Contributions to this chapter: Data were provided by Moreno Menghini. Aran Johal contributed to the segmentation of the OCT images as part of his supervised undergraduate project.

4. Retinal remodelling in photoreceptor disease

4.1 Summary

In the presence of photoreceptor death, the retina responds with a number of adaptive responses resulting in retinal remodelling. The significant structural changes can have implications for the measurement of visual function in interventional trials. A cohort of patients with X-linked retinitis pigmentosa secondary to a mutation in *RPGR* underwent OCT imaging (Heidelberg Spectralis) and microperimetry (MAIA) visual field testing of the central 10 degrees of retina. Accurate segmentation of the OCT images was performed using semi-automated software (Orion, Voxeleron LLC, Pleasanton, CA). Eccentricity analysis for 1, 3, 5 and 7 degrees of visual field was performed in MATLAB following centration of the OCT images over the fovea. This exploratory study shows that a thinner photoreceptor complex is associated with thickening in the inner retina. These changes are most marked in the central 1 degree where the thickness changes cancel each other out. Inner retinal changes maximally occur within the central 5 degrees, whereas photoreceptor thinning is present across the central 7 degrees. This shows that retinal remodelling occurs at different rates across the retina in the presence of photoreceptor disease. Visual field measurement is impacted by this retinal remodelling, with both photoreceptor thickness and inner retina thickness having a significant impact on microperimetry threshold.

4.2 Introduction to retinal remodelling

Retinal disease results in the death of photoreceptors. After dropout of the photoreceptors, there is much change in the structure of the retina. One aspect of particular interest is the significant change that occurs in the inner retina as this is secondary to what is occurring in the photoreceptors. The inner retina consists of a variety of neural cell types, critical to the

processing of light, visible on OCT as several layers. These cell types are the bipolar, amacrine, and horizontal cells as detailed in section 1.2.1.2. Several attempts at standardising the labelling of these layers have been conducted to match with what we know from histological findings (Staurenghi et al. 2014; Cruz-Herranz et al. 2016).

The top four bands of the OCT image represent the outer plexiform layer, inner nuclear layer, inner plexiform layer, and retinal nerve fibre layer (Figure 4.1). The outer plexiform layer denotes the first layer of synapses, thus bringing together spatial information from across the retina. The photoreceptors connect to the bipolar and horizontal cells. However, there is also evidence of cones carrying rod signals to the outer plexiform layer (Nelson 1997; Schneeweis and Schnapf 1995; Raviola and Dacheux 1990). The inner nuclear layer consists of cell bodies of bipolar, horizontal and amacrine cells. The connections between the bipolar axon endings and dendrites of the amacrine and ganglion cells occurs in the inner plexiform layer. There are multiple amacrine cell types, that are likely to have a variety of roles. They appear to be involved in the balance between inhibition and excitation, and creating feedback loops (Oesch and Diamond 2019). The final conduit between the eye and the brain are the ganglion cells. There are several different types of ganglion cells projecting to different layers of the lateral geniculate nucleus (LGN). The ganglion cells introduce sensitivity to different aspects of features of the visual stimulus, with this organisation being propagated along the rest of the visual system (Sanes and Masland 2015).

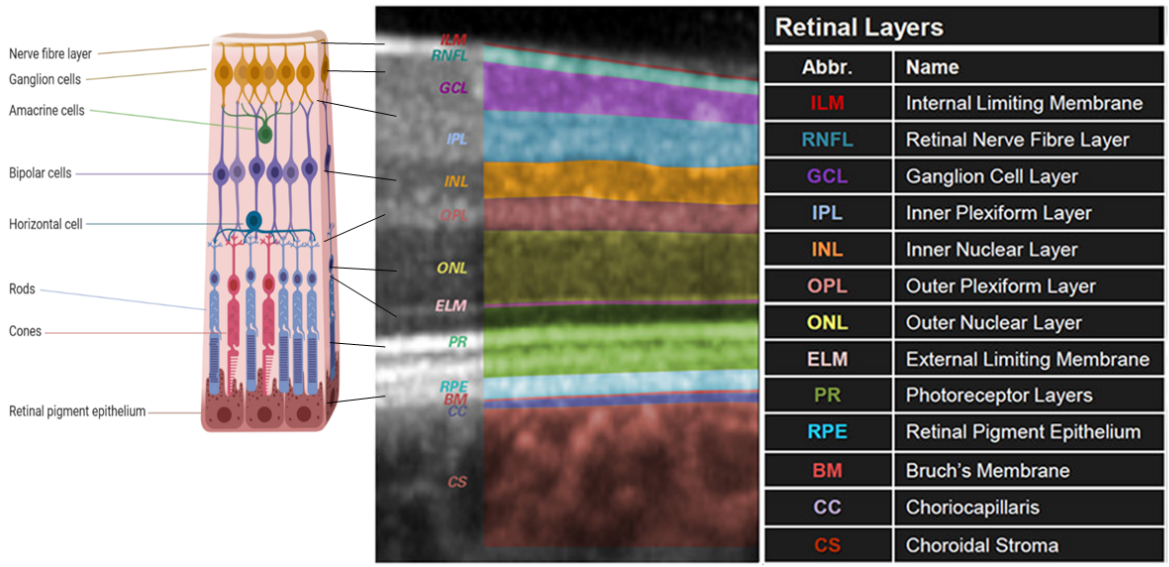


Figure 4-1: Indication of the cells likely contributing to each OCT layer. Image created from figure 1.1 and https://www.heidelbergengineering.com/int/news/know-your-retinal-layers-33401465/

The potential impact of retinal remodelling in inherited retinal diseases is the effect it could have on visual field testing, which is often a key outcome measure in clinical trials of novel interventions (Jolly, Bridge, and MacLaren 2019). Perimetry is affected by both photoreceptor density and ganglion cell density (Watson 2014). Therefore, physical reorganisation in either or both of these cell types may also contribute to the functional changes measured. Additionally, ganglion cells form many parallel pathways to carry the visual information from a range of cells in the inner retina (Kolb, Ralph, and Eduardo 1995). The visual processing starts at the level of the bipolar cells and therefore changes from this level must be considered for impact on the measurement of visual function.

Retinal remodelling has previously been reported in a variety of inherited retinal degenerations using a variety of methods. Some human studies have focussed specifically on ganglion cells and aspects of the inner retina around the optic nerve head and reported conflicting results (Hood et al. 2009; Fu et al. 2019). Other groups have used macular OCT scans and directly compared the inner retina to patterns of change in the photoreceptors. These have been based on indirect

processing of the reflectance profiles to infer the layer boundaries. The results in several rod-cone dystrophies, regardless of genetic cause indicate inner retinal thickening is associated with thinning in the outer nuclear layer. This effect appears to be maximal in the paracentral region, though the time course does change between subtypes (Aleman et al. 2007; Jacobson et al. 2009; Aleman et al. 2008; Jacobson et al. 2006).

Another approach adopted to investigate retinal remodelling is the use of computational molecular phenotyping and electron microscopy. This can only be conducted in animal models due to the requirement to sacrifice the eye. The advantage is the ability to look at a detailed view of cellular response of the remodelling process and provide a more detailed background. Remodelled retinas show abnormal wiring involving all neural cell types with remnant circuits as well as new synapses visible. However, the new synapses struggle to integrate with existing circuits in the eye. The process has been observed in a variety of retinal disease models. Interestingly, the cones do appear to have a protective effect against the remodelling process (Marc and Jones 2003). The same techniques have been used on both human and non-human primate donor eyes with rod-cone degeneration showing that reorganisation occurs continually throughout the disease process until the retina is no longer able to function visually and ultimately results in neuronal death (Jones et al. 2016).

There are now semi-automated algorithms available for the accurate segmentation of OCT data. For example Orion® by Voxeleron LLC (Pleasanton, CA, USA) has been validated against manual segmentation techniques (Seigo et al. 2012). By reducing the time taken for this step of post-processing, the whole image thickness can be feasibly analysed for different layers in patient cohorts to investigate the presence and significance of retinal remodelling. Many previous studies have focussed specifically on either the inner or outer retinal layers. Using Orion®, I was able to look at the same layers simultaneously at different eccentricities and relate these to the microperimetry sensitivity (MAIA, Centervue, Padova, Italy) in the central visual field. For this study, data from patients with X-linked retinitis pigmentosa due to a mutation in the *RPGR* gene

were chosen, as this is a photoreceptor specific mutation. This allows the impact on the inner retina which is secondary to photoreceptor disease to be studied.

4.3 Method

Optical coherence tomography (OCT) volume scans of the *RPGR* cohort were acquired between 2013 and 2019 on the Heidelberg Spectralis (Heidelberg Engineering, Heidelberg, Germany) following dilation. Scan field ranged between 30° x 15°, and 30° x 25°. Scan lengths were between 8.3 mm (768 pixels) and 10.4 mm (1536 pixels) with a lateral resolution of 5.64 to 12.53 µm/pixel. The axial resolution was 3.87 µm/pixel for all scans analysed. The average (±SD) automated real-time averaging (ART) was 8 (± 2) images per retinal location. OCT volume scans of the healthy controls acquired in 2017 were all 30 x 15° with a length of 8.5 mm (768 pixels) and an axial resolution of 3.87 µm/pixel.

Layer definitions were based on the APOSTEL recommendations (Cruz-Herranz et al. 2016). Total retinal thickness was defined as the thickness from the internal limiting membrane to Bruch's membrane. The inner retina was defined as the internal limiting membrane to the outer surface of the outer plexiform layer. The photoreceptor complex was the sum of the outer nuclear layer (inner segments) and photoreceptor outer segments, defined as the inner border of the outer nuclear layer to the inner margin of the RPE/Bruch's band (Figure 4.2 A). The automatic layer segmentation function was used on the Orion® software with further optimisation using the intelligent editor. The output was saved as a CSV file with thickness measurements at each pixel in each slice for the individual layers.

I chose to analyse the photoreceptor complex for defining photoreceptor damage instead of analysing the inner and outer segments separately for two reasons. Firstly, there is controversy around the exact border definitions with OCT imaging. Secondly, previous studies investigating visual field sensitivity have in turn used either inner or outer segment thickness. It is not known

how each part of the photoreceptor impacts the function of the cell. The outer segments contain the opsin to detect photons of light, and retinal for phototransduction. Inner segments contain the cell machinery for functioning so both segments are required for the photoreceptor to be fully functioning. Therefore, looking at the inner and outer segments together allows me to overcome both the methodological difficulties and capture the net effect of the photoreceptor.

The output from the Orion® was imported into MATLAB (version 2018a, The MathWorks, Natick, MA). The layers of interest were defined and thickness values summed at each location as appropriate. The central foveal location was recorded from Heidelberg Eye Explorer and calculated into pixel position. This was set as the central point of the data for further analysis. A circle of varying radial eccentricities (1, 3, 5 and 7 degrees) was created around this centre point and the average thickness within this circle was calculated for different eccentricities as shown in Figure 4.2 B. Each image was scaled to account for the magnification used at image acquisition.

Microperimetry was conducted with the MAIA (Centervue, Padova, Italy) with a 10-2 grid. The raw data were exported into MATLAB and processed in a similar way to above with threshold values obtained at 1, 3, 5 and 7 degrees radial eccentricity. All eyes tested had the grid centred on the fovea so the centre of the grid was used for the foveal point in the eccentricity calculation. Data from the left eye was transposed into the same plane as the right eye. The relationship between the inner retina and photoreceptor complex and microperimetry threshold was explored using a multiple linear regression model. All statistical analyses were conducted in SPSS (version 25.0, IBM Software, New York, USA).

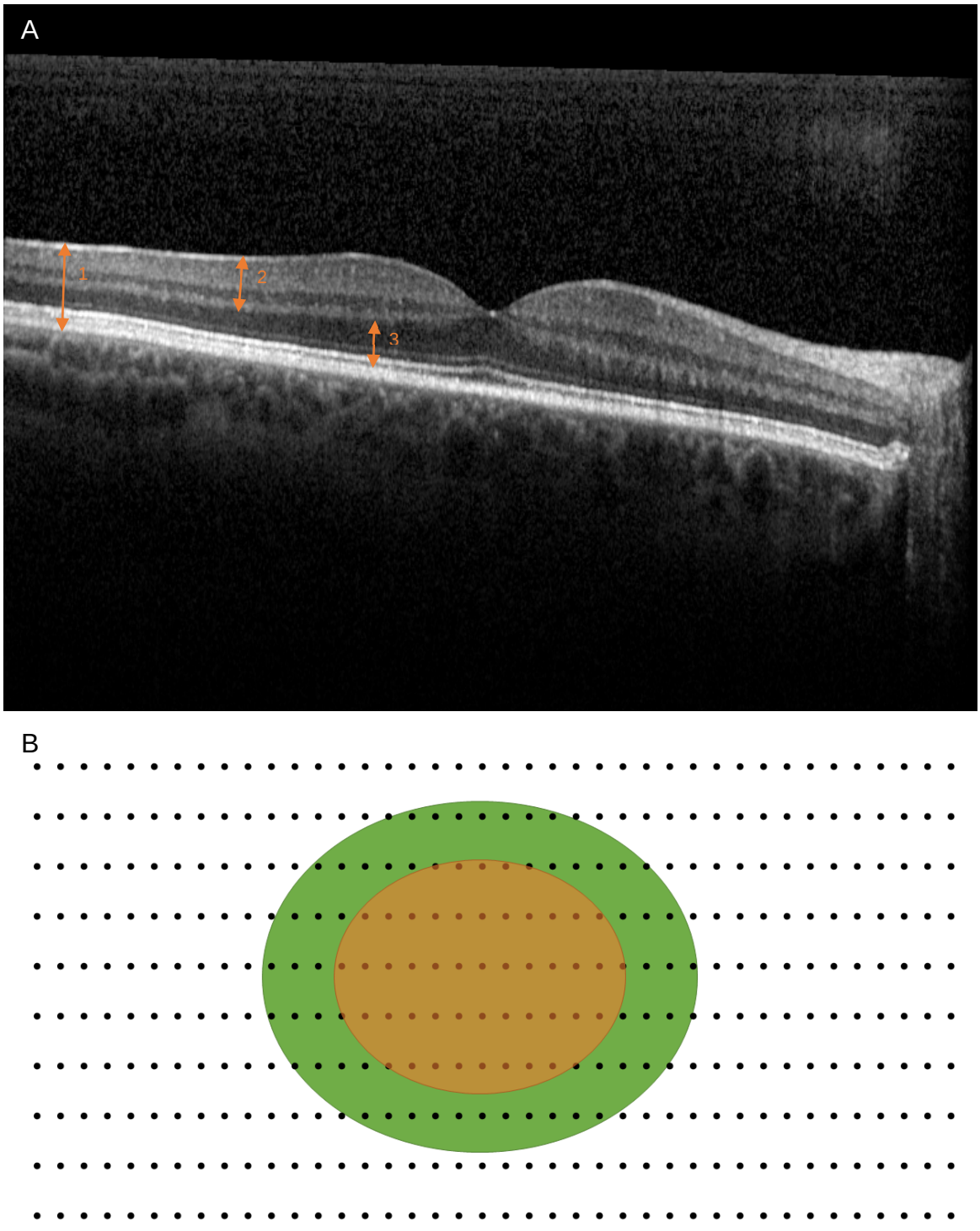


Figure 4-2: (A) Layer definitions used for further analysis. 1 = total retinal thickness; 2 = inner retina; 3 = photoreceptor complex. (B) Demonstration of method used for eccentricity calculations. Each dot represents a thickness measurement at each pixel. The circles represent zones used for calculation of average thickness at 2 different eccentricities.

4.4 Results

4.4.1 Retinal Thickness

Patient demographics are presented in Table 4.1. Twenty-one eyes from 12 patients with RPGR were examined, with 18 eyes from nine control patients. Qualitative analysis of retinal thickness shows different patterns of retinal organisation in the disease eyes compared to the control eyes. Figure 4.3 shows the retinal configurations for an eye with mild and severe disease against an age-matched healthy eye. The eye with mild disease shows a thinning of the photoreceptor complex, with concurrent thickening of the inner retina. The eye with severe disease shows overall retinal thinning, with photoreceptors being eradicated. It also has greater thickening of the inner retina. A summary of the retinal thickness measurements is shown in Table 4.2 and Figure 4.4.

Group	**Age (years)**	**Visual acuity (logMAR)**	**Scan focus (D)**	**Microperimetry threshold (dB)**
RPGR	28.8 (15 -52)	0.15 (0.00 – 0.48)	0.00 (-5.5 - +3.38	10.1 (0.6 – 21.0)
Control	26.7 (21 – 42)	N/A	-0.56 (-2.81 - +1.78)	N/A

Table 4-1: Subject demographics. All values are presented as mean with the range in brackets.

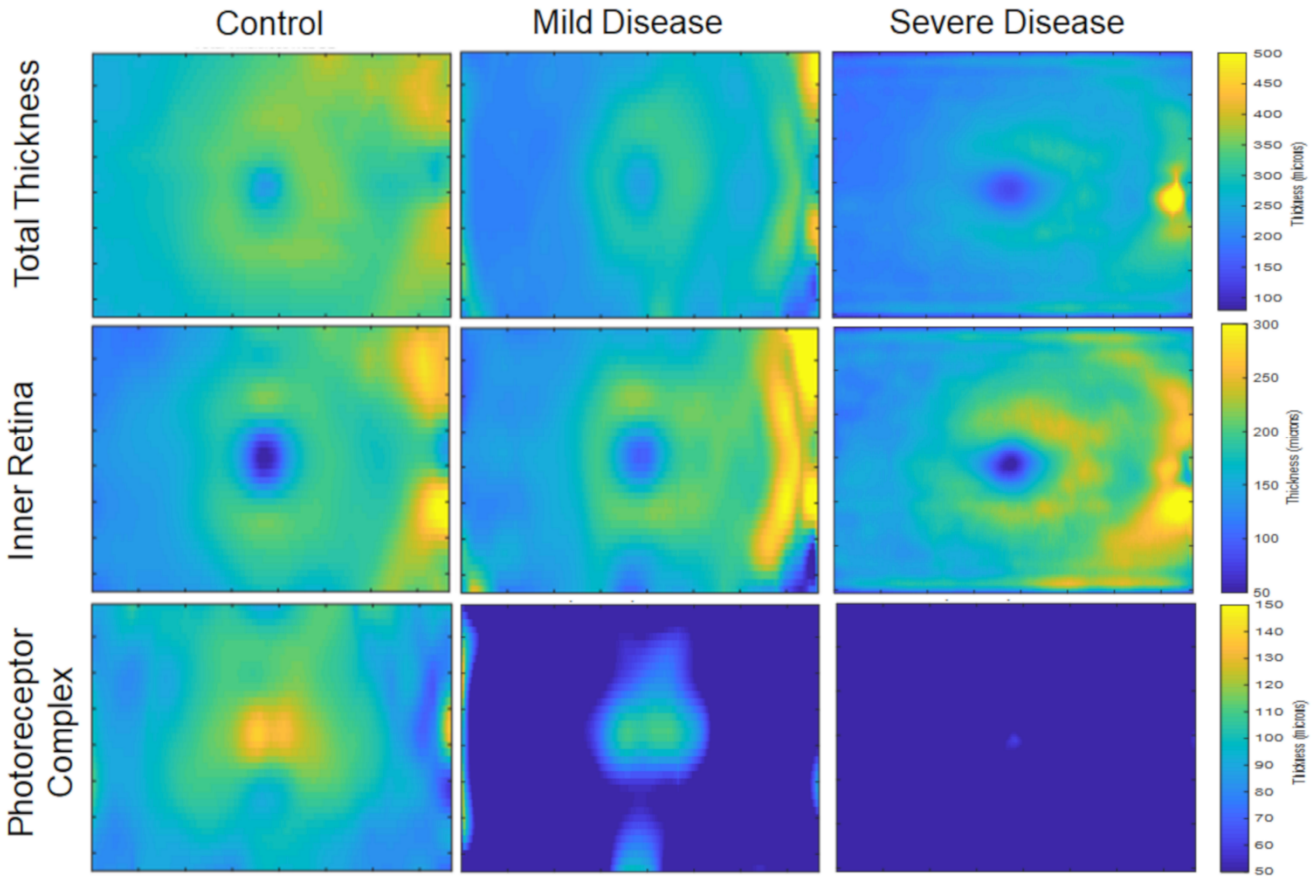


Figure 4-3: Demonstration of retinal remodelling. Sample thickness measurements from representative eyes from the control, mild and severe disease groups. Thickness measurements are shown for total thickness, inner retina and the photoreceptor complex.

Eccentricity	Layer	RPGR group OD	Control group OD	RPGR group OS	Control group OS
1 degree	Total thickness	233.05 ± 38.93	262.73 ± 19.77	224.12 ± 64.24	259.32 ± 19.20
	Inner retina	138.58 ± 74.99	61.82 ± 13.91	136.06 ± 65.29	57.03 ± 15.42
	Photoreceptor complex	95.86 ± 34.24	139.30 ± 14.72	87.26 ± 41.76	141.83 ± 5.53
3 degrees	Total thickness	279.45 ± 40.40	324.69 ± 17.44	267.24 ± 55.73	323.55 ± 15.95
	Inner retina	195.55 ± 63.58	144.08 ± 7.43	191.32 ± 47.38	142.88 ± 10.99
	Photoreceptor complex	83.50 ± 25.78	126.49 ± 10.58	73.59 ± 29.91	127.20 ± 4.73
5 degrees	Total thickness	294.96 ± 36.76	352.38 ± 14.66	279.79 ± 50.74	352.03 ± 13.89
	Inner retina	217.87 ± 56.65	182.26 ± 7.97	211.49 ± 37.35	181.34 ± 8.99
	Photoreceptor complex	74.29 ± 21.49	119.39 ± 8.37	65.11 ± 27.49	119.69 ± 5.18
7 degrees	Total thickness	290.65 ± 34.30	355.78 ± 12.00	274.83 ± 48.03	355.94 ± 12.26
	Inner retina	218.47 ± 50.44	192.15 ± 7.14	211.34 ± 31.40	191.46 ± 7.13
	Photoreceptor complex	67.26 ± 19.33	114.60 ± 6.99	59.07 ± 23.93	114.61 ± 5.11

Table 4-2: Summary of layer thickness measures (µm) across different eccentricities of the retina.

Differences between groups were assessed using the Kruskal-Wallis one-way ANOVA. Each layer range of the retina was assessed independently, and within layers Bonferroni correction for multiple comparisons was conducted. The pattern of difference between patient and control groups varied between layers, providing an insight into the impact of pathology. The photoreceptor complex was significantly thinner in patients compared to controls ($P < 0.01$) at all four eccentricities. The inner retina was significantly thicker in the patients compared to the controls ($P < 0.01$) for the central 1 and 3 degrees. The combination of these changes resulted in the difference between groups for total thickness for 3, 5 and 7 degrees ($P < 0.01$) but not in the central 1 degree ($P = 0.91$).

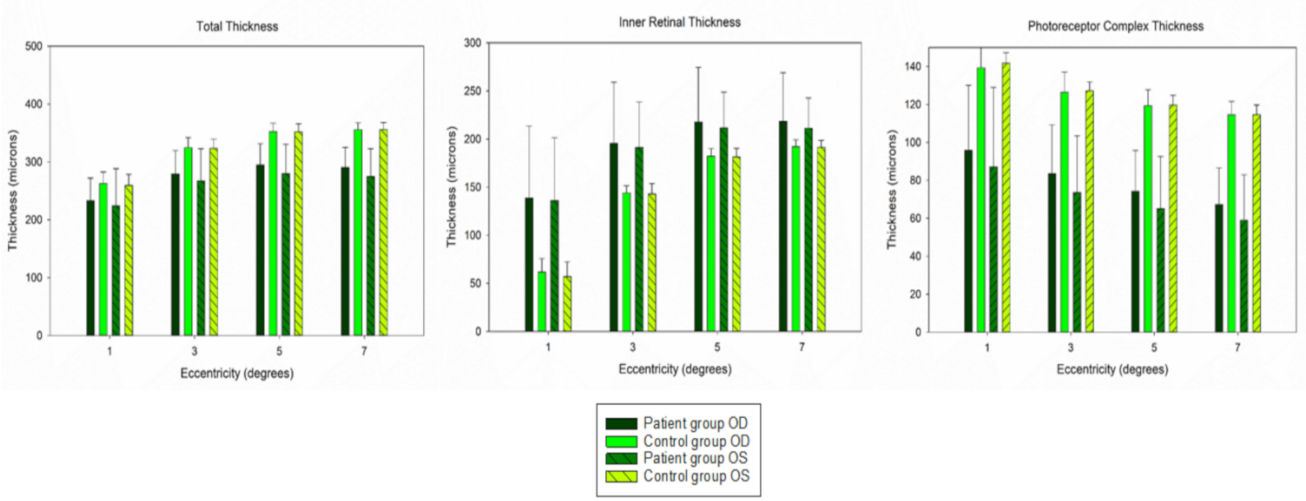


Figure 4-4: Summary of thickness measurements from table 4.2 for total thickness, inner retinal thickness and photoreceptor complex thickness at different eccentricities. Patient group in darker colours and control group in lighter colours. The right eye (OD) is represented by plain filled bars and left eye (OS) represented by the bars containing lines. The error bars show standard deviation.

4.4.2 Relationship with Visual Field

A multiple linear regression analysis was performed to explain microperimetry threshold in terms of visual field area covered, inner retinal and photoreceptor complex thickness (Figure 4.5). All assumptions required for regression analysis were checked and met. Namely linearity, independence, homoscedasticity, multicollinearity and normality of the residuals. The R^2 value showed that the model explained 91.3% of the microperimetry threshold results with those 3 factors. Photoreceptor thickness has a coefficient of 0.15 (95 % CI 0.13 to 0.18) µm thickness per dB threshold, t = 12.26, P < 0.01. Inner retinal thickness has a coefficient of 0.05 (95 % CI 0.03 to 0.06) µm thickness per dB threshold, t = 5.98, P < 0.01. Visual field extent has a coefficient of -1.48 (95 % CI -2.02 to -0.95) degree per dB threshold, t = -5.50, P < 0.01. Both changes in the inner retinal thickness and photoreceptor complex thickness affect microperimetry threshold, and the degree of change varies with eccentricity. Figure 4.5B demonstrates this correlation in an example eye. Photoreceptor thinning and reduced microperimetry threshold occur in the same areas but are not perfectly coincident (Figure 4.5 B),

with some variability in areas of the same thickness in terms of threshold measurement at that location.

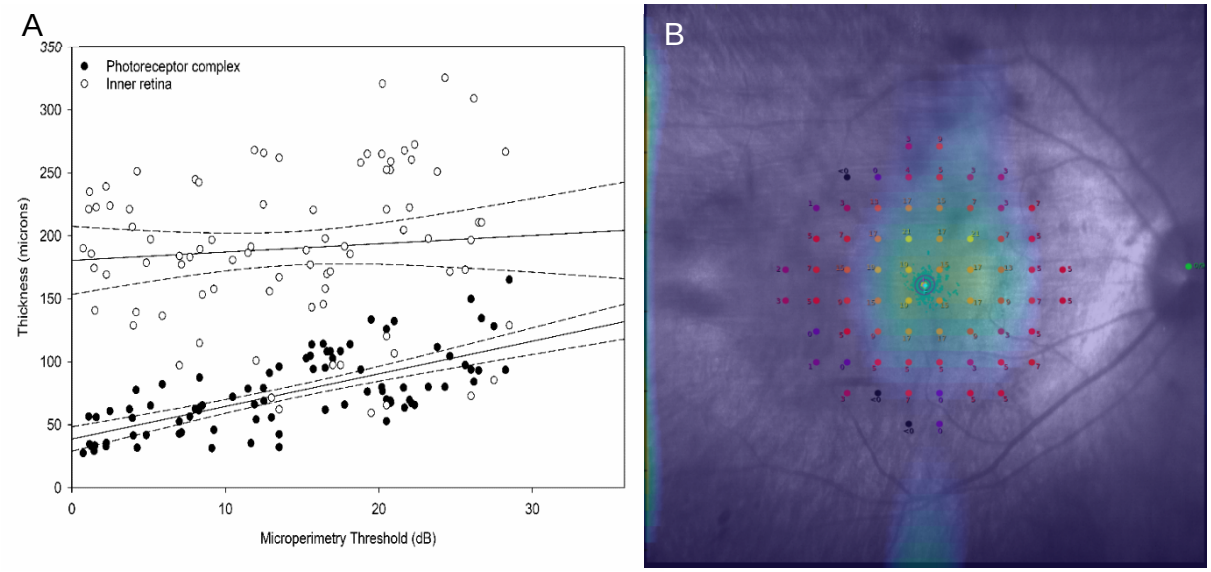


Figure 4-5: (A) Correlation between microperimetry threshold and retinal thickness. Solid lines show the regression lines with 95% confidence intervals presented by the dashed lines. A positive correlation is present between microperimetry threshold and both photoreceptor complex thickness and inner retinal thickness. (B) Microperimetry results overlaid on the photoreceptor outer segment map for subject 007 shown in figure 4.2.

4.5 Discussion

This exploratory study has shown retinal remodelling occurs in eyes affected by a genetic mutation in *RPGR* as previously reported (Aleman et al. 2007). Thinning of the photoreceptors is associated with inner retinal thickening. The photoreceptor complex thinning occurs across the retina, with the inner retinal thickening occurring primarily in the central area. This could be indicative of either the lag period between these two events, or the location of the retinal thickening being concentrated within the arcades. The remodelling likely occurs in response to the initial photoreceptor degeneration and will not be present following cell death, such as within the peripheral retina. In contrast, the difference in the photoreceptor complex between the patient and control eyes included the central one degree of retina. The decrease in the photoreceptor

thickness balances the inner retinal thickening in the central one degree resulting in no change in the total thickness of the retina. The total thickness did differ at other eccentricities. This shows the importance of not relying on total thickness measurements or individual eccentricities to infer disease processes. With the secondary effect in different layers having different magnitudes and rates of change, the thickness measurements used in any study must be targeted to the layer and topographical region of interest to reflect the disease process. In addition, investigation of photoreceptor diseases should also take into account secondary changes in the inner retina.

This is the first time the impact of retinal remodelling has been investigated on functional measures. Visual field measures are currently used to investigate both ganglion cell function, such as in glaucoma, and photoreceptor function in retinal disease. However, the sensitivity measured will be a combination of both of these factors. With retinal remodelling, the assumption of ganglion cell stability cannot be made, so characterising the impact of this on visual field results is important. Multiple regression analysis shows that both the photoreceptor thickness and inner retinal thickness have a significant relationship with microperimetry threshold. Photoreceptor thickness showed a larger coefficient and hence larger effect. Additionally, measuring a larger visual field reduced the microperimetry threshold. Sensitivity reduces with distance away from the fovea so eccentricity would be expected to have an impact on the threshold. In addition, in diseased eyes peripheral visual field will be affected before the central visual field. The increase in variability at scotoma borders is a well-documented phenomenon (Z. Wu, Jung, et al. 2015). The variability in the interplay between the outer retina and visual field sensitivity is visible around the border of central degeneration in the overlay image (Figure 4.5B). The same microperimetry threshold value appears to be associated with a range of outer segment thicknesses, showing other factors have an influence. The original modelling of the relationship between cone density and ganglion cell density to explain visual field thresholds utilises cell density (Watson 2014). Although OCT thickness cannot be directly equated to cell density (Harwerth and Wheat 2008; Menghini et al. 2015), it can provide a

surrogate marker of disease progression and has been used to look at photoreceptor thickness and visual field sensitivity (Rangaswamy et al. 2010). Additionally, thickness data can be reliably collected in human participants routinely. A larger study will therefore be valuable in establishing this relationship in different disease models.

There are several possible mechanisms to explain retinal remodelling in photoreceptor disease, and they likely interact. Inner retinal thickening has been observed in Behçet's disease, indicating an inflammatory process that persists after active disease is treated (Cheng et al. 2016). A mouse model of retinitis pigmentosa shows several processes involved in the inner retinal changes with an associated upregulation of Müller glia (Strettoi et al. 2002). This is achieved via endothelin-2 signalling from degenerating photoreceptors to the Müller glia and astrocytes (Rattner and Nathans 2005). Müller cells are vital for retinal homeostasis, production of neurotransmitters, secretion of neurotrophic factors, maintaining transparency of the retina, and phagocytosis of cone outer segments. Changes in the normal Müller cell function can result in a swelling of the neuronal cell bodies, explaining the inner retinal thickening (Reichenbach and Bringmann 2013). Additionally, the Müller cells in the retina lose their metabolic coherence in degenerating retina and this may cause a loss in the ability to maintain function (Pfeiffer et al. 2016). The concentration of Müller glia is highest in the fovea and parafovea which fits with the pattern reported here (Distler and Dreher 1996).

Molecular imaging in the presence of photoreceptor loss shows abnormal circuitry between the photoreceptors and inner retina likely as a result of abnormal signalling and deafferentation (Marc and Jones 2003). The downstream retinal circuits are also affected. Ganglion cells are preserved but do show some abnormal spike patterns. The implication for visual function is not known (Margolis et al. 2008). The presence of downstream effects on the retinal circuits has been harnessed in designing new treatments for retinal degeneration in order to prevent the secondary neural cell loss by providing increased signalling (Jolly et al. 2020). Electrical

stimulation of the retina for example has altered the gene expression and neurotransmitter expression resulting in retinal protection.

Due to the limited numbers of patients, with this being a rare disease, the right and left eyes were analysed together in the same models. I am aware this is not ideal as this may inflate the correlations. In view of this, an expanded dataset is being collected in order to ensure these conclusions are valid and prove to the case.

4.6 Conclusion

In summary, I show that retinal structure should never be monitored by measuring full retinal thickness as this may mask some of the disease processes. Retinal remodelling occurs with the photoreceptor thinning leading to inner retinal thickening in eyes with retinitis pigmentosa due to the *RPGR* gene. Additionally, the inner retinal changes may be an important consideration when interpreting microperimetry data and generalised thickness as an outcome measure.

4.7 Novel findings

Changes in the inner retina, occurring secondary to photoreceptor degeneration, can impact on functional measurements (microperimetry).

4.6 Implications for clinical practice

Monitoring inner retinal thickness in photoreceptor disease provides insights into degree of degeneration.

Chapter 5:
The Visual Brain

My contributions to this chapter: I developed the study idea, applied for ethical approval, conducted safety screening, collected both MRI, OCT and visual function data, conducted the analysis and interpretation. I developed the Octopus test and wrote the analysis code in MATLAB. Data collection took place from June 2018 to August 2019.

Contributions to this chapter: Data collection was conducted with Aislin Sheldon. MRI data acquisition was in conjunction with radiography staff. The analysis work in this chapter was conducted in collaboration with Prof Franco Pestilli's lab in the University of Indiana. MATLAB code for OCT and microperimetry analysis was written in conjunction with Daniel Bullock. Brainlife apps were written and optimised for this dataset in conjunction with Brad Caron. Colm Andrews implemented the Octopus test code on the Open Perimetry Interface.

5. Impact of visual field loss on the visual pathway investigated with diffusion MRI

5.1 Summary

With the intimate connection between photoreceptors and the retinal circuits, and the neural circuitry in the eye with the brain, secondary changes in the visual brain are an important consideration in retinal disease. White matter tracts carry visual information from the eye to the brain and preserve the visual field representation of the world in the process. Diffusion magnetic resonance imaging (MRI) allows assessment of white matter structural integrity across the brain.

Visual field was examined in the central (microperimetry threshold) versus peripheral region (octopus screening assessment). Whole brain analysis suggests that increased microperimetry threshold is associated with increased white matter integrity in a range of vision related pathways. This prompted the investigation of specific tracts.

The optic radiations exhibited a decrease in FA (fractional anisotropy), indicative of reduced white matter integrity, in both the macular and peripheral bundles in the choroideremia population compared to controls. Microperimetry threshold has a positive correlation with FA and negative correlation with mean diffusivity (MD) in the ventral stream tract (ILF) and vertical tract connecting the ventral and dorsal streams (VOF). These results indicate a reduction in tract integrity with visual loss from choroideremia. The dorsal stream does not appear to be affected by disease. This may, however, be due to the SLF tract covering a wide array of fibre bundles within it, masking impact on visual specific fibres.

5.2 Introduction

5.2.1 Visual brain in eye disease

The presence of secondary degeneration in the visual brain following retinal degeneration could potentially impose limits on the improvement in vision following treatment of the retina. There is a growing body of evidence that retinal disease has downstream effects in the visual brain (H. Brown et al. 2016; Rokem et al. 2017). Magnetic resonance imaging (MRI) white matter structural changes have been reported in a range of visual disorders. Anophthalmia presents with changes in volume of the optic tracts and reduced integrity of the optic radiations. Atrophy of the visual cortex can also be seen in patients with early vision loss. Later visual loss, including juvenile macular degeneration, age-related macular degeneration and retinitis pigmentosa have also shown white matter changes within the visual areas, including the lateral geniculate nucleus (LGN), optic radiations and visual cortex in some cohorts examined. The changes reported in glaucoma include smaller optic nerve diameter, smaller LGN, and white matter changes along the whole visual pathway (H. Brown et al. 2016). The changes reported have been attributed to a variety of processes including cortical plasticity, synaptic reorganisation, changes in both directions from both feedback and feedforward mechanisms. However, these studies are small cohorts of patients. The results have not been systematically related to the degree of eye disease present or type of visual field loss caused by the ophthalmic disease. In addition, few studies have yet gone beyond the primary visual cortex, which is key to understanding the complete visual system.

Preliminary work has shown that gene therapy for Leber Congenital Amaurosis can impact on the function of the visual cortex (Ashtari et al. 2011). Here, the authors utilised functional MRI measures in response to a checkerboard pattern of varying contrast presented in dim illumination. They report larger areas of activation in the eye previously treated with gene therapy compared to the untreated eye in three participants of varying ages. However, baseline measures were not

available and no structural data were collected, preventing adequate analysis of interventional effects. With the first gene therapy in the eye receiving regulatory and NICE approval for patient use, a precedent has been set for therapeutic intervention of genetic eye diseases. This makes it especially important and timely to understand downstream effects from the retinal degeneration to the brain.

5.2.2 White matter tracts

The white matter connects grey matter regions and is not a static attribute throughout life (Sampaio-Baptista and Johansen-Berg 2017). White matter gains its name from the myelin sheath that is widespread throughout the central nervous system (L. Swanson 2013). The white matter pathways of the visual system are the myelinated axons of the visual neurons connecting the visual areas. This begins at the back of the eye with the optic nerves (Razek et al. 2018) and progresses through the optic tracts and optic radiations as detailed in section 1.3.1. The white matter paths are dynamic throughout life in both health and disease with changes observed both in response to learning new skills (Johansen-Berg 2010) and in response to disease affecting the pathways such as in multiple sclerosis (Stone et al. 1995; Gajamange et al. 2018). Optic tract and optic radiations are affected by both ganglion cell and photoreceptor disease causing similar visual deficits demonstrating the interconnectivity of the white matter tracts of the visual system with the eye (Ogawa et al. 2014).

5.2.3 Ventral and dorsal visual streams

A key theory for the processing of visual data in the brain is the presence of two parallel processing streams, first described in monkeys, called the ventral and dorsal streams (Ungerleider and Haxby 1994). This concept was formalised using evidence based input in humans by Milner and Goodale and has since been explored further. Both streams have the same

input but process the vision in different ways, resulting in different outputs. This has the effect of maximising the amount of information that can be analysed in the minimum amount of time. The ventral stream is specialised for object recognition and spatial relations, resulting in perception. It provides object identification with form and colour, using previous information to optimise recognition, as well as providing information about the place of objects in the visual world. The dorsal stream connects the occipital and parietal cortices. It is considered the pathway to action such as reaching and grasping. The information in this stream is therefore highly reactive to the information being presented to the visual system in real time, and must compute our own egocentric location in space in relation to other objects (Milner and Goodale 2008). Evidence from optical illusions and psychophysical experiments provide mixed results as to how independent these two pathways are. It is likely, the two visual systems work together to allow us to function in the world, with the ventral stream providing perceptual information and contributing to planning for action. The dorsal stream is able to reliably execute and control action. The information is likely combined at several levels of processing (Schenk, Franz, and Bruno 2011). Visual field has differential representation in the two systems. Cortical magnification seems to be magnified in the ventral stream, emphasising central vision. Cortical magnification appears reduced in dorsal part of V1, indicating that the peripheral vision is better represented in the dorsal stream (Milner and Goodale 2008). This would suggest that peripheral visual field loss is likely to have a disproportionate impact on the dorsal stream.

The major tracts representing the ventral and dorsal streams are thought to be the inferior longitudinal fasciculus (ILF) and superior longitudinal fasciculus (SLF) respectively based on locational and functional data. Vertical tracts such as the vertical occipital fasciculus (VOF) are thought to be connectors between the streams (Figure 5.1). All three of these tracts can be reliably identified with the use of dMRI (Bullock et al. 2019).

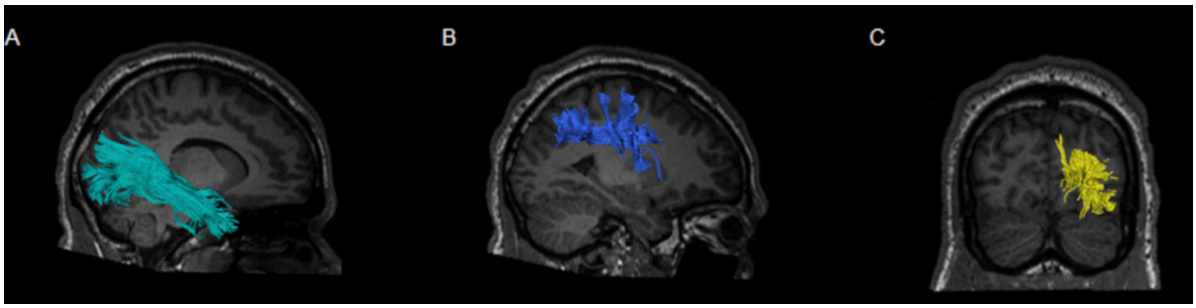


Figure 5-1: (A) Sagittal view of the inferior longitudinal fasciculus (ILF). (B) Sagittal view of the superior longitudinal fasciculus (SLF) 1 and 2. (C) Coronal view of the vertical occipital fasciculus (VOF).

The paths of the ILF and SLF tracts across the brain have been documented (Mori et al. 2002). The ILF crosses the occipital and temporal cortices, both of which are involved in visual perception. On this basis the ILF is thought to be the major tract representing the ventral visual stream (Tavor et al. 2014; Rokem et al. 2017). Fractional anisotropy (FA) and radial diffusivity (RD), both measures of white matter integrity, in the ILF have been correlated with results from behavioural experiments testing the ability to determine faces and scenes. Both of these are considered to be ventral stream processes. Both fractional anisotropy and radial diffusivity showed correlations with visual tasks, including an increased ability to recognise scene details and scene detection (Tavor et al. 2014).

The SLF is a large fibre bundle consisting of three branches with SLF 1 and 2 being the most dorsal branches. It has one end within the occipital lobe and extends into the parietal cortex (Catani et al. 2002). Visuo-spatial processing appears to be associated with SLF 2 (Thiebaut de Schotten et al. 2011). Although SLF 2 is the largest component of the SLF, SLF 1 connects to the premotor region, supporting its role in the dorsal stream (Makris et al. 2005).

Day to day tasks require an integration of multiple skill sets. For example, reading involves seeing detail with co-ordinated eye movements (Yeatman, Dougherty, Ben-Shachar, et al. 2012; Vidyasagar and Pammer 2010). The VOF is a vertical tract that appears to connect ventral and dorsal related brain areas, with this configuration being thought to enhance visual ability (Yeatman et al. 2014). This is achieved by connecting regions for both detail (ventral) and motion

(dorsal) with origins visible in both the ventral and dorsal areas of the visual cortex (Takemura et al. 2016).

5.2.4 Diffusion-weighted MRI

Diffusion-weighted MRI (dMRI) is a non-invasive method to investigate white matter tracts and their associated microstructural properties. This is a useful way of looking at the connectivity of the brain beyond the primary visual cortex (Rokem et al. 2017). Structural connectivity has important implications for functional abilities and has been shown to be affected by life experiences such as learning new skills. Adaptive processes have been noted in disease processes (Johansen-Berg 2010; Assaf, Johansen-Berg, and Thiebaut de Schotten 2019). If such processes occur in retinal disease, this could have implications for preserving visual perception in disease.

The basis of dMRI is the pattern of diffusion of water molecules in different tissues. Molecules are in constant motion at non-zero absolute temperatures. Diffusion relates to this random motion of water molecules in the brain. Diffusion is restricted by tissue boundaries and biological barriers and this property can be utilised to investigate the structure of different tissue types (Figure 5.2). White matter consists of tightly packed, coherently aligned fibrils with glial tissue borders. This provides a barrier to the diffusion of water (Beaulieu 2002). Changes in dMRI can therefore be used as a proxy for degenerative changes (Rokem et al. 2017).

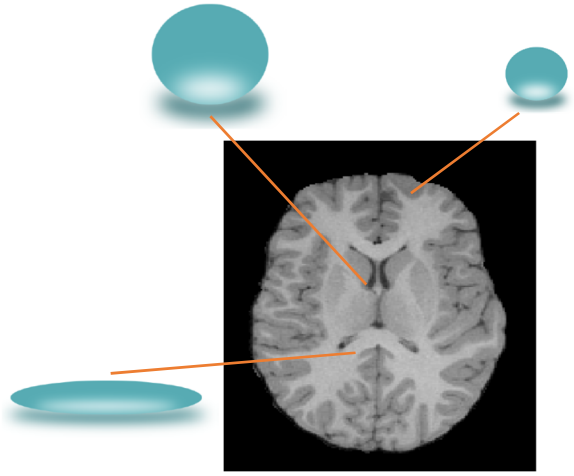


Figure 5-2: Mechanism of diffusion MRI. The circles represent free flowing water molecules in the cerebrospinal fluid and grey matter. The elongated oval represents movement water molecules constrained by the axons of white matter.

One of the key metrics used to quantify microstructure is FA which measures the degree to which water molecules move in a specific direction. The scale of measurement is from 0 to 1, where 0 indicates equal diffusion in all directions and 1 indicates a high degree of directionality. Water molecules within axons that form a tract move parallel to the tract, and will therefore have a high FA value. Those in fluid, such as cerebrospinal fluid) are free to move in all directions, and will have low FA (Figure 5.2). FA is a useful measure of white matter integrity as it is thought to represent a combination of features, including fibre complexity, membrane integrity and myelin thickness (Johansen-Berg 2010). Another key measure is MD which provides an overall measure of diffusion across a region (Pierpaoli and Basser 1996). Changes in MD can be a marker of loss of tissue integrity (Werring et al. 2000).

The aims of this chapter are to correlate visual function measures with changes in white matter tracts in patients with choroideremia compared to control patients using dMRI. In addition, I will investigate factors affecting the white matter tracts as well as changes in both the early (optic radiations) and late visual systems (connections between the primary visual cortex and higher visual centres).

5.3 Methods

This study was approved by the Health Regulatory Authority, REC reference 17/LO/1540, and adhered to the tenets of the Declaration of Helsinki. Detailed SOPs for vision tests are provided in Appendix 1.

5.3.1 Structural MRI acquisition

A high-resolution (1 mm x 1 mm x 1 mm) whole head T1-weighted MPRAGE anatomical image (TE = 3.96 ms, TR = 1900 ms, field of view = 256 mm, flip angle = 8 deg) was acquired for all patients.

5.3.2 Diffusion MRI acquisition

Scanning took place in a 3T Prisma MRI scanner (Siemens Healthcare, Erlangen, Germany) at the Functional Magnetic Resonance Imaging Centre of the Brain (FMRIB, University of Oxford), using a 64-channel head coil. The imaging parameters chosen matched the Biobank protocol in order to allow future comparisons to be made to Biobank data. The UK Biobank is an open source population dataset incorporating MRI imaging, OCT imaging and genetic information.

Diffusion-weighted data were acquired using echo planar imaging (EPI; TR = 3600 ms, TE = 92.0 ms, multiband acceleration factor = 3 with interleaved slices, and voxel size of 2 ×2 × 2 mm^3). The dMRI was collected in 104 directions in the AP direction and 6 directions in the PA direction (b-value = 2000 s/mm^2 and 1000 s/mm^2), and 8 non-DWI (B0) images were acquired.

5.3.3 Diffusion analysis

5.3.3.1 Pre-processing

Raw anatomical T1w images were pre-processed using the FMRIB Software Library (FSL) function *fsl_anat*. Within this function, the raw anatomical T1w images were cropped and reoriented, bias corrected, linearly-aligned to the MNI152 0.7mm atlas using *flirt*, and non-linearly aligned to the same atlas using *fnirt* (Jenkinson et al. 2002). The linearly-aligned T1 will be referred to as the 'acpc-aligned' T1. Following this, the acpc-aligned T1 was used for segmentation and surface generation using Freesurfer's *recon-all* function (Fischl 2012). The thalamic nuclei were segmented into its subcomponents using Freesurfer's developmental *segment_thalamic_nuclei* function (Iglesias et al. 2018). The population receptive field (pRF) maps based on functional MRI measures, including eccentricity, were then fitted to the cortical surfaces generated from Freesurfer using the Benson et al. retinotopy atlas. This created a map of the regions of V1 used for different visual field areas (Benson et al. 2012, 2014). These processes were implemented on the open cloud computing platform brainlife.io (Avesani et al. 2019).

EPI acquisitions are prone to geometric distortions that can lead to errors in tractography. To minimize this, two image sets were acquired with the phase-encoded direction reversed, "blip-up" and "blip-down" (Chang and Fitzpatrick 1992). This results in images with geometric distortions of equal magnitude but in the opposite direction allowing for the calculation of a corrected image (Andersson, Skare, and Ashburner 2003). Before correcting for geometric distortions, each image set, blip-up and blip-down, was corrected for motion and eddy-current related distortions. Eddy-current and motion correction with outlier replacement (*-repol*) was then applied via the *eddy_cuda8.0* command provided by FSL. These processes were conducted using tools from FSL (FMRIB Centre Software Library, Oxford University;

http://www.fmrib.ox.ac.uk/fsl/) (Woolrich et al. 2009; S. Smith et al. 2004). DTI images were then aligned to the T1 structural scan, which had been resampled to AC-PC orientation.

5.3.3.2 Tract based spatial statistics (TBSS)

A diffusion tensor model was fitted to each voxel. This consists of eigenvectors (λ) which describe the diffusivity across three principal directions (Pierpaoli and Basser 1996). MD is measured in $\mu m^2/ms$ and calculated by averaging the eigenvalue in each of the principal directions. The *dtifit* function in FSL was used to implement this.

$$MD = (\lambda_1 + \lambda_2 + \lambda_3) / 3$$

$$FA = \sqrt{}\left(((\lambda_1 - \lambda_2)^2 + (\lambda_2 - \lambda_3)^2 + (\lambda_1 - \lambda_3)^2) / 2(\lambda_1^2 + \lambda_2^2 + \lambda_3^2)\right)$$

To allow comparison across participants, localised statistical changes between groups can be assessed using tract based spatial statistics (TBSS). This is achieved by registering each individual's diffusion results into common space which is representative of the mean of the white matter tracts of a population (S. Smith et al. 2006). This was conducted in FSL using *randomise*. Visual function measures were included in the model as covariates and significance was thresholded at $P \leq 0.01$ following 5000 permutations and correction for multiple comparisons across space. VA, microperimetry threshold, and octopus peripheral score were entered as covariates in the analysis.

5.3.3.3 Tractography

A series of apps were utilised on Brainlife.io to create a repeatable analysis pipeline. Anatomically-constrained Tractography (ACT) was used to generate whole-brain tractograms for each participant (R. Smith et al. 2012). ACT sets strict anatomical constraints on the tractography in order to provide biologically-plausible streamlines. A grey matter - white matter

interface mask was generated using MrTrix3's *5ttgen* function and used a seed mask for tracking. The constrained-spherical deconvolution (CSD) model was fit on the full multi-shell pre-processed dMRI data using MrTrix3 to generate fibre orientation dispersion (FOD) maps across maximum spherical harmonic orders (i.e. lmax) 2,4,6 and 8 to guide tracking (R. Smith et al. 2012). Probabilistic ACT tractography was subsequently performed across lmax values of 6 and 8 with 1 million streamlines generated per lmax with a minimum streamline length of 25mm, maximum length of 220 mm, maximum angle of curvature of 35 degrees, and a step-size of 0.2mm. The two tractograms were then combined into a single tractogram and used for white matter tract segmentation.

The human white matter tracts were segmented using a custom version of white matter query language described in detail in Bullock et al, 2019 (Bullock et al. 2019). In brief, this segmentation uses known anatomical terminations and shape characteristics of white matter tracts to segment whole-brain tractograms into known tracts. From these, the SLF, ILF, and VOF were specified for further analysis. The tracts were cleaned by computing a centroid of each tract and removing streamlines that were located greater than 4 standard deviations away from the position of the centroid. This cleaning process was performed five times.

Tract profiles for each parameter (FA and MD) were generated by estimating the core representation of each tract, resampling and segmenting each streamline into 200 equally-spaced nodes, applying a gaussian weight to each streamline based on distance away from the core, and obtaining the weighted average metric at each node. This was performed using in-house MATLAB code utilizing the *Compute_FA_AlongFG* command provided by Vistasoft (code provided by Brad Caron, IU). In order to avoid partial-voluming effects and to cleanly separate tract from grey matter, the first and last 10 nodes from the tract profiles were removed. Averages were then computed for each tract, along the 180 nodes, collapsed over each group, and were displayed in Tract Profiles for group comparisons (Yeatman, Dougherty, Myall, et al. 2012).

5.3.3.4 Optic radiations tracking

Regions-of-interest (ROIs) necessary for tracking the optic radiation were generated using AFNI's 3dROIMaker's functionality (Taylor and Saad 2013). For the lateral geniculate nuclei (LGN), volumes were extracted from the thalamic nuclei segmentation previously generated using Freesurfer. Extraction ROIs used to constrain tracking of the optic radiation to biologically-relevant streamlines were generated from the subcortical (*aseg*) segmentation generated previously using Freesurfer. Specifically, exclusion ROIs included the contralateral hemisphere cerebral white matter and cortex and the ipsilateral cerebellum white matter and cortex. V1 was extracted from the visual area segmentation of the retinotopic maps generated previously.

In order to examine the potential link of functional visual field loss and white matter structure, multiple segments of the optic radiation were tracked using termination ROIs representing different cortical eccentricities. White matter microstructure modelling via eccentricity was conducted with the Tracking the Human Optic RAdiation (THORA) app. This involved a peripheral bundle being generated using regions of V1 that process visual information from 7 degrees to 90 degrees of eccentricity and a macular bundle was generated from regions representing the central 0 to 5 degrees of visual field eccentricity. Parallel transport probabilistic tractography for each bundle was performed using Trekker software (Aydogan and Shi 2019). Specifically, tracking was performed across multiple spherical harmonic orders (lmax=6,8) and minimum angles of curvature (0.25, 0.5, 0.75, 1). A minimum FOD amplitude of 0.025 and a step size of 0.05 were used for each lmax and curvature permutation. During tracking, streamlines were excluded if they entered the CSF or any of the exclusion ROIs generated previously with AFNI. A total of 1250 streamlines were generated per permutation, and the permutations for each bundle were combined to create a tractogram of 10k streamlines each. Following tracking, the bundles were cleaned twice by computing a centroid of each bundle and

removing streamlines that were located greater than 4 and 3 standard deviations away from the position of the centroid respectively.

5.3.3.5 Statistical analyses

A summary of the apps used on the Brainlife.io platform is shown in Table 5.1.

Application	Github repository	Open Service DOI
FSL Anat (T1)	https://github.com/brainlife/app-fsl-anat/tree/master	https://doi.org/10.25663/brainlife.app.273
Freesurfer	https://github.com/brainlife/app-freesurfer/tree/1.7	https://doi.org/10.25663/bl.app.0
Tissue-type segmentation	https://github.com/brainlife/app-mrtrix3-5tt/tree/binarize	https://doi.org/10.25663/brainlife.app.239
Segment Thalamic Nuclei	https://github.com/brainlife/app-segment-thalamic-nuclei/master	https://doi.org/10.25663/brainlife.app.222
pRFs / Benson14-Retinotopy	https://github.com/davhunt/app-benson14-retinotopy/master	https://doi.org/10.25663/brainlife.app.187
FSL Top-up & Eddy - CUDA	https://github.com/brainlife/app-FSLTopupEddy/master	https://doi.org/10.25663/brainlife.app.287
Mrtrix3 Preprocess	https://github.com/brain-life/app-mrtrix3-preproc/tree/1.5	https://doi.org/10.25663/bl.app.68
ROI Generation	https://github.com/brain-life/app-roiGenerator/tree/master	https://doi.org/10.25663/brainlife.app.242
Fit CSD Model For Tracking	https://github.com/brainlife/app-mrtrix3-csd/tree/ensemble	https://doi.org/10.25663/brainlife.app.238
FSL DTIFIT	https://github.com/brainlife/app-fslDTIFIT/master	https://doi.org/10.25663/brainlife.app.292
ACT Tractography	https://github.com/bacaron/app-mrtrix3-act/tree/1.3	https://doi.org/10.25663/brainlife.app.297
THORA	https://github.com/brainlife/app-trekker-roi-tracking/tree/optic-radiation-eccentricity-exclusion	https://doi.org/10.25663/brainlife.app.233
White Matter Anatomy Segmentation	https://github.com/brainlife/app-wmaSeg/tree/3.3	https://doi.org/10.25663/brainlife.app.188
Remove Tract Outliers	https://github.com/brainlife/app-removeTractOutliers/tree/1.3	https://doi.org/10.25663/brainlife.app.195
Tract Analysis Profiles	https://github.com/brain-life/app-tractanalysisprofiles/tree/1.6	https://doi.org/10.25663/brainlife.app.185
Tractography quality check	https://github.com/brainlife/app-tractographyQualityCheck/tree/1.2	https://doi.org/10.25663/brainlife.app.189

Table 5-1: List of all the apps used from the Brainlife.io platform to process the dMRI data.

The tract profiles for each participant were downloaded from Brainlife using Ubuntu and the CLI interface. Further analysis was conducted in MATLAB and SPSS.

5.3.4 Octopus visual fields

A custom test was implemented in the Open Perimetry Interface on the Octopus perimeter (Haag-Streit, Harlow, UK). This was based on the Estermann test and expanded to provide a symmetrical measure across the visual field (Figure 5.3 A) (presented at BCOVS 2018 and 2019). The test stimuli were Goldmann size V to ensure the absolute extent of the visual field was measured. Each presentation lasted 200 ms at 10 dB. Each location was tested twice and the count of the points seen output. The test was performed binocularly with room lights off. Fixation and head position were monitored through the use of the inbuilt camera. A central fixation target of four green dots was provided. Reliability was assessed through the implementation of false positive trials and set at a maximum of 20%. The output from the test consisted of CSV files providing the results of light presentations and a pictorial representation of the results (Figure 5.3 B).

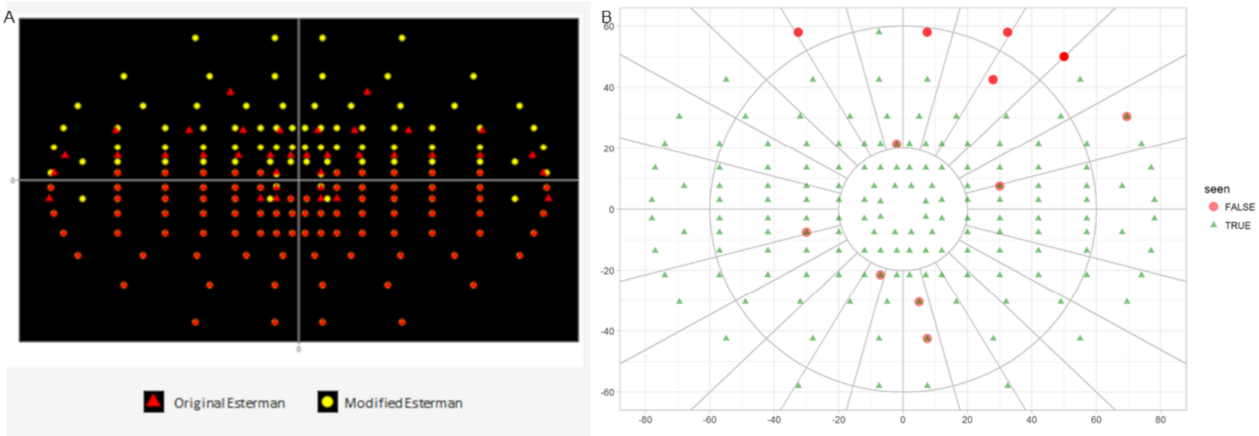


Figure 5-3: (A) Locations of stimuli presented with original Esterman test (red triangles) and the new modified test (yellow circles) to show differences between them. The new test covers a larger area of the visual field with a more even spread. (B) Example output from the test. The green triangles represent seen points and red circles not seen. Both symbols overlaid indicate that the point was seen on one presentation but not on the other.

Analysis of the results was conducted in MATLAB (version 2018a, The MathWorks, Natick, MA). The central seven degrees was disregarded as being representative of central vision. A periphery score was calculated as a percentage of the remaining points seen on either presentation.

5.3.5 Microperimetry: central visual field

Microperimetry was conducted in mesopic conditions following five minutes of adaptation, without pupil dilation (Han et al. 2018, 2017). A 10-2 grid (68 stimuli) with 4-2 staircase strategy was utilised, centred over the anatomical fovea based on the SLO image. If the fixation targets could not be seen, verbally guided microperimetry was conducted. The right eye was tested prior to the left. If the participant was microperimetry naive, a learning test was first administered. Reliability was set at fixation losses ≤ 15%. If not met, the test was repeated. The raw data were exported detailing the threshold at each point, and processed in MATLAB. The analysis code is available at https://github.com/jkjolly/OCT_scripts. It calculated the average threshold of rings of around the central 1 degree, 1-3 degrees, 3-5 degrees, and 5-7 degrees. The right and left eyes were averaged to present the overall visual field.

5.3.6 Retinal OCT

OCT examination was performed on the Heidelberg Spectralis (Heidelberg Engineering, Heidelberg, Germany). Fixation was achieved with either the internal or an external fixation target as appropriate. A 20 x 20 degree volume scan was conducted in high resolution mode with ART = 9. The scan consisted of 49 A-scan slices. Scans were imported into Orion® (Voxeleron LLC, Pleasanton, CA, USA) for accurate segmentation as described in chapter 4. The import was imported into MATLAB. The analysis code is available at

https://github.com/jkjolly/OCT_scripts. Average thickness was calculated in the rings described in chapter 5.3.5 in the right and left eyes.

5.3.7 Participants

Twenty patients with choroideremia were recruited with 15 age- and sex-matched control participants. There were 18 male patients with choroideremia and two female carriers presenting with a male phenotype. A wide range of disease severity states were included in the cohort. All subjects had sufficient vision to complete the battery of tests. Mean age was 38 years with a range of 19 to 58 years. The control group consisted of two females matching the ages of the female carriers and 13 males. Mean age of the group was 38 years with a range of 19 to 60 years. Visual function assessment and MRI scanning was successfully completed on all subjects. TBSS was successful on all subjects. One patient participant and one control participant failed completion of tractography and were excluded from the tract and optic radiations analysis. Both were males with an age of 54 years and 51 years respectively.

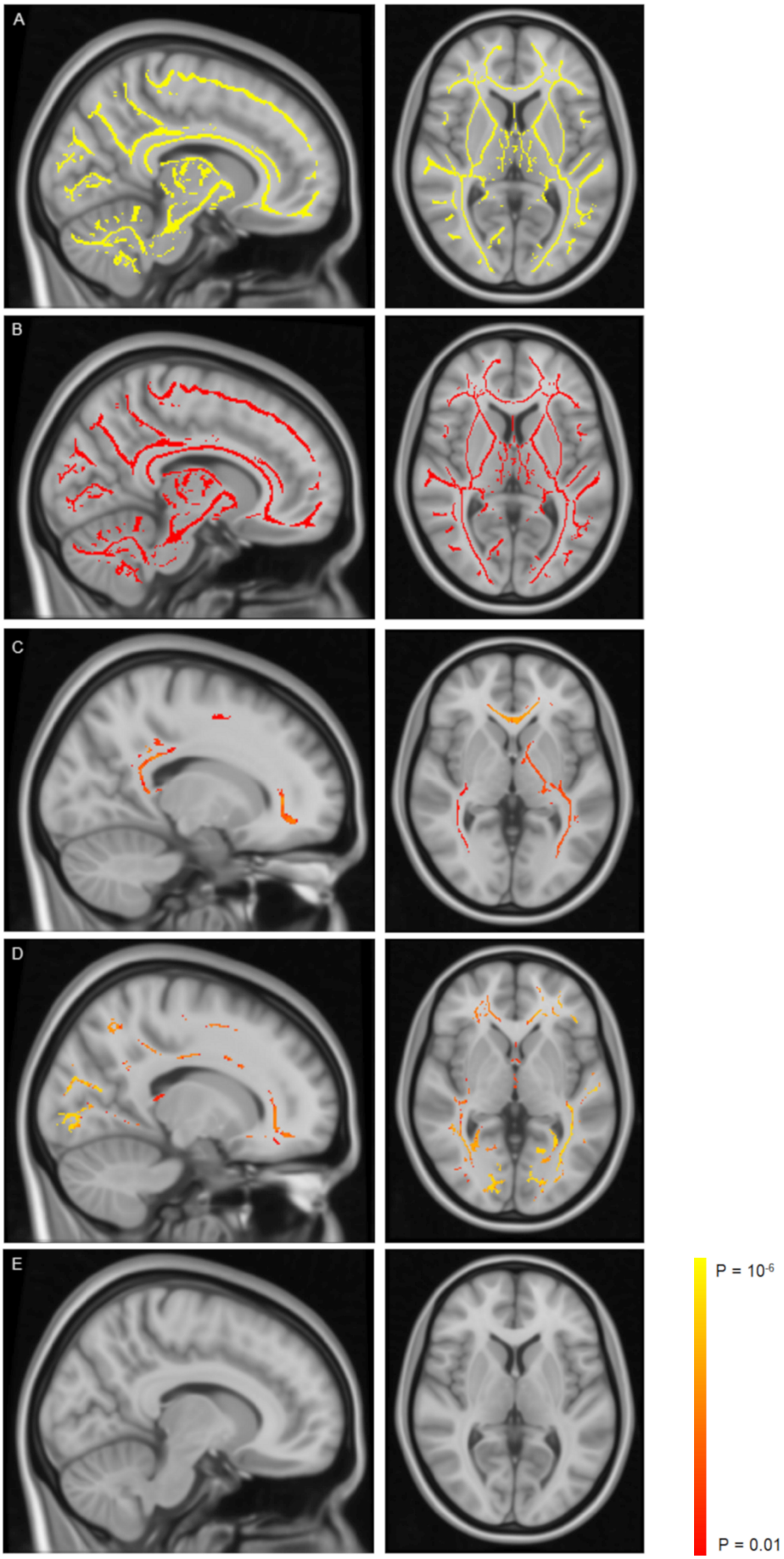
5.4 Results

5.4.1 Whole brain analysis show a correlation between white matter microstructure and visual function

The white matter tract skeleton was successfully identified in both choroideremia and control participant groups using TBSS (Figure 5.4 A and B). There was no statistical difference in the FA of the white matter tracts between the groups ($P > 0.05$). The probability maps (Figures 5.4 C – E) show the relationship between a higher FA measurement, indicating greater white matter integrity with the visual measures. Regions marked as red-yellow show a significant relationship ($P \leq 0.01$). Whole brain analyses show a correlation between white matter microstructure and

central vision, but not peripheral vision. Higher FA (greater white matter integrity) is related to higher visual acuity, particularly along the optic radiations. Mild changes are also visible in the corpus callosum. Interestingly the changes are not present in the posterior radiations, situated towards the primary visual cortex. There is an even stronger relationship with microperimetry threshold as shown by the yellow colour and increased extent of the white matter pathways involved. The full extent of the optic radiations are involved, as well as the visual cortex. Mild changes remain visible in the corpus callosum.

Figure 5-4: All data are presented as a sagittal view on the left and axial view on the right. (A) White matter tracts for the control participant group displaying the collective results across the group and registered to a standard template displayed against the MNI standard brain. (B) Same view for the choroideremia participants. Scale bar applies to images C-E. Probability maps for FA differences incorporating visual function as a covariate. The colours show voxels with a significant relationship between white matter pathways and visual function. (C) Visual acuity. (D) Microperimetry threshold of the central visual field. (E) Octopus periphery score.


A
B
C
D
E
P = 10-6
P = 0.01

5.4.2 Central visual field loss affects both macular and peripheral bundles in the optic radiations

The optic radiations form the longest white matter tract of visual specific information and were therefore examined in more detail (Figure 5.5). The tract characteristics are shown in Figure 5.6. Several areas of the tracts show a clear separation between control and choroideremia groups, with the control groups displaying a higher FA, indicating greater white matter integrity. Right and left hemispheres were analysed separately. All assumptions were met for the two-way ANOVA which examined the impact of group and tract position on the FA. There was a statistically significant difference between the macular and peripheral bundles (F (1, 58) = 10.71, P = 0.002) for the right and left (F (1, 58) = 3.92, P = 0.05) hemispheres. There was also a statistically significant difference in FA between the patient and control groups F (1, 58) = 4.75, P = 0.03 for the right hemisphere and F (1, 58) = 11.00, P = 0.002 for the left hemisphere. The interactive term was not significant (P = 0.51), indicating that the presence of visual disease did not affect the macular bundle more than the peripheral bundle in a statistically significant way. Mean FA for the macular bundle in the choroideremia patients was 0.47 ± 0.03 compared to the control group 0.49 ± 0.02, and in the peripheral bundle FA values were 0.45 ± 0.03 versus 0.46 ± 0.03 (Figure 5.6) across both hemispheres.

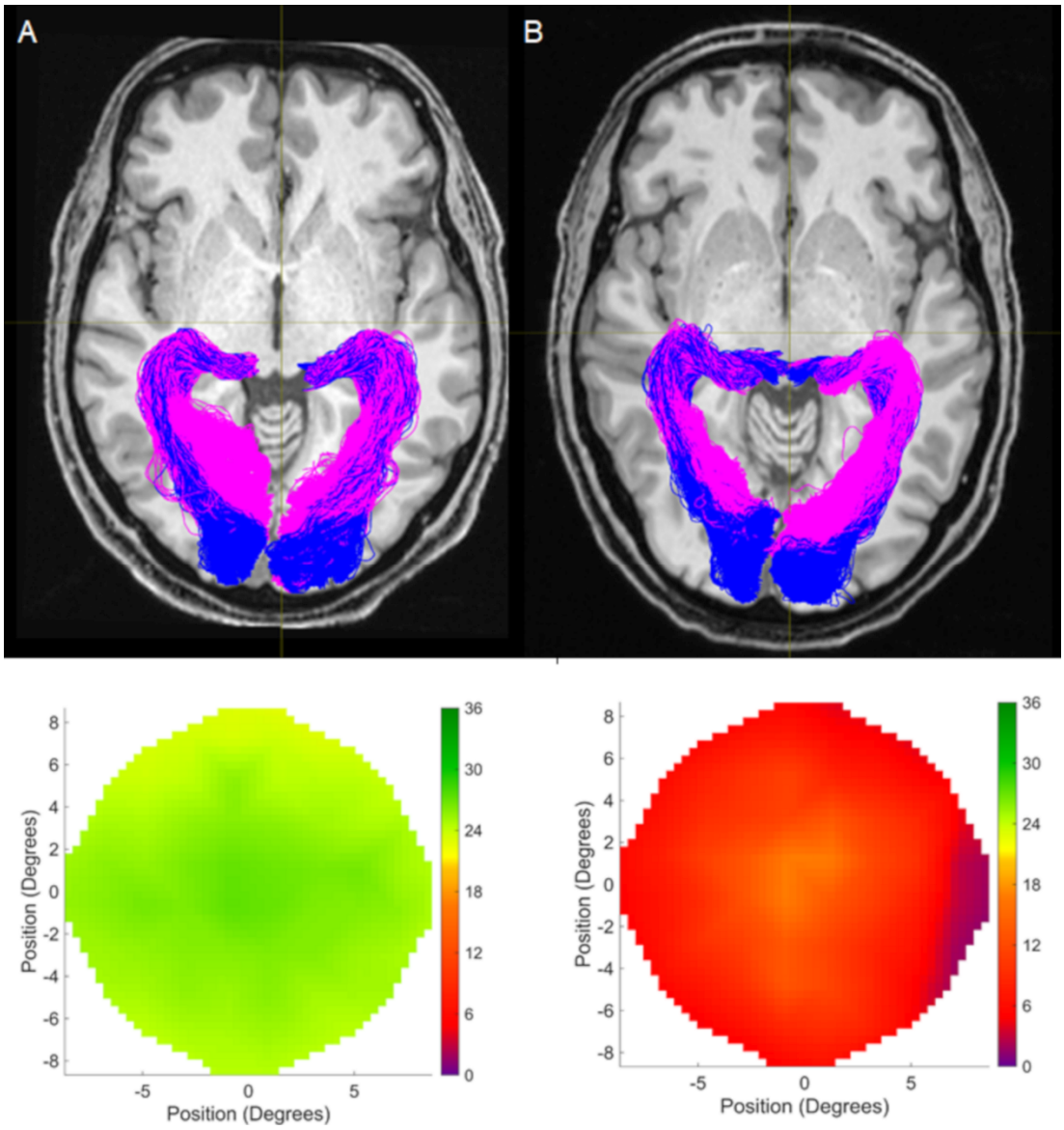


Figure 5-5: Group average representations of the optic radiations representing macular fibres in blue (central 5 degrees of vision), and peripheral vision fibres in pink (7-90 degrees of vision). Both peripheral and macular fibre bundles had lower fractional anisotropy (FA) in the patient group compared to the control group. Underneath are the average microperimetry results for the group with right and left eyes combined. (A) Control group and (B) Choroideremia group.

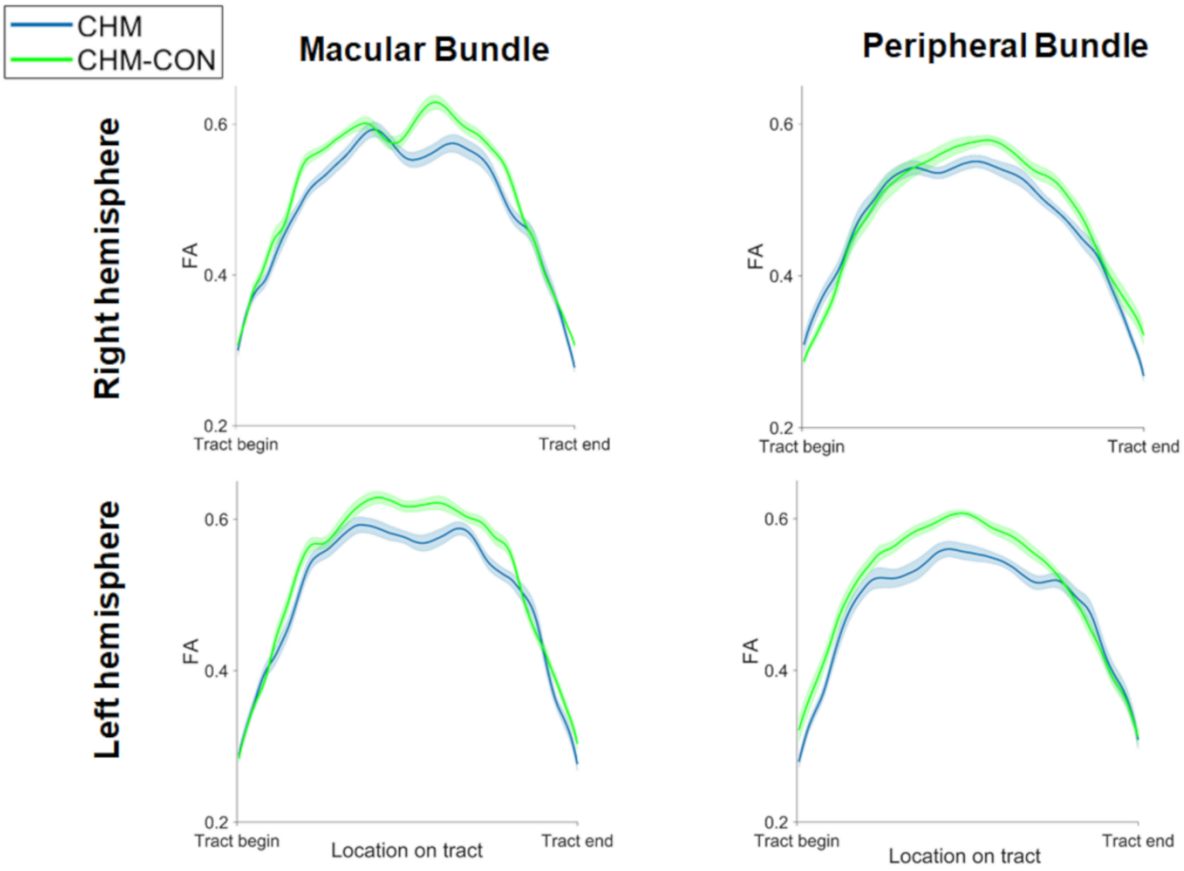


Figure 5-6: Tract profiles in choroideremia (blue) and control (green) groups showing FA values across the tracts. The top row shows tracts in the right hemisphere and bottom row shows tracts in the left hemisphere. The columns show tract profiles for the macular and peripheral bundles respectively. The shaded area around the bars represents the standard deviation, created by Rob Campbell (2020). raacampbell/shadedErrorBar (https://www.github.com/raacampbell/shadedErrorBar), GitHub.

A Generalised Estimating Equations (GEE) model was used to assess the influence of structural and functional visual field changes on the FA in both macular and peripheral optic radiations in each hemisphere. Microperimetry and OCT measures were included as covariates at 1, 3, 5 and 7 degree eccentricity. Microperimetry was averaged across eyes and the periphery score from the Octopus was a binocular measure. OCT thickness for the photoreceptor complex and inner retina from both eyes were included as a combined interactive term with microperimetry results at each eccentricity due to their interaction as shown in chapter 4. The group data for each measure is shown in Figure 5.7. Data from the right and left hemispheres were combined. The GEE model showed a significant interaction of the periphery score and retinal visual field loss

at 3 and 5 degrees on the FA measurement ($P \leq 0.02$). Peripheral bundle FA appeared to be affected by retinal visual field at 5 degrees and the peripheral score ($P < 0.01$).

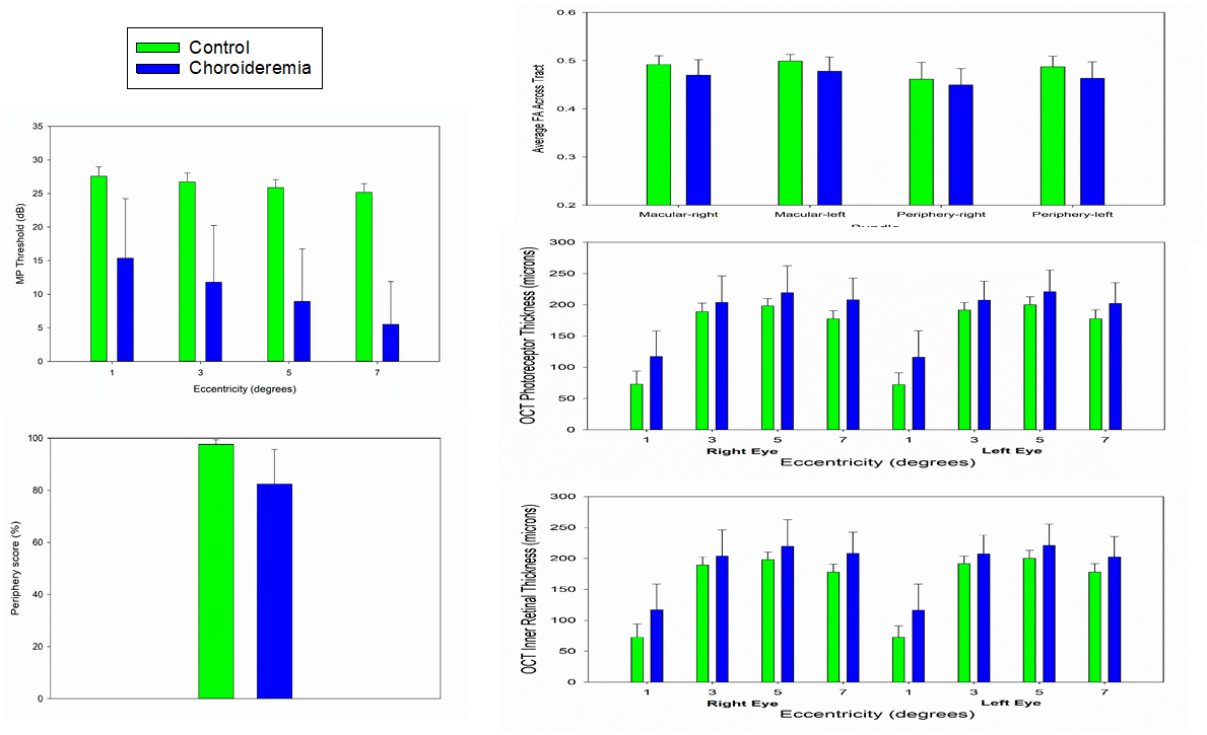


Figure 5-7: Summary of group measures with green representing control group and blue representing choroideremia patient group. Error bars show the standard deviation. Visual field results are presented in the left with combined right and left microperimetry threshold at different eccentricities and a global octopus score. On the right, the FA scores are presented in each bundle. Underneath OCT thickness measures are shown at 1,3,5, and 7 degrees eccentricity for each eye separately.

5.4.3 Impact of visual field loss on the ventral versus dorsal streams

There is clearly an effect of choroideremia on the pathways to the visual cortex as shown by the effects on the optic radiations, but it is important to understand whether there are also wider effects on the visual pathway. Tractography was used to examine the ILF, SLF and VOF tracts specifically. Right and left tracts were combined to reduce multicollinearity when combining the brain tract results with the ocular data. Summary statistics are shown in Table 5.2 and Figure 5.8.

One way MANOVA with Bonferroni correction for multiple tests was conducted to look at differences between the choroideremia and control groups. There was a statistically significant difference between choroideremia and controls F (10, 48) = 20.2, P < 0.001; Wilk's $\lambda = 0.192$, partial $\eta^2 = 0.808$. Post-hoc analysis showed significant differences were present for the ILF tracts (FA P = 0.009, MD P = 0.025), and VOF tracts (FA P = 0.050, MD P = 0.013), but not the SLF tracts (FA P = 0.602, MD P = 0.455) as shown in Figure 5.8. Examination of the ocular data showed a preservation of the VA on average across the patient group (P = 0.159). However, central visual field as measured by microperimetry threshold was reduced in choroideremia compared to control eyes (P < 0.001). Structural integrity of the central and peripheral retina was represented by OCT thickness at 1 and 7 degrees respectively. The thinning of the central retina in choroideremia was not significant (P = 0.266), but was in the peripheral retina in the disease group (P = 0.035).

Factor	**Choroideremia**	**Control Participants**
VA (letters)	83 ± 9	88 ± 13
MP (dB) *	8.4 ± 6.9	25.9 ± 1.1
OCT centre (µm)	275.2 ± 50.5	263.1 ± 21.0
OCT periphery (µm) *	51.6 ± 13.8	304.5 ± 51.6
ILF FA *	0.477 ± 0.028	0.500 ± 0.025
ILF MD (μm^2/ms) *	0.782 ± 0.030	0.765 ± 0.028
SLF FA	0.442 ± 0.015	0.445 ± 0.024
SLF MD (μm^2/ms)	0.714 ± 0.019	0.709 ± 0.027
VOF FA *	0.367 ± 0.030	0.383 ± 0.029
VOF MD (μm^2/ms) *	0.753 ± 0.027	0.734 ± 0.028

*Table 5-2: Summary measures of ventral and dorsal tracts and ocular data. Data are presented as mean ± SD. The * denotes the measures that are statistically different between groups.*

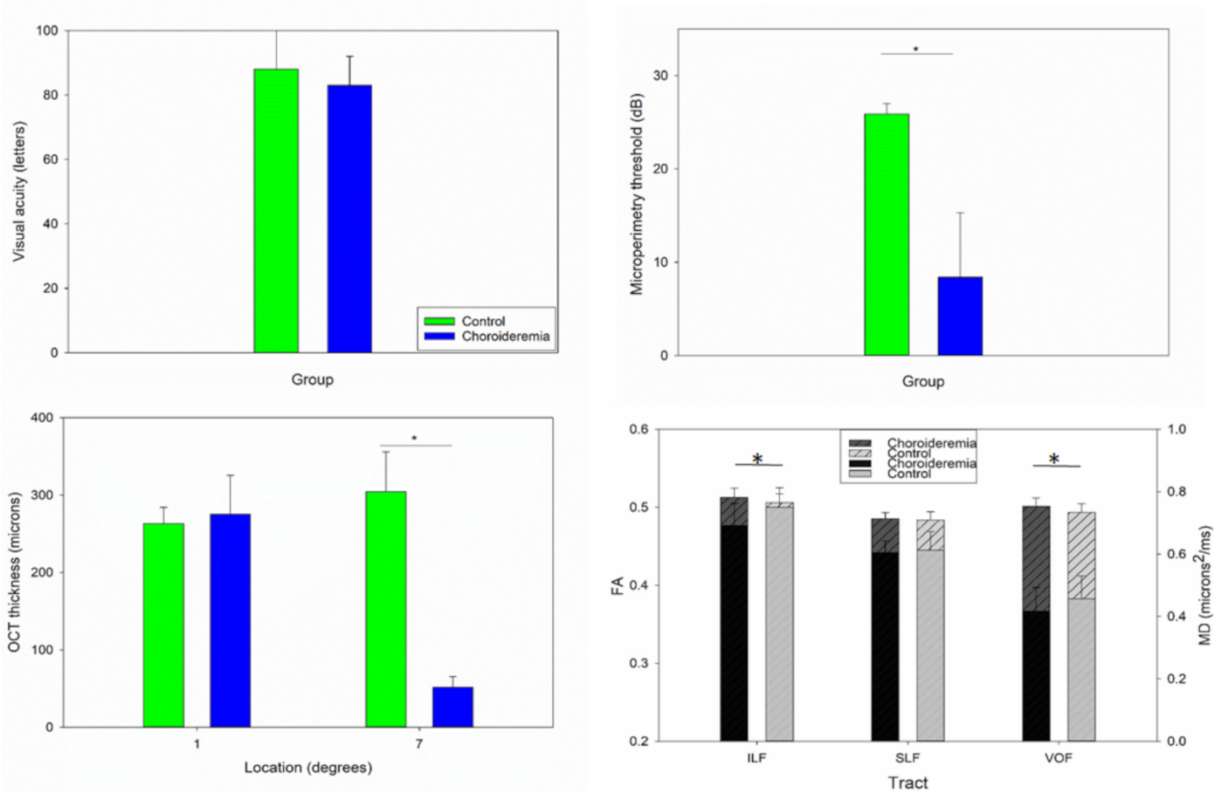


Figure 5-8: Summary statistics comparing choroideremia (black bars) and control (grey bars) groups. Plots show visual acuity, microperimetry threshold, OCT thickness within the central 1 degree and a ring located around 7 degrees from the fovea, and tract measurement with FA on the right Y axis (solid shading) and MD on the left Y axis (patterned bars). Both FA and MD show a reduction in the disease population. The error bars represent standard deviation. Stars represent a significant difference between the groups.

In order to understand the impact of visual field loss on the ILF and VOF tracts, the spearman correlation between the tract measures and microperimetry threshold was calculated (Figure 5.9). FA showed a significant positive correlation with microperimetry threshold for the ILF for both the right ($\rho = 0.55$, $P < 0.01$), and left hemispheres ($\rho = 0.48$, $P < 0.01$). There was also a significant correlation for the VOF for both the right ($\rho = 0.51$, $P < 0.01$), and left hemispheres ($\rho = 0.36$, $P = 0.04$). MD showed a negative correlation with microperimetry threshold for the ILF for both right ($\rho = -0.43$, $P = 0.01$), and left hemispheres ($\rho = -0.42$, $P = 0.01$). The negative correlation was also seen for the VOF for both the right ($\rho = -0.45$, $P < 0.01$), and left hemispheres ($\rho = -0.51$, $P < 0.01$).

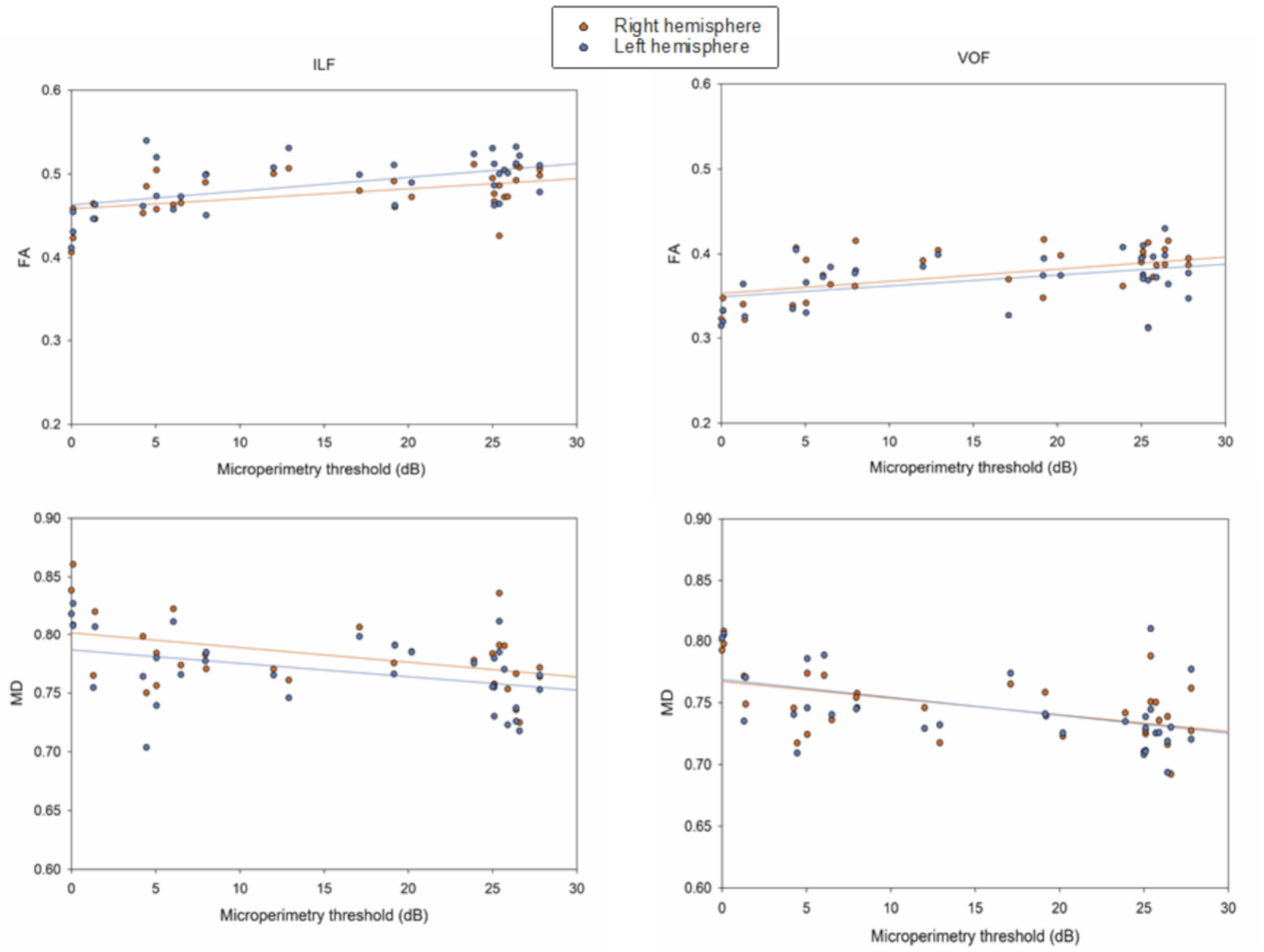


Figure 5-9: Correlation between tract measures and microperimetry threshold. A positive correlation was seen between microperimetry threshold and FA (top row) in both the ILF (left hand side) and VOF (right hand side). A negative correlation is present between threshold and MD (bottom row).

Each tract was sampled by 200 points to allow analysis of changes along the tracts. For statistical analysis this was split over 10 location bins with values averaged within the bins, with 1 denoting the point closest to the visual cortex and 10 the most distal end. This was conducted for FA (Figure 5.10) and MD (Figure 5.11). The graphs indicate a clear separation between the control and choroideremia groups at several points along the tracts for both FA and MD. The summary results are shown in the supplementary table 2.

A two-way ANOVA was conducted to examine the difference in FA between tracts and disease states at different locations along the tracts, with lower FA in the choroideremia population. Significant effects ($P < 0.01$) were noted for disease state (F (1, 0.09) = 77.9), location (F (9, 0.66) = 546.1), and tract (F (5, 0.80) = 664.9). In addition, a significant interaction ($P < 0.01$)

was noted between tracts and both location (F (45, 0.01) = 11.0) and disease state (F (5, 0.01) = 5.5), indicating the pattern of change across the tract differed with the tract being measured. Changes between the centre of the tract and the periphery were steepest in the ILF and shallowest in the SLF. There was also a significant interaction between the disease state and location, F (9, 0.003) = 2.6, P < 0.01. This is indicative of choroideremia altering the pattern of change seen across the length of the tracts. Tukey post-hoc analysis with Bonferroni correction shows the pattern of asymmetry between the right and left ILF but no significant difference between the SLF or VOF in the right and left hemispheres as seen with FA.

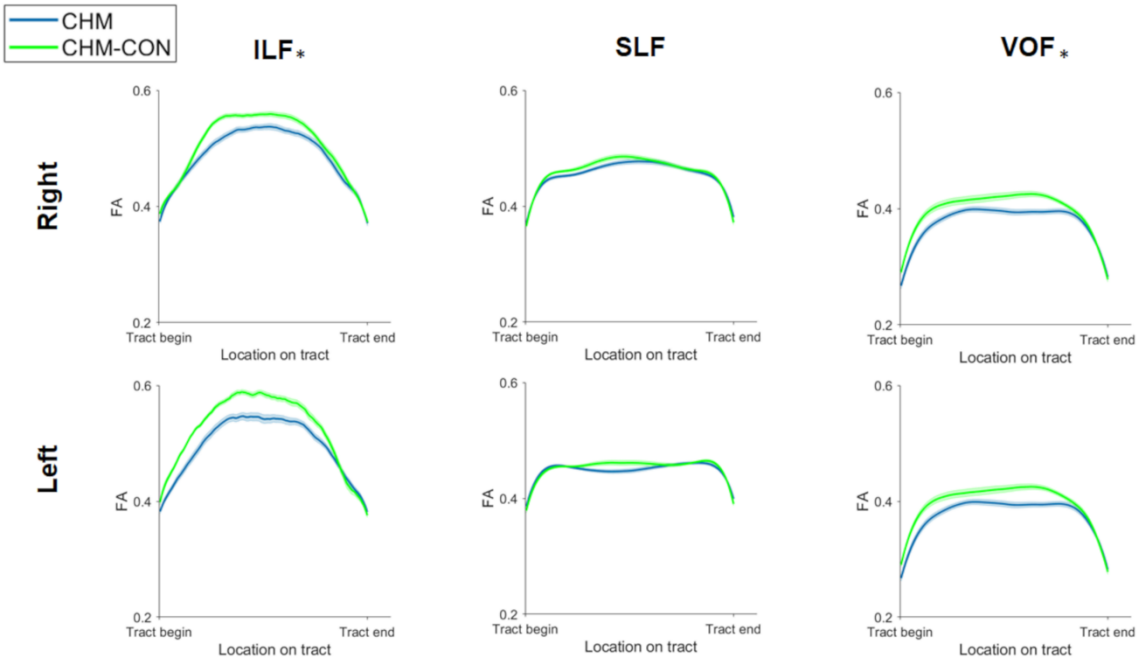


Figure 5-10: Tract profiles in choroideremia (blue) and control (green) groups showing FA values across the tracts. The top row shows tracts in the right hemisphere and bottom row shows tracts in the left hemisphere. The columns show tract profiles for the ILF, SLF, and VOF respectively. The stars by the tract name show which tracts were significantly different between the patient and control disease states. The shaded area around the bars represents the standard deviation.

This analysis was repeated for MD with the raw data shown in supplementary table 3. A two-way ANOVA was conducted to examine the difference in MD between tracts and disease state at different locations along the different tracts. Significant effects (P < 0.01) were noted for

disease state (F (1, 0.15) = 163.4), location (F (9, 0.02) = 24.5), and tract (F (5, 0.27) = 285.2). In addition, a significant interaction ($P \leq 0.01$) was noted between tracts and both location (F (45, 0.01) = 7.0) and disease state (F (5, 0.003) = 3.0). There was also a significant interaction between the disease state and location, F (9, 0.002) = 2.6, $P < 0.01$. As for FA, the pattern of MD changes across the length of the tract is dependent on both the tract being examined, and the disease state. MD was higher in the choroideremia group compared to the control population. Changes between the centre of the tract and the periphery were steepest in the ILF and shallowest in the SLF.

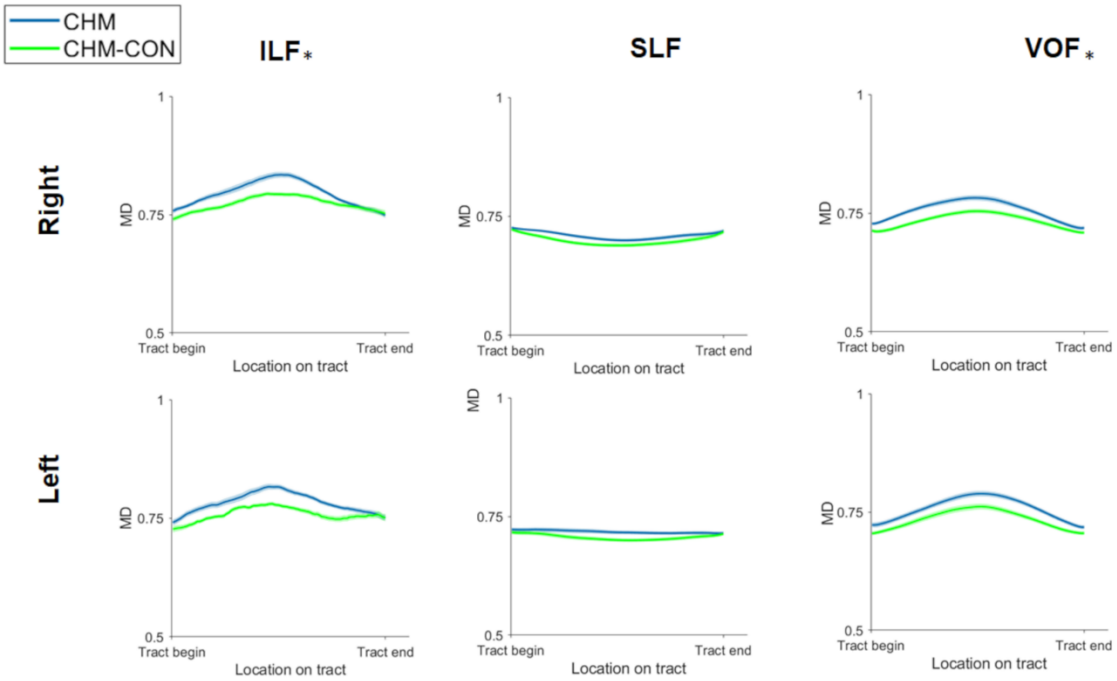


Figure 5-11: Tract profiles in choroideremia (blue) and control (green) groups showing MD values across the tracts. The top row shows tracts in the right hemisphere and bottom row shows tracts in the left hemisphere. The columns show tract profiles for the ILF, SLF, and VOF respectively. The stars show which tracts were significantly different between the patient and control disease states. The shaded area around the bars represents the standard deviation.

5.5 Discussion

TBSS showed an impact of the changes in VA and the central visual field on the white matter tracts but the peripheral visual field did not impact on the white matter tracts. Increased VA and

increased microperimetry threshold were associated with higher FA, a marker for increased white matter integrity. The greatest changes appeared to be in the optic radiations, visual cortex and corpus callosum. The corpus callosum connects the right and left hemispheres allowing inter-hemispheric communication and the stitching together of the hemi field representations of the world. There is significant visual input represented in the fibres of the corpus callosum (Pietrasanta, Restani, and Caleo 2012). A difference was likely not detected between the disease and control groups due to the range of visual deficits represented in the choroideremia group. Individual brains show a high degree of variability, so the process of warping to a standard template limits conclusions that can be drawn from TBSS about the location of changes (S. Smith et al. 2006). The specific impact on the tracts was therefore explored using tractography.

In the first instance, the optic radiations were examined as the longest visual specific white matter tract, connecting the eye and the brain. FA was lower in peripheral bundle compared to macular bundle and this pattern was present in both disease and control patients. In choroideremia, FA was reduced in both the macular and peripheral bundles and the difference between them does not appear to be magnified by disease.

Next, I examined the impact on specific tracts considered representative of the ventral visual stream (ILF), the dorsal visual stream (SLF) and a vertical tract connecting the two streams (VOF). Due to the functions of the streams and the differential cortical magnification effects, it could be expected that the peripheral visual field loss in choroideremia would have a larger impact on the dorsal stream. Differences between tracts in the choroideremia group versus controls showed a significant reduction in FA and increase in MD in the ILF and VOF but not the SLF.

Ocular data were as expected showing structural preservation with preserved VA in the choroideremia but functional defects were present as shown by the difference in microperimetry threshold. This fits with previous reports of central vision defects in choroideremia even in the

presence of preserved VA, with early defects in attributes such as colour despite normal looking central structure (Jolly et al. 2015). With central vision being so critical for quality of life (Azoulay et al. 2015), it is possible that even subtle changes in central visual function may be encouraging reshaping of the white matter pathways. The extent of visual field loss appears to be a significant factor in this change. With reducing visual field in the central area, there is a decrease in FA and increase in MD. This combination of factors is indicative of reduced white matter integrity as visual field declines.

The ILF is a large tract and encompasses more than the individual pathways of interest in the ventral visual pathway to examine visual ability (Gomez et al. 2015). There was greater asymmetry in the ILF between hemispheres compared to the other tracts. Choroideremia becomes less symmetrical between eyes as disease progresses, with relative temporal preservation (Jolly et al. 2016, 2017). The degree of functional asymmetry between the eyes may influence processes further downstream.

Assessing the change in the parameters over the length of the tracts appears to indicate the biggest difference in the centre of the tract as shown in the profile figures. This may in part be reflective of the methodology utilised. Tractography relies on identifying areas of white matter separate from the grey matter. The ends of the tracts insert into grey matter (such as LGN and V1). Therefore, variability in the FA and MD measurement is likely to increase as grey matter impedes on the tractography, reducing the significance of any change. The centre of the tracts is more likely to be exclusively white matter and, on this basis, likely to better reflect true differences in white matter microstructure.

Although the largest difference between the choroideremia and control groups was expected in the dorsal stream, no significant difference was found between groups in the SLF. The SLF does not originate in V1 and therefore may not be an adequate marker of the dorsal stream despite its connection to the motion areas (Makris et al. 2005). A logical next step would be to track from

point to point along a specific visual motion path connecting V1 and the motion complex. In view of the impact of peripheral field loss on mobility, this will be an important assessment of the true dorsal pathway. The VOF showed a difference between the choroideremia and control participants. Considering its role in connecting the two visual streams, and its origins in the cortex representing both streams, it is likely to be affected by changes in either or both streams (Takemura et al. 2016).

Central visual field changes have a significant impact on white matter integrity in areas both preceding and beyond V1. Retinal diseases causing changes in the visual field, particularly the central visual field cause downstream structural changes in the visual brain, which may need to be accounted for when treating the adult brain. The progressive nature of these changes are being investigated in the longitudinal arm of this study, which will provide information about the plasticity of the visual white matter. Once this is established, the possibility of reversing these changes can be examined. Since modern neuroscience provides a number of ways to improve plasticity in the brain, understanding these secondary changes resulting from degeneration may help to augment the effects of treatment to the eye.

5.6 Future Directions

We are currently developing a method to track along the white matter from one region of interest to the next. For example, the ventral pathway is associated with colours and detail. The colour and faces pathway in the brain follows a similar path with tracts from V1 to V2 to posterior inferior temporal region (PIT) and culminating in V4 (Conway 2009). Examining this pathway directly is likely to be the most suitable analysis of ventral stream and will be the subject of future work. For the dorsal pathway, I will track between V1 and the MT+ complex.

The next phase of this work is to incorporate functional measures across the network as measured by resting state MRI. This data has been collected and is being analysed in my postdoctoral

position. There is preliminary evidence to suggest that the functional connectivity alters in response to visual loss (Sabbah et al. 2017). By combining the datasets, structure-function correlations in the visual brain can be analysed for long range connectivity across the brain in different disease states. In addition, identical measures have been collected in patients with Stargardt disease to investigate the impact of severe central vision loss compared to the mild central vision loss seen in choroideremia. These measures will then be repeated following two years to assess whether the cortical changes continue with increasing changes in visual function. Once baseline changes have been measured and longitudinal patterns established, the impact of retinal therapy can be assessed.

5.7 Novel findings

A new peripheral supra threshold test has been developed for use on the Octopus perimeter.

This is the first time decreasing visual field has been shown to cause changes in white matter integrity in the visual pathways between the eye and V1, as well as beyond V1.

5.8 Implications for clinical practice

Changes in brain pathways occur secondary to vision loss due to defects in the eye. This change in processing likely contributes to differing adaptation to visual loss across patients. Retinal therapy alone may not be sufficient to treat vision loss. The reversibility of these changes will form the basis of future work in order to create clinical guidance.

Chapter 6:
General Discussion

6. General Discussion

6.1 Discussion

The aims of this thesis were to define a range of outcome measures for the assessment of rod-cone dystrophies, encompassing visual function measurement under different illumination levels, retinal anatomy measures and assessment of the white matter structure in the visual brain. This was driven by a lack of well-established protocols in current gene therapy trials. What I have shown is that vision is achieved and modulated by a range of circuits, which, interconnect the eye and the brain. Therefore, retinal changes must be considered in terms of their wider effects rather than in isolation.

The scoping review in chapter 1 highlights the problem with current practice regarding the measurements of visual function in gene therapy trials for the treatment of ophthalmic disease, mainly retinal disease. Established clinical measures are largely used. However, these may not be sensitive or suitable for the disease populations being studied. A few novel assessment methods have been developed but not currently universally accepted by the regulatory authorities or research teams. Herein I highlight the need for the development and validation of novel outcome measures for use in interventional trials for the treatment of retinal diseases, particularly inherited retinal degenerations (IRDs). There are three key reasons for this. Firstly, IRDs present with specific challenges, which have an impact on the practicalities of testing. For example, the reduction in visibility of objects external to the central field due to the marked visual field loss. Secondly, the heterogeneity of IRDs that means that a single measure of visual function will not necessarily capture the specific loss in any given disease. Having a deeper understanding of what each test is measuring and what is influencing it will help with the choice of the most appropriate tests in each situation. Thirdly, novel therapies require an understanding of the changes caused at a cellular level to optimally monitor the impact of therapy. By looking at effects as close as

possible to the mode of action, the ability to detect relevant changes will increase, resulting in shorter, less expensive and more effective clinical trials. It is worth noting that validation studies can be difficult in rare diseases as it can be challenging to recruit adequate numbers of patients.

Outcome measures should ideally be based on the biology of the disease and related to measurement of the therapeutic target within the eye, in order to maximise the chance of measuring a real therapeutic effect. This may change in end stage disease versus trials designed for early disease states, so suitable measures must be established for both. The balance of structural versus functional measures is likely to change in late stage versus early stage disease. However, some functional measures do remain relevant in end stage disease. If the novel outcome measures are established in the disease prior to the interventional trials, the data can be submitted to the regulatory authorities in advance of the interventional trials. This would increase the acceptability of these measures. Outcome measures should be based on an understanding of the underlying disease process as well as the impact of the gene therapy as determined by the expected impact of the viral vector and cells likely to be transfected. A significant advantage of this approach would be the likelihood of reaching the final outcome more quickly due to the use of targeted and sensitive markers of disease. The work in this thesis has contributed to more targeted testing of vision in IRD. In addition it has provided elucidation of these new testing approaches, as well as comparison with standard testing, thus paving the way for their validation and adoption.

The current key outcome identified in the scoping review was visual acuity (VA). The first half of chapter 2 therefore explores factors reducing the reliability of VA measurement in the presence of visual field loss in rod-cone dystrophies. When the visual field loss impedes on central vision, coming close to the fixation point, test-retest repeatability can be increased. This

has implications for the definition of a clinically significant change in longitudinal studies, so reducing the coefficient of repeatability increases the reliability of measurement and allows the end-point to be reached sooner. Using an electronic chart that can present the targets in the centre of the screen either as single line or as single letters reduces the requirement to track across the chart and find the letters, making the test more comfortable for the patient to conduct. Reducing the need to localise reduces the burden on the patient with fixation area being affected.

The second half of chapter 2 deals with another aspect of photopic function and cone vision; colour vision. I reviewed current colour vision testing protocols, the influence of disease on the three different cone populations with the resulting effect on testing results, as well as introducing optimisation of testing. Most colour vision tests are designed to elucidate colour perception, which is clinically useful. For clinical trials work it is more useful to infer cone photoreceptor function. I showed how an existing colour vision test can be optimised for measuring L, M and S cone function, and used in the presence of visual field loss. A tritan colour vision defect is present from early in the rod-cone dystrophy disease process, in the presence of normal visual acuity. The S cones are different from L and M cones in multiple ways. It is not clear from the current results whether the tritan defect shown is secondary to increased vulnerability of S cones to rod disease either directly or indirectly, and this requires further investigation. The implication of this for clinical trials is that any colour vision testing utilised for IRDs must include the ability to measure defects in the tritan axis as well as measure more subtle changes than clinically used tests. A significant factor that could affect the reliability of colour vision assessment is the presence of cataract. Cataract is a side effect of subretinal injections used to deliver the viral vector to the retina (Edwards et al. 2016b; Xue et al. 2018). Work is ongoing to quantify the effect of different types of cataract on the colour vision measurements so these can accurately be accounted for in interventional trials.

In chapter 3 I explore both global and local methods of measuring scotopic function. Both have a place in clinical trials settings. Full field stimulus testing (FST) is a robust measure that can be meaningful in end stage disease and reflects remaining retinal function. It is quick and easy to perform. This is the first assessment of how FST reflects dark adaptation pattern in retinal disease. However, using response to white light does not allow us to separate the contribution of rods and cones to scotopic function. This can be achieved using differential responses to red and blue lights. The two colour method is the basis of scotopic microperimetry, allowing localised changes and patterns of loss to be assessed. This is most suitable for patients with central preservation due to the demanding nature of the test. However, scotopic microperimetry is a promising technology to probe the pattern of rod loss in more central regions of the retina in retinal disease. This work is the first use of scotopic microperimetry in rod-cone dystrophies. Going forward I will be exploring a variety of genetic mutations with differential biological impacts to explore patterns of rod loss according to pathological mechanisms. For example how genetic mutations expressed as part of the rod phototransduction cascade influence patterns of photoreceptor loss versus mutations in genes affecting both rods and cones. Ciliopathies such as Usher's syndrome are likely to have a different pattern of loss compared to RPE diseases such as MERTK. Probing these differential phenotypes with scotopic microperimetry may provide insights into the natural history and mechanisms of the cell loss. Differential patterns of rod and cone cell function may also provide insights into how the rod and cone systems interact at a retinal level.

Chapters 2 and 3 show the difficulties in trying to separate out vision in terms of rod and cone function as per conventional thinking. It may be more helpful to think of how vision performs under differential light levels as this will relate more closely to patient perceived quality of life. The rod and cone systems are interlinked in multiple ways and have the ability to influence each other at multiple points along the pathway. Both chapters demonstrate the difficulty with

separating rod and cone function as independent entities, in a way that has not been highlighted previously. The relationship between rods and cones will change with differing light levels and disease state. This leads to the question of downstream effects of photoreceptor loss.

In chapter 4 I explore the structural reorganisation of the retina in response to photoreceptor disease, and show that inner retinal thickening accompanies photoreceptor thinning. MATLAB scripts were developed for the analysis of OCT and MAIA data, and made publicly available for other teams to use. This is the first example of the impact of inner retinal changes on functional measurements. Although the impact of the inner retinal changes on the microperimetry threshold measurement is smaller than the impact of the photoreceptor changes, it is still present and requires validation in larger numbers. This is particularly important because simply taking the average retinal thickness may mask the combination of thinning and thickening. For the first time I have shown a relationship between photoreceptor thinning and inner retinal thickening on microperimetry threshold changes at different eccentricities. The next stage will quantify this relationship in a larger dataset and in other retinal diseases.

In chapter 5, by using diffusion MRI to examine the structural circuits from the retina to the brain, I show changes across a number of visual white matter pathways in patients with choroideremia compared to control participants. In the optic radiations, which lead to the primary visual cortex, white matter structural integrity is affected by central visual field loss. Furthermore, a similar effect is also seen beyond V1, in two tracts connecting V1 to higher visual centres; the inferior longitudinal fasciculus (ILF) of the ventral visual pathway and the vertical occipital fasciculus (VOF) that connects the ventral and dorsal streams. The ventral stream is the pathway for perception and the dorsal stream is considered the pathway for action. Central visual field loss appears to have an impact on the ventral stream earlier in the disease process (as shown

by microperimetry loss and preservation) than expected. The dorsal stream did not show any impact related to the loss of peripheral vision, however, further work is being conducted to identify more suitable visual specific tracts to examine. This is the first comprehensive study integrating assessment of visual function, retinal imaging and brain imaging to examine the visual system as a unit in inherited retinal disease. This work shows that retinal disease causes changes throughout multiple visual circuits in the brain. This may limit the degree of improvement in vision possible by treating the retinal disease alone, as well as account for the differential adaptation that patients show to levels of vision loss.

The work investigating the visual brain in retinal disease opens up a new area of visual neuroscience. Once the baseline changes with disease state are understood, the progressive nature of these changes over time must be investigated. This will give an indication into the adaptability of the visual system at the cortical level. Visual improvement with gene therapy may be limited by secondary changes in the visual brain. If these changes are progressive, there is hope the changes are also reversible, either by re-establishing retinal integrity and thus a normal signal to the brain, or by harnessing mechanisms to increase brain adaptability. This can be done adjunct to retinal intervention, increasing the potential visual benefit following therapy, and forms an exciting future avenue of research. Being an optometrist with neuroscience training places me in a good position to conduct research into appropriate visual function measures and implementation of these into clinical practice.

6.2 Conclusion

The three aims of my thesis have been achieved. Firstly, strategies for optimising visual acuity measurement in the presence of visual field loss. This is critical in view of visual acuity being a key outcome measure in so many trials and so widely accepted. Electronic charts were able to

achieve this aim in chapter 2. The second aim was to probe different aspects of visual function, taking into account the impact of visual field loss, and develop of deeper understanding of the tests. Colour vision, FST and scotopic microperimetry were explored to achieve this aim in chapters 2 and 3. Finally, the impact of visual field loss on the visual brain was the third aim. First the changes in retinal circuits were measured via retinal remodelling in chapter 4. This impacts further downstream as seen in the white matter pathways in the brain, both leading to and from the primary visual cortex.

Evaluation and implementation of accurate and appropriate visual function testing for IRDs is an evolving field, which is being driven by the introduction of novel therapies for IRDs. Novel more sophisticated imaging and functional testing has enabled in depth phenotyping, which has highlighted important differences in how IRDs affect vision. The work in this thesis emphasises the importance of targeted measures of visual function, as well as the assessment of the contribution of the brain in health and disease. This work has also led to a number of other important research questions which are already in development to further refine visual testing in inherited retinal disease.

References

Bibliography

Ach, Thomas, Carrie Huisingh, Gerald Mcgwin Jr, Jeffrey D Messinger, Tianjiao Zhang, Mark J Bentley, Danielle B Gutierrez, et al. 2014. "Quantitative Autofluorescence and Cell Density Maps of the Human Retinal Pigment Epithelium." *Investigative Ophthalmology & Visual Science* 55 (8): 4832–41. https://doi.org/10.1167/iovs.14-14802.

Aebersold, H., O.D. Creutzfeldt, U. Kuhnt, and D. Sanides. 1981. "Representation of the Visual Field in the Optic Tract and Optic Chiasma of the Cat." *Experimental Brain Research* 42: 127–45.

Afarid, Mehrdad, Mohammad Torabi-Nami, and Bijan Zare. 2016. "Neuroprotective and Restorative Effects of the Brain-Derived Neurotrophic Factor in Retinal Diseases." *Journal of the Neurological Sciences* 363: 43–50. https://doi.org/10.1016/j.jns.2016.02.024.

Aleman, Tomas S., Artur V. Cideciyan, Alexander Sumaroka, Sharon B. Schwartz, Alejandro J. Roman, Elizabeth A.M. Windsor, Janet D. Steinberg, et al. 2007. "Inner Retinal Abnormalities in X-Linked Retinitis Pigmentosa with RPGR Mutations." *Investigative Ophthalmology and Visual Science* 48 (10): 4759–65. https://doi.org/10.1167/iovs.07-0453.

Aleman, Tomas S., Artur V. Cideciyan, Alexander Sumaroka, Elizabeth A.M. Windsor, Waldo Herrera, D. Alan White, Shalesh Kaushal, et al. 2008. "Retinal Laminar Architecture in Human Retinitis Pigmentosa Caused by Rhodopsin Gene Mutations." *Investigative Ophthalmology and Visual Science* 49 (4): 1580–91. https://doi.org/10.1167/iovs.07-1110.

Altman, Douglas G. 1990. *Practical Statistics for Medical Research*. 1st ed. London: Chapman and Hall/CRC.

Andersson, Jesper L.R., Stefan Skare, and John Ashburner. 2003. "How to Correct Susceptibility Distortions in Spin-Echo Echo-Planar Images: Application to Diffusion Tensor Imaging." *NeuroImage* 20 (2): 870–88. https://doi.org/10.1016/S1053-8119(03)00336-7.

Ashtari, Manzar, Laura L Cyckowski, Justin F Monroe, Kathleen a Marshall, Daniel C Chung, Alberto Auricchio, Francesca Simonelli, et al. 2011. "The Human Visual Cortex Responds to Gene Therapy – Mediated Recovery of Retinal Function." *J Clin Invest* 121 (6): 2160–68. https://doi.org/10.1172/JCI57377.2160.

Assaf, Yaniv, Heidi Johansen-Berg, and Michel Thiebaut de Schotten. 2019. "The Role of Diffusion MRI in Neuroscience." *NMR in Biomedicine* 32 (4): 1–16. https://doi.org/10.1002/nbm.3762.

Avesani, Paolo, Brent McPherson, Soichi Hayashi, Cesar F. Caiafa, Robert Henschel, Eleftherios Garyfallidis, Lindsey Kitchell, et al. 2019. "The Open Diffusion Data Derivatives, Brain Data Upcycling via Integrated Publishing of Derivatives and Reproducible Open Cloud Services." *Scientific Data* 6 (1): 69. https://doi.org/10.1038/s41597-019-0073-y.

Aydogan, DB, and Y Shi. 2019. "A Novel Fiber Tracking Algorithm Using Parallel Transport Frames." In *Proceedings of the 27th Annual Meeting of the International Society of Magnetic Resonance in Medicine (ISMRM)*.

Azoulay, Line, Philippe Chaumet-Riffaud, Steven Jaron, Camille Roux, Serge Sancho, Naomi

Berdugo, Isabelle Audo, José Alain Sahel, and Saddek Mohand-Saïd. 2015. “Threshold Levels of Visual Field and Acuity Loss Related to Significant Decreases in the Quality of Life and Emotional States of Patients with Retinitis Pigmentosa.” *Ophthalmic Research* 54 (2): 78–84. https://doi.org/10.1159/000435886.

Bach, Michael, Mitchell G. Brigell, Marko Hawlina, Graham E. Holder, Mary A. Johnson, Daphne L. McCulloch, Thomas Meigen, and Suresh Viswanathan. 2013. “ISCEV Standard for Clinical Pattern Electroretinography (PERG): 2012 Update.” *Documenta Ophthalmologica* 126 (1): 1–7. https://doi.org/10.1007/s10633-012-9353-y.

Bailey, Ian L., and Jan E. Lovie-Kitchin. 2013. “Visual Acuity Testing. From the Laboratory to the Clinic.” *Vision Research* 90: 2–9. https://doi.org/10.1016/j.visres.2013.05.004.

Bainbridge, James WB., Manjit S. Mehat, Venki Sundaram, Scott J. Robbie, Susie E. Barker, Caterina Ripamonti, Anastasios Georgiadis, et al. 2015. “Long-Term Effect of Gene Therapy on Leber’s Congenital Amaurosis.” *New England Journal of Medicine* 372 (20): 1887–97. https://doi.org/10.1056/NEJMoa1414221.

Bainbridge, James WB, A J Smith, S S Barker, S Robbie, R Henderson, K Balaggan, A Viswanathan, et al. 2008. “Effect of Gene Therapy on Visual Function in Leber’s Congenital Amaurosis.” *N Engl J Med* 358 (21): 2231–39. https://doi.org/10.1056/NEJMoa0802268.

Beaulieu, Christian. 2002. “The Basis of Anisotropic Water Diffusion in the Nervous System - A Technical Review.” *NMR in Biomedicine* 15 (7–8): 435–55. https://doi.org/10.1002/nbm.782.

Beck, Roy W., Pamela S. Moke, Andrew H. Turpin, Frederick L. Ferris, John Paul SanGiovanni, Chris A. Johnson, Eileen E. Birch, et al. 2003. “A Computerized Method of Visual Acuity Testing: Adaptation of the Early Treatment of Diabetic Retinopathy Study Testing Protocol.” *American Journal of Ophthalmology* 135 (2): 194–205. https://doi.org/10.1016/S0002-9394(02)01825-1.

Bennett, Jean, Jennifer Wellman, Kathleen A. Marshall, Sarah McCague, Manzar Ashtari, Julie DiStefano-Pappas, Okan U. Elci, et al. 2016. “Safety and Durability of Effect of Contralateral-Eye Administration of AAV2 Gene Therapy in Patients with Childhood-Onset Blindness Caused by RPE65 Mutations: A Follow-on Phase 1 Trial.” *The Lancet* 388 (10045): 661–72. https://doi.org/10.1016/S0140-6736(16)30371-3.

Benson, Noah C., Omar H. Butt, David H. Brainard, and Geoffrey K. Aguirre. 2014. “Correction of Distortion in Flattened Representations of the Cortical Surface Allows Prediction of V1-V3 Functional Organization from Anatomy.” *PLoS Computational Biology* 10 (3). https://doi.org/10.1371/journal.pcbi.1003538.

Benson, Noah C, Omar H Butt, Ritobrato Datta, Petya D Radoeva, David H Brainard, and Geoffrey Karl Aguirre. 2012. “The Retinotopic Organization of Striate Cortex Is Well Predicted by Surface Topology.” *Current Biology* 22 (21): 2018–85. https://doi.org/10.1016/j.cub.2012.09.014.

Berson, Eliot L. 2007. “Long-Term Visual Prognoses in Patients with Retinitis Pigmentosa The Ludwig von Sallmann Lecture.” *Experimental Eye Research* 85 (1): 7–14. https://doi.org/10.1016/j.freeradbiomed.2008.10.025.The.

Bittner, Ava K., Mohamed A. Ibrahim, Jennifer A. Haythornthwaite, Marie Diener-West, and Gislin Dagnelie. 2011. “Vision Test Variability in Retinitis Pigmentosa and Psychosocial Factors.” *Optometry and Vision Science* 88 (12): 1496–1506.

https://doi.org/10.1097/OPX.0b013e3182348d0b.

Bland, Martin J., and DG Altman. 1996a. “Measurement Error.” *British Medical Journal* 312: 1654. https://doi.org/10.1136/bmj.313.7049.106.

———. 1996b. “Measurement Error Proportional to the Mean.” *British Medical Journal* 313: 106.

———. 1999. “Measuring Agreement in Method Comparison Studies.” *Statistical Methods in Medical Research* 2802 (8): 135–60.

Boer, Michiel R de, Annette C Moll, Henrica C W de Vet, Caroline B Terwee, Hennie J M Völker-Dieben, and Ger H M B van Rens. 2004. “Psychometric Properties of Vision-Related Quality of Life Questionnaires: A Systematic Review.” *Ophthalmic & Physiological Optics : The Journal of the British College of Ophthalmic Opticians (Optometrists)* 24 (4): 257–73. https://doi.org/10.1111/j.1475-1313.2004.00187.x.

Boote, Jonathan, Wendy Baird, and Anthea Sutton. 2011. “Public Involvement in the Design and Conduct of Clinical Trials: A Narrative Review of Case Examples.” *Trials* 12 (S1): A82. https://doi.org/10.1186/1745-6215-12-s1-a82.

Brainard, David H. 2015. “Color and the Cone Mosaic.” *Annual Review of Vision Science* 1: 519–46. https://doi.org/10.1146/annurev-vision-082114-035341.

Brown, Brian, and K H Yap. 1995. “Differences in Visual Acuity between the Eyes: Determination of Normal Limits in a Clinical Population.” *Ophthalmic and Physiological Optics* 15 (3): 163–69.

Brown, HDH, Rachel L. Woodall, Rebecca E. Kitching, Heidi A. Baseler, and Antony B. Morland. 2016. “Using Magnetic Resonance Imaging to Assess Visual Deficits: A Review.” *Ophthalmic and Physiological Optics* 36 (3): 240–65. https://doi.org/10.1111/opo.12293.

Buckley, Thomas M.W., Jasleen K. Jolly, Moreno Menghini, Laura Wood, Anika Nanda, and Robert E. MacLaren. 2020. “Test-Retest Repeatability of Microperimetry in Patients with Retinitis Pigmentosa Caused by Mutations in RPGR.” *Clinical & Experimental Ophthalmology*, no. March. https://doi.org/10.1111/ceo.13753.

Bullock, Daniel, Hiromasa Takemura, Cesar F. Caiafa, Lindsey Kitchell, Brent McPherson, Bradley Caron, and Franco Pestilli. 2019. “Associative White Matter Connecting the Dorsal and Ventral Posterior Human Cortex.” *Brain Structure and Function* 224 (8): 2631–60. https://doi.org/10.1007/s00429-019-01907-8.

Burke, Tomas R, Tobias Duncker, Russell L Woods, Jonathan P Greenberg, Jana Zernant, Stephen H Tsang, R Theodore Smith, Rando Allikmets, Janet R Sparrow, and C Delori. 2014. “Quantitative Fundus Autofluorescence in Recessive Stargardt Disease.” *Investigative Ophthalmology and Visual Science* 55 (5): 2841–52. https://doi.org/10.1167/iovs.13-13624.

Byrne, Leah C., Deniz Dalkara, Gabriel Luna, Steven K. Fisher, Emmanuelle Clérin, Jose Alain Sahel, Thierry Léveillard, and John G. Flannery. 2015. “Viral-Mediated RdCVF and RdCVFL Expression Protects Cone and Rod Photoreceptors in Retinal Degeneration.” *Journal of Clinical Investigation* 125 (1): 105–16. https://doi.org/10.1172/JCI65654.

Campochiaro, Peter A., Andreas K. Lauer, Elliott H. Sohn, Tahreem A. Mir, Stuart Naylor, Matthew C. Anderton, Michelle Kelleher, Richard Harrop, Scott Ellis, and Kyriacos A.

Mitrophanous. 2017. “Lentiviral Vector Gene Transfer of Endostatin/Angiostatin for Macular Degeneration (GEM) Study.” *Human Gene Therapy* 28 (1): 99–111. https://doi.org/10.1089/hum.2016.117.

Cao, Dingcai, Joel Pokorny, Vivianne C. Smith, and Andrew J. Zele. 2008. “Rod Contributions to Color Perception: Linear with Rod Contrast.” *Vision Research* 48 (26): 2586–92. https://doi.org/10.1016/j.visres.2008.05.001.

Catani, Marco, Robert J. Howard, Sinisa Pajevic, and Derek K. Jones. 2002. “Virtual in Vivo Interactive Dissection of White Matter Fasciculi in the Human Brain.” *NeuroImage* 17 (1): 77–94. https://doi.org/10.1006/nimg.2002.1136.

Cehajic-kapetanovic, Jasmina, Kanmin Xue, Cristina Martinez-fernandez De Camara, Anika Nanda, Alexandra Davies, Laura J Wood, Anna Paola Salvetti, et al. 2020. “Initial Results from a First-in-Human Gene Therapy Trial on X-Linked Retinitis Pigmentosa Caused by Mutations in RPGR.” *Nature Medicine*. https://doi.org/10.1038/s41591-020-0763-1.

Chang, Hsuan, and J. Michael Fitzpatrick. 1992. “A Technique for Accurate Magnetic Resonance Imaging in the Presence of Field Inhomogeneities.” *IEEE Transactions on Medical Imaging* 11 (3): 319–29. https://doi.org/10.1109/42.158935.

Cheng, Dan, Yuqin Wang, Shenghai Huang, Qiuyan Wu, Qi Chen, Meixiao Shen, and Fan Lu. 2016. “Macular Inner Retinal Layer Thickening and Outer Retinal Layer Damage Correlate with Visual Acuity during Remission in Behcet’s Disease.” *Investigative Ophthalmology and Visual Science* 57 (13): 5470–78. https://doi.org/10.1167/iovs.16-19568.

Chow-Wing-Bom, Hugo, Tessa M. Dekker, and Pete R. Jones. 2020. “The Worse Eye Revisited: Evaluating the Impact of Asymmetric Peripheral Vision Loss on Everyday Function.” *Vision Research* 169: 49–57. https://doi.org/10.1016/j.visres.2019.10.012.

Ciavarella, Pio, Giuseppe Moretti, Benedetto Falsini, and Vittorio Porciatti. 1997. “The Pattern Electroretinogram (PERG) after Laser Treatment of the Peripheral or Central Retina.” *Current Eye Research* 16 (2): 111–15. https://doi.org/10.1076/ceyr.16.2.111.5094.

Cideciyan, Artur V., Geoffrey K. Aguirre, Samuel G. Jacobson, Omar H. Butt, Sharon B. Schwartz, Malgorzata Swider, Alejandro J. Roman, Sam Sadigh, and William W. Hauswirth. 2015. “Pseudo-Fovea Formation after Gene Therapy for RPE65- LCA.” *Investigative Ophthalmology and Visual Science* 56 (1): 526–37. https://doi.org/10.1167/iovs.14-15895.

Cideciyan, Artur V., T. S. Aleman, S. L. Boye, S. B. Schwartz, S. Kaushal, A. J. Roman, J.-j. Pang, et al. 2008. “Human Gene Therapy for RPE65 Isomerase Deficiency Activates the Retinoid Cycle of Vision but with Slow Rod Kinetics.” *Proceedings of the National Academy of Sciences* 105 (39): 15112–17. https://doi.org/10.1073/pnas.0807027105.

Cideciyan, Artur V., William W. Hauswirth, Tomas S. Aleman, Shalesh Kaushal, Sharon B. Schwartz, Sanford L. Boye, Elizabeth A.M. Windsor, et al. 2009. “Human *RPE65* Gene Therapy for Leber Congenital Amaurosis: Persistence of Early Visual Improvements and Safety at 1 Year.” *Human Gene Therapy* 20 (9): 999–1004. https://doi.org/10.1089/hum.2009.086.

Collison, Frederick T., Gerald A. Fishman, J. Jason McAnany, Jana Zernant, and Rando Allikmets. 2014. “Psychophysical Measurement of Rod and Cone Thresholds in Stargardt Disease with Full-Field Stimuli.” *Retina* 34 (9): 1888–95. https://doi.org/10.1038/jid.2014.371.

Constable, Ian J., Chooi May Lai, Aaron L. Magno, Martyn A. French, Samuel B. Barone, Steven D. Schwartz, Mark S. Blumenkranz, Mariapia A. Degli-Esposti, and Elizabeth P. Rakoczy. 2017. “Gene Therapy in Neovascular Age-Related Macular Degeneration: Three-Year Follow-up of a Phase 1 Randomized Dose Escalation Trial.” *American Journal of Ophthalmology* 177: 150–58. https://doi.org/10.1016/j.ajo.2017.02.018.

Conway, Bevil R. 2009. “Color Vision, Cones, and Color-Coding in the Cortex.” *Neuroscientist* 15 (3): 274–90. https://doi.org/10.1177/1073858408331369.

Corson, D. Wesley, M. Carter Cornwall, Edward F. Macnichol, Jing Jin, Randy Johnson, Fadila Derguini, Rosalie K. Crouch, and Koji Nakanishi. 1990. “Sensitization of Bleached Rod Photoreceptors by 11-Cis-Locked Analogues of Retinal.” *Proceedings of the National Academy of Sciences of the United States of America* 87 (17): 6823–27. https://doi.org/10.1073/pnas.87.17.6823.

Costa, Rogério A., Mirian Skaf, Luiz A.S. Melo, Daniela Calucci, Jose A. Cardillo, Jarbas C. Castro, David Huang, and Maciej Wojtkowski. 2006. “Retinal Assessment Using Optical Coherence Tomography.” *Progress in Retinal and Eye Research* 25 (3): 325–53. https://doi.org/10.1016/j.preteyeres.2006.03.001.

Crossland, Michael D, Adnan Tufail, Gary S Rubin, and Andrew Stockman. 2012. “Mesopic Microperimetry Measures Mainly Cones; Dark-Adapted Microperimetry Measures Rods and Cones [ARVO Abstract 4822].” *Investigative Ophthalmology & Visual Science* 53 (14): 4822.

Cruz-Herranz, Andrés, Lisanne J. Balk, Timm Oberwahrenbrock, Shiv Saidha, Elena H Martinez- Lapiscina, Wolf A Lagreze, Wolf A Schuman, et al. 2016. “The APOSTEL Recommendations for Reporting Quantitative Optical Coherence Tomography Studies.” *Neurology* 86: 2303–9.

Csaky, Karl, Frederick Ferris, Emily Y. Chew, Prashant Nair, Janet K. Cheetham, and Jacque L. Duncan. 2017. “Report from the NEI/FDA Endpoints Workshop on Age- Related Macular Degeneration and Inherited Retinal Diseases.” *Investigative Ophthalmology and Visual Science* 58 (9): 3456–63. https://doi.org/10.1167/iovs.17-22339.

Curcio, Christine A., Kimberly A. Allen, Kenneth R. Sloan, Connie L. Lerea, James B. Hurley, Ingrid B. Klock, and Ann H. Milam. 1991. “Distribution and Morphology of Human Cone Photoreceptors Stained with Anti-blue Opsin.” *Journal of Comparative Neurology* 312 (4): 610–24. https://doi.org/10.1002/cne.903120411.

Curcio, Christine A., c. Leigh Millican, Kimberly A. Allen, and Robert E. Kalina. 1993. “Aging of the Human Photoreceptor Mosaic: Evidence for Selective Vulnerability of Rods in Central Retina.” *Investigative Ophthalmology & Visual Science* 34 (12): 3278–96.

Curcio, Christine A, Kenneth R Sloan, Robert E Kalina, and Anita E Hendrickson. 1990. “Human Photoreceptor Topography.” *The Journal of Comparative Neurology* 292: 497–523.

Delori, C, Douglas G Goger, and C Kathleen Dorey. 2001. “Age-Related Accumulation and Spatial Distribution of Lipofuscin in RPE of Normal Subjects Franc.” *Investigative Ophthalmology and Visual Science* 42 (8): 1855–66.

Dias, Marina França, Kwangsic Joo, Jessica A. Kemp, Silvia Ligório Fialho, Armando da Silva Cunha, Se Joon Woo, and Young Jik Kwon. 2018. “Molecular Genetics and Emerging Therapies for Retinitis Pigmentosa: Basic Research and Clinical Perspectives.” *Progress in Retinal and Eye Research* 63: 107–31. https://doi.org/10.1016/j.preteyeres.2017.10.004.

Dimopoulos, Ioannis S., Stephanie C. Hoang, Alina Radziwon, Natalia M. Binczyk, Miguel C. Seabra, Robert E. MacLaren, Rizwan Somani, Matthew T.S. Tennant, and Ian M. MacDonald. 2018. “Two-Year Results After AAV2-Mediated Gene Therapy for Choroideremia: The Alberta Experience.” *American Journal of Ophthalmology* 193: 130–42. https://doi.org/10.1016/j.ajo.2018.06.011.

Dimopoulos, Ioannis S, Paul R Freund, Jacob A Knowles, and Ian M MacDonald. 2018. “THE NATURAL HISTORY OF FULL-FIELD STIMULUS THRESHOLD DECLINE IN CHOROIDEREMIA.” *Retina (Philadelphia, Pa.)* 38 (9): 1731–42. https://doi.org/10.1097/IAE.0000000000001764.

Distler, C., and Z. Dreher. 1996. “Glia Cells of the Monkey Retina-II. Muller Cells.” *Vision Research* 36 (16): 2381–94. https://doi.org/10.1016/0042-6989(96)00005-3.

Edwards, Thomas L., Markus Groppe, Jasleen K. Jolly, Susan M. Downes, and Robert E. Maclaren. 2015. “Correlation of Retinal Structure and Function in Choroideremia Carriers.” *Ophthalmology* 122 (6): 1274–76. https://doi.org/10.1016/j.ophtha.2014.12.036.

Edwards, Thomas L., Jasleen K. Jolly, Markus. Groppe, Alun R. Barnard, Charles L. Cottriall, Tanya. Tolmachova, Graeme C M. Black, et al. 2016a. “Visual Acuity after Retinal Gene Therapy for Choroideremia.” *New England Journal of Medicine* 374 (20): 1996–98. https://doi.org/10.1056/NEJMc1509501.

Edwards, Thomas L., Jasleen K. Jolly, Markus Groppe, Alun R. Barnard, Charles L. Cottriall, Tanya Tolmachova, Graeme C. Black, et al. 2016b. “Visual Acuity after Retinal Gene Therapy for Choroideremia.” *New England Journal of Medicine* 374 (20): 1996–98. https://doi.org/10.1056/NEJMc1509501.

Emde, Leon von der, Maximilian Pfau, Sarah Thiele, Philipp T Moller, Ruth Hassenrik, Monika Fleckenstein, Frank G Holz, and Steffen Schmitz-Valckenberg. 2019. “Mesopic and Dark-Adapted Two-Color Fundus-Controlled Perimetry in Choroidal Neovascularization Secondary to Age-Related Macular Degeneration.” *Translational Vision Science & Technology* 8 (1): 7. https://doi.org/10.1167/tvst.8.1.7.

Falcao-Reis, F. M., F. O’Sullivan, W. Spileers, C. Hogg, and G. B. Arden. 1991. “Macular Colour Contrast Sensitivity in Ocular Hypertension and Glaucoma: Evidence for Two Types of Defect.” *British Journal of Ophthalmology* 75 (10): 598–602. https://doi.org/10.1136/bjo.75.10.598.

Feuer, William J., Joyce C Schiffman, Janet L Davis, Vittorio Porciatti, Phillip Gonzalez, Rajeshwari D Koilkonda, Hiujan Yuan, Anil Lalwani, Byron L Lam, and John Guy. 2016. “Gene Therapy for Leber Hereditary Optic Neuropathy: Initial Results.” *Ophthalmology* 123 (3): 558–70. https://doi.org/10.1016/j.cogdev.2010.08.003.Personal.

Field, Greg D, and E.J. Chichilnisky. 2007. “Information Processing in the Primate Retina: Circuitry and Coding.” *Annual Review of Neuroscience* 30 (1): 1–30. https://doi.org/10.1146/annurev.neuro.30.051606.094252.

Field, Greg D, and Alapakkam P Sampath. 2016. “Behavioural and Physiological Limits to Vision in Mammals.” *Philosophical Transactions of the Royal Society B: Biological Sciences* 372: 20160072. https://doi.org/10.1098/rstb.2016.0072.

Fischer, M Dominik, Stylianos Michalakis, Barbara Wilhelm, Ditta Zobor, Regine Muehlfriedel, Susanne Kohl, Nicole Weisschuh, et al. 2020. “Safety and Vision Outcomes of Subretinal Gene Therapy Targeting Cone Photoreceptors in Achromatopsia: A

Nonrandomized Controlled Trial." *JAMA Ophthalmology*, April. https://doi.org/10.1001/jamaophthalmol.2020.1032.

Fischer, M Dominik, G Alex Ochakovski, Benjamin Beier, Immanuel P Seitz, Yousof Vaheb, Constanze Kortuem, Felix F L Reichel, et al. 2020. "CHANGES IN RETINAL SENSITIVITY AFTER GENE THERAPY IN CHOROIDEREMIA." *Retina* 40 (1): 160–68. https://doi.org/10.1097/iae.0000000000002360.

Fischl, Bruce. 2012. "FreeSurfer." *NeuroImage* 62 (2): 774–81. https://doi.org/10.1016/j.neuroimage.2012.01.021.

Fleckenstein, Monika, Peter Charbel Issa, and Frank G Holz. 2014. "Fundus Autofluorescence Imaging in Retinal Dystrophies." In *Inherited Chorioretinal Dystrophies: A Textbook and Atlas*, edited by Bernard Puech, Jean-Jacques De Laey, and Graham E Holder, 41–59. Berlin, Heidelberg: Springer Berlin Heidelberg. https://doi.org/10.1007/978-3-540-69466-3_6.

Fleckenstein, Monika, Steffen Schmitz-valckenberg, Moritz Lindner, Athanasios Bezatis, Eva Becker, Rolf Fimmers, Frank G Holz, and Fundus Autofluorescence. 2014. "The '"Diffuse-Trickling"' Fundus Autofluorescence Phenotype in Geographic Atrophy." *Investigative Ophthalmology and Visual Science* 55 (5): 2911–20. https://doi.org/10.1167/iovs.13-13409.

Flynn, Erin, Keiko Ueda, Emily Auran, Jack M Sullivan, and Janet R Sparrow. 2014. "Fundus Autofluorescence and Photoreceptor Cell Rosettes in Mouse Models." *Investigative Ophthalmology & Visual Science* 55: 5643–52. https://doi.org/10.1167/iovs.14-14136.

Foote, Katharina G, Nicholas Rinella, Janette Tang, Nicolas Bensaid, Hao Zhou, Qinqin Zhang, Ruikang K Wang, Travis C Porco, Austin Roorda, and Jacque L Duncan. 2019. "Cone Structure Persists Beyond Margins of Short-Wavelength Autofluorescence in Choroideremia." *Investigative Ophthalmology & Visual Science* 60 (14): 4931–42. https://doi.org/10.1167/iovs.19-27979.

Fraser, Rogan G., Rose Tan, Lauren N. Ayton, Emily Caruso, Robyn H. Guymer, and Chi D. Luu. 2016. "Assessment of Retinotopic Rod Photoreceptor Function Using a Dark-Adapted Chromatic Perimeter in Intermediate Age-Related Macular Degeneration." *Investigative Ophthalmology and Visual Science* 57 (13): 5436–42. https://doi.org/10.1167/iovs.16-19295.

Fu, Dun J., Kanmin Xue, Jasleen K. Jolly, and Robert E. MacLaren. 2019. "A Detailed in Vivo Analysis of the Retinal Nerve Fibre Layer in Choroideremia." *Acta Ophthalmologica* 97 (4): e589–600. https://doi.org/10.1111/aos.13973.

Fulton, Anne B, Janice Dodge, Ronald M Hansen, and Theodore P Williams. 1999. "The Rhodopsin Content of Human Eyes." *Investigative Ophthalmology & Visual Science* 40 (8): 1878–83.

Gajamange, Sanuji, David Raffelt, Thijs Dhollander, Elaine Lui, Anneke van der Walt, Trevor Kilpatrick, Joanne Fielding, Alan Connelly, and Scott Kolbe. 2018. "Fibre-Specific White Matter Changes in Multiple Sclerosis Patients with Optic Neuritis." *NeuroImage: Clinical* 17: 60–68. https://doi.org/10.1016/j.nicl.2017.09.027.

Gattass, Ricardo, Sheila Nascimento-Silva, Juliana G.M. Soares, Bruss Lima, Ana Karla Jansen, Antonia Cinira M. Diogo, Mariana F. Farias, et al. 2005. "Cortical Visual Areas in Monkeys: Location, Topography, Connections, Columns, Plasticity and Cortical Dynamics." *Philosophical Transactions of the Royal Society B: Biological Sciences* 360

(1456): 709–31. https://doi.org/10.1098/rstb.2005.1629.

Ghazi, Nicola G., Emad B. Abboud, Sawsan R. Nowilaty, Hisham Alkuraya, Abdulrahman Alhommadi, Huimin Cai, Rui Hou, et al. 2016. “Treatment of Retinitis Pigmentosa Due to MERTK Mutations by Ocular Subretinal Injection of Adeno-Associated Virus Gene Vector: Results of a Phase I Trial.” *Human Genetics* 135 (3): 327–43. https://doi.org/10.1007/s00439-016-1637-y.

Glen, Fiona C, Helen Baker, and David P Crabb. 2014. “A Qualitative Investigation into Patients ’ Views on Visual Fi Eld Testing for Glaucoma Monitoring.” *BMJ Open* 4 (e003996): 1–10. https://doi.org/10.1136/bmjopen-2013-003996.

Gomez, Jesse, Franco Pestilli, Nathan Witthoft, Golijeh Golarai, Alina Liberman, Sonia Poltoratski, Jennifer Yoon, and Kalanit Grill-Spector. 2015. “Functionally Defined White Matter Reveals Segregated Pathways in Human Ventral Temporal Cortex Associated with Category-Specific Processing.” *Neuron* 85 (1): 216–27. https://doi.org/10.1016/j.neuron.2014.12.027.

Grimes, William N., Adree Songco-Aguas, and Fred Rieke. 2018. “Parallel Processing of Rod and Cone Signals: Retinal Function and Human Perception.” *Annual Review of Vision Science* 4: 123–41. https://doi.org/10.1146/annurev-vision-091517-034055.

Gupta, Omesh P I, Eric D Weichel, Carl D Regillo, Mitchell S Fineman, Richard S Kaiser, Allen C Ho, J Arch McNamara, and James E Vander. 2007. “Postoperative Complications Associated with 25-Gauge Pars Plana Vitrectomy.” *Ophthalmic Surgery, Lasers & Imaging* 38 (4): 270–75.

Halioua-Haubold, Celine Lea, Jasleen K. Jolly, James A. Smith, Rafael Pinedo-Villanueva, David A. Brindley, and Robert E. MacLaren. 2019. “Potential Lifetime Quality of Life Benefits of Choroideremia Gene Therapy: Projections from a Clinically Informed Decision Model.” *Eye* 33 (8): 1215–23. https://doi.org/10.1038/s41433-019-0492-1.

Han, Ruofan Connie., Jasleen Kaur. Jolly, Kanmin Xue, and Robert E. MacLaren. 2017. “Effects of Pupil Dilation on MAIA Microperimetry.” *Clinical & Experimental Ophthalmology* 45 (5): 489–95. https://doi.org/10.1111/ceo.12907.

Han, Ruofan Connie, Joanna Monika Gray, Jennie Han, Robert E. Maclaren, and Jasleen Kaur Jolly. 2018. “Optimisation of Dark Adaptation Time Required for Mesopic Microperimetry.” *British Journal of Ophthalmology*, 1–7. https://doi.org/10.1136/bjophthalmol-2018-312253.

Harwerth, Ronald S., and Joe L. Wheat. 2008. “Modeling the Effects of Aging on Retinal Ganglion Cell Density and Nerve Fiber Layer Thickness.” *Graefe’s Archive for Clinical and Experimental Ophthalmology* 246 (2): 305–14. https://doi.org/10.1007/s00417-007-0691-5.

Hasler, Pascal W., Sara Brandi Bloch, Jørgen Villumsen, Josefine Fuchs, Henrik Lund-Andersen, and Michael Larsen. 2015. “Safety Study of 38 503 Intravitreal Ranibizumab Injections Performed Mainly by Physicians in Training and Nurses in a Hospital Setting.” *Acta Ophthalmologica* 93 (2): 122–25. https://doi.org/10.1111/aos.12589.

Hauswirth, William W., Tomas S. Aleman, Shalesh Kaushal, Artur V. Cideciyan, Sharon B. Schwartz, Lili Wang, Thomas J. Conlon, et al. 2008. “Treatment of Leber Congenital Amaurosis Due to *RPE65* Mutations by Ocular Subretinal Injection of Adeno-Associated Virus Gene Vector: Short-Term Results of a Phase I Trial.” *Human Gene Therapy* 19 (10): 979–90. https://doi.org/10.1089/hum.2008.107.

Heavner, Whitney, and Larysa Pevny. 2012. “Eye Development and Retinogenesis.” *Cold Spring Harbor Perspectives in Biology* 4 (12): a008391. https://doi.org/10.1101/cshperspect.a008391.

Hecht, Selig, Charles Haig, and Aurin M. Chase. 1937. “The Influence of Light Adaptation on Subsequent Dark Adaptation of the Eye.” *Journal of General Physiology* 20 (6): 831–50. https://doi.org/10.1085/jgp.20.6.831.

Heeren, Tjebo F C, Simone Tzaridis, Roberto Bonelli, Maximilian Pfau, Marcus Fruttiger, Mali Okada, Catherine Egan, Peter Charbel Issa, and Frank G Holz. 2019. “Dark-Adapted Two-Color Fundus-Controlled Perimetry in Macular Telangiectasia Type 2.” *Investigative Ophthalmology & Visual Science* 60 (5): 1760–67. https://doi.org/10.1167/iovs.18-25360.

Heier, Jeffrey S., Saleema Kherani, Shilpa Desai, Pravin Dugel, Shalesh Kaushal, Seng H. Cheng, Cheryl Delacono, et al. 2017. “Intravitreous Injection of AAV2-SFLT01 in Patients with Advanced Neovascular Age-Related Macular Degeneration: A Phase 1, Open-Label Trial.” *The Lancet* 390 (10089): 50–61. https://doi.org/10.1016/S0140-6736(17)30979-0.

Heon, Elise, Talal Alabduljalil, David B. McGuigan, Artur V. Cideciyan, Shuning Li, Shiyi Chen, and Samuel G. Jacobson. 2016. “Visual Function and Central Retinal Structure in Choroideremia.” *Investigative Ophthalmology and Visual Science* 57 (9): OCT377–87. https://doi.org/10.1167/iovs.15-18421.

Holmes, G. 1918. “DISTURBANCES OF VISION BY CEREBRAL LESIONS.” *British Journal of Ophthalmology* 2 (7): 353–84. https://doi.org/10.1136/bjo.2.7.353.

Hood, Donald C., and Vivienne C. Greenstein. 1988. “Blue (S) Cone Pathway Vulnerability: A Test of a Fragile Receptor Hypothesis.” *Applied Optics* 27 (6): 1025–29. https://doi.org/10.1364/ao.27.001025.

Hood, Donald C., Christine E. Lin, Margot A. Lazow, Kirsten G. Locke, Xian Zhang, and David G. Birch. 2009. “Thickness of Receptor and Post-Receptor Retinal Layers in Patients with Retinitis Pigmentosa Measured with Frequency-Domain Optical Coherence Tomography.” *Investigative Ophthalmology and Visual Science* 50 (5): 2328–36. https://doi.org/10.1167/iovs.08-2936.

Horton, Jonathan C., and William F. Hoyt. 1991. “The Representation of the Visual Field in Human Striate Cortex: A Revision of the Classic Holmes Map.” *Archives of Ophthalmology* 109 (6): 816–24. https://doi.org/10.1001/archopht.1991.01080060080030.

Howlett, Marcus H.C., Robert G. Smith, and Maarten Kamermans. 2017. “A Novel Mechanism of Cone Photoreceptor Adaptation.” *PLoS Biology* 15 (4): 1–28. https://doi.org/10.1371/journal.pbio.2001210.

Hoyt, William F. 1962. “Visual Fiber Anatomy in the Infrageniculate Pathway of the Primate.” *Archives of Ophthalmology* 68 (1): 94. https://doi.org/10.1001/archopht.1962.00960030098018.

Hwang, Jisoo, Dong-Hoon Lee, Seongchong Park, and Seung-Nam Park. 2013. “Measurement of Rod and Cone Effects in Mesopic Visual Sensitivity by Varying Viewing Field.” *Journal of the Optical Society of America A* 30 (10): 1929. https://doi.org/10.1364/josaa.30.001929.

Iglesias, Juan Eugenio, Ricardo Insausti, Garikoitz Lerma-Usabiaga, Martina Bocchetta, Koen Van Leemput, Douglas N. Greve, Andre van der Kouwe, Bruce Fischl, César Caballero-Gaudes, and Pedro M. Paz-Alonso. 2018. “A Probabilistic Atlas of the Human Thalamic

Nuclei Combining Ex Vivo MRI and Histology." *NeuroImage* 183 (July): 314–26. https://doi.org/10.1016/j.neuroimage.2018.08.012.

Ingram, Norianne T., Alapakkam P. Sampath, and Gordon L. Fain. 2016. "Why Are Rods More Sensitive than Cones?" *Journal of Physiology* 594 (19): 5415–26. https://doi.org/10.1113/JP272556.

Jackson, Gregory R., Cynthia Owsley, and Gerald McGwin. 1999. "Aging and Dark Adaptation." *Vision Research* 39 (23): 3975–82. https://doi.org/10.1016/S0042-6989(99)00092-9.

Jacobson, Samuel G., Tomas S. Aleman, Alexander Sumaroka, Artur V. Cideciyan, Alejandro J. Roman, Elizabeth A.M. Windsor, Sharon B. Schwartz, Heidi L. Rehm, and William J. Kimberling. 2009. "Disease Boundaries in the Retina of Patients with Usher Syndrome Caused by MYO7A Gene Mutations." *Investigative Ophthalmology and Visual Science* 50 (4): 1886–94. https://doi.org/10.1167/iovs.08-3122.

Jacobson, Samuel G., Artur V. Cideciyan, Alexander Sumaroka, Tomas S. Aleman, Sharon B. Schwartz, Elizabeth A.M. Windsor, Alejandro J. Roman, Edwin M. Stone, and Ian M. MacDonald. 2006. "Remodeling of the Human Retina in Choroideremia: Rab Escort Protein 1 (REP-1) Mutations." *Investigative Ophthalmology and Visual Science* 47 (9): 4113–20. https://doi.org/10.1167/iovs.06-0424.

Jacobson, Samuel G., Artur V. Cideciyan, Alexander Sumaroka, Alejandro J. Roman, Jason Charng, Monica Lu, Shreyasi Choudhury, et al. 2017. "Defining Outcomes for Clinical Trials of Leber Congenital Amaurosis Caused by GUCY2D Mutations." *American Journal of Ophthalmology* 177: 44–57. https://doi.org/10.1016/j.ajo.2017.02.003.

Jacobson, Samuel G., Walter J. Voigt, Jean-Marie Parel, Peter P. Apathy, Lan Nghiem-Phu, Steve W. Myers, and V. Michael Patella. 1986. "Automated Light- and Dark- Adapted Perimetry for Evaluating Retinitis Pigmentosa." *Ophthalmology* 93 (12): 1604–11. https://doi.org/10.1016/S0161-6420(86)33522-X.

Jacobson, Samuel G, Artur V Cideciyan, Ramakrishna Ratnakaram, Elise Heon, Sharon B Schwartz, Alejandro J Roman, Marc C Peden, et al. 2012. "Gene Therapy for Leber Congenital Amaurosis Caused by RPE65 Mutations: Safety and Efficacy in Fifteen Children and Adults Followed up to Three Years." *Archives of Ophthalmology* 130 (1): 9–24. https://doi.org/10.1001/archophthalmol.2011.298.Gene.

Jenkinson, Mark, Peter Bannister, Michael Brady, and Stephen Smith. 2002. "Improved Optimization for the Robust and Accurate Linear Registration and Motion Correction of Brain Images." *NeuroImage* 17 (2): 825–41. https://doi.org/10.1016/S1053-8119(02)91132-8.

Johansen-Berg, Heidi. 2010. "Behavioural Relevance of Variation in White Matter Microstructure." *Current Opinion in Neurology* 23 (4): 351–58. https://doi.org/10.1097/WCO.0b013e32833b7631.

Johnson, Mary A., Brett G. Jeffrey, André M.V. Messias, and Anthony G. Robson. 2019. "ISCEV Extended Protocol for the Stimulus–Response Series for the Dark-Adapted Full-Field ERG b-Wave." *Documenta Ophthalmologica* 6: 217–27. https://doi.org/10.1007/s10633-019-09687-6.

Jolly, Jasleen K., Holly Bridge, and Robert E. MacLaren. 2019. "Outcome Measures Used In Ocular Gene Therapy Trials: A Scoping Review Of Current Practice." *Frontiers in Pharmacology*.

Jolly, Jasleen K., Clare E Couldridge-Smith, Kanmin Xue, and Robert E. Maclaren. 2019. “The Impact of Progressive Visual Field Constriction on Reading Ability in an Inherited Retinal Degeneration.” *Ophthalmologica*. https://doi.org/10.1159/000503294.

Jolly, Jasleen K., Thomas L. Edwards, Jonathan Moules, Markus Groppe, Susan M. Downes, and Robert E. MacLaren. 2016. “A Qualitative and Quantitative Assessment of Fundus Autofluorescence Patterns in Patients With Choroideremia.” *Investigative Opthalmology & Visual Science* 57 (10): 4498. https://doi.org/10.1167/iovs.15-18362.

Jolly, Jasleen K., Joanna M Gray, Anna Paola Salvetti, Ruofan C Han, and Robert E MacLaren. 2019. “A Randomized Crossover Study to Assess the Usability of Two New Vision Tests in Patients with Low Vision.” *Optometry and Vision Science* 96 (6): 443–52. https://journals.lww.com/optvissci/Fulltext/pre-publication/A_Randomized_Crossover_Study_to_Assess_the.98143.aspx.

Jolly, Jasleen K., Markus Groppe, Jacqueline Birks, Susan M. Downes, and Robert E. MacLaren. 2015. “Functional Defects in Color Vision in Patients with Choroideremia.” *American Journal of Ophthalmology* 160 (4): 822-831e3. https://doi.org/10.1016/j.ajo.2015.06.018.

Jolly, Jasleen K., S K Wagner, P Martus, R E MacLaren, B Wilhelm, A R Webster, S M Downes, et al. 2020. “Transcorneal Electrical Stimulation for the Treatment of Retinitis Pigmentosa: A Multicenter Safety Study of the OkuStim® System (TESOLA-Study).” *Ophthalmic Research* 63 (3): 234–43. https://doi.org/10.1159/000505001.

Jolly, Jasleen K., Kanmin Xue, Thomas L Edwards, Markus Groppe, and Robert E MacLaren. 2017. “Characterizing the Natural History of Visual Function in Choroideremia Using Microperimetry and Multimodal Retinal Imaging.” *Investigative Opthalmology & Visual Science* 58 (12): 5575. https://doi.org/10.1167/iovs.17-22486.

Jones, B. W., R. L. Pfeiffer, W. D. Ferrell, C. B. Watt, M. Marmor, and R. E. Marc. 2016. “Retinal Remodeling in Human Retinitis Pigmentosa.” *Experimental Eye Research* 150: 149–65. https://doi.org/10.1016/j.exer.2016.03.018.

Kaarniranta, Kai, and Matti Kontkanen. 2003. “Visual Recovery of the Amblyopic Eye in an Adult Patient after Loss of the Dominant Eye.” *Acta Ophthalmologica Scandinavica Suppl* 81 (5): 539. https://doi.org/10.1034/j.1600-0420.2003.00127.x.

Kaiser, Peter K. 2009. “Prospective Evaluation of Visual Acuity Assessment: A Comparison of Snellen versus ETDRS Charts in Clinical Practice (An AOS Thesis).” *Transactions of the American Ophthalmological Society* 107: 311–24. http://www.pubmedcentral.nih.gov/articlerender.fcgi?artid=2814576&tool=pmcentrez&rendertype=abstract.

Kinnear, P R, and A Sahraie. 2002. “New Farnsworth-Munsell 100 Hue Test Norms of Normal Observers for Each Year of Age 5–22 and for Age Decades 30–70.” *British Journal of Ophthalmology* 86: 1408–11.

Kiser, Ava K., Derek Mladenovich, Fariba Eshraghi, Debra Bourdeau, and Gislin Dagnelie. 2005. “Reliability and Consistency of Visual Acuity and Contrast Sensitivity Measures in Advanced Eye Disease.” *Optometry and Vision Science* 82 (11): 946–54. https://doi.org/10.1097/01.opx.0000187863.12609.7b.

Klein, M., and D. G. Birch. 2009. “Psychophysical Assessment of Low Visual Function in Patients with Retinal Degenerative Diseases (RDDs) with the Diagnosys Full-Field Stimulus Threshold (D-FST).” *Documenta Ophthalmologica* 119 (3): 217–24.

https://doi.org/10.1007/s10633-009-9204-7.

Klein, Ronald, Barbara E.K. Klein, Kathryn L.P. Linton, and David L. De Mets. 1991. “The Beaver Dam Eye Study: Visual Acuity.” *Ophthalmology* 98 (8): 1310–15. https://doi.org/10.1016/S0161-6420(91)32137-7.

Kling, A., G.D. Field, D.H. Brainard, and E.J. Chichilnisky. 2019. “Probing Computation in the Primate Visual System at Single-Cone Resolution.” *Annual Review of Neuroscience* 42: 169–86. https://doi.org/10.1146/annurev-neuro-070918-050233.

Koilkonda, Rajeshwari D., Hong Yu, Tsung-Han Chou, William J. Feuer, Marco Ruggeri, Vittorio Porciatti, David Tse, et al. 2014. “Safety and Effects of the Vector for the Leber Hereditary Optic Neuropathy Gene Therapy Clinical Trial.” *JAMA Ophthalmology* 132 (4): 409. https://doi.org/10.1001/jamaophthalmol.2013.7630.

Kolb, Helga, Nelson Ralph, and Fernandez Eduardo. 1995. *The Organization of the Retina and Visual System. Webvision: The Organization of the Retina and Visual System [Internet]*. Salt Lake City (UT): University of Utah Health Sciences Center.

Kolster, Hauke, Joseph B. Mandeville, John T. Arsenault, Leeland B. Ekstrom, Lawrence L. Wald, and Wim Vanduffel. 2009. “Visual Field Map Clusters in Macaque Extrastriate Visual Cortex.” *Journal of Neuroscience* 29 (21): 7031–39. https://doi.org/10.1523/JNEUROSCI.0518-09.2009.

Kupfer, C, L Chumbley, and J C Downer. 1967. “Quantitative Histology of Optic Nerve, Optic Tract and Lateral Geniculate Nucleus of Man.” *Journal of Anatomy* 101 (3): 393–401. http://www.ncbi.nlm.nih.gov/pubmed/6051727%0Ahttp://www.pubmedcentral.nih.gov/articlerender.fcgi?artid=PMC1270921.

Lähteenvuo, Johanna, and Seppo Ylä-Herttuala. 2017. “Advances and Challenges in Cardiovascular Gene Therapy.” *Human Gene Therapy* 28 (11): 1024–32. https://doi.org/10.1089/hum.2017.129.

Lam, Byron L., Janet L. Davis, Ninel Z. Gregori, Robert E. MacLaren, Aniz Girach, Jennifer D. Verriotto, Belen Rodriguez, Potyra R. Rosa, Xiaojun Zhang, and William J. Feuer. 2019. “Choroideremia Gene Therapy Phase 2 Clinical Trial: 24-Month Results.” *American Journal of Ophthalmology* 197: 65–73. https://doi.org/10.1016/j.ajo.2018.09.012.

Lamb, T D, and E N Jr Pugh. 2004. “Dark Adaptation and the Retinoid Cycle of Vision.” *Progress in Retinal and Eye Research* 23 (3): 307–80. https://doi.org/10.1016/j.preteyeres.2004.03.001.

Latham, Keziah, Mohammad Baranian, Matthew Timmis, and Shahina Pardhan. 2015. “Emotional Health of People with Visual Impairment Caused by Retinitis Pigmentosa.” *Plos One* 10 (12): e0145866. https://doi.org/10.1371/journal.pone.0145866.

Li, Roger W., Charlie Ngo, Jennie Nguyen, and Dennis M. Levi. 2011. “Video-Game Play Induces Plasticity in the Visual System of Adults with Amblyopia.” *PLoS Biology* 9 (8): e1001135. https://doi.org/10.1371/journal.pbio.1001135.

Lindenau, Wilhelm, Heidrun Kuhrt, Elke Ulbricht, Katrin Körner, Andreas Bringmann, and Andreas Reichenbach. 2019. “Cone-to-Müller Cell Ratio in the Mammalian Retina: A Survey of Seven Mammals with Different Lifestyle.” *Experimental Eye Research* 181: 38–48. https://doi.org/10.1016/j.exer.2019.01.012.

Lois, Noemi, Anthony S Halfyard, Alan C Bird, Graham E Holder, and Frederick W Fitzke.

2004. “Fundus Autofluorescence in Stargardt Macular Dystrophy–Fundus Flavimaculatus.” *American Journal of Ophthalmology* 138 (1): 55–63. https://doi.org/10.1016/j.ajo.2004.02.056.

MacDonald, Ian M, Laurie Russell, and Chi-Chao Chan. 2009. “Choroideremia: New Findings from Ocular Pathology and Review of Recent Literature.” *Survey of Ophthalmology* 54 (3): 401–7. https://doi.org/10.1016/j.survophthal.2009.02.008.

MacLaren, Robert E. 2016. “Benefits of Gene Therapy for Both Eyes.” *The Lancet* 388 (10045): 635–36. https://doi.org/10.1016/S0140-6736(16)30783-8.

MacLaren, Robert E., Markus Groppe, Alun R. Barnard, Charles L. Cottriall, Tanya Tolmachova, Len Seymour, K. Reed Clark, et al. 2014. “Retinal Gene Therapy in Patients with Choroideremia: Initial Findings from a Phase 1/2 Clinical Trial.” *The Lancet* 383 (9923): 1129–37. https://doi.org/10.1016/S0140-6736(13)62117-0.

Maguire, Albert M., Francesca Simonelli, Eric A Pierce, Edward N Pugh, Federico Mingozzi, Jeannette L Bennicelli, Sandro Banfi, et al. 2008. “Safety and Efficacy of Gene Transfer for Leber’s Congenital Amaurosis.” *New England Journal of Medicine* 358 (21): 2240–48. https://doi.org/10.1056/NEJMoa0802315.Safety.

Maguire, Albert M, Katherine A High, Alberto Auricchio, J Fraser Wright, Eric A Pierce, Francesco Testa, Federico Mingozzi, et al. 2009. “Age-Dependent Effects of RPE65 Gene Therapy for Leber’s Congenital Amaurosis: A Phase 1 Dose-Escalation Trial.” *Lancet* 374 (9701): 1597–1605. https://doi.org/10.1016/S0140-6736(09)61836-5.Age-dependent.

Makris, Nikos, David N. Kennedy, Sean McInerney, A. Gregory Sorensen, Ruopeng Wang, Verne S. Caviness, and Deepak N. Pandya. 2005. “Segmentation of Subcomponents within the Superior Longitudinal Fascicle in Humans: A Quantitative, in Vivo, DT-MRI Study.” *Cerebral Cortex* 15 (6): 854–69. https://doi.org/10.1093/cercor/bhh186.

Marc, Robert E., and Bryan W. Jones. 2003. “Retinal Remodeling in Inherited Photoreceptor Degenerations.” *Molecular Neurobiology* 28 (2): 139–47. https://doi.org/10.1385/MN:28:2:139.

Margolis, David J., Gregory Newkirk, Thomas Euler, and Peter B. Detwiler. 2008. “Functional Stability of Retinal Ganglion Cells after Degeneration-Induced Changes in Synaptic Input.” *Journal of Neuroscience* 28 (25): 6526–36. https://doi.org/10.1523/JNEUROSCI.1533-08.2008.

Massof, R. W., and D. Finkelstein. 1979. “Rod Sensitivity Relative to Cone Sensitivity in Retinitis Pigmentosa.” *Investigative Ophthalmology and Visual Science* 18 (3): 263–72.

McCulloch, Daphne L., Michael F. Marmor, Mitchell G. Brigell, Ruth Hamilton, Graham E. Holder, Radouil Tzekov, and Michael Bach. 2015. “ISCEV Standard for Full-Field Clinical Electroretinography (2015 Update).” *Documenta Ophthalmologica* 130 (1): 1–12. https://doi.org/10.1007/s10633-014-9473-7.

Mcglothlin, Anna E, and Roger J Lewis. 2014. “Minimal Clinically Important Difference Defining What Really Matters to Patients.” *Jama* 312 (13): 1342–43. https://doi.org/10.1001/jama.2014.12660.4.

Megaw, Roly D., Dinesh C. Soares, and Alan F. Wright. 2015. “RPGR: Its Role in Photoreceptor Physiology, Human Disease, and Future Therapies.” *Experimental Eye Research* 138: 32–41. https://doi.org/10.1016/j.exer.2015.06.007.

Menghini, Moreno, J K Jolly, A Nanda, L Wood, J Cehajic-Kapetanovic, and R E MacLaren.

2020. “Early Cone Photoreceptor Outer Segment Length Shortening in RPGR X-Linked Retinitis Pigmentosa.” *Ophthalmologica*. https://doi.org/10.1159/000507484.

Menghini, Moreno, Brandon J. Lujan, Shiri Zayit-Soudry, Reema Syed, Travis C. Porco, Kristine Bayabo, Joseph Carroll, Austin Roorda, and Jacque L. Duncan. 2015. “Correlation of Outer Nuclear Layer Thickness with Cone Density Values in Patients with Retinitis Pigmentosa and Healthy Subjects.” *Investigative Ophthalmology and Visual Science* 56 (1): 372–81. https://doi.org/10.1167/iovs.14-15521.

Messias, Katharina, Herbert Jägle, Rafael Saran, André Domingos Pinto Ruppert, Rubens Siqueira, Rodrigo Jorge, and André Messias. 2013. “Psychophysically Determined Full-Field Stimulus Thresholds (FST) in Retinitis Pigmentosa: Relationships with Electroretinography and Visual Field Outcomes.” *Documenta Ophthalmologica* 127 (2): 123–29. https://doi.org/10.1007/s10633-013-9393-y.

Meur, Guylène Le, Pierre Lebranchu, Fanny Billaud, Oumeya Adjali, Sébastien Schmitt, Stéphane Bézieau, Yann Péréon, et al. 2018. “Safety and Long-Term Efficacy of AAV4 Gene Therapy in Patients with RPE65 Leber Congenital Amaurosis.” *Molecular Therapy* 26 (1): 256–68. https://doi.org/10.1016/j.ymthe.2017.09.014.

Milner, A. D., and M. A. Goodale. 2008. “Two Visual Systems Re-Viewed.” *Neuropsychologia* 46 (3): 774–85. https://doi.org/10.1016/j.neuropsychologia.2007.10.005.

Montesano, Giovanni, Luca M. Rossetti, Allison M. McKendrick, Andrew Turpin, Paolo Fogagnolo, Francesco Oddone, Paolo Lanzetta, et al. 2020. “Effect of Fundus Tracking on Structure-Function Relationship in Glaucoma.” *British Journal of Ophthalmology*, 1–7. https://doi.org/10.1136/bjophthalmol-2019-315070.

Mori, Susumu, Walter E. Kaufmann, Christos Davatzikos, Bram Stieltjes, Laura Amodei, Kim Fredericksen, Godfrey D. Pearlson, et al. 2002. “Imaging Cortical Association Tracts in the Human Brain Using Diffusion-Tensor-Based Axonal Tracking.” *Magnetic Resonance in Medicine* 47 (2): 215–23. https://doi.org/10.1002/mrm.10074.

Morshedian, Ala, and Gordon L. Fain. 2017. “The Evolution of Rod Photoreceptors.” *Philosophical Transactions of the Royal Society B: Biological Sciences* 372 (1717): 20160074. https://doi.org/10.1098/rstb.2016.0074.

Nanda, Anika, Anna P. Salvetti, Penny Clouston, Susan M. Downes, and Robert E. MacLaren. 2018. “Exploring the Variable Phenotypes of RPGR Carrier Females in Assessing Their Potential for Retinal Gene Therapy.” *Genes* 9 (12): 643. https://doi.org/10.3390/genes9120643.

Narayan, Daniel S., John P.M. Wood, Glyn Chidlow, and Robert J. Casson. 2016. “A Review of the Mechanisms of Cone Degeneration in Retinitis Pigmentosa.” *Acta Ophthalmologica* 94 (8): 748–54. https://doi.org/10.1111/aos.13141.

Nathans, Jeremy, Darcy Thomas, and David S. Hogness. 1986. “Molecular Genetics of Human Color Vision : The Genes Encoding Blue, Green, and Red Pigments.” *Science* 4747 (1984): 193–232.

Nelson, Ralph. 1997. “Cat Cones Have Rod Input : A Comparison of the Response Properties of Cones and Horizontal Cell Bodies in the Retina of the Cat.” *Journal of Computational Neurology* 172 (1): 109–35.

Nork, T. M., S. A. McCormick, G. M. Chao, and J. V. Odom. 1990. “Distribution of Carbonic Anhydrase among Human Photoreceptors.” *Investigative Ophthalmology and Visual*

Science 31 (8): 1451–58.

O'Connell, Caitlin, Leon C. Ho, Matthew C. Murphy, Ian P. Conner, Gadi Wollstein, Rakie Cham, and Kevin C. Chan. 2016. "Structural and Functional Correlates of Visual Field Asymmetry in the Human Brain by Diffusion Kurtosis MRI and Functional MRI." *NeuroReport* 27 (16): 1225–31. https://doi.org/10.1097/WNR.0000000000000682.

Oesch, Nicholas W, and Jeffrey S Diamond. 2019. "Synaptic Inhibition Tunes Contrast Computation in the Retina." *Visual Neuroscience* 36: E006. https://doi.org/10.1017/S095252381900004X.Synaptic.

Ogawa, Shumpei, Hiromasa Takemura, Hiroshi Horiguchi, Masahiko Terao, Tomoki Haji, Franco Pestilli, Jason D. Yeatman, Hiroshi Tsuneoka, Brian A. Wandell, and Yoichiro Masuda. 2014. "White Matter Consequences of Retinal Receptor and Ganglion Cell Damage." *Investigative Ophthalmology & Visual Science* 55 (10): 6976–86. https://doi.org/10.1167/iovs.14-14737.

Ogura, Shuntaro, Tsutomu Yasukawa, Aki Kato, Hideaki Usui, Yoshio Hirano, Munenori Yoshida, and Yuichiro Ogura. 2014. "Wide-Field Fundus Autofluorescence Imaging to Evaluate Retinal Function in Patients With Retinitis Pigmentosa." *American Journal of Ophthalmology* 158 (5): 1093-1098.e3. https://doi.org/10.1016/j.ajo.2014.07.021.

Oishi, Akio, Ken Ogino, Yukiko Makiyama, and Satoko Nakagawa. 2013. "Wide-Field Fundus Auto Fl Uorescence Imaging of Retinitis Pigmentosa." *Ophthalmology* 120 (9): 1827–34. https://doi.org/10.1016/j.ophtha.2013.01.050.

Owsley, Cynthia, Gregory R. Jackson, Artur V. Cideciyan, Yijun Huang, Stuart L. Fine, Allen C. Ho, Maureen G. Maguire, Virginia Lolley, and Samuel G. Jacobson. 2000. "Psychophysical Evidence for Rod Vulnerability in Age-Related Macular Degeneration." *Investigative Ophthalmology and Visual Science* 41 (1): 267–73.

Owsley, Cynthia, Gerald McGwin, Kay Scilley, and Katherine Kallies. 2006. "Development of a Questionnaire to Assess Vision Problems under Low Luminance in Age-Related Maculopathy." *Investigative Ophthalmology and Visual Science* 47 (2): 528–35. https://doi.org/10.1167/iovs.05-1222.

Paramei, Galina V, and Beata Oakley. 2014. "Variation of Color Discrimination across the Life Span." *Journal of the Optical Society of America A* 31 (4): 375–84.

Patrício, Maria I., Alun R. Barnard, Harry O. Orlans, Michelle E. McClements, and Robert E. MacLaren. 2017. "Inclusion of the Woodchuck Hepatitis Virus Posttranscriptional Regulatory Element Enhances AAV2-Driven Transduction of Mouse and Human Retina." *Molecular Therapy - Nucleic Acids* 6 (March): 198–208. https://doi.org/10.1016/j.omtn.2016.12.006.

Patryas, Laura, Neil R.A. Parry, David Carden, Daniel H. Baker, Jeremiah M.F. Kelly, Tariq Aslam, and Ian J. Murray. 2013. "Assessment of Age Changes and Repeatability for Computer-Based Rod Dark Adaptation." *Graefe's Archive for Clinical and Experimental Ophthalmology* 251 (7): 1821–27. https://doi.org/10.1007/s00417-013-2324-5.

Patterson, Sara S., James A. Kuchenbecker, James R. Anderson, Maureen Neitz, and Jay Neitz. 2020. "A Color Vision Circuit for Non-Image-Forming Vision in the Primate Retina." *Current Biology* 30 (7): 1269-1274.e2. https://doi.org/10.1016/j.cub.2020.01.040.

Peltier, Johann, Nadine Travers, Christophe Destrieux, and Stéphane Velut. 2006. "Optic Radiations: A Microsurgical Anatomical Study." *Journal of Neurosurgery* 105 (2): 294–300. https://doi.org/10.3171/jns.2006.105.2.294.

Peters, A Y, K G Locke, and D G Birch. 2000. “Comparison of the Goldmann-Weekers Dark Adaptometer and LKC Technologies Scotopic Sensitivity Tester-1.” *Documenta Ophthalmologica* 101: 1–9.

Pfau, Maximilian, Leon von der Emde, Chantal Dysli, Sarah Thiele, Philipp T Moller, Moritz Lindner, Jennifer Nadal, et al. 2019. “Light Sensitivity Within Areas of Geographic Atrophy Secondary to Age-Related Macular Degeneration.” *Investigative Ophthalmology & Visual Science* 60 (12): 3992–4001. https://doi.org/10.1167/iovs.19-27178.

Pfau, Maximilian, Moritz Lindner, Monika Fleckenstein, Robert P Finger, Gary S Rubin, Wolf M Harmening, Marco U Morales, Frank G Holz, and Steffen Schmitz-Valckenberg. 2017. “Test-Retest Reliability of Scotopic and Mesopic Fundus-Controlled Perimetry Using a Modified MAIA (Macular Integrity Assessment) in Normal Eyes.” *Ophthalmologica. Journal International d’ophtalmologie. International Journal of Ophthalmology. Zeitschrift Fur Augenheilkunde* 237 (1): 42–54. https://doi.org/10.1159/000453079.

Pfau, Maximilian, Moritz Lindner, Julia S Steinberg, Sarah Thiele, Christian K Brinkmann, Monika Fleckenstein, Frank G Holz, and Steffen Schmitz-Valckenberg. 2017. “Visual Field Indices and Patterns of Visual Field Deficits in Mesopic and Dark-Adapted Two-Colour Fundus-Controlled Perimetry in Macular Diseases.” *The British Journal of Ophthalmology*, November. https://doi.org/10.1136/bjophthalmol-2017-311012.

Pfeiffer, Rebecca L., Robert E. Marc, Mineo Kondo, Hiroko Terasaki, and Bryan W. Jones. 2016. “Müller Cell Metabolic Chaos during Retinal Degeneration.” *Experimental Eye Research* 150: 62–70. https://doi.org/10.1016/j.exer.2016.04.022.

Pierdomenico, Johnny Di, Ana Martínez-Vacas, Daniel Hernández-Muñoz, Ana M. Gómez-Ramírez, Francisco Javier Valiente-Soriano, Marta Agudo-Barriuso, Manuel Vidal-Sanz, María P. Villegas-Pérez, and Diego García-Ayuso. 2020. “Coordinated Intervention of Microglial and Müller Cells in Light-Induced Retinal Degeneration.” *Investigative Ophthalmology & Visual Science* 61 (3): 47. https://doi.org/10.1167/iovs.61.3.47.

Pierpaoli, Carlo, and Peter J. Basser. 1996. “Toward a Quantitative Assessment of Diffusion Anisotropy.” *Magnetic Resonance in Medicine* 36 (6): 893–906. https://doi.org/10.1002/mrm.1910360612.

Pietrasanta, Marta, Laura Restani, and Matteo Caleo. 2012. “The Corpus Callosum and the Visual Cortex: Plasticity Is a Game for Two.” *Neural Plasticity* 2012: 838672. https://doi.org/10.1155/2012/838672.

Rabin, Jeff. 1984. “Visual Improvement in Amblyopia after Visual Loss in the Dominant Eye.” *Optometry and Vision Science*. https://doi.org/10.1097/00006324-198405000-00008.

Rakoczy, Elizabeth P., Chooi May Lai, Aaron L. Magno, Matthew E. Wikstrom, Martyn A. French, Cora M. Pierce, Steven D. Schwartz, et al. 2015. “Gene Therapy with Recombinant Adeno-Associated Vectors for Neovascular Age-Related Macular Degeneration: 1 Year Follow-up of a Phase 1 Randomised Clinical Trial.” *The Lancet* 386 (10011): 2395–2403. https://doi.org/10.1016/S0140-6736(15)00345-1.

Rangaswamy, Nalini V., Hemaxi M. Patel, Kirsten G. Locke, Donald C. Hood, and David G. Birch. 2010. “A Comparison of Visual Field Sensitivity to Photoreceptor Thickness in Retinitis Pigmentosa.” *Investigative Ophthalmology and Visual Science* 51 (8): 4213–19. https://doi.org/10.1167/iovs.09-4945.

Ratnarajan, Gokulan, Jasleen K. Jolly, Imran H. Yusuf, and John F. Salmon. 2018. “The Effect of Trabeculectomy Surgery on the Central Visual Field in Patients with Glaucoma Using

Microperimetry and Optical Coherence Tomography." *Eye* 32 (8): 1365–71. https://doi.org/10.1038/s41433-018-0095-2.

Rattner, Amir, and Jeremy Nathans. 2005. "The Genomic Response to Retinal Disease and Injury: Evidence for Endothelin Signaling from Photoreceptors to Glia." *Journal of Neuroscience* 25 (18): 4540–49. https://doi.org/10.1523/JNEUROSCI.0492-05.2005.

Raviola, E, and RF Dacheux. 1990. "Axonless Horizontal Cells of the Rabbit Retina: Synaptic Connections and Origin of the Rod Aftereffect." *Journal of Neurocytology* 19: 731–36.

Razek, Ahmed Abdel Khalek Abdel, Nihal Batouty, Wesam Fathy, and Rania Bassiouny. 2018. "Diffusion Tensor Imaging of the Optic Disc in Idiopathic Intracranial Hypertension." *Neuroradiology* 60 (11): 1159–66. https://doi.org/10.1007/s00234-018-2078-1.

Reichenbach, Andreas, and Andreas Bringmann. 2013. "New Functions of Müller Cells." *Glia* 61 (5): 651–78. https://doi.org/10.1002/glia.22477.

Ripamonti, Caterina, G. Bruce Henning, Scott J. Robbie, Venki Sundaram, L. Ingeborgh van den Born, Ingele Casteels, Thomy J. L. de Ravel, et al. 2015. "Spectral Sensitivity Measurements Reveal Partial Success in Restoring Missing Rod Function with Gene Therapy." *Journal of Vision* 15 (20): 1–16. https://doi.org/10.1167/15.15.20.

Rokem, Ariel, Andrew S Bock, K Suzanne Scherf, Brian A Wandell, Holly Bridge, Hiromasa Takemura, Andrew S Bock, et al. 2017. "The Visual White Matter : The Application of Diffusion MRI and Fiber Tractography to Vision Science." *Journal of Vision* 17 (2): 1–30. https://doi.org/10.1167/17.2.4.doi.

Roman, Alejandro J., Artur V. Cideciyan, Tomas S. Aleman, and Samuel G. Jacobson. 2007. "Full-Field Stimulus Testing (FST) to Quantify Visual Perception in Severely Blind Candidates for Treatment Trials." *Physiological Measurement* 28 (8): N51–56. https://doi.org/10.1088/0967-3334/28/8/N02.

Roman, Alejandro J., Sharon B. Schwartz, Tomas S. Aleman, Artur V. Cideciyan, John D. Chico, Elizabeth A.M. Windsor, Leigh M. Gardner, et al. 2005. "Quantifying Rod Photoreceptor-Mediated Vision in Retinal Degenerations: Dark-Adapted Thresholds as Outcome Measures." *Experimental Eye Research* 80 (2): 259–72. https://doi.org/10.1016/j.exer.2004.09.008.

Rosser, Daniel A., Simon N. Cousens, Ian E. Murdoch, Fred W. Fitzke, and David A.H. Laidlaw. 2003. "How Sensitive to Clinical Change Are ETDRS LogMAR Visual Acuity Measurements?" *Investigative Ophthalmology and Visual Science* 44 (8): 3278–81. https://doi.org/10.1167/iovs.02-1100.

Rougier, Nicolas P., Michael Droettboom, and Philip E. Bourne. 2014. "Ten Simple Rules for Better Figures." *PLoS Computational Biology* 10 (9): 1–7. https://doi.org/10.1371/journal.pcbi.1003833.

Ruickmann, A Von, F W Fitzke, and A C Bird. 1995. "Distribution of Fundus Autofluorescence with a Scanning Laser Ophthalmoscope." *British Journal of Ophthalmology* 79: 407–12.

Russell, Stephen, Jean Bennett, Jennifer A. Wellman, Daniel C. Chung, Zi Fan Yu, Amy Tillman, Janet Wittes, et al. 2017. "Efficacy and Safety of Voretigene Neparvovec (AAV2-HRPE65v2) in Patients with RPE65-Mediated Inherited Retinal Dystrophy: A Randomised, Controlled, Open-Label, Phase 3 Trial." *The Lancet* 390 (10097): 849–60. https://doi.org/10.1016/S0140-6736(17)31868-8.

Sabbah, Norman, Nicolae Sanda, Colas N. Authié, Saddek Mohand-Saïd, José Alain Sahel, Christophe Habas, Amir Amedi, and Avinoam B. Safran. 2017. “Reorganization of Early Visual Cortex Functional Connectivity Following Selective Peripheral and Central Visual Loss.” *Scientific Reports* 7 (January): 1–19. https://doi.org/10.1038/srep43223.

Salvetti, Anna P., Maria I. Patrício, Alun R. Barnard, Harry O. Orlans, Doron G. Hickey, and Robert E. MacLaren. 2017. “Impact of Vital Dyes on Cell Viability and Transduction Efficiency of AAV Vectors Used in Retinal Gene Therapy Surgery: An In Vitro and In Vivo Analysis.” *Translational Vision Science & Technology* 6 (4): 4. https://doi.org/10.1167/tvst.6.4.4.

Sampaio-Baptista, Cassandra, Nicola Filippini, Charlotte J. Stagg, Jamie Near, Jan Scholz, and Heidi Johansen-Berg. 2015. “Changes in Functional Connectivity and GABA Levels with Long-Term Motor Learning.” *NeuroImage* 106: 15–20. https://doi.org/10.1016/j.neuroimage.2014.11.032.

Sampaio-Baptista, Cassandra, and Heidi Johansen-Berg. 2017. “White Matter Plasticity in the Adult Brain.” *Neuron* 96 (6): 1239–51. https://doi.org/10.1016/j.neuron.2017.11.026.

Sampaio-Baptista, Cassandra, Jan Scholz, Mark Jenkinson, Adam G. Thomas, Nicola Filippini, Gabrielle Smit, Gwenaëlle Douaud, and Heidi Johansen-Berg. 2014. “Gray Matter Volume Is Associated with Rate of Subsequent Skill Learning after a Long Term Training Intervention.” *NeuroImage* 96: 158–66. https://doi.org/10.1016/j.neuroimage.2014.03.056.

Sampath, Alapakkam P., Katherine J. Strissel, Rajesh Elias, Vadim Y. Arshavsky, James F. McGinnis, Jeannie Chen, Satoru Kawamura, Fred Rieke, and James B. Hurley. 2005. “Recoverin Improves Rod-Mediated Vision by Enhancing Signal Transmission in the Mouse Retina.” *Neuron* 46 (3): 413–20. https://doi.org/10.1016/j.neuron.2005.04.006.

Sanda, Nicolae, Leonardo Cerliani, Colas N. Authié, Norman Sabbah, José Alain Sahel, Christophe Habas, Avinoam B. Safran, and Michel Thiebaut de Schotten. 2018. “Visual Brain Plasticity Induced by Central and Peripheral Visual Field Loss.” *Brain Structure and Function* 223 (7): 3473–85. https://doi.org/10.1007/s00429-018-1700-7.

Sandberg, Michael A., Bernard Rosner, Carol Weigel-DiFranco, Thaddeus P. Dryja, and Eliot L. Berson. 2007. “Disease Course of Patients with X-Linked Retinitis Pigmentosa Due to RPGR Gene Mutations.” *Investigative Ophthalmology and Visual Science* 48 (3): 1298–1304. https://doi.org/10.1167/iovs.06-0971.

Sanes, Joshua R, and Richard H Masland. 2015. “The Types of Retinal Ganglion Cells: Current Status and Implications for Neuronal Classification.” *The Annual Review of Neuroscience* 38: 221–48. https://doi.org/10.1146/annurev-neuro-071714-034120.

Sassmannshausen, Marlene, Julia S Steinberg, Rolf Fimmers, Maximilian Pfau, Sarah Thiele, Monika Fleckenstein, Frank G Holz, and Steffen Schmitz-Valckenberg. 2018. “Structure-Function Analysis in Patients With Intermediate Age-Related Macular Degeneration.” *Investigative Ophthalmology & Visual Science* 59 (3): 1599–1608. https://doi.org/10.1167/iovs.17-22712.

Schenk, Thomas, Volker Franz, and Nicola Bruno. 2011. “Vision-for-Perception and Vision-for-Action: Which Model Is Compatible with the Available Psychophysical and Neuropsychological Data?” *Vision Research* 51 (8): 812–18. https://doi.org/10.1016/j.visres.2011.02.003.

Schmidt, Brian P., Ramkumar Sabesan, William S. Tuten, Jay Neitz, and Austin Roorda. 2018.

"Sensations from a Single M-Cone Depend on the Activity of Surrounding S-Cones." *Scientific Reports* 8 (1): 1–10. https://doi.org/10.1038/s41598-018-26754-1.

Schmitz-valckenberg, Steffen, Frank G Holz, Alan C Bird, and Richard F Spaide. 2008. "FUNDUS AUTOFLUORESCENCE IMAGING: Review and Perspectives." *Retina* 28: 385–409.

Schneeweis, David M, and Julie L Schnapf. 1995. "Photovoltage of Rods and Cones in the Macaque Retina." *Science* 268 (5213): 1053–56.

Schwartz, Steven H. 2010. "Visual Perception : A Clinical Orientation." New York, NY ; London.

Seabra, Miguel C, Michael S Brown, and Joseph L Goldstein. 1993. "Retinal Degeneration in Choroideremia : Deficiency of Rab Geranylgeranyl Transferase." *Science* 259 (5093): 377–81.

Seigo, Michaela A., Elias S. Sotirchos, Scott Newsome, Aleksandra Babiarz, Christopher Eckstein, E'Tona Ford, Jonathan D. Oakley, et al. 2012. "In Vivo Assessment of Retinal Neuronal Layers in Multiple Sclerosis with Manual and Automated Optical Coherence Tomography Segmentation Techniques." *Journal of Neurology* 259 (10): 2119–30. https://doi.org/10.1007/s00415-012-6466-x.

Seitz, Immanuel P., Jasleen K. Jolly, M. Dominik Fischer, and Matthew P. Simunovic. 2018. "Colour Discrimination Ellipses in Choroideremia." *Graefe's Archive for Clinical and Experimental Ophthalmology* 256 (4): 665–73. https://doi.org/10.1007/s00417-018-3921-0.

Simunovic, Matthew P. 2016. "Acquired Color Vision Deficiency." *Survey of Ophthalmology* 61 (2): 132–55. https://doi.org/10.1016/j.survophthal.2015.11.004.

Simunovic, Matthew P., Anthony T. Moore, and Robert E. MacLaren. 2016. "Selective Automated Perimetry under Photopic, Mesopic, and Scotopic Conditions: Detection Mechanisms and Testing Strategies." *Translational Vision Science and Technology* 5 (3): 1–13. https://doi.org/10.1167/tvst.5.3.10.

Simunovic, Matthew P., M. Votruba, B. C. Regan, and J. D. Mollon. 1998. "Colour Discrimination Ellipses in Patients with Dominant Optic Atrophy." *Vision Research* 38 (21): 3413–19. https://doi.org/10.1016/S0042-6989(98)00094-7.

Smith, RE., Jacques Donald Tournier, Fernando Calamante, and Alan Connelly. 2012. "Anatomically-Constrained Tractography: Improved Diffusion MRI Streamlines Tractography through Effective Use of Anatomical Information." *NeuroImage* 62 (3): 1924–38. https://doi.org/10.1016/j.neuroimage.2012.06.005.

Smith, SM., Mark Jenkinson, Heidi Johansen-Berg, Daniel Rueckert, Thomas E. Nichols, Clare E. Mackay, Kate E. Watkins, et al. 2006. "Tract-Based Spatial Statistics: Voxelwise Analysis of Multi-Subject Diffusion Data." *NeuroImage* 31 (4): 1487–1505. https://doi.org/10.1016/j.neuroimage.2006.02.024.

Smith, SM., Mark Jenkinson, Mark W. Woolrich, Christian F. Beckmann, Timothy E.J. Behrens, Heidi Johansen-Berg, Peter R. Bannister, et al. 2004. "Advances in Functional and Structural MR Image Analysis and Implementation as FSL." *NeuroImage* 23 (SUPPL. 1): 208–19. https://doi.org/10.1016/j.neuroimage.2004.07.051.

Staurenghi, Giovanni, Srinivas Sadda, Usha Chakravarthy Frcophth, Richard F Spaide, International Nomenclature, Coherence Tomography, and I N Oct. 2014. "Proposed

Lexicon for Anatomic Landmarks in Normal Posterior Segment Spectral-Domain Optical Coherence Tomography The IN OCT Consensus." *Ophthalmology* 121 (8): 1572–78. https://doi.org/10.1016/j.ophtha.2014.02.023.

Stingl, Krunoslav T., Laura Kuehlewein, Nicole Weisschuh, Saskia Biskup, Frans P.M. Cremers, M. Imran Khan, Carina Kelbsch, et al. 2019. "Chromatic Full-Field Stimulus Threshold and Pupillography as Functional Markers for Late-Stage, Early-Onset Retinitis Pigmentosa Caused by Crb1 Mutations." *Translational Vision Science and Technology* 8 (6): 45. https://doi.org/10.1167/tvst.8.6.45.

Stone, L. A., P. S. Albert, M. E. Smith, C. DeCarli, M. R. Armstrong, D. E. McFarlin, J. A. Frank, and H. F. McFarland. 1995. "Changes in the Amount of Diseased White Matter over Time in Patients with Relapsing-Remitting Multiple Sclerosis." *Neurology* 45 (10): 1808–14. https://doi.org/10.1212/WNL.45.10.1808.

Strauss, Olaf. 2005. "The Retinal Pigment Epithelium in Visual Function." *Physiological Reviews* 85 (3): 845–81. https://doi.org/10.1152/physrev.00021.2004.

Strettoi, Enrica, Vittorio Porciatti, Benedetto Falsini, Vincenzo Pignatelli, and Chiara Rossi. 2002. "Morphological and Functional Abnormalities in the Inner Retina of the Rd/Rd Mouse." *Journal of Neuroscience* 22 (13): 5492–5504. https://doi.org/10.1523/jneurosci.22-13-05492.2002.

Swanson, LW. 2013. "Basic Plan of the Nervous System. Iconoclast To Icon." In *Fundamental Neuroscience: Fourth Edition*, edited by Larry R Squire, 4th ed., 15–38. Amsterdam: Elsevier. https://doi.org/10.1016/B978-0-12-385870-2.00002-0.

Swanson, WH., D. G. Birch, and J. L. Anderson. 1993. "S-Cone Function in Patients with Retinitis Pigmentosa." *Investigative Ophthalmology and Visual Science* 34 (11): 3045–55.

Tahir, Humza J., Elena Rodrigo-Diaz, Neil R.A. Parry, Jeremiah M.F. Kelly, David Carden, and Ian J. Murray. 2017. "Slowed Dark Adaptation in Older Eyes; Effect of Location." *Experimental Eye Research* 155: 47–53. https://doi.org/10.1016/j.exer.2016.11.016.

Takemura, Hiromasa, Ariel Rokem, Jonathan Winawer, Jason D. Yeatman, Brian A. Wandell, and Franco Pestilli. 2016. "A Major Human White Matter Pathway Between Dorsal and Ventral Visual Cortex." *Cerebral Cortex* 26 (5): 2205–14. https://doi.org/10.1093/cercor/bhv064.

Takeshita, Daisuke, Lina Smeds, and Petri Ala-Laurila. 2017. "Processing of Single-Photon Responses in the Mammalian on and off Retinal Pathways at the Sensitivity Limit of Vision." *Philosophical Transactions of the Royal Society B: Biological Sciences* 372 (1717): 1–10. https://doi.org/10.1098/rstb.2016.0073.

Talib, Mays, Jasleen K. Jolly, and Camiel J.F. Boon. 2018. "Measuring Central Retinal Sensitivity Using Microperimetry." In *Methods in Molecular Biology*, 1st ed., 1715:339–49. Springer Science.

Talib, Mays, Mary J. Van Schooneveld, Alberta A. Thiadens, Marta Fiocco, Jan Wijnholds, Ralph J. Florijn, Nicoline E. Schalij-Delfos, et al. 2019. "CLINICAL and GENETIC CHARACTERISTICS of MALE PATIENTS with RPGR-ASSOCIATED RETINAL DYSTROPHIES: A Long-Term Follow-up Study." *Retina* 39 (6): 1186–89. https://doi.org/10.1097/IAE.0000000000002125.

Tavor, Ido, Maya Yablonski, Aviv Mezer, Shirley Rom, Yaniv Assaf, and Galit Yovel. 2014. "Separate Parts of Occipito-Temporal White Matter Fibers Are Associated with Recognition of Faces and Places." *NeuroImage* 86: 123–30.

https://doi.org/10.1016/j.neuroimage.2013.07.085.

Taylor, Paul A., and Ziad S. Saad. 2013. “FATCAT: (An Efficient) Functional and Tractographic Connectivity Analysis Toolbox.” *Brain Connectivity* 3 (5): 523–35. https://doi.org/10.1089/brain.2013.0154.

Testa, Francesco, Albert M. Maguire, Settimio Rossi, Eric A. Pierce, Paolo Melillo, Kathleen Marshall, Sandro Banfi, et al. 2013. “Three-Year Follow-up after Unilateral Subretinal Delivery of Adeno-Associated Virus in Patients with Leber Congenital Amaurosis Type 2.” *Ophthalmology* 120 (6): 1283–91. https://doi.org/10.1016/j.ophtha.2012.11.048.

Thiebaut de Schotten, Michel, Flavio Dell’Acqua, Stephanie Forkel, Andrew Simmons, Francesco Vergani, Declan G M Murphy, and Marco Catani. 2011. “A Lateralized Brain Network for Visuo-Spatial Attention.” *Nature Precedings*. https://doi.org/10.1038/npre.2011.5549.1.

Thompson, Debra A., Robin R. Ali, Eyal Banin, Kari E. Branham, John G. Flannery, David M. Gamm, William W. Hauswirth, et al. 2015. “Advancing Therapeutic Strategies for Inherited Retinal Degeneration: Recommendations from the Monaciano Symposium.” *Investigative Ophthalmology and Visual Science* 56 (2): 918–31. https://doi.org/10.1167/iovs.14-16049.

Tolmachova, Tanya, Silene T Wavre-Shapton, Alun R Barnard, Robert E MacLaren, Clare E Futter, and Miguel C Seabra. 2010. “Retinal Pigment Epithelium Defects Accelerate Photoreceptor Degeneration in Cell Type-Specific Knockout Mouse Models of Choroideremia.” *Investigative Ophthalmology & Visual Science* 51 (10): 4913–20. https://doi.org/10.1167/iovs.09-4892.

Ungerleider, Leslie G, and James V Haxby. 1994. “‘What’ and ‘Where’ in the Human Brain.” *Current Opinion in Neurobiology* 4: 157–65.

Verbakel, Sanne K, Ramon AC van Huet, Camiel JF Boon, Anneke I den Hollander, Rob WJ Collin, Klaver Caroline CW, Carel B Hoyng, Ronald Roepman, and B Jeroen Klevering. 2018. “Non-Syndromic Retinitis Pigmentosa.” *Progress in Retinal and Eye Research* 66: 157–86. https://doi.org/10.1007/978-3-319-95046-4_25.

Vidyasagar, Trichur R., and Kristen Pammer. 2010. “Dyslexia: A Deficit in Visuo-Spatial Attention, Not in Phonological Processing.” *Trends in Cognitive Sciences* 14 (2): 57–63. https://doi.org/10.1016/j.tics.2009.12.003.

Wan, Xing, Han Pei, Min Jian Zhao, Shuo Yang, Wei Kun Hu, Heng He, Si Qi Ma, et al. 2016. “Efficacy and Safety of RAAV2-ND4 Treatment for Leberâ (Tm) s Hereditary Optic Neuropathy.” *Scientific Reports* 6 (October 2015): 2–11. https://doi.org/10.1038/srep21587.

Wandell, Brian A., Serge O. Dumoulin, and Alyssa A. Brewer. 2007. “Visual Field Maps in Human Cortex.” *Neuron* 56 (2): 366–83. https://doi.org/10.1016/j.neuron.2007.10.012.

Wandell, Brian A., and Jonathan Winawer. 2011. “Imaging Retinotopic Maps in the Human Brain.” *Vision Research* 51 (7): 718–37. https://doi.org/10.1016/j.visres.2010.08.004.

Wang, Tian, Johan Pahlberg, Jon Cafaro, Rikard Frederiksen, A. J. Cooper, Alapakkam P. Sampath, Greg D. Field, and Jeannie Chen. 2019. “Activation of Rod Input in a Model of Retinal Degeneration Reverses Retinal Remodeling and Induces Formation of Functional Synapses and Recovery of Visual Signaling in the Adult Retina.” *The Journal of Neuroscience : The Official Journal of the Society for Neuroscience* 39 (34): 6798–6810. https://doi.org/10.1523/JNEUROSCI.2902-18.2019.

Ward, Rebecca, Joanna J Kaylor, Diego F Cobice, Dionissia A Pepe, Eoghan M McGarrigle, Susan E Brockerhoff, James B Hurley, Gabriel H Travis, and Breandan N Kennedy. 2020. “Non-Photopic and Photopic Visual Cycles Differentially Regulate Immediate, Early and Late-Phases of Cone Photoreceptor-Mediated Vision.” *Journal of Biological Chemistry* jbc.RA119. https://doi.org/10.1101/2020.02.15.950915.

Watson, Andrew B. 2014. “A Formula for Human Retinal Ganglion Cell Receptive Field Density as a Function of Visual Field Location.” *Journal of Vision* 14 (7): 1–17. https://doi.org/10.1167/14.7.15.

Weleber, Richard G., Mark E. Pennesi, David J. Wilson, Shalesh Kaushal, Laura R. Erker, Lauren Jensen, Maureen T. McBride, et al. 2016. “Results at 2 Years after Gene Therapy for RPE65-Deficient Leber Congenital Amaurosis and Severe Early-Childhood-Onset Retinal Dystrophy.” *Ophthalmology* 123 (7): 1606–20. https://doi.org/10.1016/j.ophtha.2016.03.003.

Welker, Susanne G, Maximilian Pfau, Manuel Heinemann, Steffen Schmitz-Valckenberg, Frank G Holz, and Robert P Finger. 2018. “Retest Reliability of Mesopic and Dark-Adapted Microperimetry in Patients With Intermediate Age-Related Macular Degeneration and Age-Matched Controls.” *Investigative Ophthalmology & Visual Science* 59 (4): AMD152–59. https://doi.org/10.1167/iovs.18-23878.

Werring, David J., Ahmed T. Toosy, Christopher A. Clark, Geoffrey J.M. Parker, Gareth J. Barker, David H. Miller, and Alan J. Thompson. 2000. “Diffusion Tensor Imaging Can Detect and Quantify Corticospinal Tract Degeneration after Stroke.” *Journal of Neurology Neurosurgery and Psychiatry* 69 (2): 269–72. https://doi.org/10.1136/jnnp.69.2.269.

Witkovsky, Paul. 2004. “Dopamine and Retinal Function.” *Documenta Ophthalmologica* 108 (1): 17–39. https://doi.org/10.1023/B:DOOP.0000019487.88486.0a.

Wong, Agnes M.F. 2012. “New Concepts Concerning the Neural Mechanisms of Amblyopia and Their Clinical Implications.” *Canadian Journal of Ophthalmology* 47 (5): 399–409. https://doi.org/10.1016/j.jcjo.2012.05.002.

Wood, Laura J, Jasleen K Jolly, Colm D Andrews, Iain R Wilson, Doron Hickey, Jasmina Cehajic-Kapetanovic, and Robert E MacLaren. 2020. “Low-Contrast Visual Acuity versus Low-Luminance Visual Acuity in Choroideremia.” *Clinical and Experimental Optometry* n/a (n/a). https://doi.org/10.1111/cxo.13087.

Woolrich, Mark W., Saad Jbabdi, Brian Patenaude, Michael Chappell, Salima Makni, Timothy Behrens, Christian Beckmann, Mark Jenkinson, and Stephen M. Smith. 2009. “Bayesian Analysis of Neuroimaging Data in FSL.” *NeuroImage* 45: S173–86. https://doi.org/10.1016/j.neuroimage.2008.10.055.

Wu, SM. 1991. “Input-Output Relations of the Feedback Synapse between Horizontal Cells and Cones in the Tiger Salamander Retina.” *Journal of Neurophysiology* 65 (5): 1197–1206. https://doi.org/10.1152/jn.1991.65.5.1197.

Wu, Zhichao, Lauren N. Ayton, Robyn H. Guymer, and Chi D. Luu. 2013a. “Intrasession Test-Retest Variability of Microperimetry in Age-Related Macular Degeneration.” *Investigative Ophthalmology and Visual Science* 54 (12): 7378–85. https://doi.org/10.1167/iovs.13-12617.

Wu, Zhichao, Lauren N. Ayton, Chi D. Luu, and Robyn H. Guymer. 2015. “Longitudinal Changes in Microperimetry and Low Luminance Visual Acuity in Age-Related Macular Degeneration.” *JAMA Ophthalmology* 133 (4): 442–48.

https://doi.org/10.1001/jamaophthalmol.2014.5963.

Wu, Zhichao, Lauren N Ayton, Robyn H Guymer, and Chi D Luu. 2013b. “Intrasession Test – Retest Variability of Microperimetry in Age-Related Macular Degeneration.” *The Association for Research in Vision and Ophthalmology* 54 (12): 7378–85. https://doi.org/10.1167/iovs.13-12617.

Wu, Zhichao, Chang J. Jung, Lauren N. Ayton, Chi D. Luu, and Robyn H. Guymer. 2015. “Test—Retest Repeatability of Microperimetry at the Border of Deep Scotomas.” *Investigative Ophthalmology and Visual Science* 56 (4): 2606–11. https://doi.org/10.1167/iovs.14-15977.

Xue, K, M. Groppe, A. P. Salvetti, and R. E. MacLaren. 2017. “Technique of Retinal Gene Therapy: Delivery of Viral Vector into the Subretinal Space.” *Eye* 31 (9): 1308–16. https://doi.org/10.1038/eye.2017.158.

Xue, K, Jasleen K. Jolly, Alun R. Barnard, Anna Rudenko, Anna P. Salvetti, Maria I. Patrício, Thomas L. Edwards, et al. 2018. “Beneficial Effects on Vision in Patients Undergoing Retinal Gene Therapy for Choroideremia.” *Nature Medicine* 24 (10): 1507–12. https://doi.org/10.1038/s41591-018-0185-5.

Xue, K, Marta Oldani, Jasleen K. Jolly, Thomas L. Edwards, Markus Groppe, Susan M. Downes, and Robert E. Maclaren. 2016. “Correlation of Optical Coherence Tomography and Autofluorescence in the Outer Retina and Choroid of Patients with Choroideremia.” *Investigative Ophthalmology and Visual Science* 57 (8): 3674–84. https://doi.org/10.1167/iovs.15-18364.

Yeatman, Jason D., Robert F. Dougherty, Michal Ben-Shachar, and Brian A. Wandell. 2012. “Development of White Matter and Reading Skills.” *Proceedings of the National Academy of Sciences of the United States of America* 109 (44): E3045–53. https://doi.org/10.1073/pnas.1206792109.

Yeatman, Jason D., Robert F. Dougherty, Nathaniel J. Myall, Brian A. Wandell, and Heidi M. Feldman. 2012. “Tract Profiles of White Matter Properties: Automating Fiber-Tract Quantification.” *PLoS ONE* 7 (11): e49790. https://doi.org/10.1371/journal.pone.0049790.

Yeatman, Jason D., Kevin S. Weiner, Franco Pestilli, Ariel Rokem, Aviv Mezer, and Brian A. Well. 2014. “The Vertical Occipital Fasciculus: A Century of Controversy Resolved by in Vivo Measurements.” *Proceedings of the National Academy of Sciences of the United States of America* 111 (48): E5214–23. https://doi.org/10.1073/pnas.1418503111.

Yoshimine, Shoyo, Shumpei Ogawa, Hiroshi Horiguchi, Masahiko Terao, Atsushi Miyazaki, Kenji Matsumoto, Hiroshi Tsuneoka, Tadashi Nakano, Yoichiro Masuda, and Franco Pestilli. 2018. “Age-Related Macular Degeneration Affects the Optic Radiation White Matter Projecting to Locations of Retinal Damage.” *Brain Structure and Function* 223 (8): 3889–3900. https://doi.org/10.1007/s00429-018-1702-5.

Yusuf, Imran H., Jasleen K. Jolly, Gokulan Ratnarajan, and John F. Salmon. 2018. “Microperimetry and Optical Coherence Tomography Imaging in the Fellow Eye of Patients with Unilateral Focal Ischaemic Glaucoma.” *Eye* 32 (8): 1372–79. https://doi.org/10.1038/s41433-018-0094-3.

Zein, Wadih M., Brett G. Jeffrey, Henry E. Wiley, Amy E. Turriff, Santa J. Tumminia, Weng Tao, Ronald A. Bush, et al. 2014. “CNGB3-Achromatopsia Clinical Trial with CNTF: Diminished Rod Pathway Responses with No Evidence of Improvement in Cone Function.” *Investigative Ophthalmology and Visual Science* 55 (10): 6301–8.

https://doi.org/10.1167/iovs.14-14860.

Zele, Andrew J., Michelle L. Maynard, and Beatrix Feigl. 2013. “Rod and Cone Pathway Signaling and Interaction under Mesopic Illumination.” *Journal of Vision* 13 (1): 1–19. https://doi.org/10.1167/13.1.22.

Zysk, Adam M, Freddy T Nguyen, Amy L Oldenburg, Daniel L Marks, and Stephen A Boppart. 2007. “Optical Coherence Tomography: A Review of Clinical Development from Bench to Bedside.” *Journal of Biomedical Optics* 12 (5): 51403. https://doi.org/10.1117/1.2793736.

Supplementary Data

Supplementary Data

Supplementary Table 1: Outcome measures on official registered entries for all trials relating to ocular gene therapy.

Phase	**Primary: Safety measures**	**Primary: Validated tests**	**Primary: Novel tests**	**Primary: Non-specific**	**Secondary: Safety measures**	**Secondary: Validated tests**	**Secondary: Novel tests**	**Secondary: Non-specific**
I or I/II	Adverse events and laboratory measures, inflammation, maximum tolerated dose, physical health	Visual acuity, IOP, kinetic and static perimetry		Photography, tolerability	Conversion disease type, maximum tolerated dose, number of rescue injections	Colour vision, dark adaptation, defined area or features on imaging, ERG, FST, mfERG, questionnaires, reading speed, retinal thickness, perimetry-Goldmann, perimetry-Humphrey, perimetry-microperimetry, perimetry-static, visual acuity distance (logMAR or FrACT), VA near	Dark adaptation cone recovery, light aversion, mobility door task, pupillometry	Efficacy, mobility, objective changes in vision, ophthalmic findings, pupil light reflex, psychophysical tests, quality of life, retinal function, retinal imaging, visual function, imaging

2 and 3	Adverse events	Visual acuity	Mobility (binocular)		Adverse events, laboratory measures	AF changes, colour vision, contrast sensitivity, FST, OCT ellipsoid zone, OCT RNFL, perimetry-Humphrey, microperimetry, questionnaires, VEP, visual acuity	Mobility (monocular)	AF, computerised visual field, responder analysis
Unspecified	Laboratory measures	Visual acuity			Laboratory measures	ERG, IOP, OCT RNFL, VEP		Computerised visual field

Supplementary Table 2: Summary FA measures of measures at different locations on the ventral, dorsal, and vertical tracts for both choroideremia and control participant groups.

Group	Location	Tract	Mean	Std. Deviation
CHM	1	right ILF	0.351	0.022
		right SLF	0.355	0.021
		right VOF	0.270	0.033
		left ILF	0.358	0.026
		left SLF	0.370	0.026
		left VOF	0.257	0.038
	2	right ILF	0.447	0.034
		right SLF	0.444	0.023
		right VOF	0.374	0.040
		left ILF	0.451	0.043
		left SLF	0.451	0.016
		left VOF	0.355	0.042
	3	right ILF	0.494	0.042
		right SLF	0.454	0.020
		right VOF	0.400	0.032
		left ILF	0.506	0.052
		left SLF	0.453	0.016
		left VOF	0.386	0.036
	4	right ILF	0.524	0.039
		right SLF	0.465	0.023
		right VOF	0.406	0.036
		left ILF	0.540	0.049
		left SLF	0.448	0.022
		left VOF	0.398	0.035
	5	right ILF	0.535	0.034
		right SLF	0.474	0.029
		right VOF	0.409	0.043
		left ILF	0.545	0.052
		left SLF	0.447	0.026
		left VOF	0.397	0.038
	6	right ILF	0.535	0.039

		right SLF	0.477	0.032
		right VOF	0.411	0.044
		left ILF	0.542	0.052
		left SLF	0.450	0.026
		left VOF	0.394	0.038
	7	right ILF	0.524	0.039
		right SLF	0.473	0.030
		right VOF	0.407	0.042
		left ILF	0.534	0.043
		left SLF	0.456	0.022
		left VOF	0.394	0.034
	8	right ILF	0.496	0.046
		right SLF	0.463	0.025
		right VOF	0.394	0.044
		left ILF	0.500	0.041
		left SLF	0.460	0.019
		left VOF	0.394	0.035
	9	right ILF	0.444	0.040
		right SLF	0.450	0.022
		right VOF	0.359	0.050
		left ILF	0.445	0.036
		left SLF	0.456	0.019
		left VOF	0.369	0.036
		Total	0.420	0.053
	10	right ILF	0.350	0.030
		right SLF	0.363	0.019
		right VOF	0.251	0.040
		left ILF	0.358	0.035
		left SLF	0.382	0.023
		left VOF	0.271	0.033
Control	1	right ILF	0.360	0.027
		right SLF	0.349	0.023
		right VOF	0.256	0.046
		left ILF	0.373	0.029
		left SLF	0.363	0.031
		left VOF	0.279	0.024

	2	right ILF	0.452	0.043
		right SLF	0.450	0.017
		right VOF	0.379	0.056
		left ILF	0.487	0.023
		left SLF	0.448	0.020
		left VOF	0.384	0.042
	3	right ILF	0.524	0.033
		right SLF	0.463	0.022
		right VOF	0.416	0.052
		left ILF	0.543	0.024
		left SLF	0.455	0.014
		left VOF	0.409	0.048
	4	right ILF	0.555	0.029
		right SLF	0.475	0.031
		right VOF	0.427	0.042
		left ILF	0.578	0.031
		left SLF	0.459	0.026
		left VOF	0.415	0.050
	5	right ILF	0.557	0.028
		right SLF	0.485	0.031
		right VOF	0.433	0.033
		left ILF	0.586	0.032
		left SLF	0.461	0.033
		left VOF	0.419	0.048
	6	right ILF	0.558	0.034
		right SLF	0.482	0.030
		right VOF	0.436	0.026
		left ILF	0.579	0.037
		left SLF	0.461	0.033
		left VOF	0.423	0.041
	7	right ILF	0.546	0.035
		right SLF	0.474	0.030
		right VOF	0.431	0.032
		left ILF	0.565	0.045
		left SLF	0.458	0.027
		left VOF	0.423	0.033

	8	right ILF	0.508	0.039
		right SLF	0.464	0.024
		right VOF	0.421	0.042
		left ILF	0.523	0.043
		left SLF	0.460	0.017
		left VOF	0.409	0.027
	9	right ILF	0.452	0.042
		right SLF	0.453	0.026
		right VOF	0.388	0.040
		left ILF	0.443	0.052
		left SLF	0.461	0.018
		left VOF	0.374	0.034
	10	right ILF	0.352	0.025
		right SLF	0.355	0.029
		right VOF	0.273	0.026
		left ILF	0.352	0.026
		left SLF	0.374	0.023
		left VOF	0.269	0.032

Supplementary Table 3: Summary MD measures of measures at different locations on the ventral, dorsal, and vertical tracts for both choroideremia and control participant groups.

Group	Location	Tract	Mean	Std. Deviation
CHM	1	right ILF	0.756	0.029
		right SLF	0.727	0.012
		right VOF	0.738	0.019
		left ILF	0.742	0.041
		left SLF	0.724	0.026
		left VOF	0.733	0.034
	2	right ILF	0.777	0.029
		right SLF	0.721	0.013
		right VOF	0.743	0.024
		left ILF	0.767	0.039
		left SLF	0.722	0.030

		left VOF	0.735	0.033
	3	right ILF	0.794	0.042
		right SLF	0.714	0.018
		right VOF	0.760	0.029
		left ILF	0.781	0.044
		left SLF	0.721	0.031
		left VOF	0.753	0.034
	4	right ILF	0.812	0.049
		right SLF	0.707	0.020
		right VOF	0.773	0.034
		left ILF	0.798	0.050
		left SLF	0.719	0.031
		left VOF	0.771	0.036
	5	right ILF	0.829	0.044
		right SLF	0.702	0.020
		right VOF	0.781	0.036
		left ILF	0.814	0.040
		left SLF	0.717	0.026
		left VOF	0.785	0.039
	6	right ILF	0.831	0.036
		right SLF	0.700	0.021
		right VOF	0.779	0.037
		left ILF	0.807	0.032
		left SLF	0.716	0.021
		left VOF	0.787	0.037
	7	right ILF	0.810	0.028
		right SLF	0.703	0.025
		right VOF	0.767	0.033
		left ILF	0.791	0.028
		left SLF	0.715	0.021
		left VOF	0.776	0.032
	8	right ILF	0.784	0.022
		right SLF	0.708	0.026
		right VOF	0.750	0.027
		left ILF	0.774	0.027
		left SLF	0.715	0.021

		left VOF	0.756	0.028
	9	right ILF	0.766	0.030
		right SLF	0.712	0.026
		right VOF	0.730	0.025
		left ILF	0.765	0.034
		left SLF	0.715	0.022
		left VOF	0.734	0.026
	10	right ILF	0.748	0.034
		right SLF	0.720	0.023
		right VOF	0.731	0.023
		left ILF	0.748	0.039
		left SLF	0.716	0.023
		left VOF	0.728	0.024
Control	1	right ILF	0.740	0.034
		right SLF	0.724	0.020
		right VOF	0.726	0.024
		left ILF	0.726	0.042
		left SLF	0.718	0.024
		left VOF	0.712	0.023
	2	right ILF	0.756	0.030
		right SLF	0.710	0.024
		right VOF	0.719	0.026
		left ILF	0.741	0.028
		left SLF	0.714	0.029
		left VOF	0.717	0.031
	3	right ILF	0.766	0.031
		right SLF	0.700	0.024
		right VOF	0.733	0.026
		left ILF	0.755	0.027
		left SLF	0.709	0.031
		left VOF	0.733	0.038
	4	right ILF	0.781	0.034
		right SLF	0.693	0.023
		right VOF	0.745	0.028
		left ILF	0.773	0.027
		left SLF	0.704	0.029

		left VOF	0.748	0.042
	5	right ILF	0.792	0.029
		right SLF	0.690	0.023
		right VOF	0.752	0.030
		left ILF	0.778	0.027
		left SLF	0.701	0.025
		left VOF	0.759	0.043
	6	right ILF	0.792	0.029
		right SLF	0.689	0.026
		right VOF	0.752	0.031
		left ILF	0.772	0.027
		left SLF	0.700	0.023
		left VOF	0.759	0.039
	7	right ILF	0.784	0.031
		right SLF	0.692	0.028
		right VOF	0.744	0.032
		left ILF	0.759	0.035
		left SLF	0.701	0.024
		left VOF	0.747	0.034
	8	right ILF	0.772	0.031
		right SLF	0.697	0.029
		right VOF	0.732	0.031
		left ILF	0.750	0.039
		left SLF	0.704	0.027
		left VOF	0.731	0.029
	9	right ILF	0.764	0.039
		right SLF	0.704	0.031
		right VOF	0.719	0.028
		left ILF	0.754	0.038
		left SLF	0.708	0.027
		left VOF	0.714	0.026
	10	right ILF	0.750	0.040
		right SLF	0.718	0.028
		right VOF	0.718	0.019
		left ILF	0.751	0.051
		left SLF	0.714	0.020

		left VOF	0.714	0.025
Total	1	right ILF	0.750	0.032
		right SLF	0.726	0.016
		right VOF	0.733	0.021
		left ILF	0.735	0.042
		left SLF	0.721	0.025
		left VOF	0.724	0.031
	2	right ILF	0.769	0.031
		right SLF	0.716	0.019
		right VOF	0.733	0.027
		left ILF	0.756	0.036
		left SLF	0.719	0.029
		left VOF	0.727	0.033
	3	right ILF	0.783	0.040
		right SLF	0.708	0.021
		right VOF	0.749	0.031
		left ILF	0.770	0.039
		left SLF	0.716	0.031
		left VOF	0.744	0.037
	4	right ILF	0.799	0.046
		right SLF	0.701	0.022
		right VOF	0.761	0.034
		left ILF	0.787	0.043
		left SLF	0.713	0.030
		left VOF	0.762	0.040
	5	right ILF	0.814	0.042
		right SLF	0.696	0.022
		right VOF	0.769	0.036
		left ILF	0.799	0.039
		left SLF	0.711	0.026
		left VOF	0.774	0.042
	6	right ILF	0.815	0.038
		right SLF	0.696	0.024
		right VOF	0.768	0.037
		left ILF	0.792	0.035
		left SLF	0.709	0.023

		left VOF	0.775	0.040
	7	right ILF	0.799	0.032
		right SLF	0.698	0.026
		right VOF	0.757	0.034
		left ILF	0.777	0.035
		left SLF	0.709	0.023
		left VOF	0.764	0.035
	8	right ILF	0.779	0.026
		right SLF	0.703	0.027
		right VOF	0.742	0.030
		left ILF	0.764	0.035
		left SLF	0.710	0.024
		left VOF	0.746	0.031
	9	right ILF	0.765	0.033
		right SLF	0.709	0.028
		right VOF	0.725	0.027
		left ILF	0.760	0.036
		left SLF	0.712	0.024
		left VOF	0.725	0.028
	10	right ILF	0.749	0.036
		right SLF	0.719	0.025
		right VOF	0.726	0.022
		left ILF	0.749	0.044
		left SLF	0.715	0.022
		left VOF	0.722	0.025

Appendix 1: Standard Operating Procedures

Appendix 1: Standard Operating Procedures

A1.1 Measurement of Visual Acuity with ETDRS Charts

PURPOSE

To standardise the measurement of distance visual acuity using standard ETDRS charts.

INTRODUCTION

Visual acuity is the most common measure of vision function used in both clinical work and clinical research. Visual acuity is the ability of the eye to see fine details and depends on the functions of retina, neuronal transmission, and the interpretative ability of the brain. We are measuring visual acuity with ETDRS (Early Treatment Diabetic Retinopathy Study) charts because they are especially designed for clinical studies and low vision evaluations, where accurate and repeatable visual acuity measurements is required.

SCOPE

This Standard Operating Procedure (SOP) covers the use of ETDRS charts to measure VA.

PROCEDURE

The participant will wear their optimal refractive correction and will not have dilated pupils. The participant will sit 4 metres from the ETDRS chart (followed by testing at 1 metre only if insufficient letters are read at the initial distance). Position the participant by adjusting their chair height so that their line of sight is towards the middle of the screen and that his or her back is firmly touching the back of the chair. The examiner should ensure that the participant is sitting comfortably, that the head does not move forward or backward during the test, and that the participant's eyes remain at the 4 metre distance. The participant is allowed to move their head laterally or vertically to find the optimal area of visual field for testing. The test is completed with the room lights off and internal lights on.

Testing should be performed as per the procedure below:

a. Each eye should be tested separately at 4 metres. Occlude the fellow eye to avoid the use of peripheral vision with an eye patch.

b. Use chart R to check refraction if required. Use Chart 1 to test the right eye and Chart 2 to test the left eye. By convention, first measure the right eye. Each chart should remain hidden from view until the eye in question is ready for testing. Therefore, cover both eyes with occluders before you show Chart 1 and also in between changing the charts.

c. Inform the participant the charts consist of letters. There are no numbers or symbols. The participant is asked to read from the top of the chart and to slowly read the letters (at a rate not faster than about one letter per second) in order to achieve the best identification of each letter and to not proceed until the participant has given a definite response. If the participant identifies a letter as one of two or more letters, he or she

should be asked to choose one letter and, if necessary, to guess even if the next letter has already been read.

d. It is accepted that if a participant changes their response BEFORE they have read the next letter out loud it can be counted. If the patient changes a response AFTER they have read the next letter it is not accepted.

e. Each letter read correctly should be circled. Cross out letters incorrectly identified and leave unmarked those letters that are un-attempted. The examiner should continue the test until the participant has read all the letters possible or they are unable to guess any more.

f. If less than 20 letters are read then the light box is moved to 1 metre and +0.75DS is added to the participants prescription to compensate for the closer testing distance. The participant may stand or sit for the 4 metre test, but must sit for the 1 metre test. The avoidance of any head movement forward or backward is particularly important during the 1 metre test. The participant should be asked to read only the first 6 lines at 1 metre, making 30 the maximum score at that distance.

g. Test with the low luminance filter (2 log) before testing without the filter to reduce a learning effect.

h. After the test of the right eye is completed, occlude the left eye and replace Chart 1 with Chart 2. The test is repeated for the left eye, starting at 4 metres. When testing of the left eye is completed, Chart 2 should be removed from view.

i. If no letters are seen at either working distance, test for count fingers (CF). This is done by the examiner’s hand holding 1, 2, or 5 fingers. The hand must be held steady at a distance of 2ft directly in front of the eye being examined. The non-study eye is completely occluded with a patch on the face. A light should be shown directly on the hand from behind the patient. The examiner's fingers should be presented in random order and repeated 5 times. Eccentric fixation, if present, should be encouraged. If the participant correctly identifies three of the five presentations, then count fingers vision is noted. If not, then the patient must be tested for hand movements (HM) vision.

j. In testing for HM vision, the examiner's hand with all fingers spread out should be extended two feet directly in front of the eye being examined. The non-study eye should be occluded with a patch on the participant’s face. A light should be shone directly on the hand from behind the participant. The examiner’s hand should be moved in an up-and-down direction (vertically) or in a side-to-side direction (horizontally) at a constant speed of approximately one back and forth presentation per second. The participant is instructed that the examiner’s hand will be presented and they will have to respond to the question: “What am I doing with my hand?” This should be repeated five times. Four out of five correct responses indicate that HM vision is present. If the participant does not correctly identify four of five, then you must test for light perception.

k. Testing for light perception (LP) / no light perception (NLP) vision should be done with an indirect ophthalmoscope in a darkened room. The indirect ophthalmoscope light should be held approximately 1 metre or about 3 feet away with the rheostat set at maximum voltage. From that distance the beam should be directed in and out of the eye at least four times, and the participant should be asked to respond when he or she sees

the light. If the examiner is convinced that the patient perceives the light, vision should be recorded as “light perception”; if not, vision should be recorded as “no light perception”.

l. The examiner must record the time taken to conduct the test for both eyes without the filter.

Scoring of Visual Acuity:

a. Complete the Distance Visual Acuity Score Sheet and transcribe the number of letters read for VA to the Case Report Form.

b. If 20 or more letters are read at 4 metres it is not necessary to proceed with testing at 1 metre. To calculate the total number of letters read, add 30 to the number of letters read at 4 metres as directed on the score sheet.

c. If fewer than 20 letters are read at 4 metres test distance, testing at 1 metre should be performed. Add the number of letters read at 1 metre to the number of letters read at 4 metres to calculate the total number of letters read.

d. Equivalent Snellen scores should be calculated as defined by the lowest line on which 3 or more letters were seen correctly, regardless of how many letters were seen on the letters above.

e. If no letters were read correctly, vision should be recorded as CF, HM, LP or NLP.

FORMS/TEMPLATES TO BE USED

Results can be noted on the standard Distance Visual Acuity Score Sheet. Data should be recorded in the appropriate Case Report Form.

REFERENCES

None

A1.2 Measurement of Visual Acuity with EVA Using Single Line Presentation

PURPOSE

To standardise the measurement of distance visual acuity using the Electronic Visual Acuity Tester (EVA) single line presentation.

INTRODUCTION

Visual acuity (VA) is the most common measure of vision function used in both clinical work and clinical research. Until now, little attention has been paid to the accuracy of visual acuity measurements in patients with visual field loss due to the lack of treatments for the condition. An EVA tester released by the EMMES Corporation has the ability to present letters on the centre of a computer screen in a random order, therefore negating the requirement to read down a letter chart. In order to maintain equivalency to the ETDRS charts, single line presentation of the letters in the same presentation order can be shown on the EVA system. Before this method of presentation can be accepted, the EVA tester must be shown to measure VA in a comparable way to widely accepted gold standard ETDRS charts.

SCOPE

This Standard Operating Procedure (SOP) covers the use of the EVA tester to measure VA.

PROCEDURE

The participant will wear their optimal refractive correction and should not have dilated pupils. The participant will sit 3 metres from the EVA screen. Position the participant by adjusting their chair height so that their line of sight is towards the middle of the screen. With the participant seated, his or her back should fit firmly touching the back of the chair. The examiner should ensure that the participant is sitting comfortably, that the head does not move forward or backward during the test, and that the participant's eyes remain at the 3 metre distance. The participant is allowed to move their head laterally or vertically to find the optimal area of visual field for testing. By convention, measure the right eye first. The test is completed with the room lights off.

Testing should be performed as per the procedure below:

a. Turn on the EVA system according to the manufacturer's instructions.
b. Ensure the display screen is switched on for a minimum 10 mins before use.
c. Calibrate the size and luminance as prompted by the onscreen instructions. Record this in the calibration log. This must only be done once after the machine has been switched on.
d. Turn the room lights off.
e. Power on the iPod. The code for the iPod is in the case.
f. Each eye should be tested separately at 3 metres. Fully occlude the fellow eye to avoid the use of peripheral vision.
g. Advise the participant the display consists of letters. There are no numbers or symbols. The participant is asked to read from left to right and to slowly read the letters (at a rate

not faster than about one letter per second) in order to achieve the best identification of each letter and to not proceed until the participant has given a definite response. If the participant identifies a letter as one of two or more letters, he or she should be asked to choose one letter and, if necessary, to guess even if the next letter has already been read.

h. Select “EVA” on the iPod to start. Then select ‘Chart’ from the homepage. Select ‘SLOAN Letters’ from the Optotype options. Then select ‘Single Lines’.

i. Present the participant with the 20/200 size letters by selecting “20/200” on the iPod (UK Snellen equivalent 6/60). Ask the participant to read the letters presented. Five letters will be presented for each letter size and a correct or incorrect response will be recorded on the Distance Visual Acuity Scoring Sheet. Mark a tick for a correct response and a cross for an incorrect response. Leave letters not guessed blank.

j. Once all the five letters are read on the 20/200 line, select “Smaller” on the iPod to decrease the size of the letters to 20/160. Continue this process until the participant can no longer read the letter size presented.

k. If the participant cannot read the 20/200 letters, increase the letter size by selecting “Bigger” until a letter size is presented that the participant can read. The screen may display less than five letters in which case, select “repeat” until 5 letters have been displayed per letter size. If the total letters presented with repeat is greater than 5, only accept responses for the first 5 presentations.

l. Please see the Appendix for precise order of presentation.

m. It is accepted that if a participant changes their response BEFORE the response has been recorded. If the participant changes a response AFTER the response has been recorded it is not accepted.

n. The examiner should continue the test until the participant has read all the letters possible or they are unable to guess any more. The examiner must record the score, Snellen equivalent, and time taken to conduct the test for both eyes.

Scoring of Visual Acuity:

f. If larger letters are not tested, please assume they were seen and add scores for them as seen accordingly. Sum the number of letters seen, with a maximum result of 100. See the Appendix for guidance on how to treat lines not attempted.

g. Equivalent Snellen scores should be calculated as defined by the lowest line on which 3 or more letters were seen correctly, regardless of how many letters were seen on the letters above.

h. Complete the Distance Visual Acuity Score Sheet and transcribe the number of total number of letters seen correctly and the Snellen equivalent to the Case Report Form.

FORMS/TEMPLATES TO BE USED

Results can be noted on the Distance Visual Acuity Score Sheet.

REFERENCES

EVA instruction manual.

A1.3 Measurement of Visual Acuity Using Automated EVA E-ETDRS Protocol

PURPOSE

To standardise the measurement of distance visual acuity using the automated procedure on the Electronic Visual Acuity Tester (EVA).

INTRODUCTION

Visual acuity (VA) is the most common measure of vision function used in both clinical work and clinical research. Until now, little attention has been paid to the accuracy of visual acuity measurements in patients with visual field loss due to the lack of treatments for the condition. An EVA tester released by the EMMES Corporation has the ability to present letters on the centre of a computer screen in a random order, therefore negating the requirement to read down a letter chart, which is difficult for patients with visual field loss. Before this method of presentation can be accepted, the EVA tester must be shown to measure VA in a comparable way to widely accepted gold standard ETDRS charts.

SCOPE

This Standard Operating Procedure (SOP) covers the use of the EVA tester to measure VA.

PROCEDURE

The participant will wear their optimal refractive correction and should not have dilated pupils. The participant will sit 3 metres from the EVA screen. Position the participant by adjusting their chair height so that their line of sight is towards the middle of the screen. With the participant seated, his or her back should fit firmly touching the back of the chair. The examiner should ensure that the participant is sitting comfortably, that the head does not move forward or backward during the test, and that the participant's eyes remain at the 3 metre distance. The participant is allowed to move their head laterally or vertically to find the optimal area of visual field for testing. By convention, measure the right eye first. The test is completed with the room lights off.

Testing should be performed as per the procedure below:

a. Turn on the EVA system according to the manufacturer's instructions.

b. Ensure the display screen is switched on for a minimum of 10 mins before use for the high contrast targets and 45 mins for the low contrast targets.

c. Calibrate the size and luminance as prompted by the onscreen instructions. Record this in the calibration log. This must only be done once after the machine has been switched on.

d. Turn the room lights off.

e. Power on the iPod. The code for the iPod is in the case.

f. Each eye should be tested separately at 3 metres. Fully occlude the fellow eye to avoid the use of peripheral vision.

g. Advise the participant that a letter will be presented on the middle of the screen surrounded by sides forming a box. Their task is to identify the letter in the middle, ignoring the surrounding lines. Some of the letters will be smaller than others but they must try and guess as far as possible.

h. It is accepted that if a participant changes their response BEFORE the response has been recoded. If the patient changes a response AFTER the response has been recorded it is not accepted. If a participant guesses 2 letters then they must choose one.

i. The examiner should follow the on screen prompts to conduct the test. Once it is completed, the screen will display a summary of the test results. The examiner must record the score, score ID, Snellen equivalent, and time taken to conduct the test for both eyes.

j. Record time taken to complete the test.

k. Repeat the test with the low luminance filter in place.

l. Conduct the low contrast E-ETDRS using a contrast level of 5%. This is informed in the same way. Follow the onscreen prompts.

FORMS/TEMPLATES TO BE USED

Results should be recorded in the appropriate Case Report Form.

REFERENCES

EVA instruction manual

A1.4 MAIA Microperimetry 10-2 Standard Grid

PURPOSE

To ensure that the microperimetry assessment is carried out as consistently as possible for all study participants.

INTRODUCTION

Microperimetry is used to test retinal function within the macular area. The testing protocol is based on the MAIA system (Centervue, Padova, Italy) and has been developed following initial examinations on choroideremia patient volunteers at the Oxford Eye Hospital. Each patient should be re-tested on the same machine, if possible.

SCOPE

This Standard Operating Procedure (SOP) covers the use of the MAIA system for microperimetry assessment, but a similar protocol can be used for the Nidek MP 1-3 system, if this is the only machine available.

PROCEDURE

The test should be performed prior to pupil dilation. All tests will be carried out in the same order: right eye followed by left eye. For comfort, the patient may pause the test at any time for up to 5 minutes in total per test, as long as they remain dark adapted. The MAIA operator screen should remain covered with a red filter 026 Bright Red (Lee Filters, Hampshire, UK) as much as possible. The high temperature (HT) version of the same filter should be wrapped around any lamps being used in the room in order to minimise cone stimulating wavelengths of light. Testing should be performed as per the procedure below:

a. Dark adapt the patient for minimum 20 minutes in a darkened room. A dim lamp in the corner of the room may be used during the adaptation time to allow mobility of the examiner but must be switched off before testing is commenced. The illuminance at the patient's eye level should remain below 2 lux during the adaptation time and below 1 lux during the microperimetry test. Additional neutral density filters can be used over the lamp as required to achieve this level of illumination.

b. Enter patient details on the machine. Use study code and initials instead of name if appropriate. This can be changed at the end of the trial. Set screen to dark appearance.

c. Sit the patient in front of the machine with a patch covering the non-tested eye. Adjust both the height of the machine and distance between chin and forehead rests to ensure that the patient is seated in a comfortable and stable position.

d. For the first test being performed at baseline, click "New expert exam". Select the 10-2 (68 stimuli) grid. Set eye being tested (OD before OS) and click auto alignment. Final adjustments can be made using the buttons in front of the screen. Bring the machine forward using the focussing button. It can also be adjusted horizontally and vertically

using the arrow keys. The fundal autofluorescence image should fill the screen with the macula centred and optic disc visible. If it is too far away, the fundal image will not fill the screen. If it is too close, distortion of the image will appear. Once start is pressed, the auto focus will occur. Final adjustments can be made using the + and – buttons if required. Follow the on screen adjustments during setup. If the auto alignment function is not able to line the machine up, please follow a manual process.

e. Ask the patient to keep looking at the red ring. The button must be pressed for any flashing lights seen, no matter how dim. If the red ring is not visible, the larger fixation target can be used (by pressing the button for both fixation targets for maximum visibility). If this is still not visible, guide the patient's gaze verbally based on the fundal image on the screen. Continue to verbally guide the patient throughout testing.

f. Provide encouragement during testing. Ensure head is kept still in the correct position. The machine can be moved vertically and horizontally if the eye position moves, but focussing must not be amended during testing.

g. Note reliability score and spread of fixation on completion of testing. Reliability should be above 85% or fixation losses ≤ 15%, otherwise the test must be repeated.

h. If 5 points or less are seen (i.e. sensitivity >1dB to be counted as seen) on the 10-2 grid, conduct a second test to examine the central visual field in more detail. Choose the 10^{o} standard test with 37 stimuli that has a greater concentration in the centre than the periphery. This must be done for both eyes, even if the other eye sees more.

i. For repeat testing, click on "Follow-up exam" rather than "New expert exam", to use identical settings to ensure consistency. Baseline measurements require a minimum of 3 field tests before treatment to allow for the learning effect. If appropriate, repeat both the 10-2 and 37 stimuli grids at each follow up.

FORMS/TEMPLATES TO BE USED

Results can be printed directly from the machine. Data should be recorded in the appropriate Case Report Form and raw data downloaded.

REFERENCES

- MAIA user manual
- MAIA brochure:

www.centervue.com/articms/admin/upAllegati/639/1390298079.pdf

www.centervue.com/articms/admin/upAllegati/639/1416559637.pdf

A1.5 Fundus Autofluorescence

PURPOSE

To standardise the acquisition of fundus autofluorescence (FAF) images.

INTRODUCTION

FAF aims to produce digital autofluorescence images of the patient's fundus.

SCOPE

This Standard Operating Procedure (SOP) covers FAF using the Heidelberg Spectralis® HRA+OCT imaging system (Heidelberg Engineering, Heidelberg, Germany).

PROCEDURE

a. Imaging systems:
    - Patients will be examined in mydriasis using a Spectralis® HRA+OCT system (Heidelberg Engineering, Heidelberg, Germany), at a laser power of 486 µW.

b. Recording of images:
    - There must be a facility for the transfer of images to external data storage devices.
    - Images should not be compressed.
    - Images should be saved using the following filename format so as to preserve the anonymity of the trial participant – "REGEN_AF"_"anonymous 3-digit Patient Identifier specific to the trial participant"_ "Visit Number"_"Left eye (L) or right eye (R)"_"Date in the format ddmmmyy", e.g. "REGEN_AF_123_Visit1_L_01Sep15". (The list of anonymous patient identifiers specific to each trial participant will be kept in the Investigator Site File maintained at each trial site.)

c. Standard image capture:
    - Participants' keratometry measurements should be recorded at the first visit and entered into the Heidelberg system software to standardise inter-individual retinal image magnification.
    - FAF images should be taken in High Speed (HS) at both the 30° and 55° angles of capture, in both normalised and non-normalised formats.
    - All images should be recorded at Automatic Real-Time (ART) mode 100. If not possible, use the highest possible ART number while excluding motion artefact.
    - Photographs should include the whole disc and macula in view and should avoid cutting off edges of the islands of residual retina that are typical of an FAF choroideremia phenotype, i.e. if possible include the entirety of any delineated posterior pole regions of surviving autofluorescent retinal pigment epithelium.

REFERENCES

Heidelberg user manual

A1.6 Farnsworth-Munsell 100 Hue Test

PURPOSE

To standardise the assessment of colour vision using the Farnsworth-Munsell (FM) 100 Hue Test for all study participants.

INTRODUCTION

The F-M 100-Hue test is a panel test of colour vision specifically developed to determine/quantify colour discrimination [1].

SCOPE

This Standard Operating Procedure (SOP) covers colour vision testing using the FM 100 Hue Test.

PROCEDURE

This test must be conducted prior to pupillary dilatation and clinical examination. Each eye should be tested separately and in the same order: right then left. The test is conducted with a light source that provides adequate illumination (≥270 lux) and whose spectral power distribution simulates CIE standard illuminant D65. The testing distance is 50cm.

Testing should be conducted as follows:

a. The patient is shown the first box and instructed that their task is to arrange the moveable caps in a gradual progression in colour. In practice, the easiest way for many subjects to perform the test is to choose which cap most closely matches the left-most cap in colour and to place this cap (without touching the coloured aperture) next to the fixed cap. This process is then repeated using the first placed cap as a new reference and so on until all of the caps are used.

b. It is important that the caps are randomised (by hand) prior to commencement. The randomised caps *should remain within the tray.* This is important when testing subjects with constricted fields (so that the task remains as far as possible one of colour discrimination, rather than visual search). This will also shorten the testing time. Help can be provided in finding stray caps outside the patient's visual field.

c. Once the first box is completed, the procedure is completed for the second and subsequent boxes.

d. The patient's details should be entered on the standardised score sheet and their ordering recorded for each box. It is important to check that the ordering is performed correctly and that no caps are missing.

e. Test scoring can be performed with customised software or the scoring software provided with the test. Colour vision error score should be recorded. For the purposes of the trial, data will also be analysed using the "moment of inertia" analysis of Vigrys

& King-Smith. Online analysis can be performed at www.torok.info/colorvision-v1/. Alternatively, a stand-alone BASIC program is available from the Nuffield Laboratory of Ophthalmology on request (requires Chipmunk BASIC to run). The key variables to be noted in this latter analysis are C-index, S-index and axis.

FORMS/TEMPLATES TO BE USED

Results should be recorded and scored as outlined above. Data should be recorded in the appropriate Case Report Form.

REFERENCES

1. Farnsworth D. The Farnsworth-Munsell 100-Hue and Dichotomous Tests for Color Vision. Journal of the Optical Society of America A. 1943;33:568-74.

A1.7 Cambridge Colour Low Vision Version Trivector Test

PURPOSE

To standardise the assessment of colour vision using the low vision Cambridge colour test for all study participants in FMRIB studies.

INTRODUCTION

The Cambridge Colour Test is a computerised test of colour discrimination originally developed for the assessment of colour vision in patients with congenital colour vision deficiency. This was later modified as the “low vision Cambridge Colour Test” (lvCCT) for the investigation of colour discrimination in patients with low vision/acquired colour vision deficiency and is the version used in all studies taking place in Oxford Eye Hospital [1].

SCOPE

This Standard Operating Procedure (SOP) covers colour vision testing using the lvCCT trivector test paradigm.

DEFINITIONS

CRS = Cambridge Research Systems

lvCCT = low vision Cambridge Colour Test

PROCEDURE

This test should be conducted prior to pupillary dilatation or exposure to bright lights such as retinal imaging. The test is to be performed binocularly (both eyes together). The test is conducted in a darkened room with the patient wearing their usual refractive correction. The patient must wear the most recent distance prescription. If there is any doubt over the glasses, a refraction should be performed.

Test parameters are preset and should not be changed from the following.

1. Display distance at 1500mm and field of view 26.18x14.90 degrees. White point be set to D65.
2. Set conditions to use the Azimuth colour system; with values of 0.0667, 4.8382 and 5.9852 to represent L, M & S cone responses. Randomised ordering with 3 trials per block.
3. There are 4 discs to be displayed on the screen, one coloured and the other three varying in luminance. The position and size of these has been preset by CRS. They have a radius of 2 degrees. The right disc should be positioned X 4.3 degree, Y 0 degrees. The left disc should be positioned X -4.3 degree, Y 0 degrees. The upper disc

should be positioned X 0 degrees, Y 4.3 degrees. The lower disc should be positioned X 0 degrees, Y -4.3 degrees.

4. Set stimulus duration of each disc to a maximum of 20s in order to allow localisation of the discs in patients with severely reduced visual fields.
5. A staircase method to be employed for threshold determination with 6 out of 7 reversals being used to determine the threshold. Decrease rate of 50 before 1st reversal and 12.5 after the 1st reversal. Increase rate of 25. This will occur after each response. Arithmetic threshold estimation based on troughs and peaks. Abort the test after 5 negative responses at maximum saturation (0.11). There will not be any catch trials.
6. The response will be determined by the subject's button box or using the arrow keys. A response will end the stimulus. Response time is limited to 2s following the end of the stimulus appearance. Auditory indicators should be used where possible to aid the patient with knowing when the trial is commencing. No response feedback should be provided.

Testing should be conducted as follows: Provide the patient with an appropriate set of trial lenses to account for their distance refractive error. Keep both eyes open together so centre the trial frames to ensure the participant is looking through the centre of the lenses or use own glasses.

1. Set up the colour vision testing equipment:
    1. Position the screen at 1.5 metres from the patient using the marker on the wall.
    2. Ensure the connections between the computer and the screen is robust.
    3. Plug in the button box into the slot labelled button box.
    4. Plug in the power supply of the screen first followed by the iMac.
    5. Turn on the keyboard and mouse.
    6. Enter the password to login to the iMac: 'metropsis'.
    7. Load the 'Psykinematix Sharp' application – always skip calibrator.
2. Add the subject to the system
    1. Click on 'Subjects'.
    2. Create a profile for the right eye by clicking on the '+' button.
    3. Enter the subjects birth date.
    4. Click on 'unnamed subject' in the subject list and type the subjects name.
    5. Select the subjects Gender and Handedness from the drop down menus.
3. Set up the colour vision test application
    1. Click on the 'Designer' button in the Psykinematix application.
    2. Click on the 'METROPSIS – Cambridge Colour Test – Low vision version – Trivector CHM' entry in the list.

3. Click on the ‘Play’ button.
4. From the ‘Subject ID’ drop down menu select the subjects name.
5. From the ‘Group’ drop down menu, select ‘MRI’.

4. Explain the test to the participant:
    1. ‘The test will require you to look at the screen. Four circles will appear in an ‘Up’, ‘Down’, ‘Left’ and ‘Right’ position. One of the circles will have a shade of colour to it. The other three circles will be grey with different levels of brightness. Indicate which one you think is the coloured circle using the corresponding button on the button box, for example if you think the circle in the ‘Up’ position has a shade of colour, press the ‘Up’ button. Don’t let your attention be drawn to the brightness of the circles. If you feel there is no shade of colour present, choose the circle you think is most likely or guess. The test is designed to test the limits of your colour vision so there will be circles where you don’t see the colour, we would still like you to guess in those cases and this will speed up the test. The test will take approximately 5 minutes and we will repeat the test. If you have any questions or wish to stop at any time then please ask. You can move your head around during the test but please do not sit forward or backward.’

5. Perform the colour vision test
    1. Turn off the lights.
    2. Cover the screen of the iMac.
    3. Press the ‘Enter’ button on the keyboard to begin the test.
    4. When prompted on screen, press the ‘ESC’ key on the keyboard to begin the test.
    5. Give the button box to the participant and instruct them to advise you when they are ready to begin. Press spacebar at this point as per the instructions on the screen.
    6. Monitor the patient throughout the test to ensure correct positioning i.e. sitting back against the chair and ensure they understand the correct buttons to press. Provide encouragement as required.
    7. When the test is complete, press the ‘ESC’ to return to the Psykinematix application when prompted on screen.
    8. Repeat the test either immediately or after a break, or after another test as appropriate.
    9. Use the best results for the final measurements in order to allow for learning and fatigue effects.

6. Click on ‘Plotter’
    1. Select the patient from the list.
    2. Click on ‘Data Table’.
    3. Click on the ‘Saturation’ tab and highlight all the entries in the list displayed.

4. Right-click and Save As (enter the following details with no spaces e.g. ‘JJ90OU11V’):
    1. The patients initials and last two digits of their date of birth
    2. The eye being tested – OU for both
    3. Whether this is the 1st or 2nd test
    4. Whether the test is at the 1st or 2nd visit (‘1V’ or ‘2V’)
7. Open the ‘Octave-gui’ application from the dock
    1. Set the directory to ‘metropsis_octave’
    2. Type: ‘PlotCCTtrivectorResults(‘patientdetailsxxx.txt’)
    3. In place of ‘patiendetailsxxx.txt’ type the file name as in step 6.
    4. On the window that appears, click ‘Choose’
    5. Document the values of Protan, Deutan and Tritan to 4 decimal points on the CRF
    6. Save the result as a PDF by clicking on the drop-down menu arrow and saving it in the ‘MRI’ folder on the desktop using the same name as in Step 6.
    7. Type ‘close all;clear all’ to clear the data.
    8. Repeat step 7 for each test conducted.

FORMS/TEMPLATES TO BE USED

Results can be printed directly from the machine and can be stored on the PC. Trivector test results are reported as thresholds along the protan, deutan and tritan axes. Data should be recorded in the appropriate Case Report Form.

REFERENCES

1. Simunovic MP, Votruba M, Regan BC, Mollon JD. Colour discrimination ellipses in patients with dominant optic atrophy. Vision Res. 1998 Nov; 38(21):3413-9.

A1.8 Pattern Electroretinogram

PURPOSE

To ensure that the recording of the pattern electroretinogram (PERG) is performed consistently for all study participants.

INTRODUCTION

The pattern electroretinogram (PERG) is a retinal response evoked by a reversing black and white checkerboard, which provides objective information about macular and retinal ganglion cell function. The PERG will be performed before and after vector administration according to the study schedule, in order to monitor macular function in the study eye and fellow (control) eye. It can be measured by the Espion system (Diagnosys LLC, MA, USA).

SCOPE

This Standard Operating Procedure (SOP) specified stimulus and recording parameters available on the Espion system to measure the PERG.

DEFINITIONS

PERG = pattern electroretinogram

PROCEDURE

a. The methodology for the PERG will, as appropriate, incorporate the published standard of the International Society for Clinical Electrophysiology of Vision (ISCEV; see reference below).

b. All patient details will be confirmed and recorded. The procedures will be explained in full, informed consent obtained, and any questions regarding the procedures will be answered.

c. The PERG will be performed without mydriasis and with optimal refraction for the test distance used. Testing will be prior to all procedures involving bright flashing lights (excluding microperimetry).

d. Recordings will be obtained binocularly, to help stabilise fixation during testing. In cases of strabismus or when eccentric fixation is evident, PERG will additionally be performed monocularly to aid fixation.

e. The participant should not move their head during testing and should be encouraged to remain in a relaxed state to reduce muscle noise. The patient should be instructed to fixate on a fixation target at the centre of the stimulus display during testing.

f. Gold foil corneal electrodes will be used, referenced to (10mm EEG) surface electrodes at the ipsilateral zygomatic fossae, lateral to the ipsilateral outer canthus. The gold foil corneal electrodes will be carefully positioned over the lower eyelids such that the electrode is in

contact with the corneo-scleral junction in the midline, without touching the external surface of the lower eyelid. Topical anaesthesia should not routinely be necessary, but may be needed in sensitive individual patients. The surface electrodes will be applied after routine skin preparation and will have an impedance of 5kΩ or less between any pair of electrodes.

g. The checkerboard stimulus should be generated on a CRT screen. The stimulus will consist of a reversing black and white checkerboard comprising of 50' minute checks in a 15 x 12 degree field (width and height respectively). The luminance of the white squares will be 100 $cd.m^{-2}$; contrast will be >=98%. Stimulus reversal rate will be 4.4 reversals/second. Additional testing to a 30 x 24 degree field will be performed by reducing the distance to the screen by half and adjusting the check size accordingly.

h. Normal background room lighting will be used during PERG testing, but this should be the same for all PERG recordings. Bright lights will be kept out of the patient's view, and glare from the stimulus display screen should be prevented.

i. Analysis time will be 150ms. The filter bandwidth will be 1- 100Hz (-3dB). Line frequency notch filtering (mains frequency) will not be used. Artefact rejection will be used to eliminate spuriously large signals from the average such as those produced by eye movements or blinks. In addition to the use of automated artefact rejection, the "interrupted stimulation" technique may be used to minimise small eye movements and blinking artefacts that would fall within the automated artefact reject window.

j. An adequate number of sweeps will be averaged to obtain a reliable waveform without excess noise and this will usually involve averaging a minimum of 100 sweeps. A minimum of 2 and usually more replications will be recorded, sufficient to demonstrate a high degree of reproducibility.

k. If there is any significant interocular asymmetry, all electrodes positions and skin electrode impedances will be checked and replaced/repositioned as necessary. Any other artefact intruding into the record during a test should be investigated and remedied immediately and fully documented in the patient's record.

l. PERG N35, P50 and N95 components should be marked as per the ISCEV standard. If PERG N35 is not clearly present P50 should be measured from baseline.

FORMS/TEMPLATES TO BE USED

Results can be printed directly from the machine. Data should be recorded in the appropriate Case Report Form or patient clinical notes.

REFERENCES

ISCEV standard for clinical pattern electroretinography (PERG): 2012 update.

Michael Bach, Mitchell G. Brigell, Marki Hawlina, et al.

Documenta Ophthalmologica 2013; 126 (1): 1-7.

Espion user manual

A1.9 Measurement of Dark Adaptation Curve

PURPOSE

To ensure that the measurement of the dark adaptation curve is carried out as consistently as possible for all study participants.

INTRODUCTION

The process of dark adaptation is the ability of the eye to change its sensitivity due to a change in light level from light to dark. The process is mediated by a transition from cone-dominated to rod-dominated retinal function and can be mapped over time. This investigation can be done on the Espion (Diagnosys LLC, MA, USA).

SCOPE

This Standard Operating Procedure (SOP) covers the use of the Espion system with the associated response button box and software.

PROCEDURE

The test should be performed following pupil dilation to ensure consistency of testing by reducing pupil fluctuations affecting amount of light entering the eye. All tests will be done in the same order: right eye followed by left eye. For comfort, a break should be provided between testing the eyes to improve concentration and increase reliability. The comfort break should involve walking around. Testing should be performed as per the procedure below:

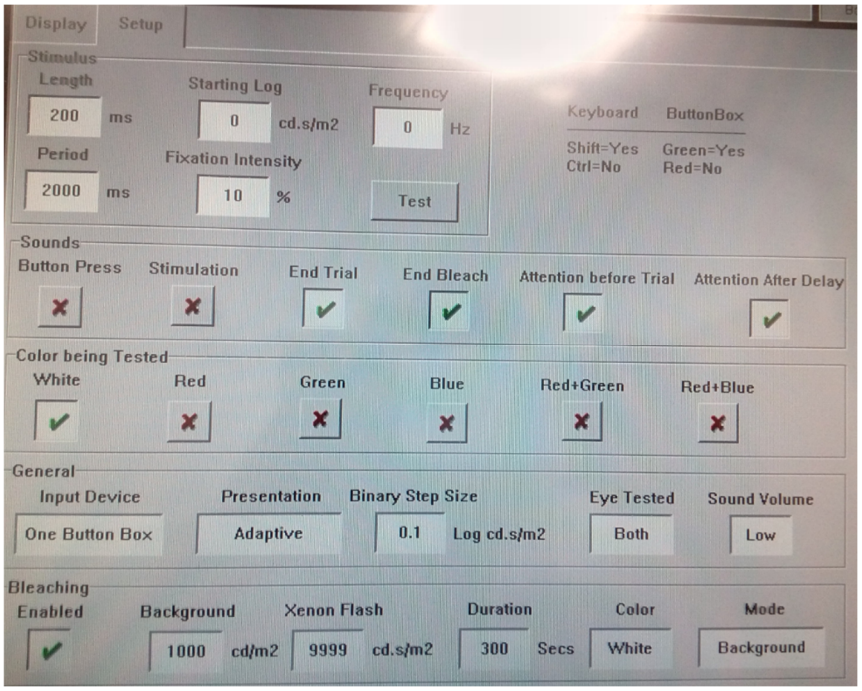
a. Plug in the button response box into the Espion Colourdome. Choose the appropriate test and calibrate the machine with the room lights off and the Colourdome cover in place. The cover should then be removed.

b. Set the parameters on both the display and settings tabs as per the following table.

Tab	**Parameter**	**Setting**
Setup	Stimulus length	200 ms
Setup	Stimulus starting log	0 cd.s/m^2
Setup	Stimulus frequency	0 Hz
Setup	Stimulus period	2000 ms
Setup	Fixation intensity	10 %
Setup	Sounds	Tick end of trial; end bleach; attention before trial. Ensure stimulation has a cross. Other boxes are optional.

Setup	Colour being tested	White
Setup	General input device	One button box
Setup	General presentation	Adaptive
Setup	General binary step size	0.1 Log cd.s/m^2
Setup	General eye tested	Select appropriate eye
Setup	Bleaching enabled	Tick
Setup	Bleaching background	1000 cd/m^2
Setup	Bleaching xenon flash	9999 cd.s/m^2
Setup	Bleaching duration	300 secs
Display	Eye	Ensure this matches the eye chosen on the setup tab
Display	Colours	Ensure this matches the colour chosen on the setup tab

This is shown clearly in the following screenshot of the setup screen:



c. Enter patient details on the machine. Study code and initials can be used instead of name. This can be changed at the end of the trial.

d. Ensure chin rest is at a comfortable height for the patient and patient's eyes are clearly visible near the centre of the camera view.

e. Measure pupil size of each eye then cover one eye ensuring no light leakage around the patch.

f. Select the eye being tested and input pupil diameter. Switch off room lights, reducing light leakage from operator screen to an absolute minimum and begin the bleaching period (5 minutes). The operator screen should be covered with a red filter 026 Bright Red (Lee Filters, Hampshire, UK). Throughout testing, keep the patient engaged by talking to them as required. NOTE: The test cannot be paused once started.

g. Once the light adaptation has finished, the light in the bowl will go out, placing the patient in the dark. Single lights of varying intensity will then be presented at the back of the bowl. The patient must respond by pressing the green button on the response box for each light seen, no matter how faint. Warn the patient, that the lights will initially be presented quickly and will slow down and get dimmer as the test progresses. Advise patient to respond for each light, no matter how faint they appear to be. Direction of fixation is not important as long as the eyes remain open.

h. There will be a series of rest periods made during the test. A single beep signals a rest period and a multiple beep signals commencement of recording. The rest periods become longer as testing progresses. The patient can be advised of this.

i. The endpoint is reached when the sensitivity curve reaches a plateau. This involves 5 consecutive points that no longer improve in sensitivity. However, the test must be run for a minimum of 25 minutes following the end of the light bleaching period, irrespective of whether a plateau is reached earlier. The test can then be stopped once the plateau has been reached. Occasionally an outlier can occur extending the time to run the test unnecessarily. Clinical judgement must be used in determining the final 5 points for the end of the test. The test must be stopped by the operator by clicking stop on the bottom tab.

FORMS/TEMPLATES TO BE USED

Results can be printed directly from the machine. Data should be recorded in the appropriate Case Report Form or patient clinical notes. Raw data can be exported.

REFERENCES

Espion user manual

A1.10 Full-Field Stimulus Threshold

PURPOSE

The purpose of this Standard Operating Procedure is to ensure the correct measurement of full field scotopic threshold (FST) using the Espion system (Diagnosys LLC, MA, USA). The SOP will ensure that the measurements are carried out as consistently as possible for all the study participants, within and across the different trials.

INTRODUCTION

The process of dark adaptation is the ability of the eye to change its sensitivity due to a change in light level from light to dark. The FST is a measure of sensitivity of the eye at the end of the dark adaptation process, i.e. maximum sensitivity of the eye. This is an alternative measure to full field ERG of retinal rod function and can be measured by the Espion system (Diagnosys LLC, MA, USA).

SCOPE

This SOP covers the use of Espion system with the associated response button box and software.

PROCEDURE

The test should be performed following pupil dilation to ensure consistency for all tests relating to the amount of light entering the eye. All tests will be done on the right eye only. For comfort, a break can be provided between testing the eyes as long as dark adaptation is maintained. Testing should be performed as per the procedure below:

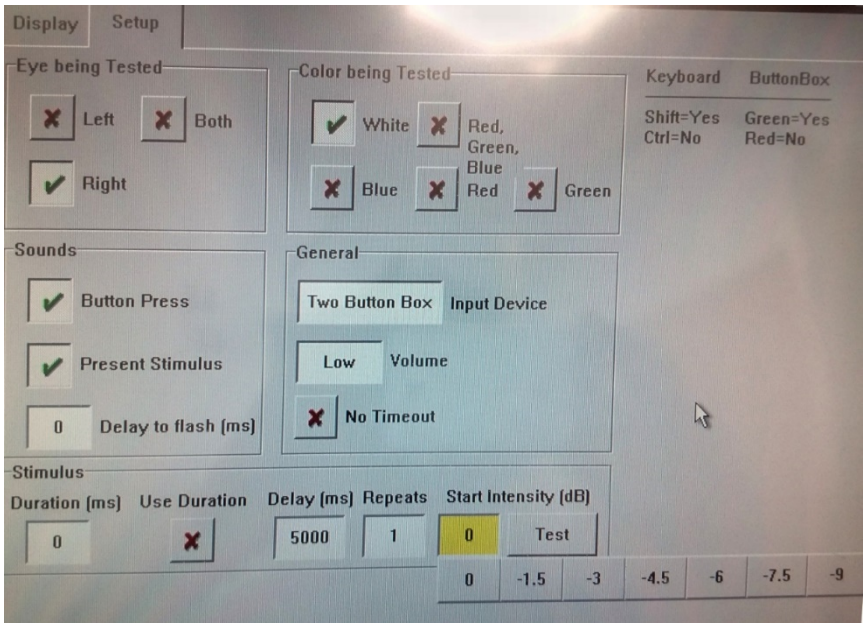
a. Plug in the button response box in to the Espion Colourdome. Choose the appropriate test and calibrate the machine with the room lights off and the Colourdome cover in place. The cover should then be removed. Calibration needs to take place only once a day, after the machine is first switched on. The automatic prompt will serve a reminder.

b. Set the parameters on both the display and settings tabs as per the following table.

Tab	**Parameter**	**Setting**
Setup	Eye being tested	Select appropriate eye
Setup	Colour being tested	Select colour being tested
Setup	Sounds	Tick button press; present stimulus
Setup	Sounds delay to flash	0 ms
Setup	General input device	Two button box
Setup	General timeout	Ensure cross so no timeout

Setup	Stimulus duration	0 ms, cross for use duration box
Setup	Stimulus delay	5000 ms
Setup	Stimulus repeats	1
Setup	Start intensity	Variable. To be set and tested before beginning.
Display	Eye	Ensure this matches the eye chosen on the setup tab
Display	Colours	Ensure this matches the colour chosen on the setup tab
Display	Results	Averages

This is shown clearly in the following screenshot of the setup screen:



c. Enter patient details on the machine. Study code and initials can be used instead of name if appropriate. This can be changed at the end of the trial.

d. Ensure chin rest is at a comfortable height for the patient and patient's eyes are clearly visible near the centre of the camera view.

e. Cover one eye with at least 2 patches, ensuring no light leakage around the patch. Dark adapt for 45 minutes. Reduce light leakage from operator screen to an absolute minimum.

f. Adjust starting point to speed up the test on the setup screen (see point b). Set starting point by clicking on the number, then click test and ask patient if the light was seen. Set the sensitivity as high as possible for the light to be seen. Start at 0dB then increase in -5, -10 or -20dB steps as appropriate (increasing then decreasing the steps to fine tune the starting point in a staircase method). This process takes a few seconds and reduces

the test time. The keypad symbol can be used to set the threshold value manually if the required value does not appear in the drop down list. Set the last point seen following one reversal as the starting point. Perform this process separately for each eye.

g. Place the button response box next to the patient with the green button on the right hand side and the red button on the left hand side. Advise the patient that the machine will beep for each flash of light. If it is seen, the patient must press the button on the right (green) and if it is not seen, press the button on the left (red). A button must be pressed for each beep in order for the test to proceed. Not seen should be the patient's default response. Advise the patient that some of the lights are extremely faint and to press if they think they saw the light.

h. Click run on the display tab to commence the test. The test will stop automatically when complete.

i. Repeat 3 times. Allow a minimum of 3 minutes dark adaptation time between tests to ensure maximum sensitivity is measured.

FORMS/TEMPLATES TO BE USED

Record test performed in the notes. Results can be printed directly from the machine.

REFERENCES

Espion user manual

A1.11 Scotopic Microperimetry

PURPOSE

The purpose of this Standard Operating Procedure is to ensure the correct measurement of retinal sensitivity using the Macular Integrity Assessment under scotopic conditions. The SOP will ensure that the measurements are carried out as consistently as possible for all the study participants, within and across the different trials.

INTRODUCTION

Scotopic microperimetry is a visual function test measuring the retinal sensitivity in the central ten degrees of retina whilst tracking eye movements using scanning laser ophthalmoscope in dark light levels. This is done on the MAIA system (Centervue SpA, Padova, Italy). A standard procedure to measure the sensitivity should be used.

SCOPE

This SOP covers the use of the scotopic MAIA microperimeter under scotopic conditions.

PROCEDURE

The test should be performed in a very dark environment following pupil dilation. This involves room lighting off and all sources of light in the room and around doors blocked out with blackout or red filter. A red lamp may be used during setup if covered with the correct red filter to prevent disruption of dark daptation. All tests will be performed on the right eye only. The participant requires a minimum of 45 minutes dark adaption prior to testing. No spectacle prescription is required to be worn for this test.

The patient should be sitting on a height adjustable chair with the MAIA microperimeter located in front of them. The participant should be asked to place their chin in the rest and with their forehead resting on the bar. They should be comfortable as they will need to remain in this position for the duration of the test. The height of the table and the chin rest can be adjusted as necessary.

The patient should be given the response button into whichever hand they prefer so that they are able to press the button located on the end of the handheld device. The occluder should be placed in position to block the left eye. The examiner should be situated at the monitoring screen. This screen should remain covered with a red film to ensure additional lighting does not interfere with the test.

Testing should be performed as per the procedure below:

1. Enter participant details on the machine. For SSN enter diagnosis or control.
2. For the 1st test being performed at baseline, click “New expert exam”. Choose the scotopic grid with concentric rings and ensure it is set to scotopic testing.

3. Explain to the patient that they will need to maintain fixation on the central target at all times throughout the test. They will be able to see lights, some bright and others faint that will flash up in the peripheral vision. Every time they are able to see one of these additional flashing lights in the periphery, they should press the button so that this is recorded. Throughout the test, they should be reminded to stay focused on the central red target. The brightness of the test can be increased and the level should be recorded on the CRF.
4. The participant should have their chin on the chin rest and the forehead placed firmly against the bar. Ensure they are comfortable and stable.
5. Set the eye being tested to OD (right eye). Press the 'Auto alignment' button on the screen. This allows the eye to be centred. The patient should be asked when they are able to see a red circle with a white dot in the centre of their vision. If after this the alignment is not possible, this can be performed manually using the 'up', 'down', 'left', 'right', 'forward' and 'back' options.
6. The cyan test should be conducted first.
7. Once aligned, the image requires focusing. Press 'start', this will automatically focus the image. Once focused the MAIA will take a screenshot of the focused image. This image will be saved and will be compared to future images to ensure alignment is correct.
8. You will be asked by the MAIA to locate the blind spot. You should click on the centre of the optic disc. Once this is completed, the test will start.
9. Provide encouragement during testing. Ensure head is kept still in the correct position. The machine can be moved vertically and horizontally if the eye position moves, but focussing must not be amended during testing. You can monitor the patients fixation by watching the central white dot located in the green fixation circle. If the white eye tracking dot moves outside of this circle the 'eye tracking alarm' will sound. At this point you may be required to remind the patient to continue looking at the fixation target or to help realign the patient.
10. If the patient becomes tired at any time, the test can be paused and restarted. For comfort, the patient may pause the test at any time, for up to 5 minutes in total per test, as long as they remain in the same light level.
11. Note reliability score and spread of fixation on completion of testing.
12. For repeat testing, click on "Follow-up exam" rather than "New expert exam", to use identical settings to ensure consistency. Complete all cyan tests before commencing testing with the red target.

FORMS/TEMPLATES TO BE USED

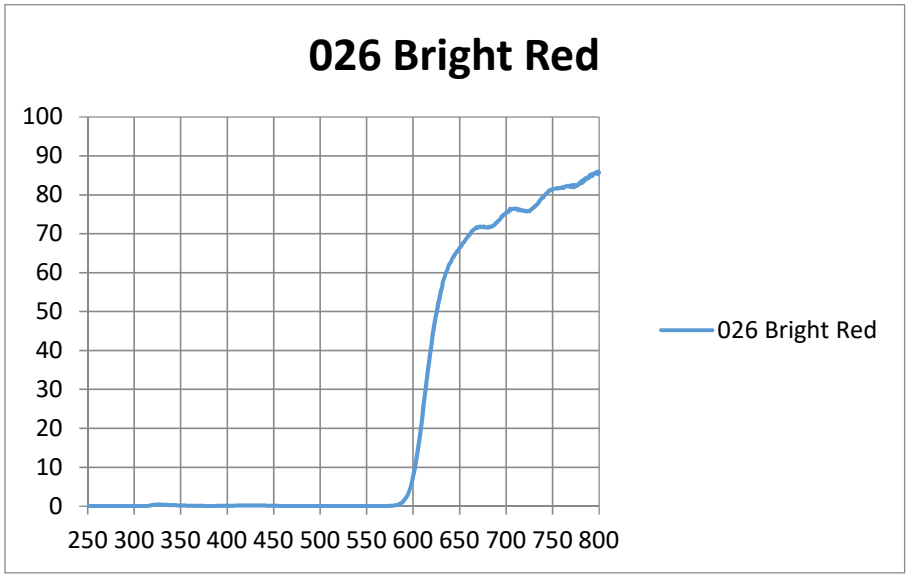
Record test performed in the notes. Results can be printed directly from the machine.

REFERENCES

http://www.centervue.com/system/datas/57/original/MAIA_Brochure_US.pdf

Pfau M, Lindner M, et al. Test-Retest Reliability of Scotopic and Mesopic Fundus-Controlled Perimetry Using a Modified MAIA (Macular Integrity Assessment) in Normal Eyes. *Ophthalmologica* 2016.

Transmission curve for 026 red filter



A1.12 Retinal Imaging With Ocular Coherence Tomography (OCT)

PURPOSE

To ensure that retinal imaging is carried out as consistently as possible for all study participants.

INTRODUCTION

Ocular coherence tomography imaging (OCT) will be performed using the spectral domain OCT system (Spectralis® HRA+OCT imaging system, Heidelberg Engineering, Heidelberg, Germany) to produce high resolution three-dimensional digital images of the patient's retina. This non-invasive imaging procedure will be performed at every visit to assess the anatomical structure of the retina, retinal pigment epithelium (RPE) and choroid to allow measurement of the retinal lesion zone.

SCOPE

This SOP covers the use of the use of spectral domain OCT systems with in-built confocal scanning laser ophthalmoscopy (SLO) image and eye tracking for the purpose of examining clinical trial participants using the Heidelberg Spectralis® HRA+OCT imaging system (Heidelberg Engineering, Heidelberg, Germany).

PROCEDURE

All tests should be performed without pupil dilation unless the participant has pupils too small to obtain adequate images. Scans of good quality (high signal, low noise) should be obtained. Image the right eye followed by the left eye.

Testing should be performed as per the procedure below:

1. Enter participant details. Enter own initials in operator and choose MRI for the study.
2. Position patient on chin and headrest to sit comfortably. Ensure height is set appropriately for the patient. Encourage participant to remain in this position throughout the procedure.
3. Ask the participant to watch the fixation target. Use the external target if the internal one cannot be seen. Verbally guide the participant and offer lots of encouragement.
4. Set the following parameters:

1. High resolution (HR)
2. ART mode 9
3. 20x20 degree volume scan
4. 49 A-scans
5. Centre over the foveola.

6. Focus the infrared image until image is optimal and fills the screen.
7. Ensure the scan appears in the top third of the scan window throughout and quality score remains above 20. If this cannot be achieved, make a note of why.
8. Follow-up OCTs should be performed at the same location using the AutoRescan function by selecting the baseline (i.e. pre-treatment) image as the reference scan. Note the baseline image will be marked by a chequered square symbol at the bottom left corner in the Heidelberg Eye Explorer software.
9. Repeat with a 7 line scan if possible.

FORMS/TEMPLATES TO BE USED

Record on the appropriate Case Report Form that OCT has been performed.

REFERENCES

https://www.heidelbergengineering.com/media/e-learning/Totara-US/files/pdf-tutorials/2238-003_Spectralis-Training-Guide.pdf

A1.13 Octopus Perimetry

PURPOSE

To ensure that Octopus perimetry assessment is carried out as consistently as possible for all study participants.

INTRODUCTION

Octopus perimetry allows characterisation of the extent of the wider visual field using a binocular suprathreshold test. This is based on the Estermann binocular test but has been customised to provide a symmetrical measure across the visual field. This has been implemented in the Open Perimetry Interface on the Octopus system (Haag-Streit, Harlow, UK).

SCOPE

This SOP covers the use of the Octopus system for binocular visual field assessment.

PROCEDURE

All tests should be performed without pupil dilation and with uptodate spectacles. The test must be repeated twice and the best results used in the analysis.

Testing should be performed as per the procedure below:

1. Ensure the Octopus is switched on at all 3 switches before switching on the computer.
2. Switch on the 0900 server and then click on R i386 3.4.3 icon on the desktop.
3. Click on File > Open script > Documents > esterman.GUI then choose Estermann.GUI.r.
4. Click Crtl A then ctrl R.
5. Set patient up on the Octopus by adjusting the height of the machine and the distance between the chin and forehead rests to ensure the participant is comfortable.
6. Move the chinrest as far to the left as possible, and ask the participant to place their chin on right hand side of the rest so most of one eye is visible on the camera. Adjustments can be made on the Octopus using the buttons on near the screen.
7. Instruct the participant to keep watching the fixation target of 4 green dots placed in a crosshair. If they can't see them all, emphasis it doesn't matter, they can pick ones can be seen and focus on them. The important thing is to keep the eyes as still as possible.
8. When prompted enter Patient ID (study ID number), visit number, Port number should be 50001, check Octopus900 and live graph on, change directory to esterman.GUI.
9. Start tracking on server. Ensure room lights off and the participant is sitting forward for calibration then click continue.

10. Watch results progress and eye position and instruct patient accordingly.
11. Repeat if false positives are above 20%
12. The test can be paused anytime but ensure the participant eye position is placed at the identical position as per the start of the test.
13. Once the test is completed, the continue button becomes active. This will save it in the results folder. Cancel deletes the results.
14. Repeat but close and restart the server in between tests.

FORMS/TEMPLATES TO BE USED

Results can be printed directly from the machine onto a USB stick. Data should be recorded in the appropriate Case Report Form.

REFERENCES

1. Octopus user manual

Appendix 2: Papers published from the thesis

A2.1 Jolly JK, Bridge H, MacLaren RE. Outcome Measures Used in Ocular Gene Therapy Trials: A Scoping Review of Current Practice. *Frontiers in Pharmacology* 2019 doi: 10.3389/fphar.2019.01076

A2.2 Jolly JK, Juenemann K, Boagey H, Nadsady M, Bridge H, MacLaren RE. Validation of Electronic Visual Acuity (EVA) Measurement Against Standardised ETDRS Charts In Patients With Visual Field Loss From Inherited Retinal Degenerations. *British Journal of Ophthalmology* 2019 doi: 10.1136/bjophthalmol-2019-315124

A2.3 Jolly JK. Rod-cone dystrophies: a guide to genetics and management. Optometry Today continuing education article December 2019

Appendix 3: Other relevant publications by Jasleen K Jolly

A3.1 **Jolly JK**, Xue K, Edwards TL, Groppe M, MacLaren RE. Characterizing the natural history of visual function in choroideremia using microperimetry and multimodal retinal imaging. Investigative Ophthalmology and Vision Science 2017; 58(12): 5575-83. DOI: 10.1167/iovs.17-22486

A3.2 **Jolly JK**, Edwards TL, Moules J, Groppe M, Downes SM, MacLaren RE. A qualitative and quantitative assessment of fundus autofluorescence patterns in patients with choroideremia. Investigative Ophthalmology and Vision Science 2016; 57:4498-4503. DOI: 10.1167/iovs.15-18362

A3.3 **Jolly JK**, Groppe M, Birks J, Downes S, MacLaren RE. Functional Defects in Colour Vision in Choroideremia. American Journal of Ophthalmology 2015; 160(4): 822-31. DOI: 10.1016/j.ajo.2015.06.018

A3.4 Han RC, **Jolly JK**, Xue K, MacLaren RE. The effects of pupil dilation on MAIA microperimetry. Clinical and Experimental Ophthalmology 2017; 45(5): 489-495. DOI: 10.1111/ceo.12907

A3.5 Han RC, Gray J, Han J, MacLaren RE, **Jolly JK**. Optimisation of dark adaptation time required for mesopic microperimetry. British Journal of Ophthalmology 2019; 103: 1092-98. doi: 10.1136/bjophthalmol-2018-312253

A3.6 Talib M, **Jolly JK**, Boon CJF. Measuring Central Retinal Sensitivity Using Microperimetry. Methods in Molecular Biology (In book: Retinal Gene Therapy, pp.339-349).

A3.6 Edwards TL, **Jolly JK**, Groppe M, Barnard AR, Cottriall CL, Tolmachova T, Black GCM, Webster AR, Lotery AJ, Holder GE, Xue K, Downes SM, Simunovic MP, Seabra MC, MacLaren RE. Long term improvement in visual acuity after retinal gene therapy for choroideremia. New England Journal of Medicine 2016; 374:1996-8. DOI: 10.1056/NEJMc1509501

A3.7 Xue K, **Jolly JK**, Barnard AR, Rudenko A, Patricio MI, Edwards TL, Groppe M, Tolmachova T, Black GC, Webster AR, Lotery AJ, Holder GE, Downes SM, Seabra MC, MacLaren RE. Retinal Gene Therapy for Choroideremia in a Multicentre Dose Escalation Phase I/II Clinical Trial. Nature Medicine 2018; 24(10): 1507-12. DOI: 10.1038/s41591-018-0185-5